Evaluation of a Chemical Genetic Approach to be used *in vivo* to Investigate the Role of the M_1 Muscarinic Acetylcholine Receptor in Learning, Memory, and Neurodegenerative Disease.

Thesis submitted for the degree of

Doctor of Philosophy

at the University of Leicester

By

Simon Mallinson Brooke MSc, BSc (Hons)

MRC Toxicology Unit

University of Leicester

2018

Abstract

In this project I performed the *in vitro* characterisation of a chemical genetic approach, using mutant receptors and an inert synthetic ligand, to dissect the role of the M_1 muscarinic acetylcholine receptor (mAChR) in learning, memory, and neurodegenerative disease. The mutant receptors being employed are designer receptors exclusively activated by designer drugs (DREADDs) and phosphorylation deficient (PD) receptors. DREADDs contain mutations within the orthosteric binding pocket; reducing the affinity and potency of the natural ligand, acetylcholine, and increasing the potency and efficacy of an inert synthetic ligand, clozapine-N-oxide (CNO). For phosphorylation deficient mutant receptors, phosphorylated serine residues were substituted for alanine residues. Using M_1-DREADD and M_1-DREADD-PD mutations *in vivo,* our ultimate aim is to study role of M_1-mAChR signalling, and G-protein dependent signalling, on learning and memory.

My investigations of the function and pharmacology of the M_1-DREADD and M_1-DREADD-PD mAChRs found the DREADD mutations significantly reduced the potency of acetylcholine, as well as the affinity of orthosteric antagonists such as N-methyl-scopolamine. These mutations also increased both the efficacy, relative to acetylcholine, and potency of CNO for the M_1 mAChR. Phosphorylation-deficient mutants were found to have impaired agonist dependent internalisation when compared to wild-type and DREADD M_1-mAChRs. Although reported to be an inert ligand, CNO was found to act in an antagonist mode at the mouse M_1, M_2, and M_4 mAChRs. This antagonistic mode, as well as the potential for CNO to be metabolised into clozapine, suggests alternative DREADD ligands need to be considered to prevent off-target side effects, even though previous transgenic studies have been successful. Given the successful modification of M_1-mAChR, these mutants can now be used to genetically engineer mice for *in vivo* studies. With these mice, behavioural studies can be performed to characterise the role played by total M_1-mAChR signalling, and its G-protein-dependent and independent signalling, on learning and memory. These observations can be used to inform drug discovery efforts targeting the M_1-mAChR, such as the treatment of Alzheimer's disease.

Publications

Papers

Butcher, A.J., Bradley, S.J., Prihandoko, R., **Brooke, S.M.**, Mogg, A., Bourgognon, J-M., Macedo-Hatch, T., Edwards, J.M., Bottrill, A.R., Challiss, R.A.J., Broad, L.M., Felder, C.C., Tobin, A.B. (2016) An Antibody Biosensor Establishes the Activation of theM1 Muscarinic Acetylcholine Receptor during Learning and Memory. The Journal of Biological Chemistry 291(17): 8862-8875.

Sophie J. Bradley, Colin Molloy, Christoffer Bundgaard, Adrian J. Mogg, Karen J. Thompson, Louis Dwomoh, Helen E. Sanger, Michael D. Crabtree, **Simon M. Brooke**, Patrick M. Sexton, Christian C. Felder, Arthur Christopoulos, Lisa M. Broad, Andrew B. Tobin and Christopher J. Langmead, (2018) Bitopic Binding Mode of an M_1 Muscarinic Acetylcholine Receptor Agonist Associated with Adverse Clinical Trial Outcomes. *Molecular Pharmacology*, 93(6) pp.645–656

Abstracts

Simon M. Brooke, Andrew B. Tobin. Evaluation of a Chemical Genetic Approach to Determine GPCR Function. *BPS 5th Focused Meeting on Cell Signalling. 28-29 April 2014. Poster Presentation.*

Simon M. Brooke, Rudi Prihandoko & Andrew B. Tobin. Evaluation of a Chemical Genetic Approach to Determine GPCR Function. *Eurotox 2014, 50th Congress of the European Societies of Toxicology. 7-10 September 2014. Poster Presentation*

Simon M. Brooke, Rudi Prihandoko & Andrew B. Tobin. Pharmacological Evaluation of CNO as a Tool to Determine *in vivo* GPCR Function. *BPS 6th Focused Meeting on Cell Signalling. 18-19 April 2016. Poster Presentation*

Simon M. Brooke, Sophie Bradley, Rudi Prihandoko & Andrew B. Tobin. Pharmacological Evaluation of Clozapine N-Oxide for its use in the in vivo Chemical Genetic Investigation of M_1 Muscarinic Acetylcholine Receptor Function. *BPS in silico and in vitro methods in modern drug discovery. 24-25 April 2017. Poster Presentation and Poster Prize*

Simon M. Brooke, Sophie Bradley, Rudi Prihandoko & Andrew B. Tobin. Pharmacological Evaluation of Clozapine N-Oxide for its use in the in vivo Chemical Genetic Investigation of M1 Muscarinic Acetylcholine Receptor Function. *FASEB SRC: G-Protein Coupled Receptor Kinases and Arrestins: From Structure to Disease: 11-16 June 2017 Poster Presentation*

Acknowledgements

Firstly, I would like to thank Prof. Andrew Tobin for the opportunity to undertake this PhD project, as well as for his support and encouragement during my time in the lab. My PhD was funded through the MRC Integrative Toxicology Training Partnership directed by Prof. Andy Smith. I would also like to thank Prof. Andy Smith for the events he organised as part of the ITTP program, and for stepping in to be my internal supervisor following the move of the Tobin group to the University of Glasgow.

I would like to especially thank the members of the Tobin group past and present for their support and guidance through my project. Special thanks go to Dr. Adrian Butcher, Dr. Sophie Bradley, and Dr. Rudi Prihandoko for their time and patience in training me in molecular pharmacology and the statistical analysis of my data. I would also like to thank the members of the group for making the lab a friendly environment to work in, and especially Sophie, Ana, Andy, Saj, Katie, and Omar for organising and getting involved with social events outside of work where we could relax and have a laugh.

I would like to thank the friends I've made within the MRC Toxicology Unit and the ITTP during my PhD. Even on the worst days where you wonder why you're still there, there was always a friendly face at lunch or in the break room to have a chat and a laugh with. Without the friendships I have made during my PhD, who knows how I would've survived, whether it be going to the cinema, the pub, siege Saturday, or Dungeons and Dragons.

Finally, I would like to thank all my family and friends outside of the MRC Tox Unit who have helped and supported me through these past 4 years. I would like to thank my parents who have supported me through so much of my education. Whether it be reading through my writing, helping me with moving in Leicester and moving all the way to Glasgow, or just being there for a chat when I've needed one.

Contents

List of Figures

List of Tables

Abbreviations

A_1AR	Adenosine A_1 Receptor
ACh	Acetylcholine
AChE	Acetylcholine Esterase
AChEI	Acetylcholine Esterase Inhibitor
AFU	Arbitrary Fluorescence Units
B_{max}	Total Receptor Density
CaSR	Calcium Sensing Receptor
CHO	Chinese Hamster Ovary
CLARITY	Clear Lipid-exchanged Acrylamide-hybridized Rigid Imaging/ Immunostaining/ in situ-hybridization-compatible Tissue hYdrogel
CNO	Clozapine N-Oxide
COPD	Chronic Obstructive Pulmonary Disease
DREADD	Designer Receptor Exclusively Activated by a Designer Drug
ECL	Enhanced Chemiluminescence
EC_{50}	Half Maximal Effective Concentration
EDTA	Ethylenediaminetetraacetic acid
ERK	Extracellular signal regulated kinases
ETC	Electrophoretic Tissue Clearing
E_{max}	Maximal Effective Concentration
FBS	Foetal Bovine Serum
FLIPR	Fluorescence Imaging Plate Reader

FOB	Fold Over Basal
FR	Fluorescence Ratio
GA	Glutaraldehyde
GFAP	Glial Fibrillary Acidic Protein
GPCR	G-Protein Coupled Receptor
GRK	G-Protein Coupled Receptor Kinase
HTRF	Homogeneous Time Resolved Fluorescence
IHC	Immunohistochemistry
IP	Inositol Monophosphate
IP_3R	Inositol Trisphosphate Receptor
i.p.	Intraperitoneal
JNK	c-Jun N-Terminal Kinase
K_d	Equilibrium Dissociation Constant
K_{off}	Dissociation Rate Constant
K_{on}	Association Rate Constant
LABA	Long Acting β_2-AR Agonist
LAMA	Long Acting Muscarinic Antagoinist
LSC	Liquid Scintillation Counting
LSFM	Light Sheet Fluorescence Microscopy
LSM	Light Sheet Microscope
mAChR	Muscarinic Acetylcholine Receptor
MAPK	Mitogen activated protein kinase

NMS	N-Methyl Scopolamine
pA2	Negative log of the concentration of antagonist that shifts EC_{50} by a factor of 2
PBS	Phosphate Buffered Saline
PBSTX	Phosphate Buffer Saline with 0.1% Triton X-100
PBZ	Phenoxybenzamine
PD	Phosphorylation Deficient
PIP_2	Phosphatidylinositol 4,5-Bisphosphate
PI3K	Phosphoinositide 3-Kinase
PKA	Protein Kinase A
PKC	Protein Kinase C
PLCβ	Phospholipase C β
RASSL	Receptor Activated Solely by a Synthetic Ligand
RI	Refractive Index
RIMS	Refractive Index Matching Solution
RIPA	Radioimmunoprecipitation Assay
ROCK	Rho-Associated Protein Kinase
ROI	Region of Interest
SPIM	Single Plane Illumination Microscopy
TBPB	1-(1'-(2-methylbenzyl)-1,4'-bipiperidin-4-yl)-1*H*-benzo[*b*]imidazole-2(3*H*)-1
TBS	Tris Buffered Saline
TBST	Tris Buffered Saline containing 0.1% Tween-20

WT	Wild-Type
5-HT	5-Hydroxytramptamine

Chapter 1 Introduction

1.1 G-Protein Coupled Receptors

G-protein coupled receptors (GPCRs) are the largest superfamily of membrane receptors, with 791 members identified within the human genome (Bjarnadóttir et al., 2006). GPCRs all share common structural characteristics: seven transmembrane α-helices, an intracellular C-terminus, an extracellular N-terminus, 3 extracellular loops, and 3 intracellular loops. Although they share these structural traits, GPCRs can be activated by a wide range of stimuli including extracellular signalling molecules such as peptides, hormones, neurotransmitters and even sensory inputs such as photons, odorants, and tastants. GPCRs are expressed throughout the body in various tissues, playing roles in physiological control, behaviour, and sensory perception. GPCRs have incredible potential as therapeutic targets; as well as their ubiquitous expression, GPCRs can also be targeted using small molecule ligands (Mason et al., 2012). Up to 50% of drugs on the market and 20% of the top 50 drugs either directly or indirectly target GPCRs (Ma and Zemmel, 2002).

GPCRs are split into 2 major groups: olfactory, and non-olfactory receptors; with non-olfactory GPCRs being further classified based on structural and functional similarities using the A-F system. For the A-F system, a database of known GPCR DNA sequences was analysed to identify common sequences which made up the fingerprint (Attwood and Findlay, 1994).These classes, labelled A-F, break down GPCRs into; rhodopsin-like, secretin-like, metabotropic glutamate-like, fungal mating pheromone receptors, cAMP receptors, and frizzled/smoothened receptor families. The fingerprint could be used to classify new receptor sequences as they were discovered. This classification system was based on the genomes of both vertebrates and invertebrates, with classes D and E not being present within vertebrates. Within these 5 major groups, GPCRs are organised into subfamilies e.g. mAChRs, dopamine receptors, histamine receptors, free fatty acid receptors, and 5-hydroxytryptamine (5-HT) receptors. Members of these subfamilies contain highly conserved regions, such as the orthosteric binding pocket, and share common ligands.

Muscarinic acetylcholine receptors are one such subfamily of class A GPCRs consisting of 5 receptor sub-types, labelled M_1-M_5. Found within the central and peripheral nervous systems, mAChRs play crucial roles in cognitive function, smooth muscle contraction, heartrate, and the regulation of insulin release. They are named after muscarine, a muscarinic acetylcholine receptor agonist isolated from ergot in 1869 (Schmiedeberg and Koppe, 1869). Studying its function, they identified its ability to: lower, and even arrest, heart rate; induce gastrointestinal smooth muscle contraction; stimulate tear, saliva, and mucus secretion; constrict the pupils and; even cause dyspnoea. All members of this family are activated by acetylcholine, the first neurotransmitter to be identified (Dale, 1914; Ewins, 1914; Loewi and Navratil, 1926). Although there was a large body of work performed on muscarinic acetylcholine receptors (Barlow et al., 1976; Fraser, 1957; Riker and Wescoe, 1951; Roszkowski, 1961), the confirmation of their existence as a subtype of the acetylcholine receptors, and the identity of their subtypes, was not determined till the 1980s. The differentiation between mAChR subtypes was first performed through assessments of their functional and pharmacological properties. Noticeable differences were found both in the function of the subtypes and the binding affinity of ligands including pirenzepine, gallamine and carbachol in different tissues (Birdsall and Hulme, 1983; Hammer et al., 1980; Hammer and Giachetti, 1982). Although at this early stage there were believed to be only 3 members of the family, eventually 5 members of the mAChR family were identified within the mammalian genome (Akiba et al., 1988; Bonner et al., 1991, 1988, 1987; Kubo et al., 1986; Peralta et al., 1987). Differences in function arise from the Gα subunit with which the receptor preferentially couples. M_1, M_3, and M_5 couple to $G\alpha_{q/11}$, which mediates stimulatory pathways through activation of phospholipase C such as inositol-1,4,5-trisphosphate signalling. M_2 and M_4 couple with $G\alpha_i$ mediating inhibitory pathways by inhibiting the generation of cyclic AMP by adenylyl cyclase (Brown, 2010; Burford et al., 1995). This project will focus on the evaluation of a model utilising mutant receptors and a synthetic ligand. This model is aimed towards understanding the role of the M_1-mAChR, and its downstream signalling pathways in neurodegenerative disease.

1.1.1 GPCR Signalling

GPCRs mediate signals from a wide range of inputs including lipids, peptides, and amino acids, and are also responsible for the propagation of signals from photons in the retina. Signals are propagated by GPCRs through two distinct pathways: G-protein dependent, and phosphorylation/arrestin dependent pathways. The first of these pathways, the G-protein dependent pathway, involves the coupling of heterotrimeric G-proteins to the intracellular portion of the receptor following agonist stabilisation of the active conformation of the receptor (Rasmussen et al., 2011). Heterotrimeric G-proteins consist of 3 subunits termed α, β, and γ. 16 different G_{α} subunits have been identified, as well as 5 G_{β} subunits and 11 G_{γ} sub units. Gα subunits are divided into 4 categories based on functional and sequence similarities: $G_{\alpha i}$, $G_{\alpha q}$, $G_{\alpha s}$, and $G_{\alpha 12/13}$ (Hurowitz et al., 2000; Wilkie et al., 1992). G_{β} subunits are divided into 2 groups, $G_{\beta 1\text{-}4}$ and $G_{\beta 5}$, based on sequence homology and intron positions. The G_{γ} subunits are categorised into 3 groups based on amino-acid sequence homology and functional similarities. Differences between the signalling of GPCR subtypes arises from preferential coupling to particular heterotrimeric G-proteins (Gilman, 1987; Strathmann and Gautam, 1991). Studies have shown that the G_{α} subunit of heterotrimeric G-proteins is what couples to GPCRs (Conklin and Bourne, 1993; Oldham and Hamm, 2008; Rasmussen et al., 2011). On coupling, a molecule of GDP bound to the G_{α} sub unit, is exchanged for a molecule of GTP. This exchange leads to a conformational change of the G_{α} subunit and its separation from the $G_{\beta\gamma}$ dimer. The G_{α} and $G_{\beta\gamma}$ sub units then go on to activate their respective signalling pathways. $G_{\alpha q}$ has been shown to activate phospholipase C β (PLCβ) and RhoA, $G_{\alpha i}$ inhibits the activity of adenylyl cyclase, $G_{\alpha s}$ activates adenylyl cyclase, and $G_{\alpha 12/13}$ activates the RhoA pathway. $G_{\beta\gamma}$ has been shown to activate PLCβ, phosphoinositide 3-kinase (PI3K), and SRC (Fig. 1.1). GPCR coupling with heterotrimeric G-proteins can be promiscuous, with evidence being found for receptors being able to interact with heterotrimeric G-proteins containing different Gα subunits (Hermans, 2003; Kostenis et al., 2005; Milligan, 1997). mAChRs have been found to couple with either $G_{\alpha q}$ or $G_{\alpha i}$ depending on the receptor sub-type; M_1, M_3, and M_5 mAChRs primarily couple to $G_{\alpha q}$ and M_2 and M_4 mAChRs couple to $G_{\alpha i}$. There is also evidence to suggest individual mAChRs can be promiscuous in their interactions with heterotrimeric G-proteins. For example, studies inhibiting $G_{\alpha i}$ using pertussis toxin uncovered activation

of $G_{\alpha s}$ and $G_{\alpha q}$ signalling pathways by the M_2 mAChR (Griffin et al., 2007; Michal et al., 2007). There is also evidence to suggest that the activation of mAChRs by different muscarinic ligands could trigger changes in the affinity of G-proteins to the M_1-mAChR (Akam et al., 2001; Gurwitz et al., 1994). With these mAChRs, investigations into these alternative heterotrimeric G-protein interactions were performed using pertussis toxin or multiple muscarinic ligands. The ability of different ligands to alter the heterotrimeric G-protein coupling to the receptor *in vitro* is an interesting phenomenon. These interactions may not be physiologically relevant as the ligands used are not naturally produced, but may be of importance in the characterisation of new ligands. In pertussis toxin models, the toxin inhibits the binding of $G_{\alpha i}$ to GPCRs (Locht et al., 2011; Mangmool and Kurose, 2011). Preventing $G_{\alpha i}$ competing for activated GPCRs may reveal lower affinity G-protein binding, but is not necessarily an interaction that will be physiologically relevant. Although this coupling of multiple G_{α} classes have been identified, the process leading to this promiscuity is poorly understood. It is thought this variation in G-protein coupling to GPCRs may increase the complexity of signalling pathways downstream of a given receptor (Tuček et al., 2002).

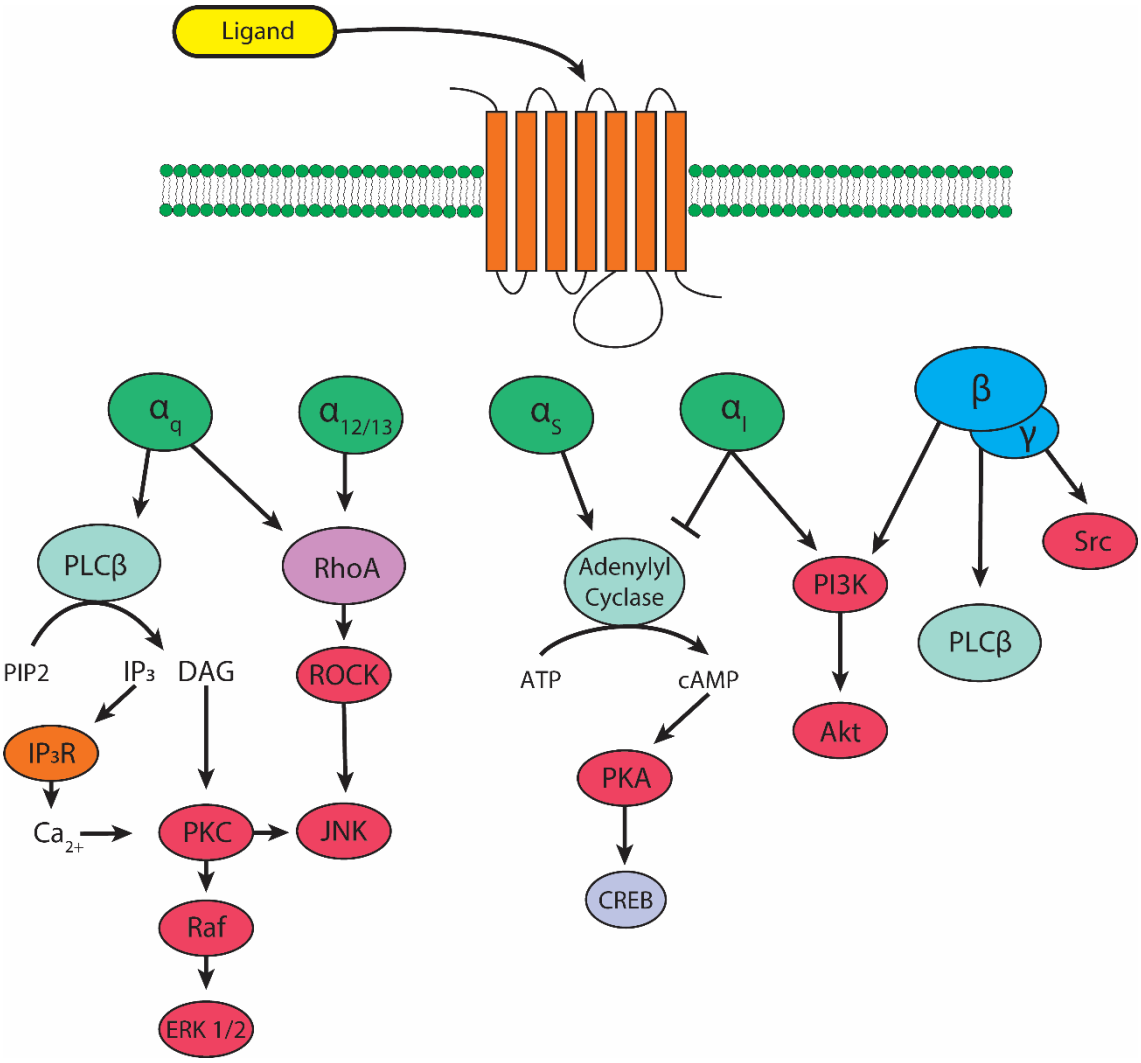

Figure 1.1. Overview of G-protein dependent signalling pathways.

Binding of an agonist to GPCRs leads to a conformational change which allows coupling of heterotrimeric G-proteins to the intracellular surface of the receptor. This interaction causes a conformational change in the G_α subunit causing the exchange of a molecule of GDP for GTP and the separation of the G_α subunit from the $G_{\beta\gamma}$ subunit. These two subunits then go on to activate their respective downstream signalling pathways, represented above. Diacylglycerol (DAG), Inositol trisphosphate receptor (IP_3R), c-Jun N-terminal kinase (JNK), Phosphatidylinositol 4,5-bisphosphate (PIP_2) Protein Kinase A (PKA), Rho-associated protein kinase (ROCK).

Phosphorylation of the intracellular sites of GPCRs plays an important role in the regulation of G-protein dependent signalling and receptor internalisation. Phosphorylation of GPCRs is controlled by secondary messenger protein kinases such as PKA (Benovic et al., 1985) and PKC (Bouvier et al., 1987), as well as a group of serine/threonine kinases called G-protein coupled receptor kinases (GRKs) (Pitcher et al., 1992). GRKs are a family of 7 serine/threonine kinases involved in the regulation of GPCR signalling through receptor phosphorylation and complex formation. GRKs are further divided into 3 distinct groups; GRK1-like, GRK2-like, and GRK4-like. GRKs can also be categorised into 2 groups; Visual GRKs, GRK1 and GRK7; and non-visual GRKs, GRK2 - GRK6. The GRK1-like group consists of GRK1 and GRK7 and are found within the rod and cone cells respectively (Ferguson, 2001). GRK 1 and GRK7 are found at the cell membrane, localised through posttranslational farnesylation within the C-terminus (Yang and Xia, 2006). The GRK2-like group consists of GRK 2 and GRK 3, also known as the β-adrenergic receptor kinases, are ubiquitously expressed through tissues, and localised within the cytosol. GRK4, GRK5, and GRK6, make up the GRK4-like group which are localised at the cell membrane. GRK4 and GRK6 are localised to the cell membrane by post translational palmitoylation of the C-terminus. Localisation of GRK5 to the cell membrane requires interaction with phosphatidylinositol 4,5-bisphosphate and lipid binding with the C-terminus (Pronin et al., 1998).Unlike GRK5 and GRK6 which are widely expressed, GRK4 is localised within the testes (Premont and Gainetdinov, 2007).

Phosphorylation by secondary messenger protein kinases and GRKs both play a role in receptor desensitisation (Lefkowitz, 1998); but it has been shown that GRK dependent phosphorylation is more critical in mediating GPCR internalisation than phosphorylation through other protein kinases (Lohse et al., 1992). GRK2-type mediated phosphorylation of GPCRs requires trafficking of the kinases from the cytosol to the cell membrane (Premont et al., 1995). $G_{\beta\gamma}$ has been shown to form a complex with GRK2 and facilitate its trafficking to the cell membrane, and induce a conformational change in GRK2, activating the kinase (Lodowski et al., 2003; Sarnago et al., 2003). Secondary messenger protein kinases and calmodulin, a calcium binding protein, have been found to regulate the function of GRKs. Calcium bound calmodulin inhibition has been found to occur through binding to GRKs and blocking their interaction with GPCRs. Calmodulin binding

also triggers autophosphorylation of C-terminal residues within GRK5, inhibiting its function (Pronin et al., 1997). PKC dependent phosphorylation of C-terminal GRK5 residues, distinct from those autophosphorylated following calmodulin binding, inhibit GRK5 function (Pronin and Benovic, 1997). Phosphorylation of GRK2 by PKC has been found to reverse the inhibition of calmodulin, with phosphorylation sites of PKC having been identified within the calmodulin binding pocket (Krasel et al., 2001). Studies of β_2-adrenergic receptor phosphorylation by PKA has been shown to reduce the affinity of $G_{\alpha s}$ and increased the affinity of $G_{\alpha i}$ (Daaka et al., 1997). This change in affinity has been thought of as both a desensitisation of $G_{\alpha s}$ dependent signalling and to initiate a new set of signalling through the $G_{\alpha i}$ pathway. Unlike secondary messenger protein kinases, GRKs usually require GPCRs to be in an active conformation to couple to and phosphorylate the receptor. An exception to this is the constitutive phosphorylation of the D1 dopaminergic receptor by GRK4 (Rankin et al., 2006). Knock-out studies have identified that GRK3, which is highly expressed within the olfactory epithelium (Schleicher et al., 1993), is integral to olfactory desensitisation (Peppel et al., 1997). Studies have shown that the pattern of intracellular phosphorylation sites, also known as a phosphorylation barcode, can depend on the ligand used to activate the receptor, and the cell type in which the receptor is expressed (Tobin et al., 2008). Individual kinases have been attributed to the phosphorylation of specific sites (Yang et al., 2017); differing expression profiles between tissues could be a source of cell type specific phosphorylation barcodes. In the M_3-mAChR, different patterns of phosphorylation intensity were seen at multiple sites in both a cell-type and ligand dependent manner (Butcher et al., 2011). Studies using free fatty acid receptor 4 (FFAR4) receptors containing mutations within phosphorylation clusters have shown that the removal of said clusters can alter receptor desensitisation to varying degrees (Prihandoko et al., 2016).

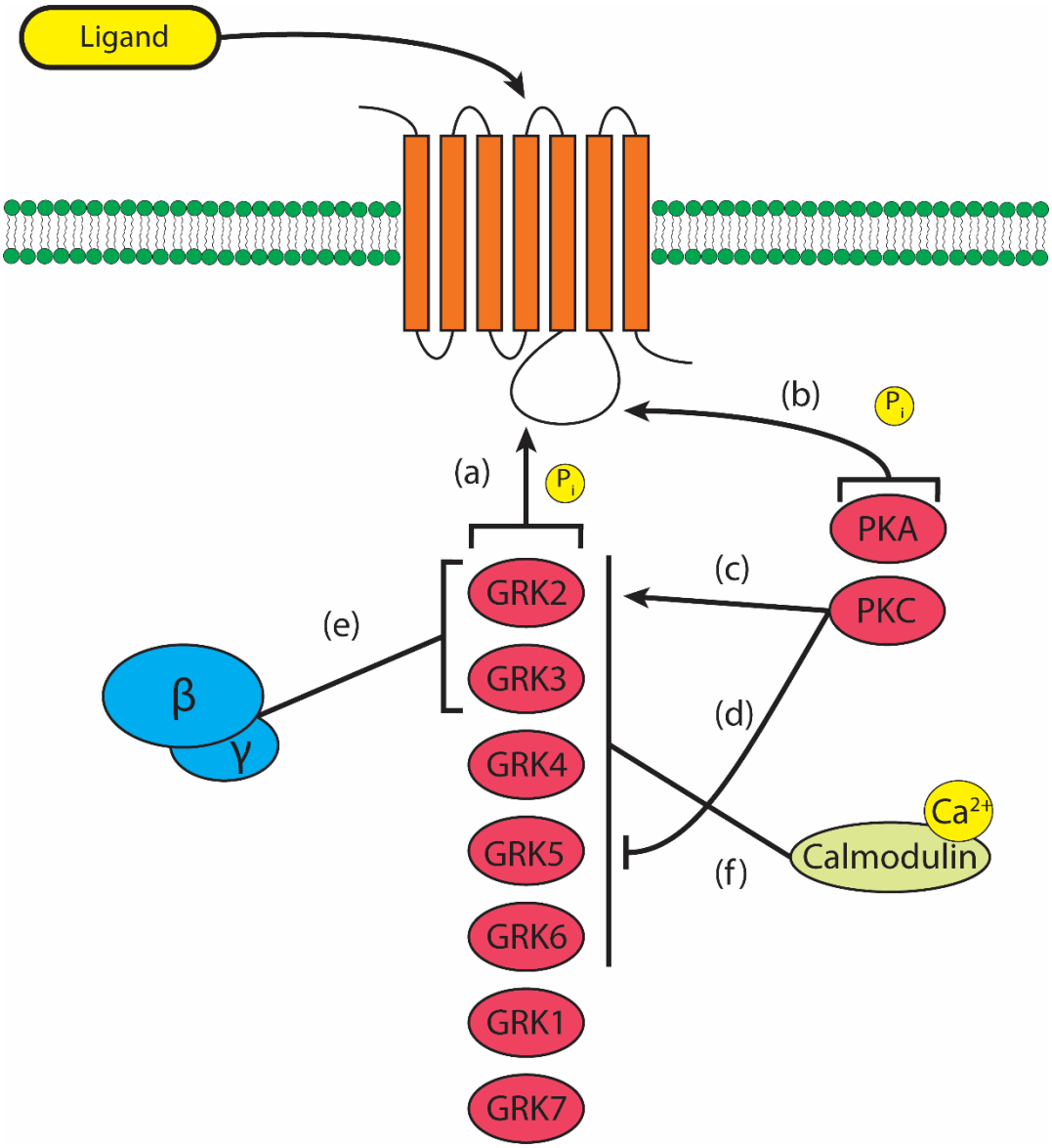

Figure 1.2. Overview of G-protein coupled receptor phosphorylation.

Phosphorylation is an important step in the regulation of GPCR signalling, playing a role in both the desensitization and internalisation of the receptor. Intracellular regions of GPCRs are phosphorylated by GRKs (**a**) and secondary messenger protein kinases such as PKA and PKC (**b**), whose activity is then potentially regulated by other proteins and molecules. PKC has also been shown to promote the translocation of GRK2 to the cell membrane (**c**) and to inhibit GRK5 activity (**d**). The $G_{\beta\gamma}$ subunit, once separated from the G_{α} subunit, has been found to traffic GRK2 and GRK3 to the cell membrane (**e**). Calcium bound calmodulin (**f**) can bind to GRK2-6 with varying affinities, and inhibit GRK phosphorylation of GPCRs.

Phosphorylation of the intracellular regions of GPCRs leads to receptor internalisation through complex formation with proteins such as arrestins (Prihandoko et al., 2016), and GRKs, and interact with clathrin coated pits (Shiina et al., 2001). Certain receptor subtypes however, such as the angiotensin II type 1A receptor and the M_2-mAChR, have been found to internalise in a clathrin independent manner (Wan et al., 2015; Zhang et al., 1996). Although clathrin independent internalisation has been identified in GPCRs it is poorly characterised. Arrestins are a family of 4 proteins, with 2 visual and 2 non-visual. The first arrestin molecule to be identified was S-arrestin, a visual arrestin identified within the rod cells of the retina and selectively couples to rhodopsin (Kühn et al., 1984). Coupling of S-arrestin to the rhodopsin blocks activation of transducin (Gurevich et al., 1994) , a form of heterotrimetic G-protein found within the cone and rod cells (Lerea et al., 1986). S-arrestin was later also identified within the brain heart lung and kidney (Breitman et al., 1991; Smith et al., 1994) and found to translocate to the members of the Secretin family of receptors (Oakley et al., 2000). The discovery of S-arrestin was followed by the consecutive discoveries of the non-visual arrestins β-arrestin 1 (Lohse et al., 1990) and 2 (Attramadal et al., 1992) and finally X-arrestin, the second visual arrestin (Cheryl et al., 1994; Murakami et al., 1993). β -arrestin 1 and 2 are expressed throughout the body with multiple splice variants having been identified (Sterne-Marr et al., 1993). S-Arrestin, β -arrestin 1 and 2, and X-arrestin, are also referred to as Arrestins 1-4 respectively. Phosphorylation of the receptor and arrestin coupling desensitizes GPCRs by blocking the intracellular regions, preventing G-protein coupling. Once coupled, arrestins regulate receptor internalisation, recycling and degradation, as well as mediating the activation of downstream signalling pathways. Arrestin-mediated receptor internalisation occurs through interactions with clathrin and adaptor protein 2 within the clathrin coated pits (Fernandez et al., 2008; Goodman et al., 1996; Laporte et al., 2000, 1999; Marchese et al., 2003; Pula et al., 2004; Qian et al., 2014). In some receptors, such as the protease-activated receptor-2, neurokinin-1 receptor, and orexin receptor, studies have found that phosphorylation of sites within the C-terminal tail are vital for arrestin-mediated internalisation (Jaeger et al., 2014; Mundell et al., 2010; Pal et al., 2013; Pula et al., 2004; Reiner et al., 2009; Singh et al., 2011). In the human M_1 mAChR it was identified that internalisation required domains within the third intracellular loop (Lameh et al., 1992); with mass spectrometry of the

M_1- and M_3-mAChRs identifying phosphorylation sites primarily within their 3rd intracellular loops (Butcher et al., 2016, 2011). To further investigate this one study used mutant M_3-mAChRs where the phosphorylation sites within the 3rd intracellular were replaced with alanine residues. These mutations were found to reduce agonist-induced arrestin recruitment and, through lowered PKD1 activation, lower insulin secretion from pancreatic islets (Kong et al., 2010).

Once internalised, the recycling or degradation of the receptor is controlled through arrestin interacting with pro-degradation E3 ubiquitin ligases and pro-recycling deubiquitinases (Goodman et al., 1996; Shenoy et al., 2009). Arrestin-dependent pathways can further silence G-protein dependent signalling pathways through degradation of secondary signalling molecules while initiating their own signalling cascades. This negative feedback activity is important in controlling receptor function; without a control mechanism, receptor function could potentially continue unchecked. The activation of diacylglycerol kinase by arrestin converts diacylglycerol into phosphatidic acid (Nelson et al., 2007). Degradation of diacylglycerol inhibits the activation of signalling pathways downstream of PKC. Biological functions have been attributed to phosphatidic acid such as vesicular trafficking (Tu-sekine et al., 2014; WANG et al., 2006) and activation of mTOR (Fang et al., 2001; Foster, 2009); and by acting as a scaffold, arrestins can activate and regulate members of downstream signalling cascades such as extracellular-signalling regulated kinases (ERK) 1/2 within the mitogen activated protein kinase (MAPK) pathway (Scott et al., 2006).

An important consideration in the development of new ligands is that agonists binding to the same receptor will not necessarily activate downstream signalling pathways to the same degree. This phenomenon, known as functional selectivity or signalling bias, is where different ligand-receptor binding leads to the stabilisation of unique conformational structures (Kenakin, 1995) which differentially activate intracellular signalling pathways. With mathematical models and methods being devised to better characterise signalling bias (Evans et al., 2011; Kenakin et al., 2012), it is thought that biased agonism could be harnessed for the development of superior therapeutic agents (Kenakin, 2012). In the β_2-adrenergic receptor, the β-arrestin biased ligand carvedilol was found to differentially phosphorylate the receptor when compared to the unbiased

isoproterenol (Nobles et al., 2011). Characterisation of the physiological outcomes of this differential phosphorylation could be used in the future for the screening of new potential therapeutic agents. Coupled with these studies into the characterisation of biased ligands, it will also be important to investigate the physiological relevance of signalling pathways *in vivo*, to understand how modulations of these pathways could be used to more efficiently treat disease.

1.2 Muscarinic Acetylcholine Receptors

1.2.1 Muscarinic Acetylcholine Receptor Distribution and Function

1.2.1.1 Central Nervous System

All mAChRs can be found throughout the central nervous system, with M_1, M_2, and M_4 subtypes being the most abundant (Levey et al., 1991). The M_1 mAChR is the most abundant receptor in the cortex, found within the postsynaptic dendrites and spines of pyramidal cells (Mrzljak et al., 1993). The M_2 mAChR has been identified primarily at the cell membrane of non-pyramidal neurons and the cytoplasm and Golgi of pyramidal neurons (Mrzljak et al., 1998, 1996) both pre- and postsynaptically. The highest levels of M_2 mAChR within the central nervous system are within the cortex (Gomeza et al., 1999a). M_4 mAChR expression within the cortex is localised to the perikarya (Volpicelli and Levey, 2004). Hippocampal expression of the M_1 mAChR makes up around 36% of the total central nervous system expression and 60% of mAChR expression within the hippocampus (Volpicelli and Levey, 2004). The M_1 mAChR is expressed throughout the hippocampus, at highest levels within the pyramidal neurons of the CA1 and dentate gyrus. M_2 mAChR expression is roughly 33% of the hippocampal mAChR expression, and is well defined within the stratum pyramidale of the CA3 and CA1 regions. Hippocampal M_4 mAChR expression makes up around 26% of hippocampal mAChR expression and is localised to the molecular layer of the dentate gyrus and the stratum radiatum of the CA1. M_3 mAChRs are expressed at low levels throughout the hippocampus, with elevated levels of expression within the stratum lucidum and stratum orens of the CA3 and the stratum lacunosum-moleculare in the CA1 (Levey et al., 1995). M_5 mAChRs are expressed at low levels within the hippocampus, substantia nigra and the ventral tegmental area (Tayebati et al., 2003; Vilaró et al., 1990) and have also been identified within the cerebral vascular beds where it is thought to control the dilation of arteries

and arterioles (Tayebati et al., 2003; Yamada et al., 2003). M_1 and M_2 mAChRs have been associated with higher cognitive functions such as spatial memory and learning. This link has been confirmed in knock-out models where removal of either the M_1 or M_2 mAChR leads to significant cognitive deficits in mice and rats (Gautam et al., 2006a; Porter et al., 2002; Seeger et al., 2004; Tzavara et al., 2003; Veeraragavan et al., 2011). Phosphorylation deficient models of the M_3 mAChR reveal changes in cognition and behaviour (Poulin et al., 2010) in mouse models, with the mice showing a reduced response to both contextual and cued stimuli during following fear conditioning. Studies have shown that the M_4 mAChR acts in an inhibitory capacity, negatively regulating locomotor activity and dopamine release in response to drugs of abuse from the D_1 dopaminergic pathways (Gomeza et al., 1999b; Jeon et al., 2010; Onali and Olianas, 2002). There is evidence that M_5 mAChRs expressed in dopaminergic neurons within the substantia nigra are involved in substance dependence. M_5 mAChR knock out models do not develop opiate dependency on exposure to morphine, without negating the analgesic properties of morphine (Basile et al., 2002; Yamada et al., 2003).

1.2.1.2 Peripheral Nervous System and Non-Neuronal Tissue

In the peripheral nervous system, the M_1 mAChRs have been found within the salivary glands, along with the M_3 mAChR, where they control salivary secretion (Gautam et al., 2004). M_2 mAChRs are highly expressed within the heart, (Hulme et al., 1990) and play a major role in heart pace making (Dhein et al., 2001). M_2 mAChRs have also been identified along with the M_3 mAChR within in the bladder, triggering detrusor muscle contraction (Noronha-Blob et al., 1989; Wang et al., 1995). Although the M_2 mAChR outnumbers the M_3 mAChR 9:1 in rat bladder and 3:1 within other species, the M_3 mAchR contributes towards around 95% of bladder smooth muscle contraction (Fetscher et al., 2002; Matsui et al., 2000; Wang et al., 1995). All members of the mAChR family have been identified within the alimentary tract; M_1 and M_3 in parenchymal tissue, M_2 and M_3 smooth muscle, M_1, M_3, M_4, and M_5 in blood vessels, and M_1 and M_4 in neuronal tissue (Tobin et al., 2009). Within the gastrointestinal smooth muscle, M_2 and M_3 mAChRs have been shown to control the strength and frequency of small intestine motor activity (Tanahashi et al., 2013). M_1 and M_3 mAChRs have been shown to control vasodilation of mesenteric arteries (Tangsucharit et al., 2016). M_2 and M_3

mAChRs have been identified within airways (Ikeda et al., 2012), with the M_3 mAChR expressed within the smooth muscle initiating airway contraction and the M_2 mAChR express inhibiting acetylcholine release and airway constriction (Fryer and Jacoby, 1998). Knock-out M_3 mAChR mouse models revealed poor glucose homeostasis in both oral and intravenous glucose tolerance tests, a reduction in the muscarinic receptor stimulated release of both insulin and glucagon, as well as a reduction in appetite and weight gain compared to control animals (Duttaroy et al., 2004; Gautam et al., 2006b; Yamada et al., 2001b). The M_4 and M_5 mAChRs have little known function within the peripheral nervous system, although some studies have provided evidence for the M_5 mAChRs involvement in contraction of ciliary processes within the eyes of dogs and rabbits (Eglen and Nahorski, 2000).

The integral functions mAChRs play within the central nervous, cardiovascular, and respiratory systems has made them targets of multiple therapeutic agents. Major therapeutic strategies in Alzheimer's disease (Langmead et al., 2008), chronic obstructive pulmonary disease (Alagha et al., 2014; Calzetta et al., 2017), and bradycardia (Papastylianou and Mentzelopoulos, 2012) have been centred around the mAChRs. In spite of their potential, the difficulty in identifying highly selective compounds has led to newer drugs, with potentially beneficial therapeutic effects, failing in clinical trials (Mirza et al., 2003). The importance of mAChRs within the alimentary canal, respiratory system, and heart, mean poor selectivity can lead to wide ranging symptoms which make these potentially beneficial ligands intolerable for chronic use. To avoid these issues the next generation of ligands need to focus on the more selective bitopic and allosteric ligands.

1.2.2 Muscarinic Acetylcholine Receptors in Disease and Therapy

GPCRs have been a long-standing feature in drug discovery efforts. They have wide range of potential physiological outputs, they are sensitive to a variety of molecules, and they have target sites easily accessible from the cells surface. Major drug discoveries targeted at GPCRs include beta-blockers, anti-histamines, antipsychotics, and sedatives. The development of the first beta-blocker, propranolol (Black et al., 1964), was a major breakthrough in the management of cardiovascular disease such as atrial arrhythmia (Harrison et al. 1965) and angina pectoris (Gillam & Prichard 1965) through the

antagonism of the β_2-adrenergic receptor. The first antipsychotic developed, chlorpromazine, is a dopamine receptor and serotonin receptor antagonist, with additional antagonistic properties at cholinergic, adrenergic and histaminergic receptors. Antagonism of the dopaminergic D2 receptor by first generation antipsychotics caused extrapyramidal side effects such as parkinsonian-like movement disorders (Sykes et al., 2017). The antipsychotic clozapine was also a receptor antagonist primarily at the serotoninergic and dopaminergic receptors, although it has been shown to interact with a wide range of GPCRs (Roth et al., 2004). Clozapine was a member of the second generation of antipsychotic agents which were called 'atypical' because of their reduced incidence of extrapyramidal side-effects, having a lower affinity for the D_2 dopaminergic receptor subtype than the first generation antipsychotic compounds (Ashby and Wang, 1996; Seeman et al., 1997). Clozapine was successful in the management of treatment-resistant schizophrenia; although it was not implemented as a first line therapy due to potentially fatal agranulocytosis, in which the white blood cell count of the patient drops dangerously low (Crilly, 2007). The terms typical and atypical antipsychotic have been questioned in recent years because of studies showing that the 'generations' of drugs are not in fact homologous groups and the differences in side effects such as extrapyramidal motor control side-effects arising from the strength of the drug, rather than the activity of the drug (Leucht et al., 2009; Tyrer and Kendall, 2009). β_2-adrenergic receptor agonists such as salbutamol are primary therapeutic agents for the treatment of the acute symptoms of asthma (Jat and Khairwa, 2013). The symptoms of asthma, constriction of the airway smooth muscle and an increase in mucus secretion, are caused by an abnormal immune response. Activation of the smooth muscle β_2-adrenergic receptor leads to an increase in intracellular cAMP. This increase in cAMP is thought to aid in smooth muscle relaxation through activation of PKA, inhibition of both the release of intracellular calcium stores and entry of calcium into the cells, as well as triggering the sequestration of intracellular calcium (Johnson, 2001; Knox and Tattersfield, 1995).

The prevalence of the mAChRs in the cardiovascular, nervous, and respiratory systems, as well as their well characterised roles in regulating physiological functions, has made them attractive targets for therapeutic agents (Wess et al., 2007). One treatment option

for sufferers of chronic obstructive pulmonary disease (COPD) and moderate to severe persistent asthma is long-acting muscarinic antagonists (LAMAs). The LAMAs tiotropium bromide and glycopyrronium bromide are prescribed in COPD and have been found to improve the quality of life of COPD sufferers (Vincken et al., 2002; Watz et al., 2016). Atropine is a non-specific muscarinic antagonist; in bradycardic patients, atropine is administered to antagonise the vagal control of heart rate through the atrioventricular and sinoatrial node (Jones, 2016; Papastylianou and Mentzelopoulos, 2012). Atropine can also be used to reduce salivary and gastric secretions, and to reduce or totally inhibit gastric motility, depending on the concentrations used (Higgins et al., 1989).

Although the direct involvement of mAChRs in disease is disputed, their potential as therapeutic targets has been proven in multiple conditions. The localisation and levels of M_1 mAChR expression within the hippocampus and cortex has driven research into understanding its role in cognitive disorders such as schizophrenia and dementia. In schizophrenia both the M_1 and M_4 mAChRs have been implicated with studies showing a reduction in expression within the prefrontal cortex (Dean et al., 2002; Gibbons et al., 2013) and hippocampus (Scarr et al., 2007) respectively. The evidence tying M5 mAChR functions to substance dependency lead to targeting the receptor in rehabilitation therapy. The role of the M_5 mAChR in neurological disorders such as Parkinson's disease(Yamada et al., 2003) and Alzheimer's disease (Yamada et al., 2001a), and the regulation of D1 dopaminergic receptor neuron controlled locomotor activity by the M_4 mAChRs, presented these receptors as potential therapeutic targets. In major depressive disorders the M_2 and M_3 mAChRs have been reported to express at lower levels within the cortex. This being said, highly conserved regions between the mAChRs, such as the orthosteric binding pocket can make the discovering of highly selective molecules difficult. The critical roles that mAChRs play in central and peripheral nervous system makes the design of a selective model important for the development of clinically well tolerated therapeutic agents.

In post mortem tissue from schizophrenic patients, reduced levels of the M_1 and M_4 mAChR were observed in the anterior cingulate cortex when compared to control samples (Zavitsanou et al., 2004), dysfunction in this area has previously been associated with schizophrenia (Adam and David, 2007). Xanomeline, an M1/M4 mAChR selective

agonist, reached phase II trials for the treatment of schizophrenia (Bodick et al., 1997; Shekhar et al., 2008). Although xanomeline is M_1/M_4 selective, it still binds to other members of the mAChR family (Grant and El-Fakahany, 2005; Machová et al., 2007; Noetzel et al., 2009a, 2009b). Xanomeline significantly improved learning, memory, and the psychiatric rating scores in schizophrenic patients over the placebo group. This therapeutic efficacy of xanomeline was however overshadowed by a high drop-out from the clinical trial due to severe gastrointestinal distress experienced by the patients. In *in vivo* studies, xanomeline was seen to increase motility in the small intestine and colons of ferrets, and was found to increase heart rate in rats (Shannon et al., 1994).

Neurodegenerative diseases are a rising problem across the world and the care of those affected costs healthcare organisations billions of pounds a year. The Global Impact of Dementia report by Alzheimer's Disease International (Prince et al., 2015) and a previous meta-analysis (Prince et al., 2013) revealed that between 2010 and 2015 the number of cases of dementia were increasing in the Americas, Africa, and Asia. These studies also found that the projected rates of increase in low- and middle-income countries was higher than in high income countries. These projections suggest an increased strain on the healthcare services in countries which may already find it more difficult to provide funding, and more strain on families who cannot afford to care for their loved ones. Increases in the incidence of dementia in these low to middle income countries have been linked to risk factors such as cardiovascular health which, although improving in high income countries, is deteriorating in low to middle income countries (Wortmann, 2015). A report published by Dementia UK (Kane and Terry, 2015) revealed that, in 2015, 850,000 people were living with dementia in the UK, with projections of over 1,100,000 people by 2025 and over 2,000,000 by 2051. The rising care costs for those afflicted with a neurodegenerative disease will continue to strain healthcare organisations and the public globally unless therapies can be developed to treat or better alleviate the symptoms that sufferers experience. Reports from Dementia UK show that the cost of Dementia in the UK, £23 billion in 2012 and £26.3 billion in 2015, was covered by families through unpaid care and individual social care, with projection on an increase in Alzheimer's sufferers leading to increased costs (Alzheimer's Society and Society, 2014).

It is widely believed that dysregulation of cholinergic receptors within the hippocampus and cortex, primarily of M_1 mAChR signalling, is important in the progression of Alzheimer's disease. Studies have shown that in Alzheimer's disease the level of M_1 mAChRs expression does not significantly change within the hippocampus and cortex but coupling of M_1 mAChR to G-proteins appeared to be impaired (Overk et al. 2010; Tsang et al. 2006). The current therapeutic agents used in the management of Alzheimer's are almost all acetylcholinesterase inhibitors (AChEIs) apart from one NMDA receptor antagonist, memantine (Langmead et al., 2008). Amyloid β aggregation in Alzheimer's disease has been shown to cause dysregulation of glutamatergic NMDA receptors. The aggregated amyloid protein activates NMDA receptors, causing an increase in intracellular Ca^{2+} and reactive oxygen species which, over a prolonged period of time, will lead to cell death (Malinow, 2012; Mota et al., 2014). Memantine is a medium affinity, voltage dependent antagonist that blocks amyloid β activation of the receptor, but will dissociate from the receptor during synaptic activation, maintaining the plasticity of the synapse (Danysz and Parsons, 2003; Wenk et al., 2006). AChEIs slow the breakdown of acetylcholine in cholinergic synapses by acetylcholine esterase, increasing acetylcholine signal intensity and duration. Although effective in the short term, AChEIs cannot be used for long term management of Alzheimer's disease. As well as not preventing the progression of disease, these drugs effect the acetylcholinesterase enzymes across the cholinergic system, causing gastrointestinal side effects, sleep disturbances, muscle cramps and headaches (Mimica and Presecki, 2009). Although memantine has been found to delay disease progression, to a certain extent, and AChEIs can counteract the cholinergic deficit, disease progression continues and the poorly tolerated side effects of AChEIs means these therapeutic agents are ineffective in the long term.

Members of the GPCR subfamilies often contain highly conserved regions, including within the orthosteric binding pocket. These highly conserved regions makes it difficult to generate selective ligands which target the orthosteric binding pocket (Liu et al., 2015). Without selectivity, drugs can cause unwanted off target effects which can lead the ligands to be poorly tolerated (Machová et al., 2007). As an alternative, ligands can be used to target sites outside of the orthosteric binding pocket called allosteric sites.

Allosteric sites can be less conserved between subfamily members and provide a target for more selective ligands (Conn et al., 2009). A more selective ligand may be of more benefit to the patients, reducing the attrition rates of drugs in clinical trials by reducing off-target side effects (Langmead and Christopoulos, 2014). The identification of more selective and efficacious ligands is therefore vital to the future of drug development. Even if reversal of the disease was not possible with late stage Alzheimer's, the ability to reduce the care needs of patients would significantly reduce the financial burden of Alzheimer's on both families and health care systems. A recent study from the Tobin group used a prion model of neurodegeneration to test the efficacy of M_1 mAChR selective positive allosteric modulators (Bradley et al., 2016a). In Alzheimer's disease, positive allosteric modulators should be able to alter signalling in the same way as AChEIs, although they will be far more selective. This study found that the positive allosteric modulators BQZ12 and BQCA were able to significantly slow disease progression, recover learning and memory deficits, and increase survival time of the animals. This study shows the potential promise in the use of allosteric modulators for the treatment of Alzheimer's disease where previous therapeutic agents have failed.

As discussed previously, GPCRs signal through G-protein dependent and phosphorylation dependent pathways, but different agonists will not necessarily activate these pathways in equal amounts (Violin and Lefkowitz, 2007); a phenomenon known as signalling bias or functional selectivity. Depending on the disease being targeted it may be important to activate one specific downstream pathway over another. This may be to avoid on-target side effects or to promote the therapeutically beneficial pathway. Agonists with this property have already been identified at the 5-HT_4 (5-hydroxytryptamine) receptor (Gaven et al., 2013); as well as putative bitopic ligands, ligands which bind to both the orthosteric and an allosteric site, at the M_1 mAChR (Digby et al., 2012; Keov et al., 2013). Biased ligands have also been identified for the μ-opioid receptor (DeWire et al., 2013) and the angiotensin II type 1 receptor (Kim et al., 2012). The μ-opioid receptor biased ligand, TVR130, is biased towards the G-protein dependent pathway, reducing receptor desensitisation and prolonging the analgesic properties. TRV027, the angiotensin II type 1 receptor ligand, is biased towards the β-arrestin dependent pathway decreasing blood pressure and increasing renal blood

flow. This ligand is designed to be used therapeutically in acute heart failure in the place of diuretics and vasodilators. Impaired interactions between M_1-mAChRs and heterotrimeric G-proteins have also been identified within Alzheimer's disease tissue samples (Overk et al., 2010; Shiozaki et al., 2001; Tsang et al., 2006). In this case the use of a G-protein dependent signalling biased ligand could increase G-protein dependent signalling. In the case of targeting the adenosine A_1 receptor (A_1AR) for cardioprotection, agonists at higher doses caused on-target side effects including bradycardia. By utilizing a bitopic agonist at the A_1AR (Valant et al., 2014) it has been shown that cardioprotection can still be achieved without the on-target bradycardia.

1.3 The Chemical Genetic Approach

As well as the development of more selective ligands, there is a growing effort to produce functionally selective compounds. An important part of this process is understanding the physiological and behavioural roles played by the separate downstream signalling pathways of GPCRs. Classical methods of determining a receptors function *in vivo* involve either using receptor antagonists or generating transgenic knock-out models. Although both models work to observe receptor function, they do have their drawbacks. Receptor antagonists can successfully silence receptor function; but without specific ligands, *in vivo* changes in behaviour and physiology may be due to interactions with multiple receptors. Transgenic receptor knock-out models are specific in silencing receptor function, but the activity cannot be reclaimed in the same animal. A way to overcome these issues is with the chemical genetic approach. This system utilises mutations within the binding pocket of a GPCR which prevents activation by the orthosteric ligand, whilst simultaneously engendering activity to a previously biologically inert synthetic ligand.

The first generation of these engineered receptors, known as receptors activated solely by synthetic ligands (RASSLs), involved molecular evolution of the β_2-adrenergic receptor (Strader et al., 1991) to reduce the affinity of the natural ligand for the receptor and engender affinity and potency for a synthetic ligand. This method was repeated in the κ-opioid receptors (Coward et al., 1998), α_{2A} adrenoceptor (Pauwels and Colpaert, 2000), 5-HT_4 receptor (Claeysen et al., 2003), and the H1 histamine receptors (Bruysters et al., 2005). An issue with this first generation of receptors was the high affinity and

potency of the synthetic ligands for the wild-type receptors. The ligands used to activate the κ-opiod RASSL mutant, spiradoline and bremazocine (Coward et al., 1998), were potent and selective agonists of the wild-type κ-opiod receptor (Dortch-Carnes and Potter, 2005; Von Voigtlander and Lewis, 1988). A screen of ligands at the α_{2A} adrenoceptor and a series of RASSL mutants found the most efficacious agonists of the RASSL receptors were full or medium strength partial agonists of the wild-type receptors. The two agonists described at the 5-HT_4 RASSL mutant, GR 113808 and ML 10375, were antagonists of the wild-type 5-HT_4 receptor. This lack of ligand selectivity could lead to difficulties deciphering the role of the transfected RASSL receptor in tissue where the wild-type receptor is present.

To bypass this issue a second generation of mutant receptors known as designer receptors exclusively activated by a designer drugs (DREADDs) was developed (Armbruster et al., 2007) using the M_3 mAChR. The mutations required for the M_3-DREADD mAChR were discovered by molecular evolution through random mutagenesis of the wild-type human M_3 mAChR. The mutants were then functionally and pharmacologically screened with the natural ligand acetylcholine and the synthetic ligand CNO. This screen was used to identify the mutations which best reduced the affinity and potency of acetylcholine while simultaneously increasing the affinity, potency, and maximal receptor activation of CNO. CNO was chosen as the ligand for the mAChR DREADD mutants based on the high affinity of clozapine for the M_3 mAChR, its bioavailability in humans and rats (Bender et al., 1994; Chang et al., 1998), and its apparent lack of activity. This screening found that the combination of 2 mutations, $Y^{3.33}C$ and $A^{5.46}G$, were the best combination for the generation of the M_3-DREADD mAChR. This notation format, the Ballesteros-Weinstein numbering scheme, labels the amino-acid sequence using 2 sets of numbers based on helix 1-7, and the position of the amino acid in relation to the most highly conserved residue within the helix being 50. For example, amino acid 5.42 would be found within the 5^{th} transmembrane domain 8 residues before the most highly conserved, that being a proline$^{5.50}$ (Isberg et al., 2015). These residues are conserved within the mAChR family and were found to illicit the same functional and pharmacological changes in the other mAChRs. When introduced *in vivo* these receptors should not interact with the natural mAChR ligand acetylcholine. If

knocked into the endogenous locus, the animal should have the same physiological and behavioural changes as are seen in knock out animals. Following administration of CNO, the receptor will be activated and normal function restored. DREADDs can also be transfected through microinjection into specific cell groups to understand the physiological and behavioural relevance of receptor activation in these select groups *in vivo*.

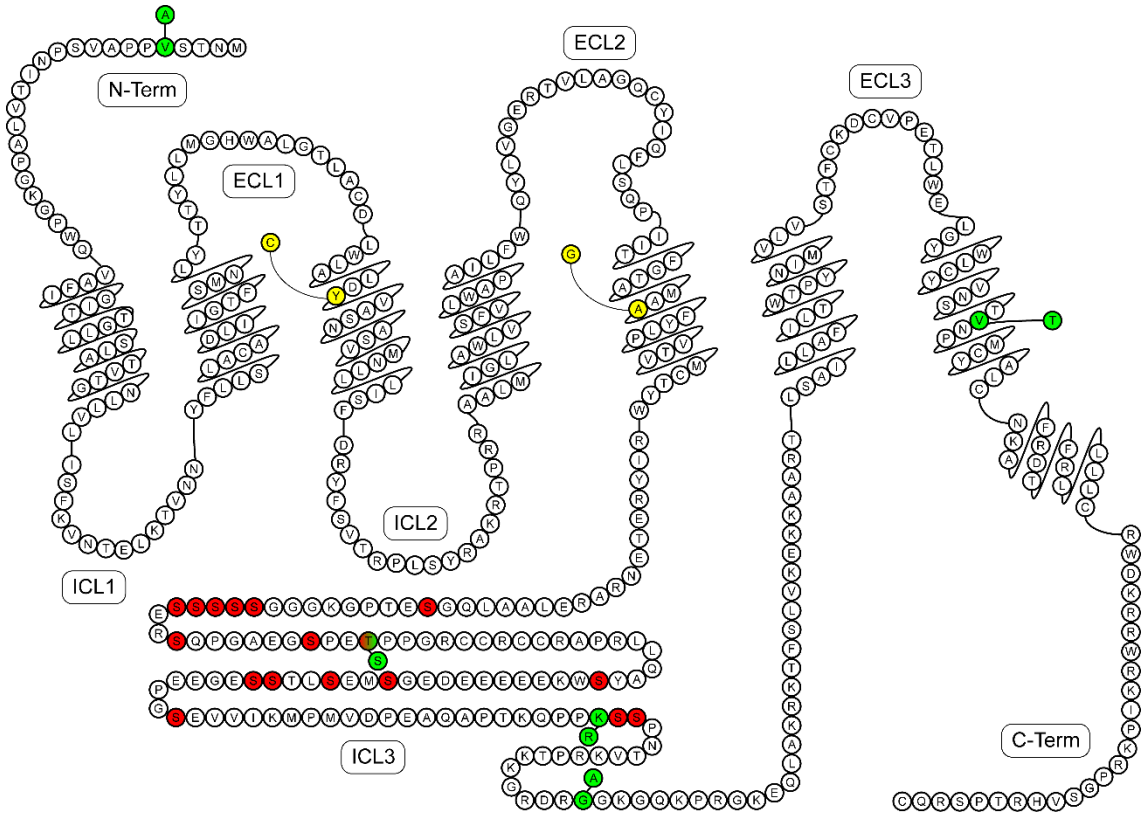

Figure 1.3. Snake-like plot of the amino-acid sequence of mouse M_1 mAChR; showing the positions of humanizing, DREADD, and Phosphorylation Deficient mutations.

Amino-acid sequence and junctions between transmembrane and the extracellular and intracellular regions were derived from the Uniprot knowledgebase (ascension: P12657). Residues mutated to humanise the mouse receptor and the new residue are coloured green. DREADD mutation sites and the introduced residues are labelled in yellow. Intracellular residues mutated into alanine in the PD mutant are shown in red. ICL refers to the intracellular loops, ECL refers to the extracellular loops.

Following the development of these receptors, they have been used to functionally characterise GPCR signalling in cell groups within the brain (Hartog et al., 2016; Warthen et al., 2016; Wasserman et al., 2016) and β-cells within the pancreas (Guettier et al., 2009). Within the brain, cell groups were virally transfected with either the M_3-DREADD or M_4-DREADD mAChR. Activation of these receptors, following administration of CNO, allows for the interrogation of either $G_{\alpha q}$ signalling using the M_3-DREADD mAChR, or $G_{\alpha i}$ signalling using the M_4-DREADD mAChR. Control of β-cells used 2 transgenic animal models containing either M_3-DREADD mAChRs or an M_3-DREADD mAChR whose intracellular loops 2 and 3 were replaced with that of the β_1-adrenergic receptor. The modifications were made to promote coupling of $G\alpha_s$ to the DREADD receptor, allowing for the investigation of $G\alpha_s$ signalling on β-cell physiology. In 2009, an M_3-DREADD receptor was modified to contain the IL2 and IL3 of the β_1-adrenergic receptor (Guettier et al., 2009). This modification generated M_3-DREADD mAChR which coupled to $G_{\alpha S}$, rather than to $G_{\alpha q}$. By expressing these mutant receptors under the transcriptional control of a fragment of the rat insulin promoter, the authors could selectively express the receptors within pancreatic β-cells, to study the roles of G-protein signalling on β-cell function.

Through chemical genetic modifications to the receptor is possible to produce a biased receptor which can only signal down either G-protein dependent pathways or phosphorylation dependent pathways. In the advent of functional selectivity, it will become more important to learn the specific effects of signalling pathways on behaviour and physiology. With this information it may be possible to identify biased ligands which are better tolerated than currently available drugs; selectively activating therapeutically beneficial pathways and avoiding those which drive on-target side effects.

A method of differentiating signalling pathways was developed involving introducing a single point mutation, R165L, into an M_3-DREADD mAChR (Nakajima and Wess, 2012), creating an arrestin/phosphorylation biased receptor. In 2016 (Hu et al., 2016), the same lab generated a G_q biased receptor through mutating 4 serine residues within the c-terminal tail and removal of the 3rd intracellular loop. In BRET assays, this mutant receptor no longer interacted with β-arrestin 1 or 2. Calcium mobilisation assays confirmed there was no significant difference in $G_{\alpha q}$ activation. A study within the Tobin

group used alanine substitution of putative phosphorylation sites to interfere with phosphorylation dependent signalling and arrestin coupling without interfering with protein folding, generating a G-protein biased M_3 mAChR (Bradley et al., 2016b; Kong et al., 2010; Poulin et al., 2010). Within airways, removal of the phosphorylation sites from the M_3 mAChR significantly reduced the maximum contraction and the potency of carbachol in the stimulation of smooth muscle contraction. Within the pancreas, where the M_3 mAChR plays a role in the regulation of insulin release and glucose homeostasis (Gautam et al., 2006c), removal of phosphorylation sites interfered with M_3 mAChR activation of protein kinase D1, an important regulator of insulin release (Sumara et al., 2009). Reduction in protein kinase D1 activation lead to decreased insulin secretion and the impaired regulation of glucose homeostasis. In fear conditioning studies, transgenic animals expressing the phosphorylation deficient M_3 mAChR had significantly lower response in contextual and cued fear conditioning tests. Lower expression of c-Fos, a marker of neuronal activity (Bullitt, 1990), was detected within the CA3 and dentate gyrus of the hippocampus in transgenic mice compared to wild-type mice. Combining the DREADD and biased signalling mutations, it will be possible to interrogate the functions of total receptor signalling and specific pathways on behaviour and function *in vivo*. The understanding of physiological roles of individual cell signalling pathways could provide researchers with vital information in the development of new, biased, drugs.

CNO is one of the two major metabolites of clozapine, the other being N-desmethylclozapine (NDMC) (Volpicelli et al., 1993; Weigmann and Hiemke, 1992). Metabolism of clozapine into CNO is mediated by the CYP3A4 isoform of cytochrome P450 (Eiermann et al., 2003; Linnet and Olesen, 1997; Pirmohamed et al., 1995) and is reversible (Chang et al., 1998). Clozapine has been detected in humans, guinea pigs, and Long-Evans rats after administration of CNO (Jann et al., 1994; MacLaren et al., 2016). N-desmethylclozapine (NDMC) and clozapine have also been detected in Lewis rat urine (Lin et al., 1996). Concentrations used for metabolite analysis were 5mg/kg intraperitoneal (i.p.) injection (MacLaren et al., 2016) or 20mg/kg orally dosed (Lin et al., 1996). Both clozapine and NDMC are promiscuous ligands, having been found to interact with members of multiple receptor families (Heinrich et al., 2009; Heusler et al., 2011;

Olianas et al., 2009, 1999; Wenthur and Lindsley, 2013). They have both been found to depress synaptic transmission in cultured rat hippocampal neurons (Ohno-Shosaku et al., 2011). A study in mice found NDMC has an inhibitory effect on exploratory locomotor function, which the authors speculated was downstream of mAChR activation (Maehara et al., 2011). The potential presence of these promiscuous and active molecules *in vivo* has led to the development of a new generation of DREADD ligands with the hope of generating a more potent DREADD agonist which doesn't have potentially confounding metabolites. Two new ligands, DREADD agonist 21 (DA21) and perlapine have been identified as potential alternatives to CNO *in vivo* (Chen et al., 2015). DA21 was first identified as part of a screen of 19 CNO analogues against the hM_3 and hM_3-DREADD mAChRs (Chen et al., 2015). The seven ligands with the lowest activity at the hM_3-WT mAChR were also screened against four non-muscarinic aminergic GPCRs, 5-HT_{2A}, 5-HT_{3C}, α_{1A} adrenergic, and H1 histamine receptors, to investigate the selectivity of these new compounds. Out of these screens DA21 was found to perform significantly better than CNO. A separate screen of existing compounds in the same study (Chen et al., 2015) also identified perlapine as a potent hM_3-DREADD agonist. As well as activating the hM_3-DREADD mAChR in the FLIPR (fluorescence imaging plate reader) Ca^{2+} mobilisation assay, perlapine showed significant, >10,000-fold, selectivity for the hM_3-DREADD mAChR over the hM_3-WT mAChR. Perlapine was first described in 1973 (Stille et al., 1973) as a sedative and promotor of sleep. In later studies it has been found to have nanomolar affinity for dopaminergic (Roth et al., 1995) and serotonergic receptors (Roth et al., 1994) GPCRs, similar to other benzodiazepine compounds. Although selective for the M_3-DREADD receptor screening needs to be carried out at wild-type and M_1-DREADD and M_1-DREADD-PD mutant mAChRs to ensure the selectivity of the ligands.

The project aims to characterise the pharmacology and function of 2 mutant receptors (Fig 1.1) and the synthetic ligand CNO. The first of these receptors is a human M_1 mAChR containing the DREADD mutations, and the second is the human M_1 mAChR containing the DREADD mutations and alanine substitutions of the phosphorylated serine residues within the 3rd intracellular loop. These receptors will be used *in vivo* to study the role of the M_1 mAChR and phosphorylation dependent signalling on learning and memory. The M_1-mAChR has been found to be crucial to learning and memory (Leaderbrand et al.,

2016), however current therapeutic agents targeting the M_1-mAChR in Alzheimer's disease lack selectivity and do not provide long-term disease modification. Using our chemical genetic approach, we can understand how M_1-mAChR signalling effects behaviour, and identify signalling pathways which are therapeutically beneficial or detrimental.

1.4 Aims and Objectives

In this project I aim to characterise the function and pharmacology of 2 mutant receptors and the synthetic ligand CNO as part of a chemical genetic approach to understand the role of GPCR signalling *in vivo*. The first of these receptors, both based on the M_1 mAChR, will contain the DREADD mutations $Y^{3.33}C$ and $A^{5.46}G$. The second will utilise alanine substitution of phosphorylated serine residues within the 3rd intracellular loop as well as the same DREADD mutations. The *in vitro* characterisation of the receptors will involve radioligand binding and cell signalling assays to assess the changes to ligand binding and receptor function caused by the mutations. I will also study the synthetic ligand CNO, to understand its interactions with the mAChR family. It is important to investigate the ligand to ensure it will not cause any confounding factors within the *in vivo* model. These receptors can then be used in transgenic studies with tests that will explore different learning and memory paradigms, such as contextual (Yoshii et al., 2016) and spatial memory (Conrad et al., 2003), as well as measuring anxiety (Poulin et al., 2010). Although the therapeutic potential of mAChRs is well documented, issues with ligand selectivity and efficacy have made the treatments for diseases such as Alzheimer's disease intolerable for chronic use. By using chemical genetic approaches, it may be possible to better understand the physiological relevance of the M_1 mAChR and its downstream signalling pathways. This information could then be used in the development of new selective and potentially biased ligands, which will be more efficacious and better tolerated therapeutic agents.

Chapter 2 Materials and Methods

2.1 Materials:

All lab reagents and chemicals were procured from Sigma-Aldrich Ltd (Dorset, UK) and ThermoFisher Scientific (Rugby, UK) unless otherwise stated.

2.1.1 Cell Lines

Human and mouse M_1, M_1-DREADD, M_1-DREADD-PD, and M_4 mAChRs were expressed in CHO-FlpIn cells using the pcDNA5/FRT expression vector; hygromycin B was used as the selection agent. M_2 and M_3 mAChRs were expressed in CHO-K1 cells using the pcDNA3 expression vector; Geneticin, also known as G418, was used as the selection agent. The human influenza haemagglutinin (HA) epitope tag was incorporated into these receptors. In the mouse M_1-, M_1-DREADD, M_1-DREADD-PD, and M_4-mAChRs the HA tag is incorporated into the C-terminal region of the receptors. In human M_1- and M_2-mAChRs the HA tag is incorporated into the N-terminal region. Untransfected CHO-FlpIn cell lines were also used as experimental controls. These cell lines were developed within the Tobin group prior to the start of this project by Dr. Adrian Butcher.

2.1.2 Cell Culture

HAMS F-12 media, Dubelco's phosphate buffered saline (PBS), penicillin-streptomycin, and Zeocin used in tissue culture were obtained from ThermoFisher Scientific (Rugby, UK). Heat-inactivated foetal bovine serum (FBS) was obtained from Labtech.com (Uckfield, UK). G-418 solution was purchased from Sigma-Aldrich Ltd (Dorset, UK). Hygromycin B was purchased from Santa Cruz Biotechnology (Heidelberg, Germany).

2.1.3 Specific Reagents

2.1.3.1 Western Blotting

For Western blotting, the 30% acrylamide/bis solution, stacking gel buffer, and resolving gel buffer were from Bio-Rad (Hemel-Hempstead, UK). Tris glycine SDS PAGE buffer 10X was purchased from National Diagnostics (Hessle, UK).

2.1.3.2 Antibodies

Anti-phospho-p44/42 MAPK (ERK1/2) (Thr202/Tyr204), anti-p44/42 MAPK (ERK1/2), and anti-GAPDH (14C10) antibodies were from New England Biolabs Ltd (Hitchin, UK).

Anti-HA High affinity and Anti-HA-Fluorescein were from Roche Diagnostics Ltd. (Burgess Hill, UK). Anti-rabbit and anti-mouse HRP conjugated antibodies were from Bio-Rad (Hemel-Hempstead, UK)

2.1.3.3 Cell Signalling Assays

IP-One HTRF® assay kits and Phospho-ERK (Thr202/Tyr204) Cellular assay kits were obtained from Cisbio Bioassays (Codolet, France). Fura-2-AM and probenecid for the calcium mobilisation assays were procured from ThermoFisher Scientific (Rugby, UK).

2.1.3.4 Radioligand Binding

^{3}H-N-methyl scopolamine (^{3}H-NMS) and ULTIMA Gold scintillant cocktail were from Perkin Elmer, Inc. (Seer Green, UK).

2.1.3.5 CLARITY

40% acrylamide and 2% bis-acrylamide solutions for the hydrogel were from Bio-Rad (Hemel-Hempstead, UK). VA-044 initiator was from Alpha Laboratories Ltd. (Eastleigh, UK).

2.2 Methods:

2.2.1 Cell Culture

2.2.1.1 Cell Line Maintenance

All cells were grown in Ham's F-12 Nutrient mix containing GlutaMAX™ with 10% FBS and 1% penicillin/streptomycin. Media used for untransfected CHO-FlpIn cells also contained Zeocin at 100 µg/mL. Media used for human and mouse M_1 wild-type (hM_1-WT and mM_1-WT respectively) mAChRs, M_1-DREADD, M_1-DREADD-PD, and human M_4-WT mAChR transfected cells also contained 400 µg/ml hygromycin B. Cell lines transfected with the M_2 and mouse M_3-WT mAChRs were maintained in the same media containing 450 µg/ml G418 rather than hygromycin B. Cells were maintained in a 5% CO_2, 95% air, humidified incubator at 37°C.

2.2.1.2 Cell Counting

Cells were counted using the CASY TTC cell counter and analyser. 100 µl of cell suspension was mixed with 9.9 ml of isotonic measuring buffer. Three samples were counted and the average concentration obtained.

2.2.2 Radioligand Binding

For all radioligand binding assays, cells were plated at 50,000 cells per well in 24 well cell culture plates. Cells were cultured in their relevant supplemented HAMS F-12 media for 48 hours at 37°C to come to 90% confluency. After lysis, all samples were loaded into scintillation tubes and mixed with 5 ml Ultima GOLD scintillant cocktail, and quantified using liquid scintillation counting (LSC).

2.2.2.1 Saturation Binding

Wells of confluent cells were washed 3 times with 1 ml Krebs buffer (10 mM HEPES, 118 mM NaCl, 4.3 mM KCl, 1.17 mM $MgSO_4$, 1.29 mM $CaCl_2$, 25 mM $NaHCO_3$, 1.18 mM KH_2PO_4, 11.7 mM glucose) and loaded with 447 µl of Krebs for 15 minutes. Half the wells were treated with atropine to a final concentration of 200 µM to estimate non-specific binding. 50 µl of ^{3}H-NMS in ½ log dilutions were added and the samples left to reach equilibrium in the incubator at 37.5°C for 1 hour. 2 wells per plate were not treated with drug or NMS to be used for protein quantification using the Bradford assay. After equilibrating, the cells were washed three times with 1 ml Krebs buffer and lysed with 300µL of RIPA buffer (10 mM Tris-HCL, 2 mM EDTA, 1% NP-40, 0.5% deoxycholic acid, 250 mM NaCl) or 0.1 M NaOH for 30 minutes.

2.2.2.2 Competition Binding

The cells were washed twice with 1 ml Krebs buffer and then loaded in duplicate with 400 µl of Krebs for 15 minutes. The wells were then treated in duplicate with 50 µl log concentration dilutions of each ligand for 15 minutes. For hM_1-WT and mM_1-WT expressing cell lines 50 µl of 10x K_d concentration ^{3}H-NMS was added for a final K_d concentration and left to reach equilibrium in the incubator at 37.5°C for 1 hour. For the M_2, mM_3, and hM_4-WT mAChR expressing cell lines, 3 concentrations of ^{3}H-NMS were used, one at the K_d concentration, one at 10 K_d, and one at 0.25-0.3 K_d. The experiment was halted by washing the wells three times with ice cold Krebs buffer on ice, and lysis of the cells with either 300 µl RIPA or 0.1M NaOH.

2.2.2.3 Dissociation Binding

Wells were washed 3 times with 1 ml binding assay buffer and were then incubated for 15 minutes in 400 µl Krebs buffer. After 15 minutes 50 µl of Krebs was added to all wells

except for the wells to be used to calculate non-specific binding (NSB) which were treated with atropine for 15 minutes. The wells were treated with 50 µl of 1 K_d ^{3}H-NMS and incubated for 4 hours at room temperature to reach equilibrium. For non-specific binding, one well for each condition was treated with atropine. After equilibration, wells were treated with unlabelled antagonist, atropine, at a concentration 1000-fold higher than that of the radioligand at time points up to 90 minutes. Once the treatment was complete the cells were washed twice with ice cold 0.9% NaCl and lysed with 500 µl 0.1M NaOH.

2.2.2.4 Association Binding

Wells were washed 3 times with 1 ml Krebs buffer and were then incubated for 15 minutes in 400 µl Krebs buffer. After 15 minutes 50 µl of Krebs was added to all wells except for the NSB well which was treated with atropine for a further 15 minutes. Wells were then treated with a K_d concentration of ^{3}H-NMS for time points up to 120 minutes. Once the treatment was complete the cells were washed twice with ice cold 0.9% NaCl and lysed with 500 µl 0.1M NaOH.

2.2.3 ERK 1/2 Activation

2.2.3.1 Western Blotting

300,000 cells per well were loaded into a 12 well plate and cultured at 37.5°C 24 hours prior to experimentation. After incubation the cells were washed 3 times in Krebs buffer and were left in 900 µl of Krebs buffer for 1 hour. After incubation the cells were treated with 100 µl of the log concentration drug dilutions for 5 minutes. After 5 minutes the media was removed and 300µL of RIPA buffer containing protease and phosphatase inhibitors was added to each well. The lysates were then transferred to tubes and centrifuged at 18000g for 10 minutes and the supernatants were transferred to new tubes. The protein content of the samples was determined and 5µg of each sample was mixed 1:1 with 2x loading buffer (100 mM Tris, 200 mM dithiothreitol, 4% SDS, 0.2% bromophenol blue, 20% glycerol) and heated at ~65°C for 5 minutes. The samples were then run on a 10% SDS-PAGE gel and transferred to a nitrocellulose membrane. The membranes were probed with antibodies against phosphorylated ERK 1/2 to measure ERK activation over basal, with the membranes being stripped and re-probed with anti-ERK 1/2 antibodies as a loading control. Horseradish peroxidase (HRP) secondary

antibodies were used, along with enhanced chemiluminescence (ECL) reagent and ECL film to visualise the bands. Densitometry was performed on the film using ImageJ, with the data normalised using the total ERK 1/2 loading control. The stimulation time of 5 minutes was chosen as it is the standard stimulation time within the lab, and has been used in the literature (Miao et al., 2016; Schrage et al., 2015; Valant et al., 2012; Wan et al., 2015). A time course assay was used to confirm this stimulation time.

2.2.3.2 Homogeneous Time Resolved Fluorescence (HTRF) Assay

Assays were carried out using the Cisbio HTRF (homogeneous time resolved fluorescence) Phospho-ERK1/2 (Thr202/Tyr204) assay kit. This assay kits uses 2 tagged anti-phosphorylated ERK 1/2 antibodies to detect the amount of phosphorylated ERK 1/2 within the well. One antibody is conjugated with a fluorescent donor molecule, Lumi4®Tb, and the other with a fluorescent acceptor, d2. When the donor is excited in close proximity to an acceptor, a photon is emitted and absorbed by the acceptor. The acceptor, excited by this photon, emits a photon of light itself. The ratio between the emission of the acceptor and donor fluorophores is used as the result for each point. 50,000 cells per well were loaded into a 96 well plate for 24 hours before the assay. Wells were washed 3 times with 200 µL Krebs buffer and incubated for 1 hour at 37°C in 180 µl of Krebs. Ligands were made up in Krebs buffer at 10x the final reaction concentration. After the incubation, wells were treated with 20 µL of increasing concentrations of agonist at 37°C for 5 minutes, after which the agonist was removed by flicking and 50 µL of lysis buffer was added for 30 minutes at room temperature. 16 µl of the lysate was then added to a 384 well plate where 4 µl of a mixture of the two HTRF anti-ERK 1/2 (Thr202/Tyr204) antibodies conjugated with either Eu^{3+}-cryptate or d2. The antibody solutions were mixed with the lysis buffer on a plate shaker at room temperature for at least 2 hours, with the signal stability lasting for 24 hours. Plates were read within 24 hours on the CLARIOstar plate reader and data exported using the MARS data analysis software provided.

2.2.4 Inositol Monophosphate (IP1) Accumulation: HTRF IP-One kit

Assays were carried out using the Cisbio HTRF IP-One assay kit. This HTRF kit measures inositol monophosphate (IP1) accumulation using an anti-IP1 antibody tagged with the fluorescent Lumi4® Tb cryptate donor, an IP1 molecule tagged with the d2 acceptor, and

lithium chloride to inhibit inositol monophosphatase and prevent the breakdown of IP1 into myo-inositol. Following receptor activation, IP1 produced by the cell competes with the tagged IP1 for the conjugated anti-IP1 antibody. An increase in IP1 production results in a reduction in the signal measured. Cells were plated into a 384 well plate at 10,000 cells per well and incubated in supplemented HAMS F-12 media for 48 hours at 37.5°C. The media was then removed and 20 µl of ligand, diluted in stimulation buffer, was added and incubated at 37.5°C for 1 hour. After stimulation the buffer was removed and 7.5 µl of lysis buffer containing the IP-d2 conjugate was added, followed by 7.5 µl of lysis buffer containing the anti-IP cryptate-Tb^{3+} conjugate. The plate was then incubated at room temperature for 1 hour on a plate shaker. After shaking the plates were read on the CLARIOstar platform and the data exported to Excel using the MARS data analysis software provided.

2.2.5 Single Cell Calcium Microscopy

Cells were seeded onto glass coverslips in 6 well plates at a density of 750,000 cells per well for 24 hours or 350,000 for 48 hours in suitable supplemented HAMS F-12. Wells were washed 3 times with 2 ml Krebs and incubated at 37°C with Krebs containing 2.5 mM probenecid and 2 µM Fura-2-AM for 30 minutes under reduced light. Fura-2-AM is a ratiometric, calcium binding, fluorescent dye used to detect changed in the concentration of intracellular calcium. Probenecid is an organic-anion transporter inhibitor which prevents the egestion of the dye. After incubation, the coverslip was washed three times with Krebs and loaded into a coverslip holder with 900 µl of Krebs and placed on the heated stage of the microscope. Ligands were made up in Krebs buffer at 10x the final reaction concentration. After a baseline reading was established for 30 seconds, 100 µl of ligand was added and measurements were taken for a further 4 minutes. Data was collected as maximum peak height from the subsequent images using MetaFluor 4.

2.2.6 Flexstation Calcium Signalling Assay

Cells were seeded into clear bottom 96 well plates at a density of 50,000 cells per well for 24 hours. Before stimulation, wells were washed 3x with Krebs, and then incubated with Krebs containing 2.5 mM probenecid and 2 µM Fura-2-AM at 37°C for 30 minutes. After incubation cells were washed and loaded with 100 µl of Krebs buffer and loaded

into a Flexstation plate reader to carry out the assay. Ligands were prepared in a 96 well plate at double the final assay concentration in Krebs buffer and the plate was placed into the Flexstation. To measure the calcium response, the plate reader took measurements for the first 16 seconds to calculate the baseline level of fluorescence. At 16 seconds the Flexstation added 100 µl of ligand to the well and continued to measure changes in fluorescence for up to 90 seconds. Measurements for each concentration were calculated as area under the curve. The Flexstation measures fluorescence from 8 wells simultaneously, unlike calcium microscopy which can only measure 1 point at a time.

2.2.7 Immunocytochemistry (IHC)

Cells were loaded onto 18 mm sterilized glass coverslips in 12 well plates at 100,000 cells per well and incubated for a minimum of 24 hours at 37°C in HAMS F-12 media. Wells were washed and incubated for 1 hour with 990 µL of Krebs buffer. Cells were then stimulated at intervals between 0 and 120 minutes, after which they were fixed for a minimum of 1 hour with 4% paraformaldehyde (PFA). After fixing, the cells were permeabilized for 30 minutes with PBS – 0.5% Triton X-100 to allow for antibody penetration into the cells. The slides were blocked using antibody diluent containing PBS – 0.1% Triton X100 (PBSTX) with 0.3% BSA. Samples were treated with primary antibodies in antibody diluent at a suitable concentration for 1-2 hours and were then washed 3 times for 10 minutes each with PBST. The coverslips were then treated for 1-2 hours with secondary antibodies at a suitable dilution in antibody diluent in subdued lighting conditions, to avoid bleaching of the fluorophore tags on the secondary antibodies. Following secondary antibody treatment, the coverslips were washed again with PBST 3 times for 10 minutes and were mounted onto slides with hard set anti-fade mounting medium containing DAPI. After the mounting solution set, the slides were sealed using clear nail varnish before confocal microscopy.

2.2.8 CLARITY

2.2.8.1 Perfusion Fixation

To prepare tissue for CLARITY processing it must be fixed by perfusion fixation with an acrylamide hydrogel (4% acrylamide, 0.05% bis-acrylamide, 0.25% VA-044, 4% paraformaldehyde in PBS). Once perfused with the hydrogel solution, the organs and

tissues of interest were removed and placed in a tube containing the hydrogel solution for 3-4 days at 4°C. This incubation step was performed to allow for complete diffusion of the hydrogel monomers throughout the samples.

2.2.8.2 Degassing and Polymerisation

Once the incubation was complete the samples were degassed, this is a necessary step before hydrogel polymerisation to remove any air bubbles from the tissue. These bubbles can expand during clearing and will disrupt the structure of the tissues mounted in the hydrogel, and the oxygen can inhibit the hydrogel polymerisation. For degassing, the samples were placed within a desiccation chamber in open Falcon tubes containing enough hydrogel solution to leave a 2cm gap between the sample and the surface. A vacuum pump was then used to evacuate the air from the chamber. The samples were then left under vacuum for at least 10 minutes to remove any dissolved air within the hydrogel solution. After 10 minutes the vacuum pump was turned off and nitrogen, or another inert gas, used to refill the chamber. The lid of the desiccation chamber was then removed and the lids carefully placed on the tubes. The tubes were then incubated for at least 3 hours at 37°C in a water bath to polymerise the hydrogel. After polymerisation excess hydrogel was removed and the samples were washed 3 times for 1 hour in clearing solution (200mM boric acid and 4% SDS in water, pH 8.5) to remove any unpolymerised hydrogel solution. Excess hydrogel was removed from the sample to reduce the amount of material for antibodies to diffuse through during the labelling process.

2.2.8.3 Sectioning and Clearing

Before the sample is cleared it may be necessary to section or cut the sample to make it easier to visualise the region of interest. This can be performed using a sharp razor blade and a sectioning mould. Samples were cleared using either passive tissue clearing or electrophoretic tissue clearing. For passive clearing, samples were incubated in clearing solution at 37°C using either a water bath or an incubator. For electrophoretic tissue clearing (ETC), the sample was placed in an electrophoretic tissue clearing chamber, with the power supply set to 20 V and 900 mA, and a perfusion pump to circulate the clearing solution. The pH of the clearing solution was checked regularly and maintained at 8.5,

and the solution itself was replaced twice a week. The clearing step was halted once the sample was clear.

2.2.8.4 Staining and Visualisation

After clearing, the samples were washed 3 times for 24 hours with PBS containing 0.1% Triton X-100 (PBSTX). Samples were then treated with primary antibodies in PBSTX for 2 days at 37°C for every 1 mm depth of staining. This antibody incubation was followed by washing in PBSTX for 1 day for every 2 days' antibody incubation, changing the PBSTX every day. Cleared tissue was incubated with secondary antibodies with the same conditions as those used for primary antibodies. A final wash was performed after the secondary incubation with the same conditions as in the previous wash.

Before the samples were visualised their refractive index (RI) was matched to that of the immersion medium used. An 85% glycerol solution was used as the refractive index matching solution (RIMS) for CLARITY samples, with a RI around 1.45. The samples were submerged in the solution for a minimum of 12 hours before observation to ensure equilibration of the refractive index throughout the sample; this time was dependent on this thickness of the tissue, with thicker samples requiring a longer equilibration time.

Image acquisition was performed using either a confocal microscope using an objective with a suitable working distance or using a light sheet fluorescence microscope (LSFM). Image analysis for confocal microscopy images was performed using Carl Zeiss Zen Lite 2012 and Arivis Vision 4D for the LSM images.

2.3 Data Analysis

Quantification of Western blots was performed using ImageJ; these densitometry results were normalised to loading controls. Preliminary processing of numerical data was performed using Microsoft Excel. Statistical analysis of the data was carried out using Graphpad Prism 6 and 7.

For ^{3}H-NMS saturation binding assay data, values for non-specific binding were subtracted from their equivalent total binding value to calculate the specific binding. This specific binding curve was than analysed using the one site – total and nonspecific binding protocol in Prism, using the following equation:

(Equation 1)

$$Y = \frac{B_{max} * [X]}{K_d + [X]} + NS * [X]$$

Where Y is total radioligand binding, B_{max} is the total receptor density, K_d is the equilibrium dissociation constant, [X] is the concentration of the radioligand, and NS is non-specific binding. For association radioligand binding, the association rate constant (K_{on}) was calculated with the one-phase association protocol, which uses equation 2. Dissociation binding assay data were analysed using the one-phase decay protocol with equation 3 to calculate the dissociation rate constant (K_{off}). The dissociation constant for the radioligand was then calculated from the K_{on} and K_{off} using equation 4.

(Equation 2)

$$Y = Y0 + (Plateau - Y0) * (1 - \exp(-K_{on} * T))$$

(Equation 3)

$$Y = (Y0 - Plateau) * \exp(-K_{off} * T) + Plateau$$

(Equation 4)

$$K_d = \frac{K_{off}}{K_{on}}$$

Where Y is binding, Y0 is binding at time 0, Plateau is the Y value at infinite time, and K is the rate constant, expressed as a reciprocal of the time units, T. Data from the competitive binding assays was analysed using the one site – Fit Ki protocol. This protocol uses the following equations:

(Equation 5)

$$Y = \frac{Top - Bottom}{1 + 10^{(U - logEC_{50})}} + Bottom$$

(Equation 6)

$$logEC_{50} = \log\left(10^{logK_i} * \left(1 + \frac{HotnM}{HotKdnM}\right)\right)$$

Where Top stands for the maximum plateau, Bottom represents the minimum plateau, U is the log molar concentration of unlabelled ligand, HotnM is the concentration of radioligand used, HotKdnM is the dissociation constant for the radioligand used, $logEC_{50}$ is the logarithmic value for the half maximal effective concentration, and log K_i is the log of the equilibrium constant of the unlabelled ligand.

Analysis of all concentration response assay data were performed using log [agonist] vs response – variable slope (four parameters), and equation 5. In this equation R is the response, which increases as C, the concentration of ligand, increases, and Top and Bottom are the plateaus, in the same units as R.

(Equation 7)

$$R = Bottom + \frac{Top - Bottom}{1 + 10^{((logEC_{50} - C) * Hill\ slope)}}$$

The data sets for the antagonism assay were analysed using the Gaddum/Schild EC_{50} shift program with the following equations:

(Equation 8)

$$Antag = 1 + \left(\frac{B}{10^{-1*pA2}}\right)^{Schild\ Slope}$$

(Equation 9)

$$EC50 = 10^{LogEC_{50}}$$

(Equation 10)

$$Log\ EC = Log(EC_{50} * Antag)$$

(Equation 11)

$$R = Bottom + \frac{Top - Bottom}{1 + 10^{(LogEC - D) * HillSlope}}$$

Where B is the concentration of antagonist, pA2 is the negative log of the concentration of antagonist that shifts the EC_{50} by a factor of 2, the Schild slope quantifies how well the shifts correspond to the prediction of competitive interaction, D is the log dose of agonist, and the Hill slope is the steepness of the family of concentration response curves. To generate the data for the Schild plot, the log (concentration ratio-1) was plotted against the log concentration of antagonist used.

(Equation 12)

$$Log(concentration\ ratio - 1) = Log\left(\left(\frac{A`}{A}\right) - 1\right)$$

Where A` is the molar EC_{50} in M of the agonist in the presence of antagonist and A is the molar EC_{50} of the agonist in the absence of antagonist.

For the statistical analyses of data, the appropriate method was chosen based upon nature of the comparisons. For the direct comparison of 2 data sets, a two-tailed Student's t-test was performed with $P<0.05$ being accepted statistically significant. When making comparisons with more than 2 groups one- or two-way ANOVA was used to analyse the data. Suitable post-hoc tests were then employed to analyse statistically significant data ($P<0.05$).

Chapter 3 Evaluation of the Pharmacology and Signalling of the M_1-DREADD and M_1-DREADD-PD Receptors

3.1 Introduction

GPCRs are well established therapeutic targets, being the focus of multiple drug discovery campaigns for neurodegenerative (Shannon et al., 1994; Veroff et al., 1998), cardiovascular (Black et al., 1964; Harrison et al., 1965), respiratory (Alagha et al., 2014; Disse et al., 1999; Watz et al., 2016), and psychological conditions (Catapano and Manji, 2007; Kane et al., 1988). Despite these successes, only ~15% of the so called druggable genome of GPCRs has been targeted therapeutically (Hauser et al., 2018, 2017). Designing experiments whereby GPCRs can be selectively targeted and that probe key aspects of *in vivo* GPCR signalling would likely dismantle many of the barriers to understanding the fundamental biology of GPCRs and unlock the full potential of this receptor superfamily. In this chapter I aim to address these two questions by using chemical genetics and a mutation strategy that will generate a G protein biased receptor variant.

Investigations of the physiological relevance of GPCR signalling pathways have revealed that certain pathways downstream of the target receptor can be the cause of adverse events and others that drive therapeutically beneficial effects (Baltos et al., 2016; Bolognini et al., 2016). Recent studies have also identified ligands which are able to preferentially activate either heterotrimeric G-protein-dependent or phosphorylation-dependent pathways (Stallaert et al., 2011; Urban et al., 2007). This phenomenon, known as signalling bias or functional selectivity, has triggered drug discovery efforts with the goal of developing functionally selective ligands which lack the adverse events observed with previous agents (Kim et al., 2012; McPherson et al., 2010; Violin et al., 2010). One example of a therapeutically viable biased ligand is oliceridine, also called TRV130, a G-protein dependent signalling biased agonist of the μ-opioid receptor (DeWire et al., 2013). This ligand preferentially activates G-protein dependent signalling pathways, bypassing the on-target, B-arrestin 2 dependent, side effects of Opiod receptor agonists such as morphine (Benyamin et al., 2008; Bohn et al., 2000, 1999; Matthes et al., 1996; Singla et al., 2017; Soergel et al., 2014; Sora et al., 1997). It is not

certain that biased ligands will be more therapeutically beneficial ligands; but understanding the physiological roles of separate signalling pathways could reveal crucial information for drug discovery efforts. To study these characteristics for the M_1-mAChR requires the ability to selectively activate the receptor subtype, and to preferentially drive specific downstream signalling pathways. One approach to the investigation of the roles of M_1-mAChR, and its signalling pathways, is a chemical genetic approach utilising DREADD mAChRs.

DREADD mutations within the mAChR binding pocket reduce the affinity of orthosteric ligands, such as acetylcholine and scopolamine, while simultaneously increasing both the affinity and potency of the synthetic, biologically inert ligand, CNO (Armbruster et al., 2007). *In vivo*, M_1-DREADD mAChR should remain inactive when exposed to acetylcholine, acting as a knock-out, and will become activated upon administration of CNO, restoring receptor function (Alexander et al., 2009; Armbruster et al., 2007). The administration of CNO can then be used to selectively activate these receptors and observe the effects of their signalling. These mutant receptors have previously been successfully transfected into specific brain regions, such as the medial prefrontal cortex (Warthen et al., 2016) and the nucleus accumbens (Zhu et al., 2016), to investigate the roles of $G_{\alpha q}$ and $G_{\alpha i}$ signalling. To investigate functional selectivity, DREADD mutants can be further modified to preferentially drive G-protein dependent or arrestin/phosphorylation dependent pathways (Hu et al., 2016; Kong et al., 2010; Nakajima and Wess, 2012). These modifications involve the mutation of intracellular regions to weaken the coupling of heterotrimeric G-proteins (Hu et al., 2016; Kong et al., 2010), or arrestins (Nakajima and Wess, 2012) to GPCRs. In animal models, differences in physiology and behaviour observed can then be attributed to specific pathways, potentially revealing a signalling blueprint for the identification of new, more tolerable, compounds.

The ultimate aim of this project in the Tobin lab is to employ a chemical genetic approach, introducing DREADD modified M_1-mAChRs into the endogenous M_1-mAChR locus to study their role *in vivo*; a novel use of the DREADD mutant receptors. These mice will initially act as a knock-out model, with the mutant receptors remaining inactive in the presence of acetylcholine. CNO can then be administered to the mice to activate

the receptor, hopefully returning the animals' behaviour to that of the controls. By substituting the intracellular phosphorylation sites with alanine residues a phosphorylation deficient (PD), G-protein biased, M_1-DREADD-PD mAChR can be produced (Kong et al., 2010). The behaviour of these M_1-DREADD-PD mAChR expressing mice can then be compared to that of the M_1-DREADD mAChR mice to understand the *in vivo* roles of signalling pathways and effects of signalling bias. Before conclusions can be made about the functional role of the M_1-mAChR these mutant models need to be characterised and compared to the wild-type receptor. To use these mutants as a model of M_1-mAChR function, CNO-mediated activation of the M_1-DREADD mAChR needs to be characterised *in vitro* to confirm its signalling is comparable to that of the wild-type receptor.

This chapter includes the *in vitro* characterisation of the pharmacology and function of M_1-DREADD and M_1-DREADD-PD mAChRs in tandem with the human and mouse M_1-mAChR. Radioligand binding studies and cell signalling assays were used to; confirm the changes to ligand-receptor interactions caused by the DREADD mutations, ensure that the M_1-DREADD and human and mouse M_1-mAChR signal through the same effectors, and understand how the PD mutations effect receptor function.

3.2 Results

3.2.1 Radioligand Binding Studies

3.2.1.1 Saturation Binding

Initial saturation radioligand binding studies (Fig. 3.1) were performed to assess both receptor expression and radioligand affinity towards: hM_1, mM_1, M_1-DREADD, and M_1-DREADD mAChRs in my recombinant cell models. Cells were treated with a range of half log dilutions of ^{3}H-NMS, from 30 nM to 0.3 pM. To distinguish specific and non-specific binding duplicate wells were used, with one set being treated with the muscarinic antagonist atropine, to compete with ^{3}H-N-methyl scopolamine (^{3}H-NMS) at the orthosteric site of the M_1 mAChR. The activity from remaining bound radioligand, the non-specific binding, can be subtracted from the activity of the untreated well, total binding, to provide a value for specific bound ^{3}H-NMS.

Western blotting confirmed expression of hM_1-WT, mM_1-WT, M_1-DREADD, and M_1-DREADD-PD mAChRs in the recombinant cell lines. Using the Welch's t-test, no significant difference was found between the affinity of ^{3}H-NMS for the hM1-WT and mM_1-WT mAChRs, although the B_{max} of the mouse receptor was found to be slightly higher, 1418 ± 85.6 fmol mg^{-1} protein, than for the human M_1-WT mAChR, 1171 ± 77.6 fmol mg^{-1} protein. The highest concentrations of ^{3}H-NMS used with the M_1-DREADD or M_1-DREADD-PD mAChRs did not reach a saturating concentration. This therefore did not allow for either the level of expression or the affinity of ^{3}H-NMS to be determined. Although these values cannot be calculated, this data supports the notion that the affinity of ^{3}H-NMS for the M_1 mAChR has been greatly reduced through the addition of the DREADD mutations. Comparing receptor expression in western blotting (Fig 3.1(e)), human and mouse M_1-WT and M_1-DREADD-PD mAChRs were expressed at similar levels, with the M_1-DREADD mAChRs expressing at higher levels. The blots revealed that the M_1-DREADD cell line had higher receptor expression than either of the wild-type or the M_1-DREADD-PD cell lines; which had reasonably similar expression.

3.2.1.2 Association and Dissociation Binding

Since saturation binding studies were not able to determine an affinity for ^{3}H-NMS at the M_1-DREADD or M_1-DREADD-PD mAChRs, association and dissociation binding studies were used as an alternative approach. Through determining the K_{on} and K_{off} of ^{3}H-NMS with association and dissociation binding respectively, an estimate for the K_d of ^{3}H-NMS can be calculated.

For the human M_1-mAChRs, the K_{on} and K_{off} for ^{3}H-NMS were calculated to be 0.0568 ± 0.0034 $M^{-1}s^{-1}$ and 0.0529 ± 0.0047 s^{-1} respectively. The K_{on} and K_{off} for mouse M1-mAChR were calculated as 0.0522 ± 0.0029 $M^{-1}s^{-1}$ and 0.0569 ± 0.0052 s^{-1} respectively. These values were then used to calculate estimates of 8.97 and 9.04 for the pK_d of ^{3}H-NMS at the hM_1- and mM_1-mAChRs respectively. These values are comparable to the K_d values calculated using saturation binding studies, validating this as an alternative approach to determining affinity.

Even though curves could be fitted to the association and dissociation binding data for the M_1-DREADD and M_1-DREADD-PD mAChRs, the R^2 for these curves is too low to accurately determine the K_{on} or K_{off} for ^{3}H-NMS at these receptors. The maximum specific binding activity of the M_1-DREADD and M_1-DREADD-PD mAChRs was also found to be significantly lower than that of the hM_1-WT and mM_1-WT mAChRs ($p<0.0001$) (Fig. 3.3) when analysed using two-way ANOVA using the Bonferroni correction. This could mean that the concentration of ^{3}H-NMS used for the M_1-DREADD and M_1-DREADD-PD mAChRs was lower than K_d. Although neither technique was successful in calculating the affinity of ^{3}H-NMS at the DREADD M_1-mAChRs, conclusions can still be drawn from these results. The inability of these approaches to determine a K_d for orthosteric ligands, in this case NMS, is consistent with the notion that the DREADD mutations have interfered with the binding of orthosteric ligands to such a degree that it precluded the accurate determination of the K_d of ^{3}H-NMS.

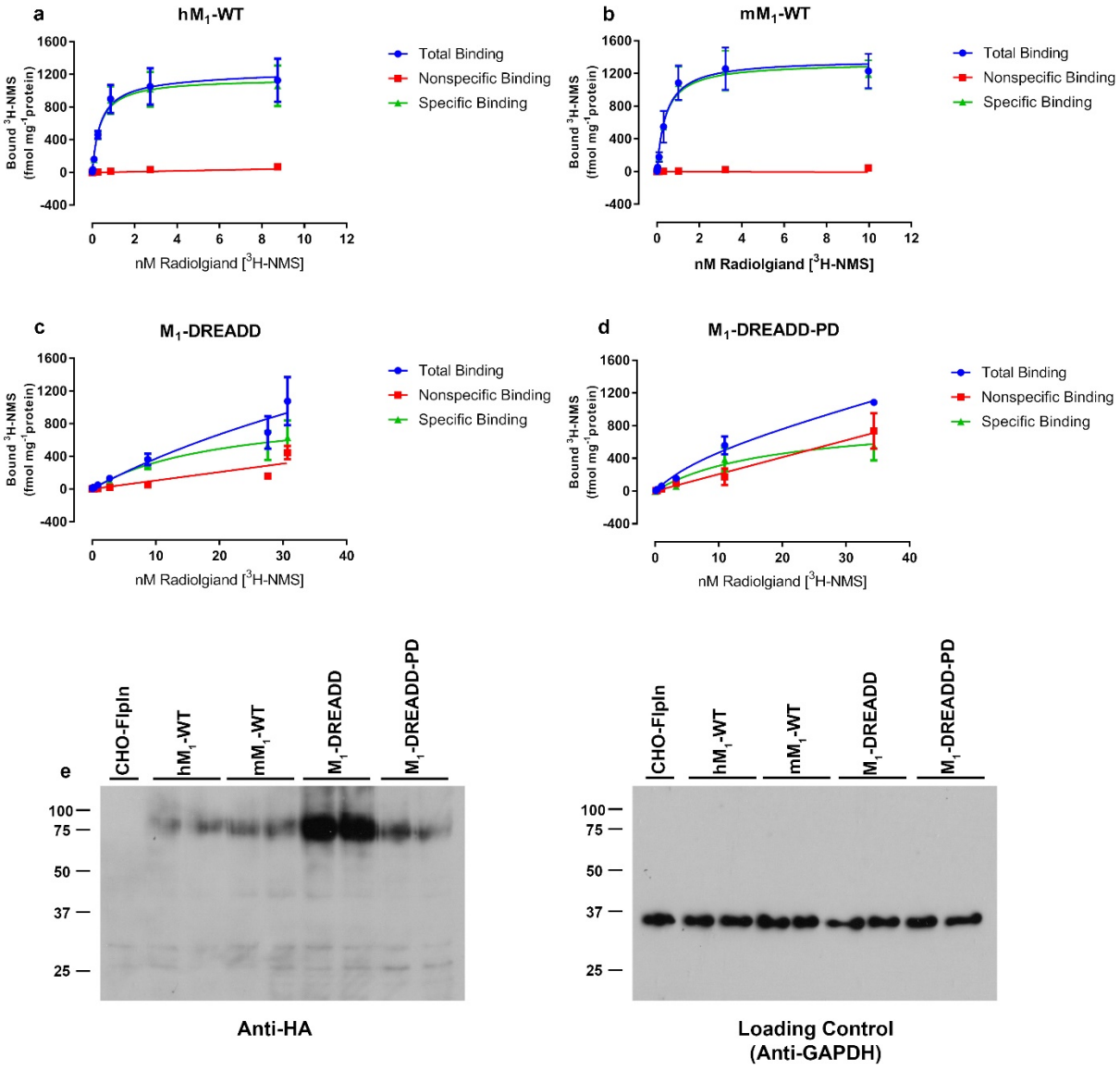

Figure 3.1: Saturation radioligand binding studies with hM$_1$-WT, mM$_1$-WT, M$_1$-DREADD, and M$_1$-DREADD-PD mAChRs using ^{3}H-NMS.

For saturation binding studies, cells expressing hM$_1$-WT (**a**), mM$_1$-WT (**b**), M$_1$-DREADD (**c**), and M$_1$-DREADD-PD (**d**) mAChRs were treated with increasing concentrations of ^{3}H-NMS at 37°C in the presence and absence of a saturation concentration of atropine to determine NSB and total binding respectively. Comparison of receptor expression was also performed with western blotting (**e**) against the HA epitope tag incorporated into the receptors using anti-HA antibody, and anti-GAPDH as a loading control. Data are shown as mean ± SEM; n=3.

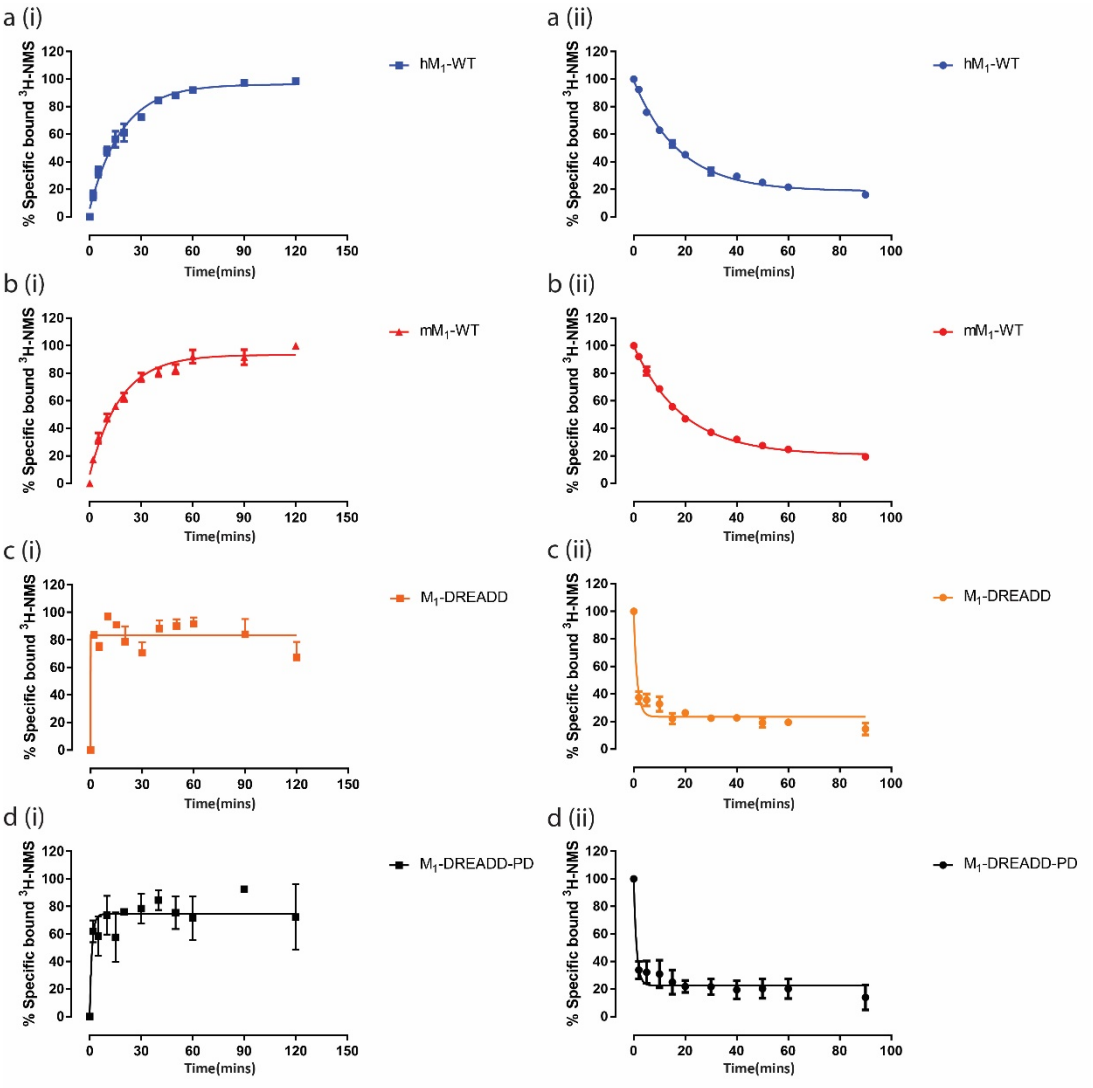

Figure 3.2: Association and dissociation binding studies using ^{3}H-NMS.

Association binding (**i**) and dissociation binding (**ii**) studies were performed on cells expressing hM$_1$-WT (**a**), mM$_1$-WT (**b**), M$_1$-DREADD (**c**), and M$_1$-DREADD-PD (**d**). For association binding, cells were incubated with a K_d concentration of ^{3}H-NMS at room temperature at different time points up to 120 minutes. One well containing a saturating concentration of atropine was used to calculate NSB. For dissociation binding, cells were preincubated with a K_d concentration of ^{3}H-NMS at room temperature for 4 hours. After incubation atropine was added to the cells at time points up to 90 minutes. Data are shown as mean ± SEM; n=3.

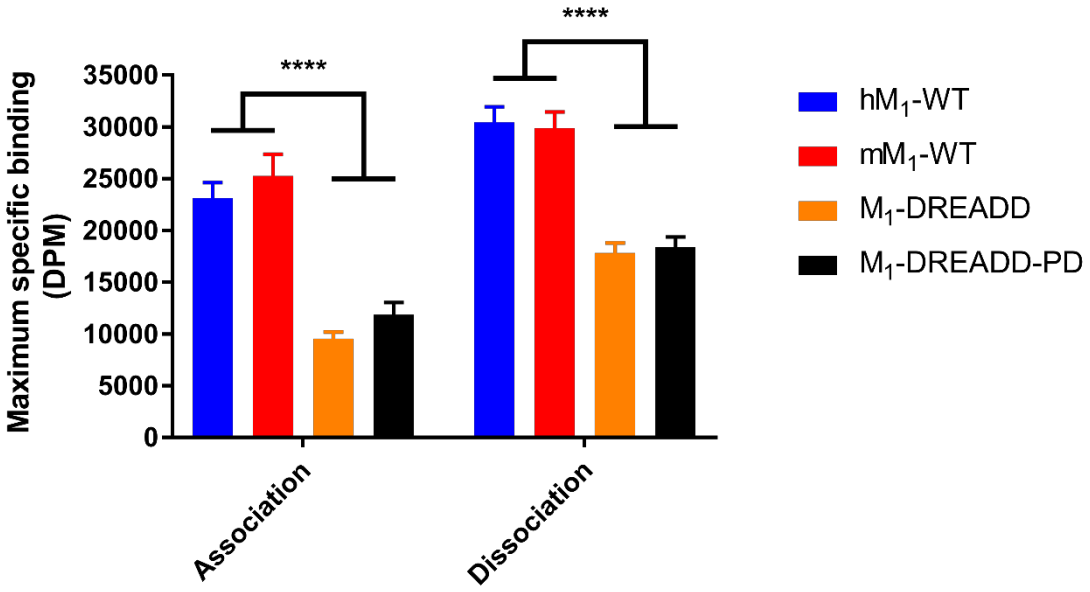

Figure 3.3: Maximum specific binding activity for hM$_1$-WT, mM$_1$-WT, M$_1$-DREADD, and M$_1$-DREADD-PD mAChRs in association and dissociation binding studies.

In both association and dissociation binding studies, the maximum specific binding for the M$_1$-DREADD and M$_1$-DREADD-PD mAChR expressing cell lines were significantly lower than that of the hM$_1$-WT and mM$_1$-WT mAChR expressing cell lines ($p<0.0001$). Data were analysed with two-way ANOVA using the Bonferroni correction. Data are shown as mean ± SEM; n=3.

	hM_1-WT	mM_1-WT	M_1-DREADD	M1-DREADD-PD
Saturation Binding				
B_{max} (fmol/mg)	1171 ± 78	1418 ± 86	*	*
pK_d	9.49 ± 0.16	9.34 ± 0.01	7.29 ± 0.38	8.06 ± 0.22
Association/ Dissociation Binding				
K_{on} ($M^{-1}s^{-1}$)	0.0568 ± 0.0034	0.0522 ± 0.0029	*	*
K_{off} (s^{-1})	0.0529 ± 0.0047	0.0569 ± 0.0052	*	*
pK_d	~8.97	~9.04	*	*

Table 3.1: Pharmacological Data for hM_1-WT, mM_1-WT, M_1-DREADD and M_1-DREADD-PD using ^{3}H-NMS.

* Curves incomplete so no value could be calculated. Data shown as mean ± SEM or ~ for approximate values; n=3.

3.2.2 Cell Signalling Assays

3.2.2.1 ERK 1/2 Activation

In vitro activation of ERK 1/2 was used to investigate the function of hM_1-WT, mM_1-WT, M_1-DREADD, and M_1-DREADD-PD mAChRs. Activation of ERK 1/2 was assessed using densitometry of western blots and HTRF plate-based assay kits.

Western blotting (Fig. 3.4-6) showed that the DREADD mutations reduced the potency of acetylcholine at the M_1 mAChR, and increased the potency of CNO. Concentrations of CNO were too low to confirm whether CNO has lower maximum effect than acetylcholine at the hM_1-WT or mM_1-WT mAChRs. Statistical analysis with one-way ANOVA using the Bonferroni correction found that CNO achieved a significantly lower maximum effect (E_{max}) with M_1-DREADD and M_1-DREADD-PD cell lines, 109.4 ± 4.57 and 114.8 ± 20.8-fold over basal (FOB) respectively, than acetylcholine in the human and mouse M_1-WT cell lines, 390.3 ± 18.6 and 375.6 ± 17.8 FOB respectively, where $P<0.0001$. The small dynamic range of densitometry when using ECL for western blotting means that basal activation could not always be detected.

With the HTRF assay (Fig. 3.7), the E_{max} of CNO at the M_1-DREADD mAChR, 649 ± 12.7 fluorescence ratio (FR), was not significantly different to that of acetylcholine at the hM_1-WT, 703.2 ± 31.8 when compared using one-way ANOVA with Bonferroni corrections. The E_{max} of acetylcholine at the mM_1-WT mAChR was significantly higher, 1257 ± 56.85, than at the hM_1-WT with a $P<0.0001$, although there is no significant increase in the response to CNO. Both acetylcholine and CNO have a higher E_{max} at the M_1-DREADD-PD mAChR, 839.4 ± 50.24 and 1186 ± 18.1 respectively, than with the M_1-DREADD mAChR. This increase in the maximal response, even though the M_1-DREADD-PD mAChRs were expressed at lower levels, may be due to the lack in receptor desensitisation expected from the PD mutations introduced. Statistical analysis of pEC_{50} using two-way ANOVA found significant difference in the potency of acetylcholine at the hM_1-WT and mM_1-WT cell lines, 6.90 ± 0.13 and 6.77 ± 0.14 respectively. Unlike in the western blotting there is a significant between the pEC_{50} values of CNO at the M_1-DREADD and M_1-DREADD-PD, 7.81 ± 0.08 and 8.49 ± 0.05 respectively where $P<0.0001$. There is no significant difference between the pEC_{50} of acetylcholine at the M_1-DREADD-PD, 4.01 ± 0.15, or M_1-DREADD, 3.54 ± 0.22.

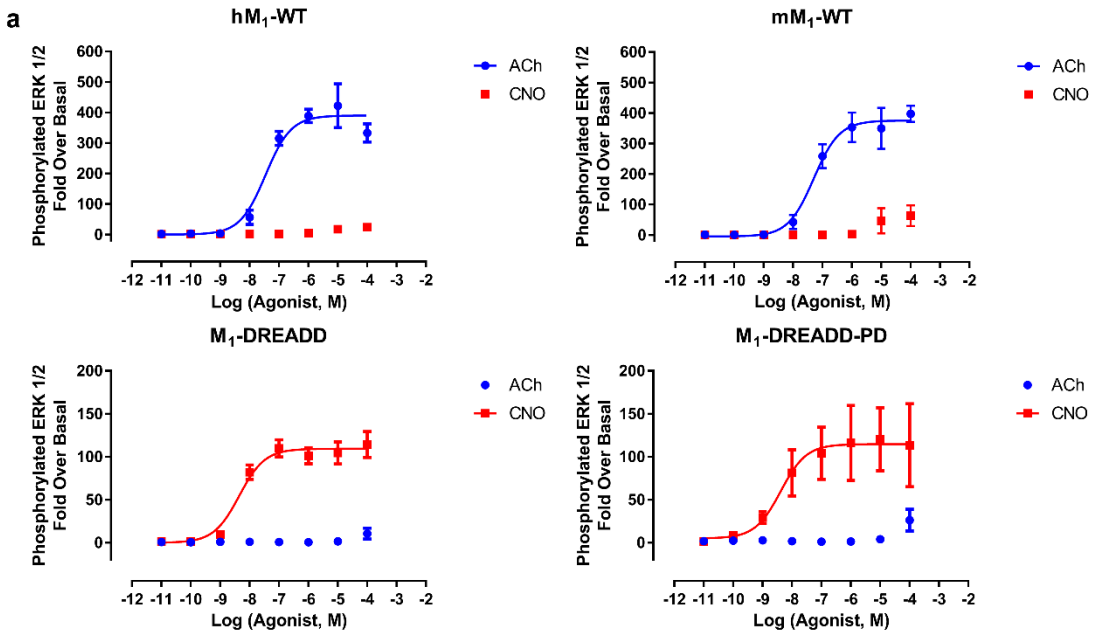

Figure 3.4: Concentration dependent activation of ERK 1/2 by acetylcholine or CNO using western blotting.

Cells expressing hM_1-WT, mM_1-WT, M_1-DREADD and M_1-DREADD-PD mAChRs were treated with increasing concentrations of acetylcholine (ACh) or CNO for 5 minutes at 37°C. Signalling was halted using ice cold RIPA lysis buffer. A western blot was performed on the lysate, probing with the phospho-p44/42 MAPK (Erk1/2) antibody (b-e i, ii) and the total p44/42 MAPK (Erk1/2) antibody (b-e iii, vi) as the loading control. Data were collected using densitometry with ImageJ, and the data expressed as fold over basal, after normalisation using total ERK 1/2 as a control (a). Data are shown as mean ± SEM; n=3.

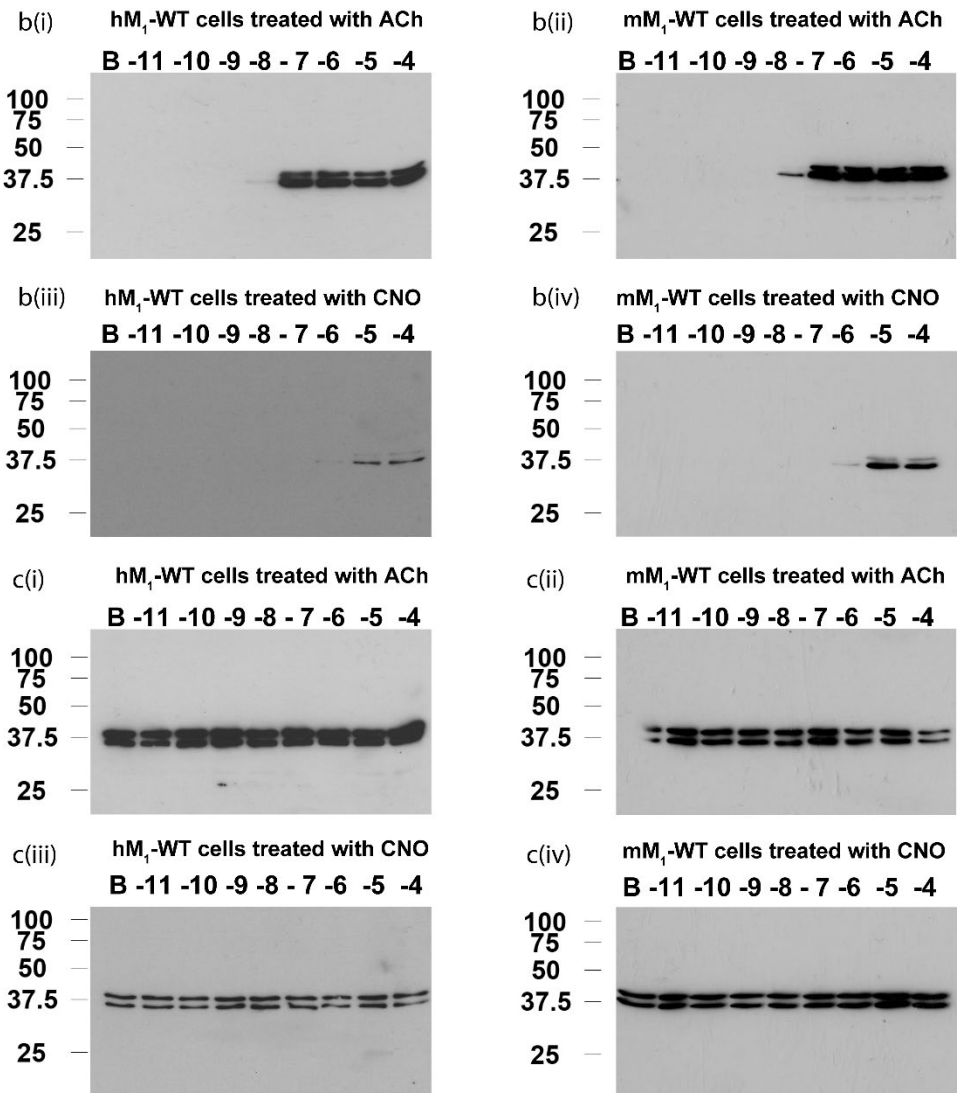

Figure 3.5: Concentration dependent activation of ERK 1/2 by Acetylcholine and CNO using western blotting cont.

Cells expressing hM_1-WT, mM_1-WT, M_1-DREADD and M_1-DREADD-PD mAChRs were treated with increasing concentrations of acetylcholine (ACh) or CNO for 5 minutes at 37°C. Signalling was halted using ice cold RIPA lysis buffer. A western blot was performed on the lysate, probing with the phospho-p44/42 MAPK (ERK1/2) antibody (b, d i-iv) and the total p44/42 MAPK (ERK1/2) antibody (c, e i-iv) as the loading control. Data were collected using densitometry with ImageJ, and the data expressed as fold over basal, after normalisation using total ERK 1/2 as a control (a).

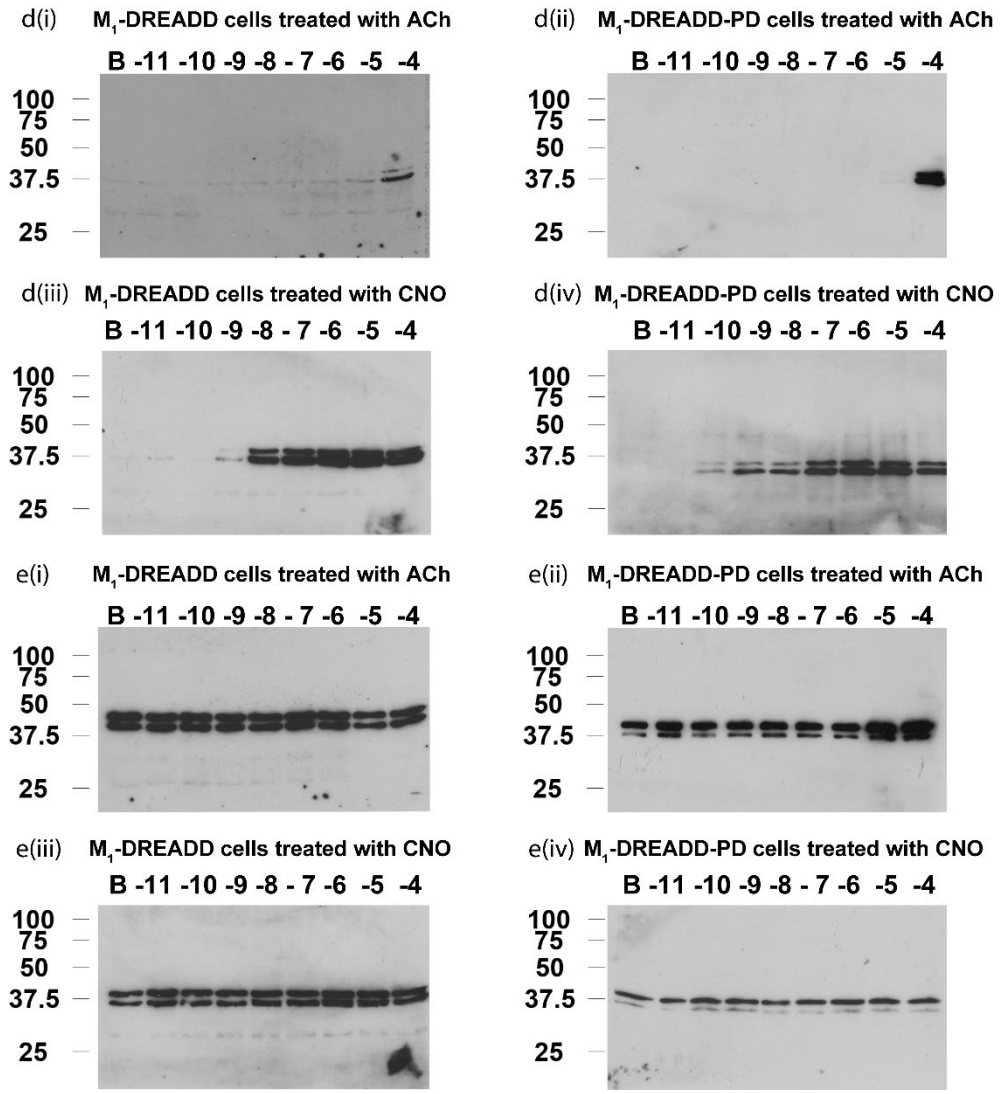

Figure 3.6: Concentration dependent activation of ERK 1/2 by acetylcholine and CNO using western blotting cont.

Cells expressing hM_1-WT, mM_1-WT, M_1-DREADD and M_1-DREADD-PD mAChRs were treated with increasing concentrations of acetylcholine (ACh) or CNO for 5 minutes at 37°C. Signalling was halted using ice cold RIPA lysis buffer. A western blot was performed on the lysate, probing with the phospho-p44/42 MAPK (ERK1/2) antibody (b-e i, ii) and the total p44/42 MAPK (ERK1/2) antibody (b-e iii, vi) as the loading control. Data were collected using densitometry with ImageJ, and the data expressed as fold over basal, after normalisation using total ERK 1/2 as a control (a).

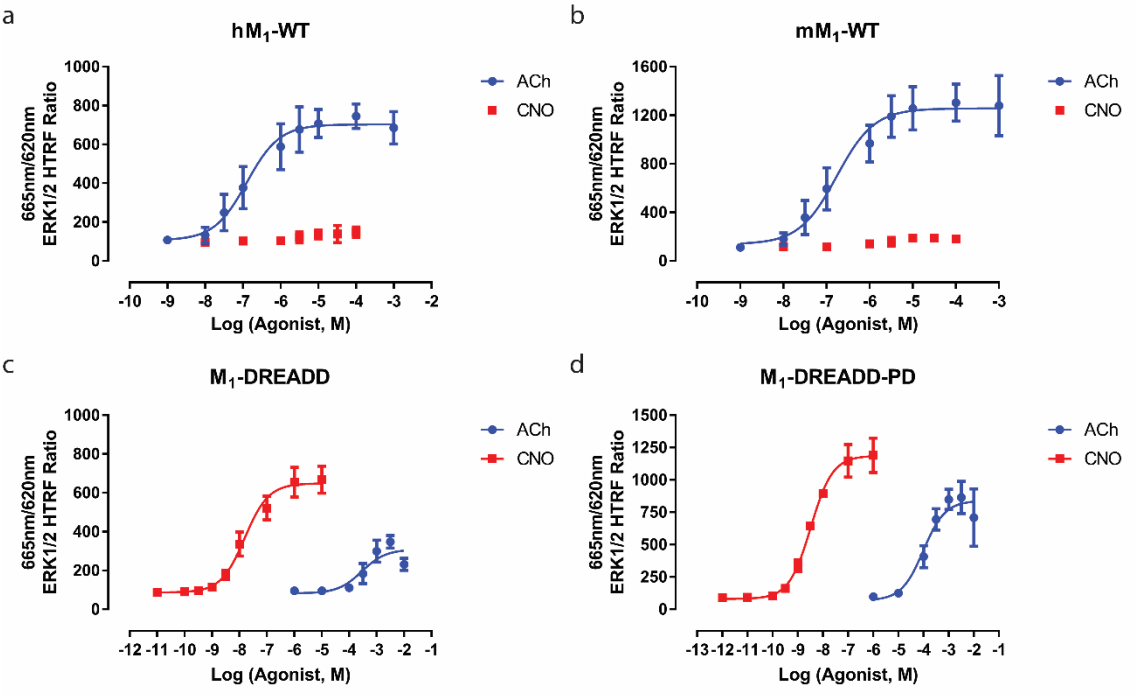

Figure 3.7: Concentration dependent activation of ERK 1/2 by acetylcholine and CNO using HTRF.

Cells expressing hM_1-WT (**a**), mM_1-WT (**b**), M_1-DREADD (**c**), and M_1-DREADD-PD (**d**) mAChRs were treated with increasing concentrations of acetylcholine or CNO for 5 minutes at 37°C. Signalling was halted using the HTRF assay kit lysis buffer. Lysates were mixed with the 2 HTRF anti-phospho-ERK 1/2 antibodies labelled with d2 acceptor and Eu^{3+}-cryptate in a 384 well plate. Following incubation while shaking for 2 hours, the plate was read in a CLARIOstar plate reader and data expressed as a ratio of the emission at 665 nm over 620 nm. Data are shown as mean ± SEM; n=3.

3.2.2.2 Inositol Monophosphate Accumulation – IP-One

The IP-One HTRF assay measures the accumulation of inositol monophosphate (IP1) through the inhibition of inositol monophosphatase. Inositol monophosphate is a breakdown product of inositol-1-4-5-trisphosphate, a signalling molecule produced following activation of phospholipase C.

The pEC_{50} values of acetylcholine at the hM_1-WT or the mM_1-WT receptors, 6.04 ± 0.07 and 5.33 ± 0.07 respectively, were comparable (Fig. 3.8). CNO was found to act only as a weak partial agonist of the human and mouse M_1-mAChR compared to acetylcholine. At the M_1-DREADD and M_1-DREADD-PD mAChRs, acetylcholine had a lowered pEC_{50} than at the human and mouse M_1-mAChRs, 2.39 ± 0.13 and 2.98 ± 0.11 respectively; with CNO achieving a higher pEC_{50}, 8.27 ± 0.14 and 8.64 ± 0.11 respectively, and acting as a full agonist of the receptor. In this IP-One experiment, both acetylcholine and CNO were full agonists of the M_1-DREADD and M_1-DREADD-PD mAChRs. As in the previous functional assays, IP-One further confirms that the introduction of DREADD mutations into the M_1-mAChR both reduces the potency of acetylcholine, and increases the potency and relative efficacy of CNO for the M_1-mAChR.

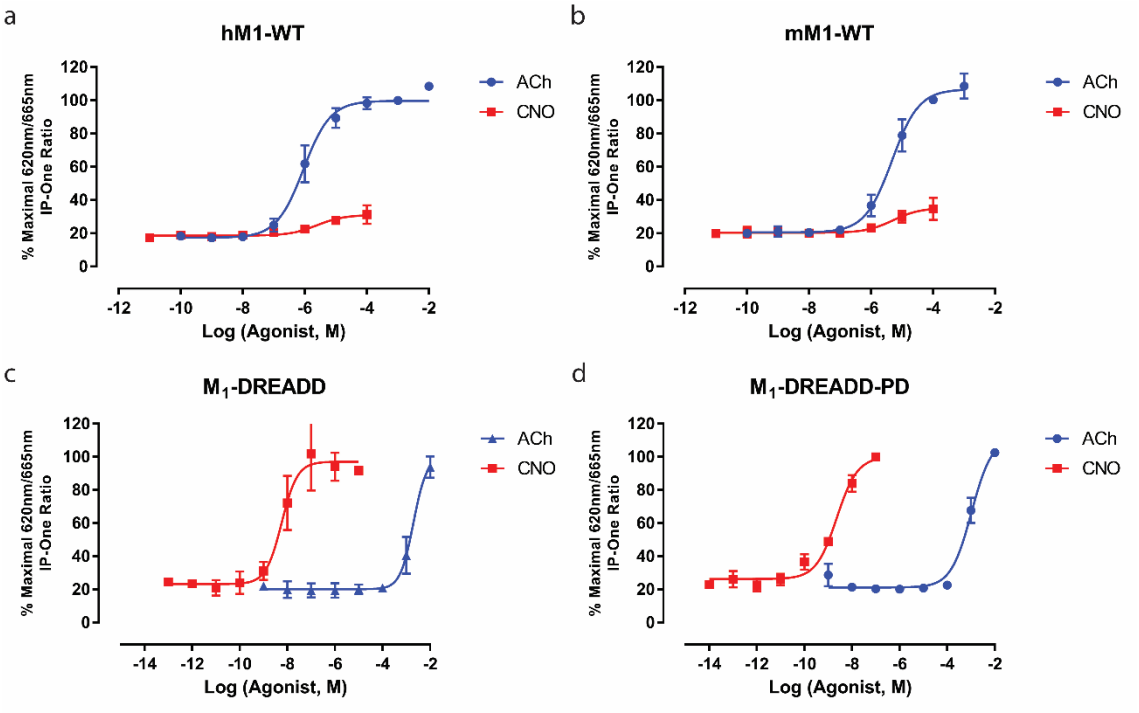

Figure 3.8: Concentration dependent accumulation of inositol monophosphate from acetylcholine and CNO.

Cells expressing hM$_1$-WT (**a**), mM$_1$-WT (**b**), M$_1$-DREADD (**c**), and M$_1$-DREADD-PD (**d**) mAChR cell lines were treated with increasing concentrations of acetylcholine or CNO for 1 hour at 37°C in stimulation buffer containing lithium chloride. Reactions were halted by removing stimulation buffer and addition of two lysis buffers, one containing d2 acceptor antibodies and the other containing Eu^{3+} conjugated IP1. Plates were shaken for a minimum of 1 hour after which the signal was read on a CLARIOstar plate reader. Data are expressed as a ratio of the emission at 665 nm over 620 nm. Data are shown as mean ± SEM; n=3.

3.2.2.3 Calcium Signalling

Measuring the concentration-dependent increase in intracellular calcium is another way of measuring $G\alpha_q$ mediated signalling. Intracellular calcium release is initiated by the signalling molecule inositol-1-4-5-trisphosphate activating the inositol-1-4-5-trisphosphate receptor in the endoplasmic reticulum.

Calcium mobilisation assays (Fig 3.9, 3.10), identified a significant shift in the pEC_{50} of acetylcholine and CNO in M_1-DREADD and M1-DREADD-PD mAChRs compared to the human and mouse M_1 mAChR (Table 3.2). The DREADD mutations reduced the pEC_{50} of acetylcholine with the hM_1-mAChR from 8.38 ± 0.16 to 4.10 ± 0.14 in calcium microscopy and from 7.95 ± 0.12 to 3.73 ± 0.37 in the plate-based assay. CNO was found to partially activate the human and mouse M_1-mAChRs at µM to mM concentrations. In the M_1-DREADD and M_1-DREADD-PD mAChRs CNO was now a full agonist of the receptor, and reached the E_{max} at sub-µM concentrations. Acetylcholine was a full agonist of the M_1-DREADD and M_1-DREADD-PD mAChRs, with pEC_{50} values 3-4 orders of magnitude lower than with the human and mouse M_1-mAChRs. Comparable E_{max} values were found between acetylcholine at the hM_1-WT and mM_1-WT mAChRs, and CNO at the M_1-DREADD and M_1-DREADD-PD mAChRs. In calcium microscopy the E_{max} of acetylcholine at the human and mouse M_1-WT mAChR were 1.29 ± 0.04 and 1.27 ± 0.04 respectively, compared to 1.21 ± 0.06 for CNO at the M_1-DREADD mAChR. The E_{max} values for acetylcholine at the human and mouse M_1-WT mAChRs using the Flexstation were 126.1 ± 5.9 and 153.9 ± 5.9 respectively, and for CNO at the M_1-DREADD mAChR was 139.7 ± 6.1. The similarities in the E_{max} values of CNO at the M_1-DREADD mAChR and acetylcholine at the human and mouse M_1-mAChR (see Table 3.2), as well as reduction in acetylcholine potency for the M_1-DREADD mAChR, adds to the argument that these mutant receptors are a valid model for studying M_1-mAChR function.

Comparing the time course of intracellular calcium reveals differences between the signalling of the M_1-DREADD and M_1-DREADD-PD mAChR expressing cell lines (Fig. 3.11). Treatment of M_1-DREADD-PD mAChR with CNO caused a prolonged increased in intracellular calcium compared to that seen with activation of the M_1-DREADD mAChR. This prolonged signalling is consistent with the reduced receptor desensitisation expected with the PD mutations.

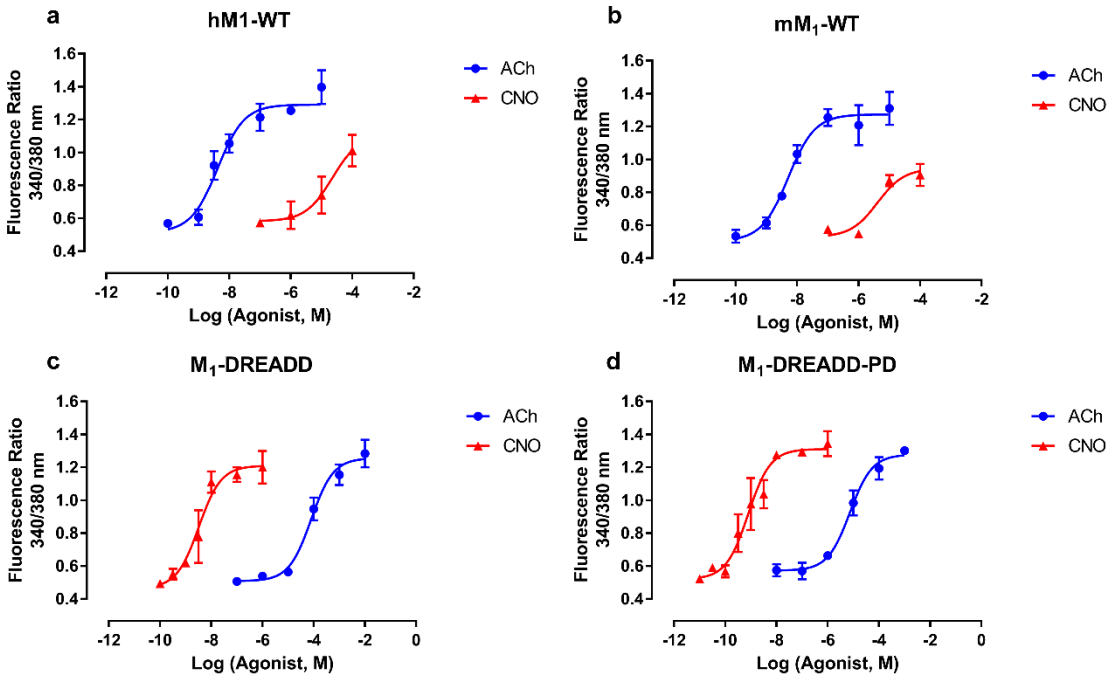

Figure 3.9: Concentration dependent increase in intracellular calcium by acetylcholine and CNO using single cell calcium microscopy.

Cells expressing hM_1-WT (**a**), mM_1-WT (**b**), M_1-DREADD (**c**), and M_1-DREADD-PD (**d**) mAChR cell lines were loaded with Fura-2-AM for 30 minutes at 37°C after which the Fura-2-AM was replaced with Krebs and a baseline reading was taken for 30 seconds. Cells were then treated with increasing concentrations of acetylcholine or CNO and measured for 2 minutes. Peak measurements were used to define each point. Data are shown as mean ± SEM; n=3 separate experiments consisting of 30-60 cells.

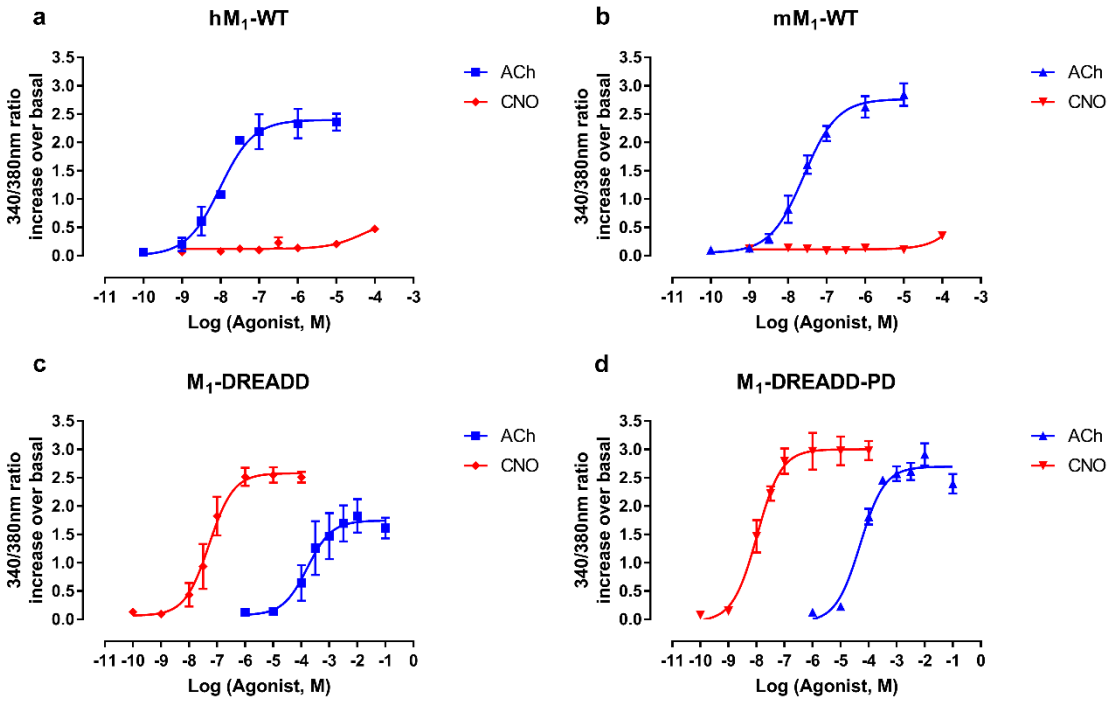

Figure 3.10: Concentration dependent increase in intracellular calcium by acetylcholine and CNO with the Flexstation plate reader.

Cells expressing hM_1-WT (**a**), mM_1-WT (**b**), M_1-DREADD (**c**), and M_1-DREADD-PD (**d**) mAChR cell lines were loaded with Fura-2-AM for 1 hour at 37°C, after which the Fura-2-AM was replaced with Krebs. The 96-well plate was then placed in the Flexstation plate reader with another 96-well plate containing ligands at 2X the concentration required. Cells were then treated with increasing concentrations of acetylcholine or CNO and measured for 74 seconds after a 16 second baseline reading was taken. Peak measurements were used to define each point as an increase over the basal fluorescence signal. Data are shown as mean ± SEM; n=3.

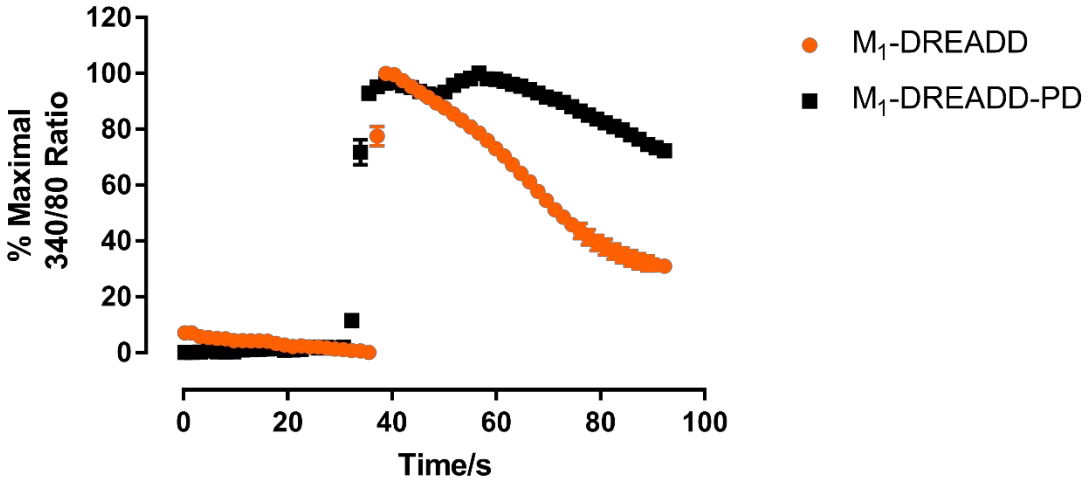

Figure 3.11: Comparison of calcium signalling curves for M_1-DREADD and M_1-DREADD-PD mAChRs treated with CNO.

Cells expressing M_1-DREADD, and M_1-DREADD-PD mAChR cell lines were loaded with Fura-2-AM for 30 minutes at 37°C after which the Fura-2-AM was replaced with Krebs and a baseline reading was taken for 30 seconds. Cells were then treated with CNO and measured for a further 90 seconds. Data are shown as mean ± SEM of 30-60 cells.

		hM_1-WT	mM_1-WT	M_1-DREADD	M_1-DREADD-PD
ERK 1/2 Activation – Western Blot					
pEC_{50}	ACh	7.46 ± 0.15	7.30 ± 0.16	*	*
	CNO	*	*	8.35 ± 0.14	8.38 ± 0.52
E_{max}	ACh	390.3 ± 18.6	375.6 ± 17.8	*	*
(FOB)	CNO	*	*	109.4 ± 4.6	114.8 ± 20.8
ERK 1/2 Activation – HTRF Assay					
pEC_{50}	ACh	6.90 ± 0.13	6.77 ± 0.14	3.54 ± 0.22	4.01 ± 0.15
	CNO	*	*	7.81 ± 0.08	8.49 ± 0.05
E_{max}	ACh	703.2 ± 31.8	1257 ± 56.85	308.9 ± 19.4	839.4 ± 50.24
(FR)	CNO	*	*	649 ± 12.7	1186 ± 18.1
IP-One					
pEC_{50}	ACh	6.04 ± 0.07	5.33 ± 0.07	2.39 ± 0.13	2.98 ± 0.11
	CNO	*	*	8.27 ± 0.14	8.64 ± 0.11
Calcium Mobilisation – Single Cell Microscopy					
pEC_{50}	ACh	8.38 ± 0.16	8.29 ± 0.16	4.10 ± 0.14	5.13 ± 0.13
	CNO	*	5.39 ± 0.33	8.49 ± 0.20	9.10 ± 0.16
E_{max}	ACh	1.29 ± 0.04	1.27 ± 0.04	1.26 ± 0.04	1.28 ± 0.04
(Peak FR)	CNO	*	0.95 ± 0.06	1.21 ± 0.06	1.31 ± 0.05
Calcium Mobilisation – Flexstation					
pEC_{50}	ACh	7.95 ± 0.12	7.46 ± 0.08	3.73 ± 0.37	4.35 ± 0.19
	CNO	*	*	7.10 ± 0.12	7.82 ± 0.08
E_{max}	ACh	126.1 ± 5.9	153.9 ± 5.6	81.4 ± 10.7	135.2 ± 6.4
(AUC)	CNO	*	*	139.7 ± 6.1	156.1 ± 4.2

Table 3.2: Functional data for the hM1-WT, mM1-WT, M1-DREADD, and M1-DREADD-PD cell lines using acetylcholine and CNO.

* High enough concentrations of agonist were not used to complete the concentration response curve. Data are shown as mean ± SEM; n=3-4.

3.2.3 Receptor Internalisation

Agonist dependent receptor internalisation and receptor expression was observed using immunocytochemistry with antibodies targeting the HA epitope tag (Fig.3.12, 3.13). Immunocytochemistry confirmed that the transfected M_1-mAChRs were expressed at the cell membrane. Endocytic vesicles containing the internalised receptors can be identified as stained dots within the cytoplasm. In hM_1-WT and mM_1-WT mAChR expressing cell-lines stimulated with acetylcholine, and M_1-DREADD mAChR expressing cell lines stimulated with CNO, ligand induced receptor internalisation can be observed. In comparison, there was no internalisation seen in the M_1-DREADD-PD mAChR expressing cell line following stimulation with CNO above what was seen in the unstimulated sample (Fig. 3.12(c) 3.13(c)). Internalised receptors can be seen within the cytoplasm of all four untreated samples, most probably due to constitutive internalisation of the receptors. Levels of internalised receptor appears higher in the M_1-DREADD mAChR expressing cell-line. This apparent increase may be due to the increased expression of the M_1-DREADD mAChR; where although the quantity of internalised receptors is higher, the proportion of internalised receptors to receptors expressing at the cell membrane was the same as the other cell lines.

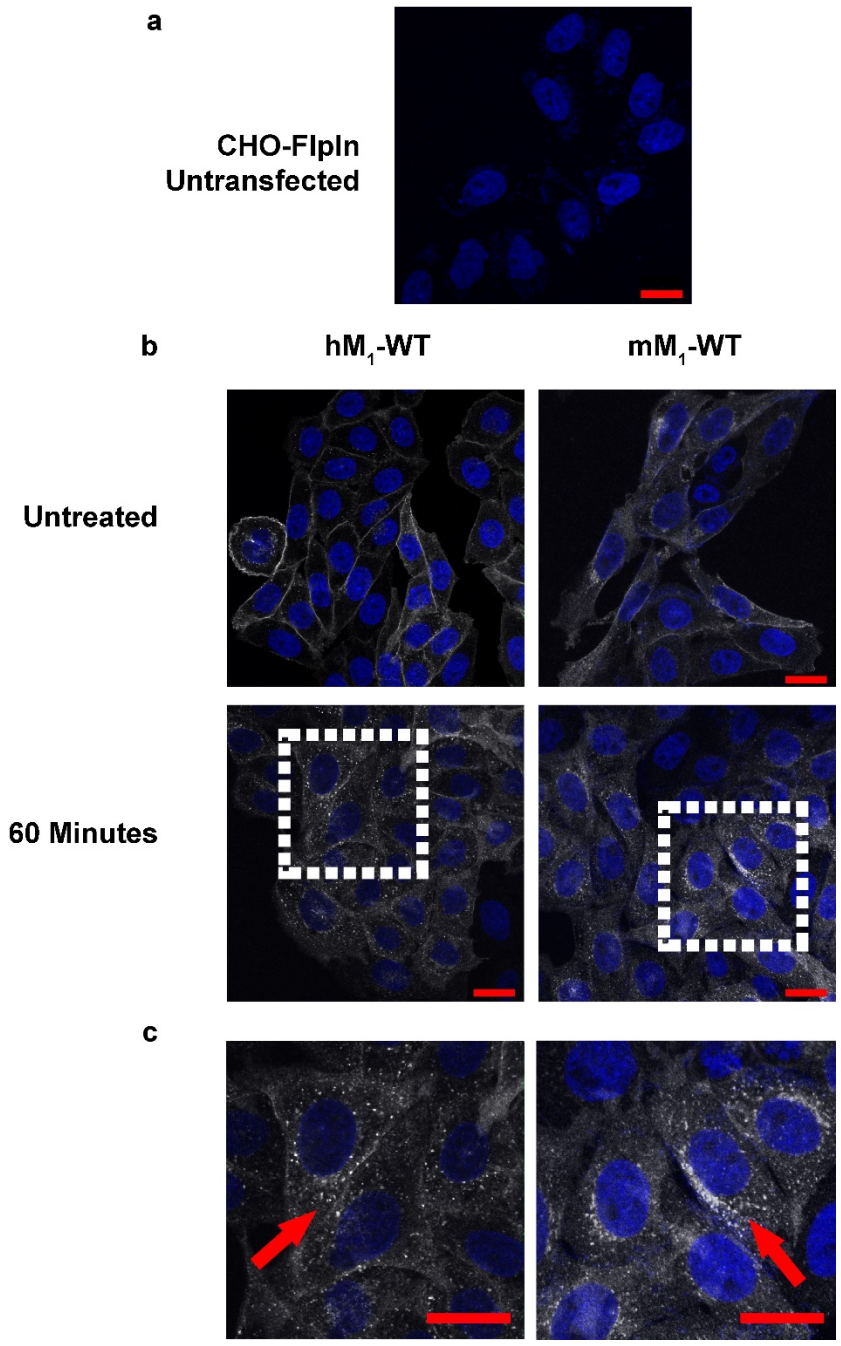

Figure 3.12: Agonist dependent receptor internalisation using immunocytochemistry targeting the HA-epitope tag.

(**a**) CHO-FlpIn cells were incubated with anti-HA antibody to ensure no non-specific staining from the primary antibody. Cells expressing the hM_1-WT and mM_1-WT (**b**), M_1-DREADD, and M_1-DREADD-PD (**d**) were loaded onto coverslips and treated with maximal concentrations of either acetylcholine (hM1-WT and mM_1-WT) or CNO (M_1-DREADD and M_1-DREADD-PD). (**c, e**) Close up sections from highlighted areas in (**b, d**) showing punctate dots of internalised receptors (red arrow) in all apart from M_1-DREADD-PD cell lines. Red scale bars equate to 20µm.

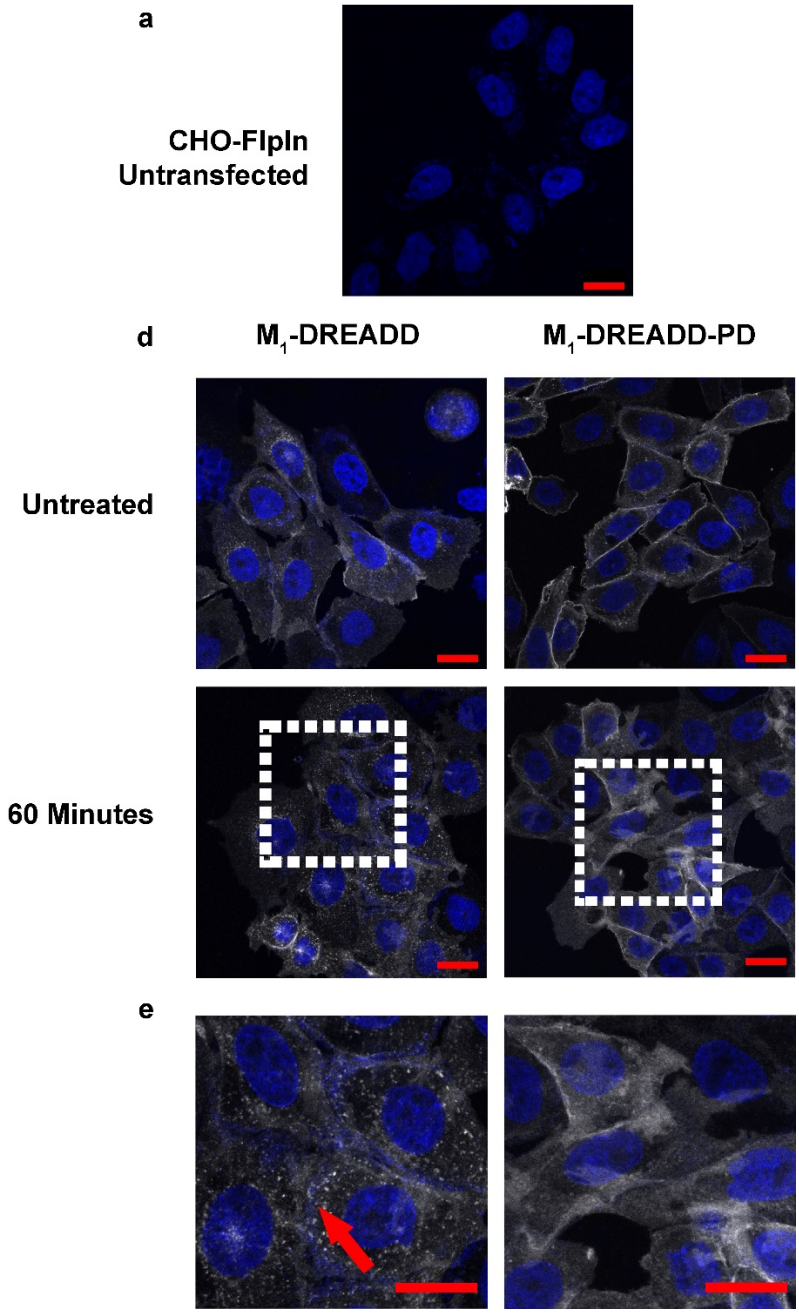

Figure 3.13: Agonist dependent receptor internalisation using immunocytochemistry targeting the HA-epitope tag continued.

(**a**) CHO-FlpIn cells were incubated with anti-HA antibody to ensure no non-specific staining from the primary antibody. Cells expressing the hM_1-WT and mM_1-WT (**b**), M_1-DREADD, and M_1-DREADD-PD (**d**) were loaded onto coverslips and treated with maximal concentrations of either acetylcholine (hM1-WT and mM_1-WT) or CNO (M_1-DREADD and M_1-DREADD-PD). (**c, e**) Close up sections from highlighted areas in (**b, d**) showing punctate dots of internalised receptors (red arrow) in all apart from M_1-DREADD-PD cell lines. Red scale bars equate to 20µm.

3.3 Discussion

This chapter presents the data from pharmacological and functional studies used to understand the behaviour of the M_1-DREADD and DREADD-PD mAChRs in relation to the hM_1-WT and mM_1-WT mAChRs. Data in the original DREADD paper (Armbruster et al., 2007) studied the function and pharmacology of the M_1-M_5 WT and DREADD mAChRs, investigating function with calcium mobilisation and inositol phosphate accumulation. Data showing the effects of the PD mutations on M_1 mAChR function had not been previously published. Before introducing these mutant receptors into an animal model for behavioural experimentation it is important that the effects of the modifications have been fully understood.

Saturation binding studies using ^{3}H-NMS and western blotting confirmed receptor expression; and immunocytochemistry showed the wild-type and mutant receptors were expressed at the cell membrane. Radioligand binding found no species difference between the affinity of ^{3}H-NMS binding at the human and mouse M_1-mAChRs. With the M_1-DREADD and M_1-DREADD-PD mAChRs, the maximum concentrations of ^{3}H-NMS used were not high enough to reach a saturating concentration. Without reaching saturating concentrations it is not possible to accurately determine the affinity of ^{3}H-NMS for the M_1-DREADD and M_1-DREADD-PD mAChRs. Another method of determining radioligand binding affinity is using association and dissociation binding. For human and mouse M_1-WT mAChRs, estimates of pK_d calculated using this method were comparable to those calculated using saturation binding. This method however was not successful in determining the K_d of NMS at the DREADD mutant receptors. Curves were fitted to the data for both association and dissociation rate data, but the fit for these curves was too poor to determine an accurate estimate of the affinity. Although neither method I used was able to determine the affinity of ^{3}H-NMS, the results seen would be expected from the DREADD mutations reducing the binding affinity of orthosteric ligands. The reduction in the K_d of ^{3}H-NMS at the M_1-DREADD and M_1-DREADD-PD mAChRs was later confirmed in homologous competition binding studies carried out by Dr. Sophie Bradley (Fig. 3.14, Table 3.3). Homologous competition binding involves competing off a single concentration of radiolabelled ligand with the unlabelled form, in this case ^{3}H-NMS and unlabelled NMS. The pK_d of NMS using homologous competition at the hM_1-WT and

mM_1-WT mAChRs, 9.61 ± 0.07 and 9.51 ± 0.08, were similar to the values acquired using saturation binding studies, 9.49 ± 0.16 and 9.34 ± 0.01. This assay was able to determine the binding affinity of NMS for both the M_1-DREADD and M_1-DREADD-PD mAChRs, 7.68 ± 0.05 and 7.65 ± 0.05 respectively. These data confirms that the DREADD mutations have interfered with the binding of orthosteric ligands to the receptor binding pocket.

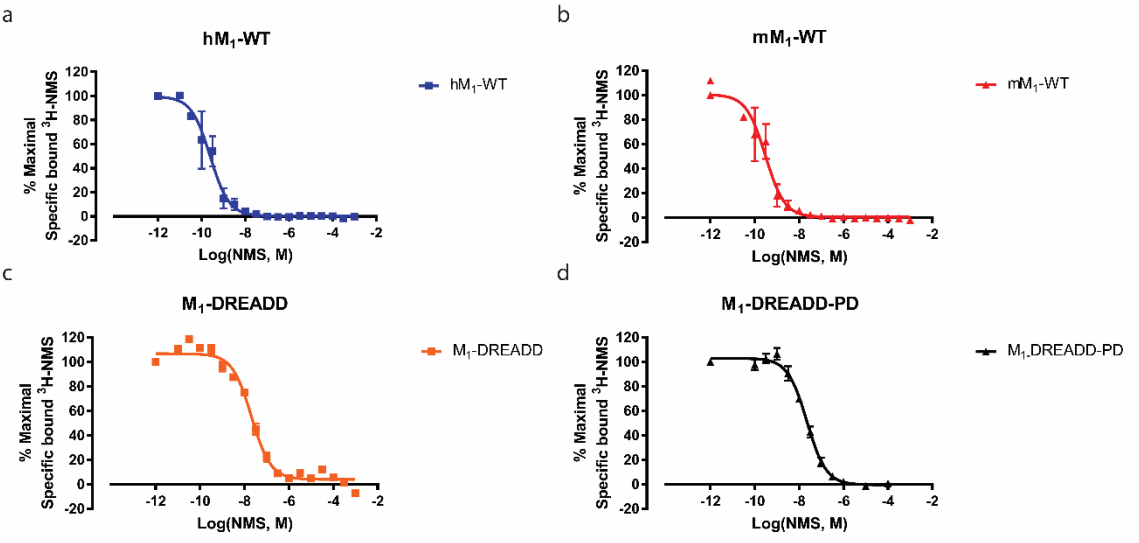

Figure 3.14: Homologous competition binding curves using ^{3}H-NMS and unlabelled NMS. Experiments carried out by Dr. Sophie Bradley.

Homologous competition experiments were carried out on hM_1-WT (**a**), mM_1-WT (**b**), M_1-DREADD (**c**), and M_1-DREADD-PD (**d**) mAChRs, competing off a single concentration of ^{3}H-NMS with increasing concentrations of unlabelled NMS. Experiments were carried out in the presence and absence of a saturating concentration of atropine to determine the non-specific and total binding respectively. Non-specific binding was subtracted from the total to provide a value for specific bound ^{3}H-NMS. Data are shown as mean ± SEM; n=3-4

	hM_1-WT	mM_1-WT	M_1-DREADD	M_1-DREADD-PD
pK_d	9.61 ± 0.07	9.51 ± 0.08	7.68 ± 0.05	7.65 ± 0.05

Table 3.3: Homologous competition radioligand binding with the hM_1-WT, mM_1-WT, M_1-DREADD, and M_1-DREADD-PD mAChRs using ^{3}H-NMS and unlabelled NMS.

Data are shown as mean ± SEM; n=3-4.

Functional studies were performed to confirm the ability of the DREADD mutations to change the potency and relative efficacy of acetylcholine and CNO. ERK 1/2 activation, inositol phosphate accumulation, and calcium mobilisation assays were used, all of which are G-protein dependent signalling pathways. Functional assays confirmed the ability of the DREADD mutations to reduce the potency of acetylcholine at the M_1-mAChR. At the human and mouse M_1-mAChRs functional assays also showed the weak partial agonism of the receptors by CNO. This agonism has been identified previously (Armbruster et al., 2007) but it would be beneficial to perform further studies on the pharmacology of CNO at the wild-type mAChRs. Being a partial agonist, CNO may illicit an antagonistic effect on wild-type receptors *in vivo* as has been described with other partial agonists (Hoyer and Boddeke, 1993). Although CNO was found to be selective for the M_1-DREADD and M_1-DREADD-PD mAChRs over the wild-type, antagonism of other mAChRs may make it necessary to identify other, more selective ligands to use for the chemical genetic approach. A study generating of a series of ligands based on clozapine, and their characterisation alongside a small group of other benzodiazepine compounds, (Chen et al., 2015) identified perlapine and DREADD agonist 21 as potential alternatives to CNO.

To assess the effects of the phosphorylation-deficient mutations on GPCRs, agonist induced internalisation was studied using ICC. Following agonist stimulation, human and mouse M_1-WT and M_1-DREADD mAChRs were found to internalise. There was no agonist induced internalisation seen in the M_1-DREADD-PD cell line following 1 hour of stimulation. This confirms that the mutations used to generate our phosphorylation-deficient receptor have successfully altered phosphorylation-dependent signalling. The findings align with previous studies using a phosphorylation-deficient M_3-mAChR model where a reduction in agonist induced β-arrestin-2 recruitment was observed (Kong et al., 2010; Poulin et al., 2010). The removal of intracellular phosphorylation sites was found to alter the signalling of the M_1-DREADD mAChR. Previously, removal of intracellular phosphorylation sites at the M_3-mAChR raised the plateau following the signalling peak in calcium signalling assays (Kong et al., 2010). This raising in the plateau being due to a lack in receptor desensitisation halting G-protein-dependent signalling. In my own calcium signalling assay (Fig. 3.11) this same prolonged signalling can be seen

when comparing M_1-DREADD and M_1-DREADD-PD intracellular calcium time courses. In my functional assays, acetylcholine and CNO were both found to have a higher potency at the M_1-DREADD-PD mAChR than at the M_1-DREADD mAChR. The loss of receptor desensitisation will allow for continued G-protein-dependent signalling to occur, increasing the relative efficacy of lower concentrations of ligands.

Overall, the above data supports the conclusion that the DREADD and PD mutant models used for our chemical genetic approach have successfully altered the function and pharmacology of the M_1-mAChR. Although the modifications are successful, findings around the partial agonist properties of CNO require further study. CNO has been used successfully in previous *in vivo* studies using DREADD receptors (Fortress et al., 2015; Parnaudeau et al., 2015; Sco et al., 2015; Yau and Mcnally, 2015) it is important to characterise and understand these interactions. The next chapter (see Chapter 4) will focus on characterising the relationship between CNO and the M_1-M_4 mAChRs, and performing the initial functional characterisation of perlapine and DREADD agonist 21 at the human and mouse M_1-, M_1-DREADD, and M_1-DREADD-PD mAChRs.

Chapter 4 Characterisation of Clozapine N-Oxide to Assess its Suitability for *in vivo* Models.

4.1 Introduction

In studying the role of the M_1-mAChR *in vivo*, a key advantage to the DREADD mAChR model is the selectively of the biologically inert ligand; in this case, CNO. However, the results in Chapter 3 have shown that CNO acts as a weak partial agonist at both the human and mouse M_1-WT mAChRs. Along with its weak agonist activity at the wild-type M_1-mAChRs, it is possible for CNO, as a partial agonist, to act in an antagonist mode in the presence of an orthosteric agonist (Henderson et al., 1990; Paronis et al., 2012; Rollema et al., 2007). Depending on the selectivity of CNO for the M_1-DREADD and M_1-DREADD mAChRs, the dose of CNO administered to our genetically engineered mice for *in vivo* studies could partially activate native mAChRs or antagonise the signalling of acetylcholine. Although *in vivo* studies have indicated that CNO has little off target activity (Alexander et al., 2009; Ray et al., 2011), the potential of CNO as an antagonist of acetylcholine signalling at wild-type mAChRs has yet to be considered fully. In this chapter I aim to explore this possible antagonistic mode, investigating whether CNO is able to interfere with *in vitro* acetylcholine signalling at the M_1-, M_2-, M_3-, and M_4-mAChRs.

In addition to the characterisation of CNO I will test recently published alternative ligands for the DREADD mAChRs. Pharmacokinetic studies of CNO have detected clozapine in the plasma and urine of guinea pigs, Long-Evans rats and humans (Jann et al., 1994; MacLaren et al., 2016) and both NDMC and clozapine have been identified in Lewis rat urine (Lin et al., 1996). Both clozapine and NDMC have well characterised activity with multiple GPCR families present within the central nervous system (Heinrich et al., 2009; Wenthur and Lindsley, 2013). These metabolites may not be present in mice due to interspecies differences in metabolism (Graham and Lake, 2008; Hucker, 1970), however their potential presence, as well as the weak partial agonism of CNO, prompted research into alternative ligands for these DREADD mAChRs. A second generation of DREADD ligands have been developed to avoid the potential confounding factors of CNO. Two benzodiazepine ligands, perlapine and DREADD agonist 21 (DA21), have been

proposed as agonists for the DREADD system, following pharmacological and functional screens at a panel of wild-type GPCRs and the M_3-DREADD mAChR. These ligands were found to be highly selective for the M_3-DREADD mAChR over the wild-type receptors, including the hM_3-WT mAChR (Chen et al., 2015), and fully activated the receptor in the calcium signalling assays. In this chapter I will perform functional assays comparing DA21 and perlapine to CNO at the mutant M_1-mAChRs, and to acetylcholine and CNO at the wild-type M_1-mAChRs.

4.2 Results

4.2.1 Competition Binding– hM_1, mM_1-WT mAChRs

Functional assays performed on the human and mouse M_1-WT mAChRs previously have shown that CNO is a partial agonist (Fig 3.4-10). As weak partial agonist, CNO may be able to compete for the orthosteric binding site and inhibit the activity of a full agonist such as acetylcholine. Here I used competition radioligand binding to compare the pK_i values of acetylcholine and CNO.

Competition radioligand binding (Fig 4.1) is a technique used to investigate the binding affinity of a ligand using a radiolabelled antagonist with a known affinity. Human and mouse M_1-WT cell lines were pretreated with increasing concentrations of CNO (10 nM to 1 mM) and acetylcholine (10 nM to 10 mM) after which ^{3}H-NMS was added at a K_d concentration and incubated at 37.5°C for 1 hour. One well for each experiment was pretreated with a high concentration of atropine to determine the non-specific binding. The pK_i of CNO was found to be around half a log higher than that of acetylcholine at both human M_1-WT (Fig 4.1 a), 5.31 ± 0.06 and 5.85 ± 0.03 respectively, and the mM_1-WT (Fig 4.1 b), 5.19 ± 0.05 and 5.65 ± 0.05 respectively. Welch's t-test, used over the student's t-test for the comparison of these independent samples, found a significant difference was found between the CNO and acetylcholine at the hM_1-WT and between CNO and acetylcholine at the mM_1-mAChR. Depending on the concentration of acetylcholine released within the cholinergic synapse, and the dose of CNO required for *in vivo* studies, this means CNO may be able to interfere with acetylcholine signalling. Further investigations need to be made into any functional antagonism CNO may exhibit on the activity of acetylcholine, as well as its pharmacological and functional properties with the other members of the mAChR family.

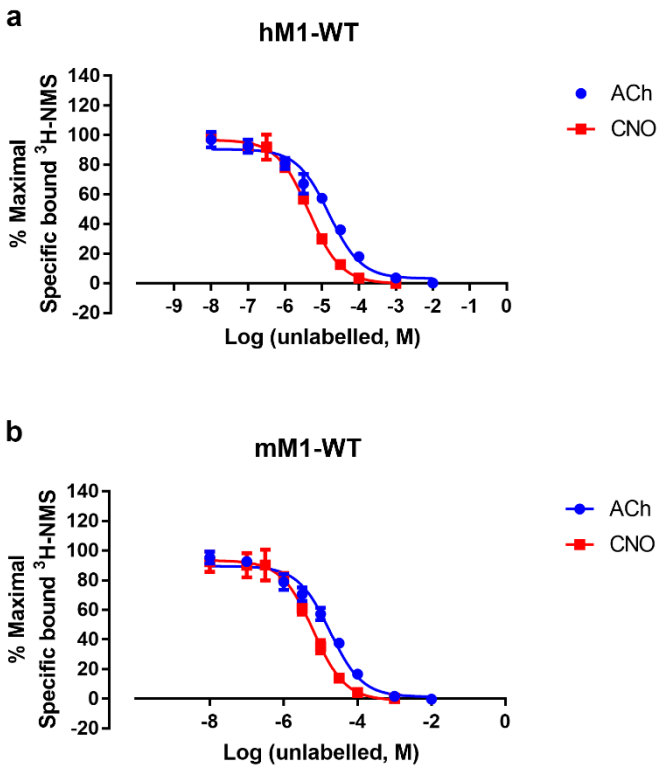

Figure 4.1: Competitive interactions of acetylcholine and CNO and the hM_1-WT and mM_1-WT mAChRs.

Cells expressing hM_1-WT (**a**), mM_1-WT (**b**), were pretreated for 15 minutes with increasing concentrations of acetylcholine or CNO before incubation with a K_d concentration of ^{3}H-NMS for 1 hour. Reaction was terminated by washing with ice-cold buffer and lysis with 0.1M NaOH. Data were collected by liquid scintillation counting of the lysate. Data are shown as mean ± SEM; n=3.

4.2.2 Functional Antagonism – hM_1, mM_1-WT mAChRs

Competition radioligand binding data (Fig 4.1) showed that CNO was able to displace the radiolabelled antagonist ^{3}H-NMS from both the human and mouse M_1 mAChRs. CNO was only found to evoke a weak response in ERK 1/2 activation, IP-One, and calcium cell signalling assays (Fig 3.4-10) suggesting that CNO may have other pharmacological activities. To investigate if CNO can inhibit the signalling of the full agonist acetylcholine, functional antagonism experiments were performed using the HTRF IP-one assays.

Cells expressing the hM1-WT and mM1-WT mAChR were initially pre-treated for 30 minutes with increasing concentrations of CNO (1 nM - 10 µM) followed by the addition of acetylcholine. Atropine was included in the assay as a control to confirm the validity of the assay. 10 µM of CNO was chosen as the top concentration as in previous experiments this concentration was shown to be the lowest concentration to activate the receptor. With hM1-WT and mM1-WT, the control experiments confirmed the antagonistic properties of atropine, producing pA_2 values of 8.38 ± 0.07 and 9.04 ± 0.08 respectively, which are similar to the reported K_d values for atropine (Birdsall et al. 2016). In hM1-mAChR expressing cell line, there is no observed rightward shift in the acetylcholine concentration response curve following treatment with CNO (Fig 4.2 b (i)). The basal level of receptor activation was increased with 10µM CNO. This is consistent with previous data (Fig 3.8) showing that 10 µM CNO was able to evoke receptor response. CNO was observed to weakly antagonise acetylcholine signalling at the mM1-WT mAChR at CNO concentrations above 1 µM (Fig 4.2 d (i)). Although this apparent functional antagonism is low (pA_2 ~ 5.4) it may still be an important consideration in the selection of the doses of CNO for *in vivo* experiments. The conservation of residues within the orthosteric binding pocket through members of the mAChR family means the functional antagonism seen within the mouse M_1 mAChR could also been observed in other mAChR subtypes.

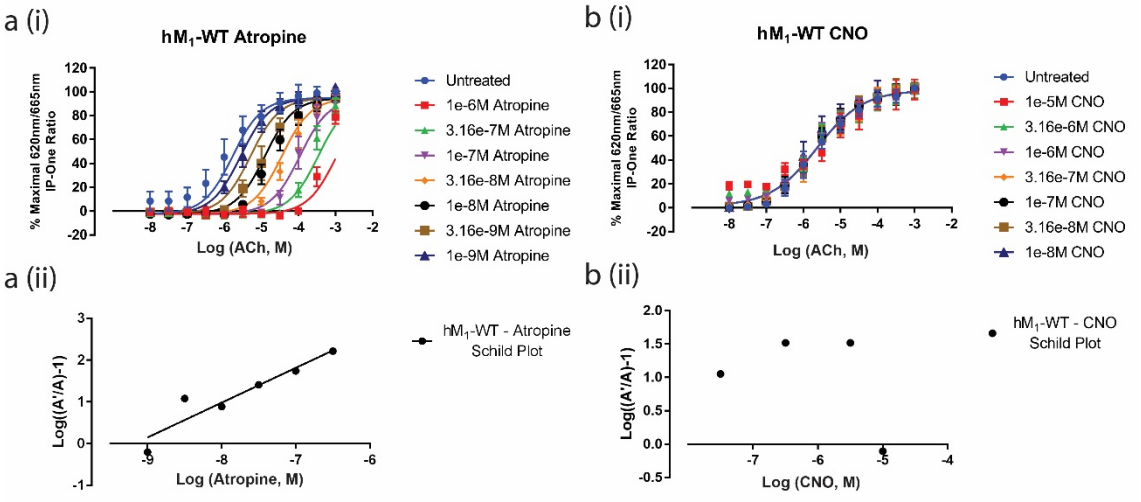

Figure 4.2: Effects of CNO and atropine on acetylcholine-mediated signalling of human and mouse wild-type M_1 mAChRs.

Cells expressing the human M1 mAChRs were pre-treated with increasing concentrations of either atropine (**a**) or CNO (**b**) for 30 min at 37°C before stimulation with acetylcholine for 2 h at 37°C. Receptor stimulation was terminated by rapid aspiration of the media, and cellular signalling was detected using the HTRF IP-One assay. (i) Curves show non-linear regression analysis of concentration response curves after pre-treatment for 30 min with increasing concentrations of atropine or CNO; including untreated control. (ii) Schild analysis of respective data sets. Data are shown as mean ± SEM; n=3.

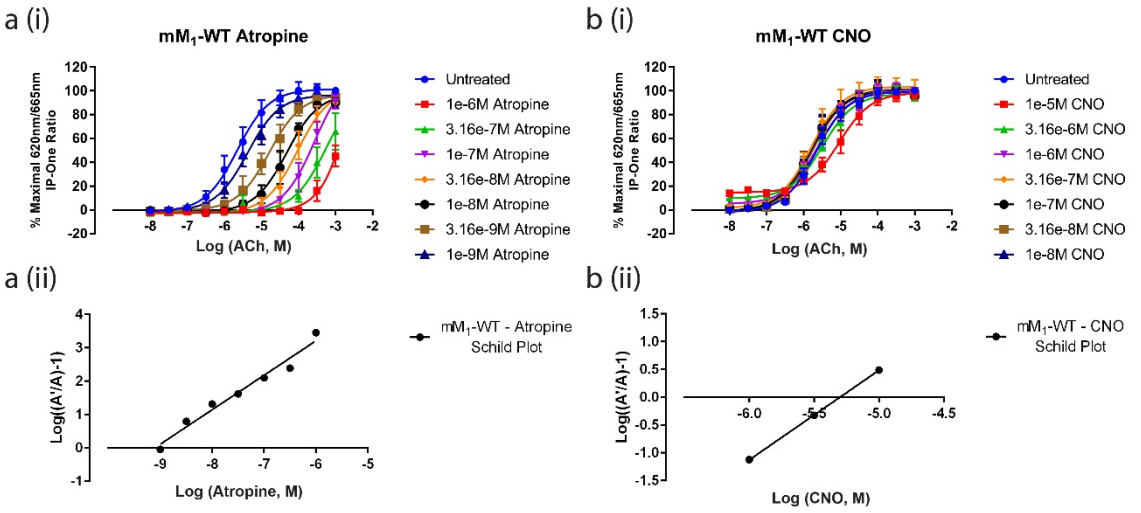

Figure 4.3: Effects of CNO and atropine on acetylcholine-mediated signalling of human and mouse wild-type M_1 mAChRs continued.

Cells expressing the mouse M1 mAChRs were pre-treated with increasing concentrations of either atropine (a, c) or CNO (b, d) for 30 min at 37°C before stimulation with acetylcholine for 2 h at 37°C. Receptor stimulation was terminated by rapid aspiration of the media, and cellular signalling was detected using the HTRF IP-One assay. (i) Curves show non-linear regression analysis of concentration response curves after pre-treatment for 30 min with increasing concentrations of atropine or CNO; including untreated control. (ii) Schild analysis of respective data sets. Data are shown as mean ± SEM; n=3.

		hM_1-WT	mM_1-WT
Competition Binding			
pK_i	ACh	5.31 ± 0.06	5.19 ± 0.05
	CNO	5.85 ± 0.03	5.65 ± 0.05
p-value		<0.001	<0.001
Functional Antagonism			
pA_2	Atropine	8.38 ± 0.07	9.04 ± 0.08
	CNO	*	5.35 ± 0.09

Table 4.1: Competitive properties of CNO at the human and mouse M_1-WT mAChRs.

* No functional antagonism was seen. Data are shown as mean ± SEM; n=3.

4.2.3 Saturation Binding – M_2, mM_3, hM_4-WT mAChR

To quantify the K_d of CNO in cell lines expressing other members of the mAChRs, saturation binding needs to be performed on these cells to calculate the K_d of ^{3}H-NMS and compare the B_{max} values of each cell line.

Saturation binding studies (Fig 4.4) were performed on M_2, mM_3, and M_4-WT expressing cell lines. Cells were incubated for 1.5 hours with increasing concentrations of ^{3}H-NMS (300 pM – 10 nM) in the presence and absence of a saturating concentration of atropine. Saturation binding found that the M_2, mM_3, and M_4-mAChRs had comparable K_d values, 9.54 ± 0.11, 9.49 ± 0.08, and 9.29 ± 0.08 respectively. Studies found that the B_{max} for the M_2-WT, 570.6 ± 34.4 fmol mg^{-1} protein, and M_4-WT, 664.8 ± 37.36 fmol mg^{-1} protein, are similar, although half that of the hM_1-WT and mM_1-WT cell lines, 1171 ± 77.6 and 1418 ± 85.6 fmol mg^{-1} protein respectively. The B_{max} of the mM_3-WT cell line was lower, 182.3 ± 8.3 fmol mg^{-1}, than any of the other wild-type expressing cell lines.

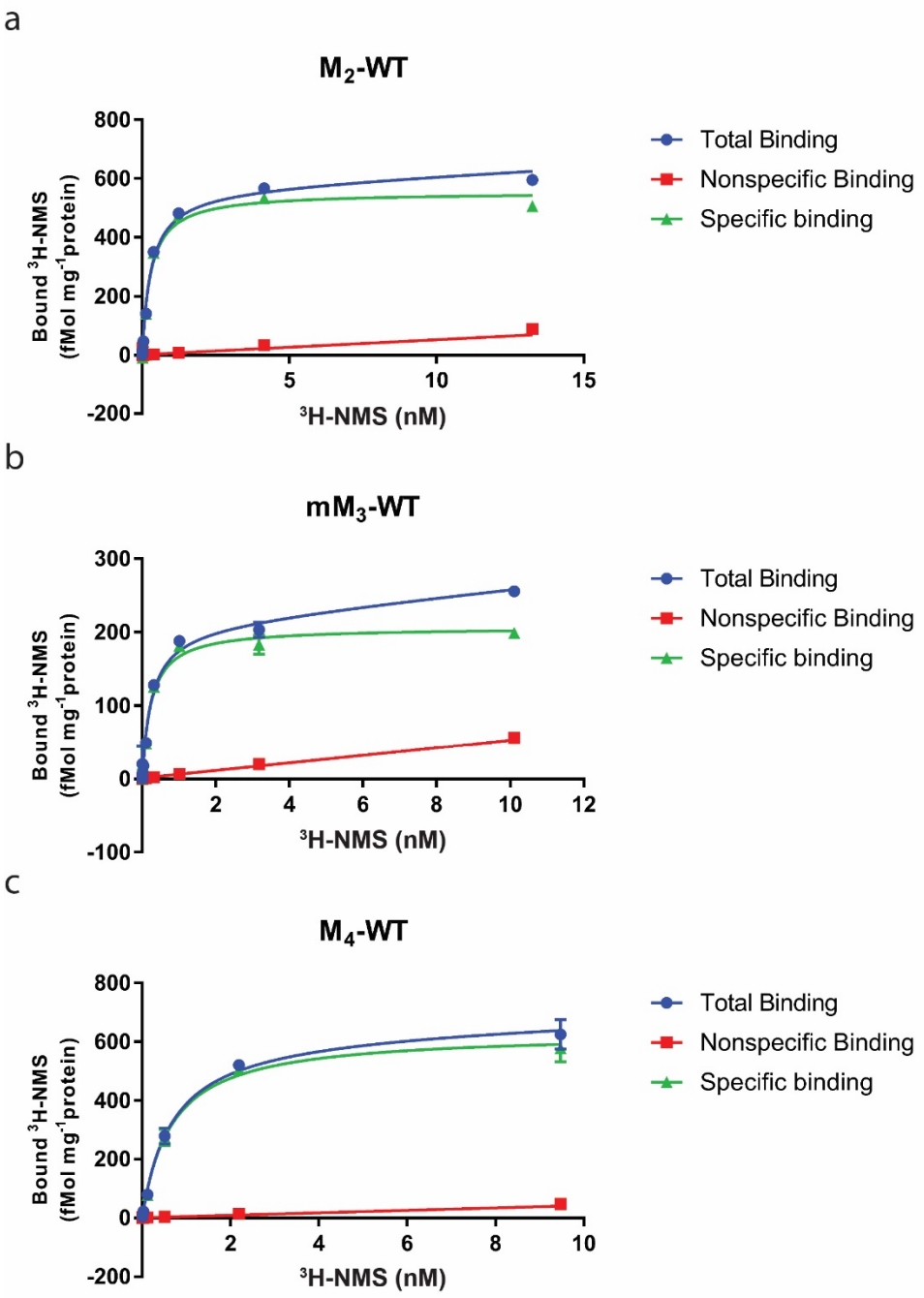

Figure 4.4: Saturation binding studies at the M_2-WT, mM_3-WT, and M_4-WT mAChRs with ^{3}H-NMS.

In saturation binding studies, cells expressing M_2-WT (**a**), mM_3-WT (**b**), and M_4-WT (**c**) mAChRs were incubated with increasing concentrations of ^{3}H-NMS, in the presence and absence of a saturating concentrations of atropine, for 1 hour at 37°C. Cells were washed with ice-cold 0.9% NaCl and lysed with 0.1M NaOH. Radioactivity was measured by liquid scintillation counting. Curves shown are representative of data n=3.

4.2.4 Competition Radioligand Binding – M_2, mM_3, hM_4-WT mAChR

Competition radioligand binding with the human and mouse M_1-mAChRs (Fig 4.1) found CNO can fully dissociate ^{3}H-NMS. The conservation of residues between the muscarinic acetylcholine receptors (Thal et al., 2016) means that CNO may interact competitively with other members of the mAChR family. To investigate these interactions, competition binding studies were performed on M_2-WT, mM_3-WT and hM_4-WT expressing cell lines.

Competition binding at the hM_1-WT and mM_1-WT mAChRs found CNO competitively bound to the receptor, which would suggest that it will also competitively interact with other members of the mAChR family. Using K_d concentrations of ^{3}H-NMS, it was found that the CNO did not fully dissociate the radioligand; however, the curves were not found to reach a lower plateau (Fig 4.5 (iii)). To investigate this further competitive binding using 2 more concentrations of ^{3}H-NMS, ~10x K_d, and ~0.25x K_d ^{3}H-NMS was performed. Using a lower concentration of ^{3}H-NMS it may be possible to determine the K_i of CNO. Observations of the 3 curves can be made to identify the mode of interaction of CNO. If the interaction is competitive then the change in radioligand concentration will cause the competition curve to shift. If the interaction is allosteric then the reduction in radioligand binding would be due to negative cooperativity, and there would not be a shift in the competition curve with differing radioligand concentrations. With the M_2, M_3, and M_4-mAChRs, there is a shift in competition binding curves for CNO between the differing concentrations of radioligand, suggesting that it is competing for ^{3}H-NMS, in line with the human and mouse M_1-mAChRs where CNO was found to bind competitively also (Fig 4.5). Using 0.25-0.3 K_d concentrations of ^{3}H-NMS in competition binding studies at the M_2, mM_3, and hM_4-WT mAChRs the pK_i of CNO were calculated as, 3.85 ± 0.11, 3.05 ± 0.23 and 3.16 ± 0.20 respectively. This shows that CNO has a markedly lower affinity than acetylcholine for the M_2, mM_3, and mM_4-WT mAChRs, around 1-2 orders of magnitude lower.

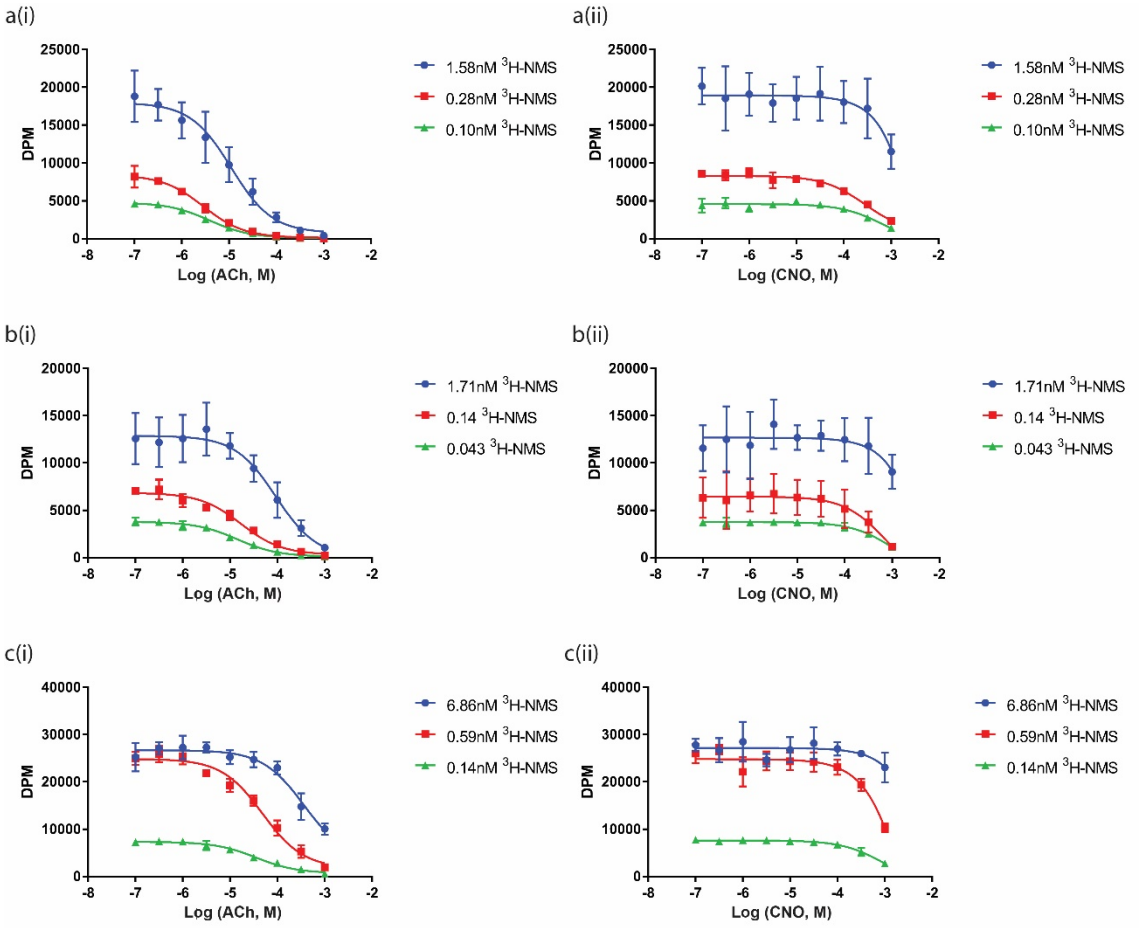

Figure 4.5: Competition binding assays with acetylcholine and CNO at M_2-WT, mM_3-WT and hM_4-WT mAChRs.

Competition binding studies were performed on M_2-WT (**a**), mM_3-WT (**b**), and hM_4-WT (**c**) expressing cell lines. Cell lines were pretreated with increasing concentrations of acetylcholine (**i**) or CNO (**ii**) for 15 minutes before incubating for 1 hour with 3 concentrations of ^{3}H-NMS. Reactions were terminated by washing with ice cold 0.9% NaCl. Cells were lysed with 0.1M NaOH and radioactivity calculated using LSC. Data are shown as mean ± SEM; n=3.

4.2.5 ERK1/2 Activation – M_2, mM_3, hM_4-WT mAChR

Functional studies have identified CNO as a weak partial agonist of the human and mouse M_1-mAChRs, and competition binding has found that CNO competitively interacts with M_2-WT, mM_3-WT and hM_4-WT mAChRs (Fig. 4.4). To test whether CNO is also a partial agonist of the M_2, M_3, and M_4-mACHRs, ERK 1/2 activation assays were performed using the HTRF assay kits. Treatment with increasing concentrations acetylcholine produced pEC_{50} values of 7.94 ± 0.13, 7.17 ± 0.13, and 7.64 ± 0.13 for the M_2, M_3, and hM_4-WT mAChRs respectively. CNO was not found to have any agonistic properties of the M_2, M_3, or M_4-mAChRs, not eliciting any detectible increase in ERK 1/2 phosphorylation over basal levels with up to 100 μM of CNO. This lack of detected agonism may be due to the weaker interaction between CNO and these mAChRs observed in the competition binding studies.

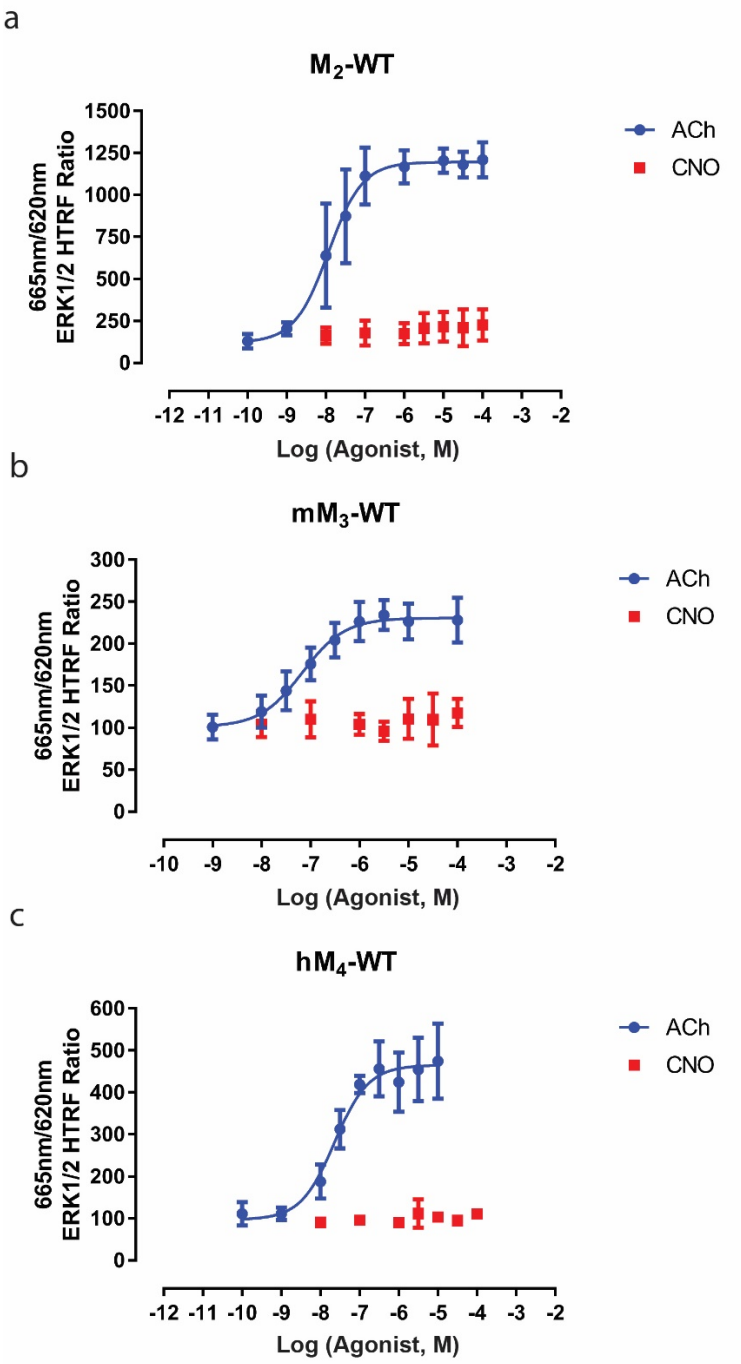

Figure 4.6: Concentration dependent activation of ERK 1/2 by acetylcholine and CNO at the M_2, M_3, and hM_4-WT mAChRs using HTRF.

Cells expressing M_2-WT (**a**), mM_3-WT (**b**), and hM_4-WT (**c**) mAChRs were treated with increasing concentrations of acetylcholine or CNO for 5 minutes. Reaction was terminated by removal of the stimulation buffer and lysis of the cells. A portion of the lysate was then mixed for a minimum of 2 hours with ERK 1/2 HTRF kit antibodies and the samples were measured using a CLARIOstar plate reader. Data are shown as mean ± SEM; n=3.

4.2.6 Functional Antagonism – M_2, mM_3, hM_4-WT mAChR

I have previously found that CNO competes with ^{3}H-NMS at the M_2, mM_3, hM_4-WT mAChRs (Fig. 4.5), but has no detectible agonism in the ERK 1/2 activation assay up to 100μM (Fig. 4.6). As with the mouse M_1-mAChR (Fig. 4.2(d)) this suggests that CNO may antagonise acetylcholine signalling at M_2, mM_3, or hM_4 mAChRs. To investigate this, a functional antagonism assay was carried out using the ERK 1/2 HTRF assay kit (Fig. 4.6).

Cells expressing M_2-WT, mM_3-WT, and hM_4-WT mAChRs were preincubated with increasing concentrations of CNO (1 μM to 100 μM) or atropine (10 nM to 1 μM) as a control, after which they were treated with increasing concentrations of acetylcholine (1pM to 1mM). 100 μM was chosen as the maximum dose of CNO as using higher concentrations would be prohibitively expensive and the concentration of CNO within experimental animals would never be this high. Gaddum/Schild analysis of the atropine functional antagonism data with M_2-WT, mM_3-WT, and hM_4-WT produced pA_2 values, 8.65 ± 0.07, 9.21 ± 0.20, 9.82 ± 0.17 respectively, which were within the range of reported K_d values for atropine (Christopoulos et al., 2017). At the mM_3-WT mAChR, no shift was seen with CNO in the concentration-response curve of acetylcholine, meaning CNO did not act as a functional antagonist within this concentration range. At the M_2-WT and hM_4-WT mAChRs CNO antagonised acetylcholine signalling, causing a rightward shift in the concentration-response curves. At the M_2-WT mAChR the Schild analysis produced a pA_2 value of 4.32 ± 0.12. This value is lower than at the mM_1-WT mAChR and correlates with the lower affinity of CNO for the M_2-WT mAChR. At the hM_4-WT mAChR however, CNO is a more potent antagonist of acetylcholine signalling, with the Schild analysis producing a pA_2 value of 6.07 ± 0.13. This higher pA_2 value does not correlate with the pK_i calculated for CNO at the hM_4-WT mAChR, 3.16 ± 0.20; the interaction between CNO and the hM_4-WT mAChR being the weakest of all the mAChRs tested. This may be due to the reduced affinity of ACh for the hM_4-WT mAChR compared to the other mAChRs tested, which would mean a lower concentration of CNO was required to compete with acetylcholine.

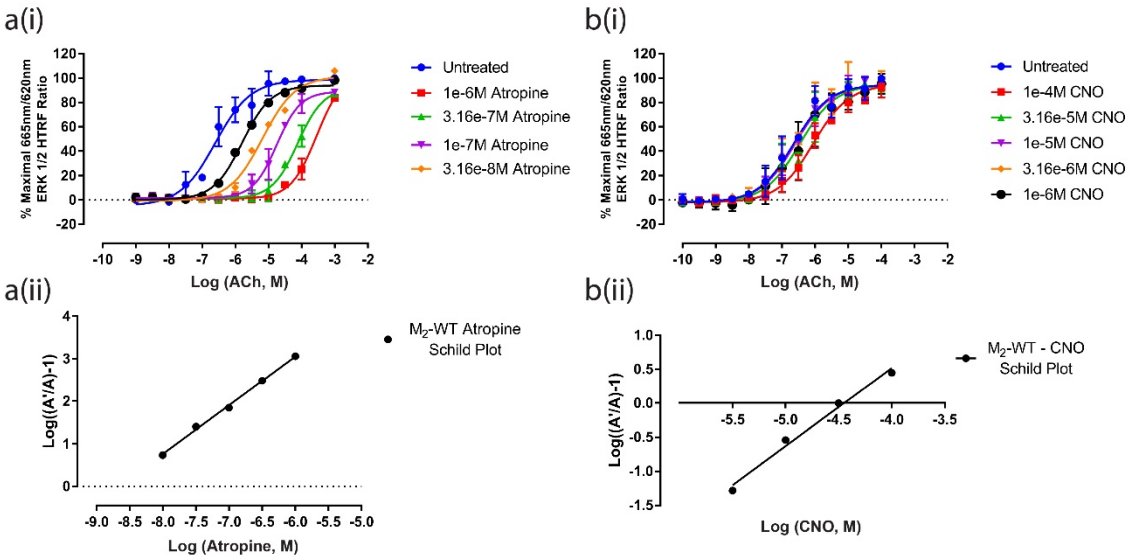

Figure 4.7: Effects of Atropine and CNO on acetylcholine activation of the M_2-WT, mM_3-WT, and hM_4-WT mAChRs using the ERK 1/2 activation HTRF assay.

Cells expressing M_2-WT mAChR were preincubated with increasing concentrations of atropine (**a**) or CNO (**b**) for 15 minutes before treatment with increasing concentrations of acetylcholine for 5 minutes. Reactions were halted with removal of the stimulation buffer and lysis of the cells. A portion of the lysate was then mixed for a minimum of 2 hours with ERK 1/2 HTRF kit antibodies and the samples were measured using a CLARIOstar plate reader. (i) Curves show non-linear regression analysis of concentration response curves after pre-treatment for 30 min with increasing concentrations of atropine or CNO; including untreated control. (ii) Schild analysis of respective data sets. Data are shown as mean ± SEM; n=3.

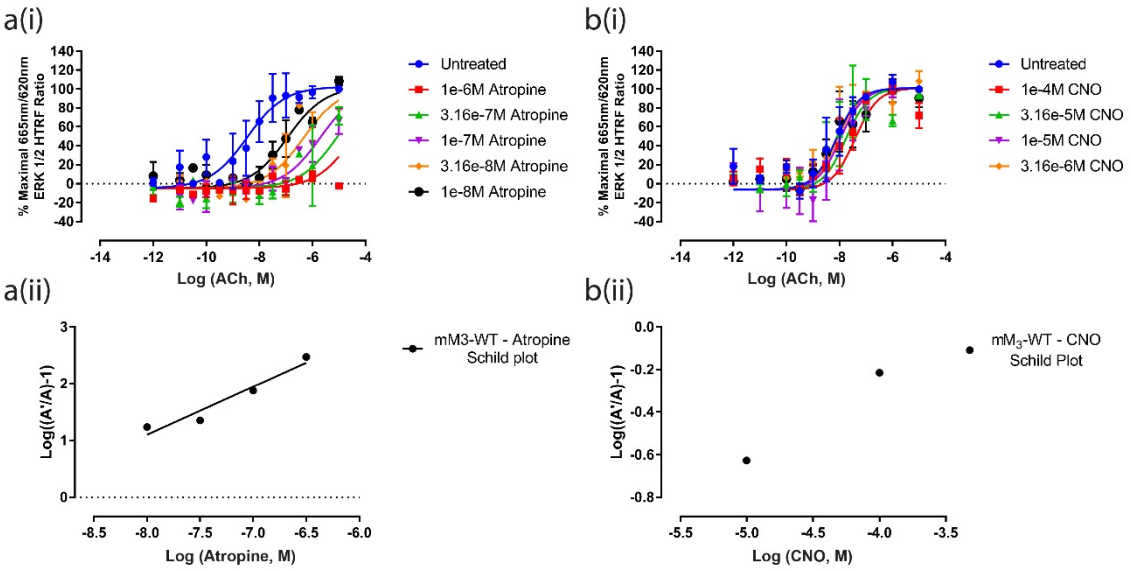

Figure 4.8: Effects of Atropine and CNO on acetylcholine activation of the M_2-WT, mM_3-WT, and hM_4-WT mAChRs using the ERK 1/2 activation HTRF assay continued.

Cells expressing mM_3-WT mAChRs were preincubated with increasing concentrations of atropine (**a**) or CNO (**b**) for 15 minutes before treatment with increasing concentrations of acetylcholine for 5 minutes. Reactions were halted with removal of the stimulation buffer and lysis of the cells. A portion of the lysate was then mixed for a minimum of 2 hours with ERK 1/2 HTRF kit antibodies and the samples were measured using a CLARIOstar plate reader. (i) Curves show non-linear regression analysis of concentration response curves after pre-treatment for 30 min with increasing concentrations of atropine or CNO; including untreated control. (ii) Schild analysis of respective data sets. Data are shown as mean ± SEM; n=3.

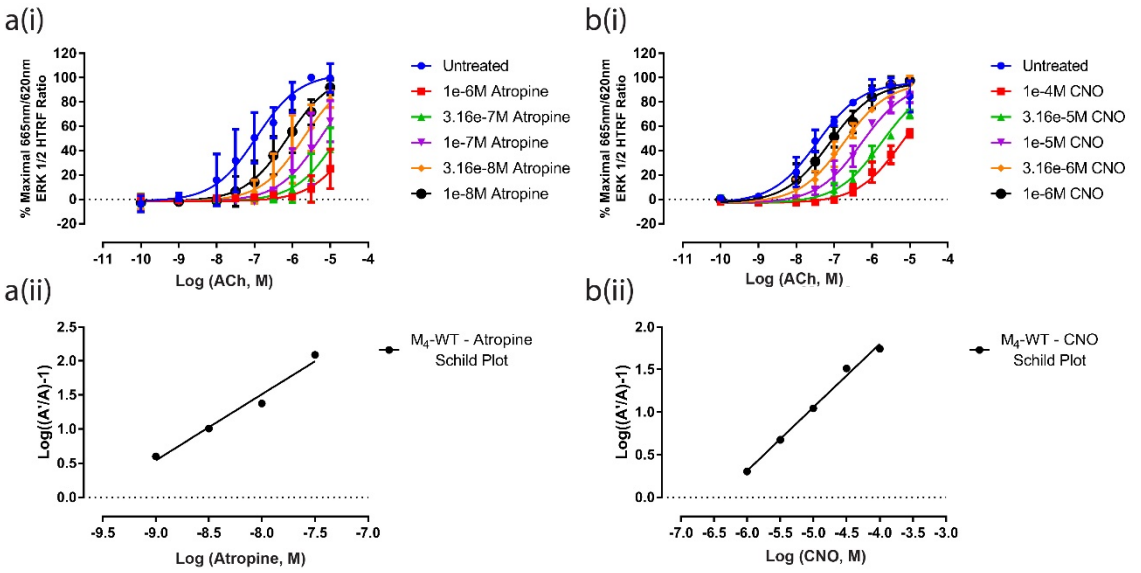

Figure 4.9: Effects of Atropine and CNO on acetylcholine activation of the M_2-WT, mM_3-WT, and hM_4-WT mAChRs using the ERK 1/2 activation HTRF assay continued.

Cells expressing hM_4-WT mAChRs were preincubated with increasing concentrations of atropine (**a**) or CNO (**b**) for 15 minutes before treatment with increasing concentrations of acetylcholine for 5 minutes. Reactions were halted with removal of the stimulation buffer and lysis of the cells. A portion of the lysate was then mixed for a minimum of 2 hours with ERK 1/2 HTRF kit antibodies and the samples were measured using a CLARIOstar plate reader. (i) Curves show non-linear regression analysis of concentration response curves after pre-treatment for 30 min with increasing concentrations of atropine or CNO; including untreated control. (ii) Schild analysis of respective data sets. Data are shown as mean ± SEM; n=3.

		M_2	mM_3	hM_4
Saturation binding				
B_{max}		570.6 ± 34.4	182.3 ± 8.3	664.8 ± 37.4
pK_d		9.54 ± 0.11	9.49 ± 0.08	9.29 ± 0.08
Competition Binding				
pK_i	ACh	5.84 ± 0.06	4.92 ± 0.08	4.64 ± 0.08
	CNO	3.85 ± 0.11	3.05 ± 0.23	3.16 ± 0.20
ERK 1/2 activation - HTRF				
pEC_{50}	ACh	7.94 ± 0.13	7.17 ± 0.13	7.64 ± 0.13
	CNO	*	*	*
Functional Antagonism				
pA_2	Atropine	8.65 ± 0.07	9.21 ± 0.20	9.82 ± 0.17
	CNO	4.32 ± 0.12	+	6.07 ± 0.13

Table 4.2: Functional and pharmacological characterisation of CNO and acetylcholine at the M_2, mM_3, and hM_4 mAChR.

* Concentrations of ligand used were not high enough to generate a full concentration response curve. + No functional antagonism was seen. Data are shown as mean ± SEM; n=3.

4.2.7 Alternative DREADD mAChR ligands

These interactions, as well as the potential for CNO to be metabolised into its parent molecule clozapine (Chang et al., 1998; Lin et al., 1996), suggest potential confounding factors when using the ligand *in vivo*. Although CNO has been successfully used in the past with DREADD mAChR models, the interactions of CNO with wild-type mAChRs characterised here and its metabolism into clozapine are potential confounding factors in *in vivo* studies. The identification and implementation of more selective compounds, and compounds which are not metabolised into bioactive molecules such as clozapine, for DREADD mAChR models could negate the possible off-target effects of CNO. Two alternative ligands have been proposed for use with the mAChR DREADDs, DREADD Agonist 21 (DA21) and perlapine (Chen et al., 2015). As an initial assessment, here I have compared them to acetylcholine and CNO at the hM_1-WT and mM_1-WT mAChRs and to CNO at the M_1-DREADD and M_1-DREADD-PD mAChRs using the IP-One accumulation HTRF assay.

At the hM_1-WT and mM_1-WT mAChRs, cells were treated with increasing concentrations of acetylcholine (1 nM to 10 mM), CNO, DA21, or perlapine (10 nM to 100 µM). For the M_1-DREADD and M_1-DREADD-PD mAChRs, cells were treated with increasing concentrations of CNO, DA21, or perlapine (1 pM to 10 µM). At both hM_1-WT and mM_1-WT mAChRs, perlapine concentrations used produced no agonist response, and DA21 only appearing to act as a weak partial agonist. At the M_1-DREADD mAChR, DA21, 8.54 ± 0.04, and perlapine, 8.20 ± 0.03, both achieved higher pEC_{50} values than CNO, 7.86 ± 0.02, and reach comparable E_{max} values. The higher potency of both perlapine and DA21 presents these ligands as potentially beneficial alternatives; however the novelty of DA21 (Chen et al., 2015) and the sedative properties of perlapine (Stille et al., 1973) means the pharmacology and function of these ligands needs to be comprehensively characterised to ensure they are suitable for *in vivo* DREADD mAChR studies.

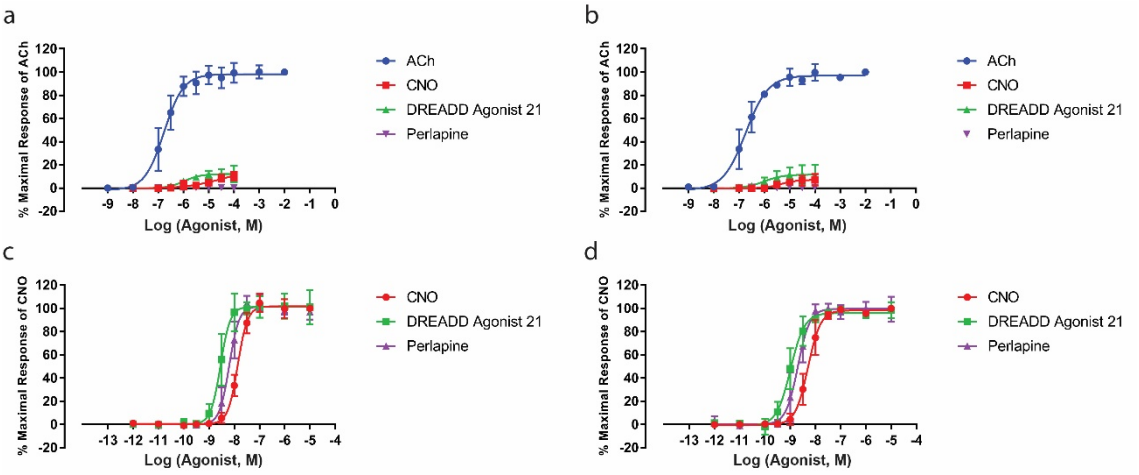

Figure 4.10: Comparison of DA21 and perlapine to acetylcholine and CNO activity at hM_1-WT, mM_1-WT, M_1-DREADD, and M_1-DREADD-PD with the IP-One accumulation HTRF assay.

hM_1-WT (**a**) and mM_1-WT (**b**) expressing cell lines were treated with increasing concentrations of acetylcholine, CNO, DA21, and perlapine for 5 minutes at 37°C. M_1-DREADD (**c**) and M_1-DREADD-PD (**d**) expressing cell lines were treated with increasing concentrations of CNO, DA21, and perlapine. Signalling was terminated with removal of the stimulation buffer and addition of ice-cold lysis buffer. Lysate was mixed with ERK 1/2 HTRF antibodies for 2 hours and plate was read using a CLARIOstar plate reader. Data are shown as mean ± SEM; n=3.

		M_1-DREADD	M_1-DREADD-PD
pEC_{50}	CNO	7.86 ± 0.02	8.30 ± 0.03
	DA21	8.54 ± 0.04	8.99 ± 0.05
	Perlapine	8.20 ± 0.03	8.69 ± 0.04
E_{max}	CNO	100	100
	DA21	99.6 ± 2.4	97.8 ± 1.8
	Perlapine	99.9 ± 1.9	101.5 ± 2.1

Table 4.3: Data from the IP-One assay comparing the pEC_{50} and E_{max} of CNO, DA21 and perlapine at the M_1-DREADD and M_1-DREADD mAChRs.

E_{max} is expressed as % maximum CNO response. Data are shown as mean ± SEM; n=4.

4.3 Discussion

The work contained within this chapter aimed to investigate the activity and interactions of the synthetic ligand CNO at the M_1-M_4-Wt mAChRs using pharmacological and cell signalling assays. This study was performed to evaluate the suitability of CNO for use *in vivo*. The function of CNO and acetylcholine was also compared to two alternative DREADD agonists proposed to improve the chemical genetic approach.

This study confirmed previous reports that CNO has a low affinity, <1 µM, for members of the mAChR family (Armbruster et al., 2007). The order of the affinities for CNO at the mAChR from the strongest are: hM_1-WT > mM_1-WT > M_2-WT > M_4-WT > M_3-WT. In cell signalling assays, CNO exhibited only very weak or no agonism towards the M_2, mM_3, and hM_4-WT mAChRs. Despite CNO having a weak affinity for members of the mAChR family, the affinity of acetylcholine was also found to be lower than 1 µM; this suggests that, at high enough concentrations, CNO could compete with acetylcholine for the mAChR orthosteric binding pocket.

To investigate whether CNO could act in an antagonist mode in the presence of acetylcholine, functional antagonism assays were performed using IP-One with the hM_1 and mM_1-WT mAChRs (Fig. 4.2,4.3) and with ERK 1/2 activation assays at the M_2, mM_3, and hM_4-WT mAChRs (Fig 4.7-9). At the hM_1-WT and mM_3-WT mAChRs CNO administration caused no significant shift in the potency of acetylcholine concentration-response curves. At the M_2-WT mAChR a modest shift in the pEC_{50} can be seen using the highest concentrations of CNO. CNO had a substantially stronger effect on the potency of acetylcholine signalling at the hM_4 and mM_1-WT mAChRs. These results show that CNO possesses an antagonistic mode in the presence of the orthosteric agonist acetylcholine. *in vivo*, this antagonist mode may lead CNO administration to antagonise acetylcholine signalling, confounding the study. The extent of these effects will depend on the concentration of acetylcholine and CNO achieved within the synapse.

Modelling studies attempting to estimate synaptic acetylcholine concentrations have to take into account the quantity of acetylcholine within the synaptic vesicles, the number of vesicles released into the synapse, the rate of breakdown of acetylcholine by AChEs within the synapse, and the sensitivity of the quantification itself (Aidoo and Ward,

2006; Nirogi et al., 2010; Scimemi and Beato, 2009). Although techniques have been developed in an attempt quantify synaptic neurotransmitter concentrations, the methods currently employed are unable to reliably and accurately quantify synaptic acetylcholine (Tsai, 2000; Zhang and Beyer, 2006). Microdialysis, the method used to collect intrasynaptic fluid is too slow to detect the rapid changes in acetylcholine concentration which occur during neuronal signalling (Bruno et al., 2006). Certain techniques have attempted to use AChEIs to prevent the breakdown of synaptic acetylcholine and aid in its quantification (Ajima and Kato, 1987; Liu and Kato, 1994; Xu et al., 1991); however AChEIs have been shown to alter neuronal activity, reducing the physiological relevance of their quantification (de Boer et al., 1990).

In spite of the weak partial agonist and antagonist modes of CNO, functional studies have confirmed that CNO is selective for the M_1-DREADD mAChRs. The concentration of CNO required to maximally activate the M_1-DREADD and M_1-DREADD-PD mAChRs, ~100nM, and the lowest concentration of CNO found to antagonise a member of the mAChR family, 1 μM. Given this functional selectivity, it may be possible to select a suitable dosage of CNO for *in vivo* studies that will avoid its off-target function. DREADD receptors have been used in *in vivo* mouse models for the investigation of neuronal circuits and specific cell groups (Alexander et al., 2009; Avaliani et al., 2016; Ray et al., 2011; Sco et al., 2015; Varela et al., 2016). In these studies, administration of CNO lead to a change in behaviour consistent with the activation of the DREADD receptors, without observing any significant effects on the control animals.

Notwithstanding the success of DREADD mAChR models using CNO, there is evidence to suggest that CNO may be back-metabolised into clozapine, as seen in Long-Evans rats (MacLaren et al., 2016). Clozapine is a pharmacologically promiscuous ligand with proven affinity for multiple GPCR families including the mAChRs, dopaminergic receptors, and serotoninergic receptors (Bolden et al., 1992; Coward, 1992; Wenthur and Lindsley, 2013), and so is a potential confounding factor within the animal studies. This prospect led to the identification of alternative ligands, based upon clozapine, for use in DREADD model (Chen et al., 2015). These ligands, perlapine and DA21, have previously been characterised for their activity at the M_3-WT and M_3-DREADD mAChRs. At the M_3-DREADD mAChR these ligands were both shown to have higher potency than

CNO, while showing very little or no activity at the M_3-WT mAChR. This activity, coupled with their lack of metabolism into a more efficacious ligand, makes them attractive options for future *in vivo* experimentation.

At the human and mouse M_1- mAChRs perlapine had no observable agonist activity up to 100 μM. At both the M_1-DREADD and M_1-DREADD-PD mAChRs, perlapine was a full agonist with a nearly half-log higher potency for the receptors than CNO. DA21 was also a full agonist of the M_1-DREADD and M_1-DREADD-PD mAChRs, and achieved higher potency than either perlapine or CNO. At the hM_1 and mM_1-WT mAChRs however, DA21 acts as a weak partial agonist. The poor efficacy of perlapine relative to acetylcholine at the human and mouse M1-WT mAChRs makes it an attractive replacement for CNO *in vivo*; earlier studies (Stille et al., 1973) have shown perlapine to be a neuroleptic drug in rats, with nanomolar affinity for D_2 and D_4-dopamine receptors and the 5-HT_{2A} receptor (Seeman et al., 1997). Perlapine was also licensed for use in human for insomnia in Japan (Roth, 2016). Unlike perlapine, DA21 has not be extensively characterised outside of the original study (Chen et al., 2015). As a benzodiazepine type compound, DA21 could still interact with multiple receptor families, as has been found with clozapine and perlapine. Investigations into the pharmacology and function of DA21 and perlapine need to be performed to understand their interactions with members of the mAChR family, among others, to confirm their suitability as agonists for our chemical genetic approach.

Chapter 5 Final Discussion

5.1 Discussion and Critical Analysis

The ultimate aim of this project within the Tobin group is the development of an animal model to study the function of the M_1-mAChR by utilising a chemical genetic approach. The mutations selected for this approach, the mAChR DREADD mutations, and phosphorylation-deficient mutations, were chosen to allow for the remote activation of the M_1-mAChR, and its downstream signalling pathways. Before being integrated into a transgenic animal model, both the M_1-DREADD mAChRs and CNO need to be characterised *in vitro* to ensure they fit certain criteria. Firstly, the DREADD mutations must reduce the potency of acetylcholine signalling at the M_1-mAChR. Secondly, the mutations must engender activity for the biologically inert synthetic ligand CNO. Finally, when activated by CNO, the M_1-DREADD mAChR must activate downstream signalling pathways comparable to the wild-type M_1-mAChR. For CNO to be suitable within the chemical genetic approach it must fully activate the M_1-DREADD mAChRs and show a high level of selectivity for the M_1-DREADD mAChR over wild-type mAChRs. Functional studies are also required to characterise any potential changes in M_1-DREADD mAChR signalling following the introduction of the PD mutations.

Results from the pharmacological investigations support the conclusion that the DREADD mutations successfully reduced the affinity and potency of orthosteric ligands for the M_1-mAChR. The DREADD mutations also engendering activity for CNO; finding the ligand to be a full agonist of the M_1-DREADD mAChR, activating the same signalling pathways as tested with the wild-type M_1-mAChRs. Although selective for the M_1-DREADD mAChR, CNO was found to act in an antagonist mode in the presence of acetylcholine at the mouse M_1-, M_2-, and M_4-mAChRs *in vitro*. The observed selectivity of CNO, and the published successful use of the DREADD mAChRs with CNO, suggests the selection of an appropriate dose *in vivo* can avoid the off-target effects of CNO. Given this, potential back-metabolism of CNO into clozapine, as well as its observed interactions with the mAChRs, drove investigation into alternatives to CNO. These alternative ligands, DA21 and perlapine, were found to have a higher potency for the M_1-DREADD and M_1-DREADD-PD mAChRs than CNO. With this in mind detailed pharmacological and pharmacokinetic studies will need to be performed. These studies

are required to understand the interactions of DA21 and perlapine with native receptors, ensure that these ligands are not back-metabolised into clozapine, and verify that, following administration, these ligands pass through the blood-brain barrier and reach their intended target.

Saturation binding assays of the wild-type mAChRs (Fig. 3.1 and 4.3) revealed that there are significant differences between the expression levels of the different WT cell lines. The human and mouse M_1-mAChRs were found to be expressing at around double the concentration of the M_2- and M_4- mAChRs. The mM_3-WT mAChR were expressed at the lowest concentration of all, around half the concentration of the M_2, and M_4-mAChRs. In the western blot comparing the quantity of receptor in the hM_1-WT, mM_1-WT, M_1-DREADD, and M_1-DREADD-PD mAChR expressing cell lines, M_1-DREADD were found to be expressed at higher concentrations of the other receptors. Comparison of the pharmacology and function of GPCRs is more reliable when receptors are expressing at similar concentrations. Although the cells used in this project did show differing receptor expression levels, reducing the receptor concentration will not significantly shift the E_{max} or pK_d of ligands for the receptors, unless the expression levels are below that of what would be the receptor reserve(Gazi et al., 1999). EC_{50}, however, can be lowered by the reduction in receptor expression. When comparing the shift in the potency of acetylcholine between the wildtype and mutant M_1-mAChRs, higher expression in the M_1-DREADD mAChR cell lines could be reducing the size of the shift caused by the DREADD mutations. The difference between the potencies of acetylcholine and CNO at the M_1-DREADD and M_1-DREADD-PD mAChRs may also be increased, with the higher expression of the M_1-DREADD mAChR potentially increasing the measured potency.

In recombinant cell lines, transfected receptors are often over expressed, leaving a receptor reserve. With a receptor reserve, the amount of ligand required to reach the EC_{50} is lower than the amount of ligand required to occupy 50% of the receptors (Hoyer and Boddeke, 1993). In functional antagonism assays, a receptor reserve can mask the full extent of an antagonist's activity; the antagonist may not achieve a high enough occupancy to block agonist dependent activation of the receptor. Although in the functional antagonism assays found CNO was the most potent at the hM_4-WT, the receptor expression of the mM_1-WT cell line was around double that of the hM_4-WT cell

line. This increased receptor expression could mean that although CNO appears to be a more potent antagonist of the M_4-mAChR, this difference could be significantly reduced. With the M_3-mAChR expressing cells, CNO was not found to cause a shift in the acetylcholine concentration response curve. As the M_3-mAChR-expressing cell line had the lowest expression, it is unlikely that a receptor reserve is masking the antagonistic properties of CNO. For more accurate calculations and comparisons of the pA_2, experiments should be performed to titrate receptor expression and remove the receptor reserve from the cell lines.

With the *in* vitro characterisation showing that, given certain caveats, the mutant M_1-mAChRs and synthetic ligand CNO fit the criteria for the chemical genetic approach, these receptors can now be employed *in vivo*. These models can then be evaluated using behavioural studies, such as contextual fear conditioning, to observe how alterations in M_1-mAChR signalling effect learning and memory. Contextual fear conditioning measures changes in hippocampus-dependent learning and memory (Phillips and LeDoux, 1992), a process known to involve mAChRs (Birdsall et al., 2001; DD et al., 1995). Although no data are available to be presented here, initial studies with the M_1-DREADD and M_1-DREADD-PD mAChR KI mice support the conclusion that the chemical genetic approach has successfully altered M_1-mAChR.

5.2 Future Directions

To further evaluate the antagonistic mode of CNO, and to interrogate other potential DREADD ligands, receptor titration experiments can be performed. Titrating receptor expression levels in each cell line using phenoxybenzamine (PBZ) is a method used to reduce the receptor reserve for functional antagonism assays. By reducing this receptor reserve, any antagonistic properties masked by the overexpression of receptors in recombinant cell lines may be revealed. Phenoxybenzamine is a concentration dependent alkylation agent which irreversibly binds to the orthosteric binding site of GPCRs including the muscarinic receptor family (Buck and Burcher, 1987; Eglen et al., 1994; Eglen and Harris, 1993). Preliminary experiments can be carried out by incubating cells in increasing concentrations of PBZ and performing an ERK 1/2 activation or IP-One accumulation assay. The optimal concentration of PBZ will be just high enough as to deplete the receptor reserve without having an effect on the E_{max}. Cells can then be preincubated with this concentration of PBZ in a functional antagonism assay. Without the receptor reserve, functional antagonism assays will be able to better compare the function of CNO as an antagonist of acetylcholine signalling. Within the functional antagonism studies more concentrations of the antagonist should also be used, with concentration both antagonising and not antagonising the signalling, this will allow for better definition of the Schild plot and will provide a more accurate pA_2 value.

A more comprehensive battery of pharmacological and functional assays will need to be performed on DA21 and perlapine. Although functional selectivity for DREADD mAChRs has been observed (Fig. 4.10) (Chen et al., 2015), these ligands could hold the same observed antagonistic properties as CNO (Fig. 5.3, 5.7, 5.9). Pharmacokinetic studies should also be performed on these ligands to confirm their bioavailability and their ability cross the blood brain barrier. If these alternative ligands are not broken down into active metabolites, as CNO is metabolised into clozapine, they will be more attractive compounds for the chemical genetic model.

A recent paper published in part by members of the Tobin group presented further pharmacological and functional studies of perlapine and DA21 against the M_1 and M_4 mAChRs, as well as their DREADD mutant counterparts (Thompson et al., 2018). Competition binding studies found the affinities of both DA21 and perlapine to be higher

than that of acetylcholine at the M_1- and M_4-mAChRs. Functional antagonism assays at the M_1- and M_4-mAChRs using DA21 revealed antagonism of acetylcholine signalling. DA21 also antagonised the signalling of dopamine at the D_1-dopanimergic receptor and quinpirole, a selective agonist of the D_2- and D_3- dopaminergic receptors, at the D_2-dopanimergic receptor. This antagonism occurs at concentrations of 1µM and above, higher than required to activate the DREADD mAChRs, meaning the selection of the correct dose may avoid the off-target effects of DA21. This paper also found that following administration of CNO, clozapine was found within plasma and the brain in a dose dependent manner, but CNO was only detected within the plasma, suggesting that clozapine is activating the DREADD-mAChRs *in vivo*, rather than CNO. Although previous studies have successfully activated signalling pathways within mouse models using the DREADD mAChR and CNO, the clear presence a promiscuous ligand such as clozapine is still a concern for future studies. The pharmacokinetic analysis found that both DA21 and perlapine were detectable within the plasma and brain in a dose dependent manner. The findings in this study bring to light the unsuitability of CNO as a ligand for the DREADD mAChRs, and the need to replace CNO with alternative ligands such as DA21 in *in vivo* studies.

To further develop this chemical genetic approach, research could also be carried out to identify an allosteric modulator which could be used to rescue *in vivo* receptor function. A suitable allosteric modulator would be able to act on the M_1-DREADD and M_1-DREADD-PD mAChRs to increase the potency of ACh for the receptor. This method of activation would allow the M_1-DREADD mAChR to respond to natural acetylcholine signals, providing a more physiologically relevant response. This method of receptor activation is also potentially safer than the use of agonists. In normal neural function acetylcholine is rapidly cleared from the synapse by AChEs, whereas synthetic ligands can persist within the synapse and stabilise the receptors in an active conformation for longer. This prolonged activation of the receptor does not accurately mimic the normal signalling in cholinergic synapses (May et al., 2007). The M_1-mAChR selective positive allosteric modulator BQCA has been previously tested at the M_1-DREADD mAChR (Abdul-Ridha et al., 2013). This study found that BQCA did not act at the M_1-DREADD receptor in the same was as it acts with the wild-type receptor. BQCA was found to have

high positive cooperativity with acetylcholine signalling at the M_1-DREADD mAChR. This cooperativity was not as high as with the M_1-WT mAChR and BQCA was not found to modulate the binding affinity of acetylcholine for the M_1-DREADD mAChR. In this *in vitro* study BQCA was not able to fully recover the function of ACh at the M_1-DREADD receptor, but future studies using new M_1-mAChR selective positive allosteric modulators could help to refine the M_1-DREADD mAChR model.

With the *in vitro* characterisation of the M_1-DREADD and M_1-DREADD-PD mAChRs verifying their modification of M_1-mAChR function and pharmacology, these mutants can now be employed in a transgenic model to study M_1-mAChR function. Initial comparisons of the M_1-DREADD mAChR expressing mice with M_1 mAChR knock-out and wild-type mice in behavioural studies will assess whether the DREADD mutations successfully prevent acetylcholine signalling *in vivo*. If acetylcholine signalling at the M_1-DREADD mAChR has been modified, behavioural experiments can be carried out in the presence and absence of an appropriate DREADD ligand in an attempt to rescue M_1 mAChR function and restore a normal behavioural response. Comparisons between the responses of M_1-DREADD and M_1-DREADD-PD mAChR KI mice following administration will investigate how removal of the phosphorylation dependent pathways of the M_1-mAChR effects learning and memory *in vivo*. The characterisation and implementation of a phosphorylation-dependent signalling biased M_1-DREADD mAChR into our chemical genetic approach would allow us to better understand the role of G-protein dependent signalling in M_1-mAChR controlled learning and memory (Nakajima and Wess, 2012; Roth, 2016). Understanding how the selective activation of receptor signalling pathways effects physiological and behavioural outcomes may reveal any negative outcomes, such as seizure-like activity, or identify a specific signalling pathway as important in driving the M_1-mAChRs normal function. These discoveries could then inform drug discovery efforts, directing efforts into the design of biased ligands if the studies suggest this to be therapeutically beneficial in the treatment of disorders such as Alzheimer's disease.

5.3 Conclusions

Bearing the critiques in mind, conclusions can still be drawn from the evaluation of the chemical genetic approach presented in this thesis. The DREADD mutations used were successful in modifying the pharmacology of the M_1-mAChRs, and CNO was found to be a weak partial agonist that binds competitively to the wild-type mAChRs as was seen in the initial study (Armbruster et al., 2007). Functional antagonism assays discovered that CNO can act in an antagonistic mode in the presence of acetylcholine, mode not previously reported in the literature. With this activity in mind, and in combination with the potential for CNO to be metabolised into clozapine *in vivo*, alternative DREADD agonists such as DA21 and perlapine need to be considered for future *in vivo* studies utilising the DREADD mAChR model.

Chapter 6 Appendix: Advanced Tissue Processing and Imaging Techniques

6.1 Introduction

Histological investigation of *ex vivo* tissue allows for the observation of morphological changes within organs (Nizri et al., 2016), as well as the changes in cell populations (Bradley et al., 2016a), and protein expression (Schlederer et al., 2014; Söderquist et al., 2015). These observations can be used, in tandem with molecular and functional analyses to interrogate the molecular mechanisms of a disease and track disease progression (Dower et al., 2017; Phillips et al., 2006; Rakha et al., 2010; Shao et al., 2006; Wipke and Allen, 2001). Standard histological analysis of tissue involves slicing thin sections containing the region of interest (ROI). These sections are then stained using chemical stains or antibodies to label cellular components. Investigations through large areas of tissue require serial sectioning, where several sections are cut from different levels through the tissue (Braumann et al., 2007). With enough sections taken through the tissue, programs can construct a 3D model (Ourselin et al., 2001; Wang et al., 2015). Without the use of automated tissue processing, embedding, and staining equipment, this method is incredibly time consuming.

6.1.1 Optical Clearing of Large Tissue Sections to Whole Organs

As an alternative to serial sectioning, chemically clearing tissue may be a more efficient alternative to analyse these larger sections of tissue. Tissue clearing is the use of chemical agents to optically clear the sample to allow visualisation of organ architecture or protein expression profiles. This first chemical clearing protocol was Spalteholz's technique, developed in 1911 using methyl salicylate and benzyl benzoate for the visualisation of cardiac vasculature (Spalteholz, 1911). This method was effective, but the long-term incubation of the tissue in organic solvents causes severe tissue damage. From 2007, several new techniques for chemical tissue clearing have been developed (Liu et al., 2016). These techniques can range from short, Clear^{T}, Clear^{T2}, and SWITCH (Kuwajima et al., 2013; Murray et al., 2015), to long, CLARITY and Scale (Chung et al., 2013; Hama et al., 2011; Susaki et al., 2014). Some clearing techniques can use complex mixtures of chemicals, CUBIC, (Susaki et al., 2014), or can involve merely dehydrating and altering the refractive index (RI) the tissue, BABB/Murray's Clear, 3DISCO, and iDISCO (Dodt et al., 2007; Ertürk et al., 2012; Renier et al., 2014). The RI of the cleared

tissue needs to be matched to that of a suitable imaging medium. Without matching the refractive index of the tissue, light will refract when passing between substances with differing refractive indexes. This refraction will distort the images acquired, produce chromatic aberrations, and reduce the resolution. RI matching is easier with the chemically cleared tissues, such as; CLARITY, Clear^{T}/Clear^{T2}, Scale, SeeDB or SWITCH (Ke et al., 2013), as the refractive index of the tissue itself is lowered. Tissues which have only been dehydrated need to be placed in higher refractive index solutions; dibenzyl ether (DBE) for iDISCO and 3DISCO, or benzyl benzoate in BABB/Murray's clear. These higher RI solutions can damage microscope equipment and be highly toxic. Although the proper controls can be put in place for their use, their inconvenience makes the use of other methods more attractive. The nature of each process can mean they are more or less suitable for certain investigations (Liu et al., 2016). Only certain techniques are compatible with the use of lipophilic dyes or IHC, and changes in tissue size due to the process could limit the use of these techniques on delicate samples.

The CLARITY (Clear Lipid-exchanged Acrylamide-hybridized Rigid Imaging/ Immunostaining/ in situ-hybridization-compatible Tissue hYdrogel) method of tissue embedding and clearing was developed in 2013 by the Diesseroth lab at Stamford University, California (Chung et al., 2013). This protocol (Fig. 6.1) involved the perfusion-fixation of tissue using a paraformaldehyde (PFA) and acrylamide-based hydrogel mixture. Once the mixture has completely diffused through the tissue, the sample and hydrogel solution are degassed and incubated at 37°C to activate the thermal initiator of acrylamide polymerisation, embedding the tissue in a PFA-acrylamide cross-linked hydrogel. Lipids can then be removed from the sample using sodium dodecyl sulphate (SDS) and boric acid, with (Chung et al., 2013) or without (Yang et al., 2014) electrophoresis, 'clearing' the tissue. If the protein of interest does not contain a fluorescent tag, samples can then be incubated with antibodies. The tissue is then optically cleared by incubating them in a refractive index matching solution (RIMS), in this case 85% glycerol which has a refractive index (RI) of 1.45. Once cleared the samples can be imaged and this set of images can be processed and a 3D model generated of the imaged area.

Following on from CLARITY, a newer protocol termed SWITCH was published (Murray et al., 2015) from the lab of Dr. Chung, the primary author of the CLARITY protocol article. SWITCH still uses PFA to fix the tissue, but instead of using acrylamide, uses glutaraldehyde (GA) to form the matrix within the tissue. A solution of PFA and glutaraldehyde in a PBS at pH 3, called SWITCH-OFF, is perfused into the mouse and the brain is removed and incubated in the same solution to allow the glutaraldehyde to fully diffuse through the tissue. Once the glutaraldehyde has fully diffused, it is transferred to a pH 7 solution at 4°C, SWITCH-ON, to initiate polymerisation. Through the ability to control when polymerisation occurs, it is possible to have full diffusion of the matrix medium through the tissue before polymerisation, unlike in CLARITY where polymerisation can occur, if slower, at low temperatures. Lipids are cleared from the sample using a solution of boric acid, lithium hydroxide and an anti-browning agent at pH 9 at 60-80°C. This high temperature clearing step increases the rate of clearance compared to CLARITY, but does lead to yellowing of the sample. Once the sample has been cleared they are labelled with antibodies and finally incubated in the 85% glycerol RIMS. The high temperatures used in SWITCH clearing make the process significantly faster than passive tissue clearing (PTC), around 2 weeks rather than 2-3 months. Although faster, the high temperatures of SWITCH clearing can denature proteins with fluorescent tags such as GFP (Murray et al., 2015). To use these expressed markers, clearing must be performed at the same temperatures used within the CLARITY protocol. Samples are then imaged using Light-sheet fluorescence microscopy (LSFM).

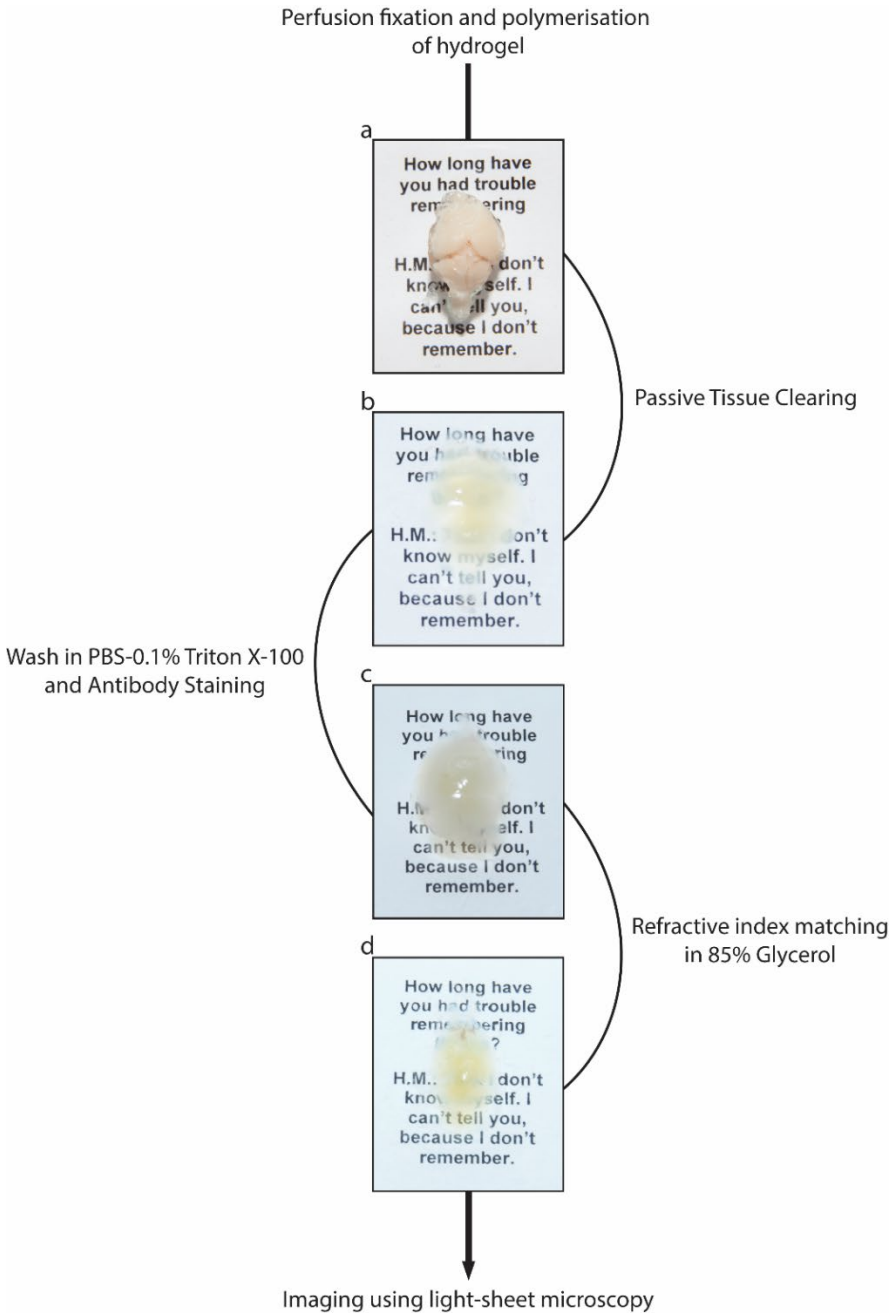

Figure 6.1: Flow diagram representing the CLARITY process including pictures of mouse brains at major steps

Tissue was taken from mice which were perfused with CLARITY hydrogel and incubated at 4°C to allow the hydrogel to fully diffuse. Hydrogel was then polymerised by degassing and incubating at 37°C. After polymerisation the sample is removed from the hydrogel and washed (**a**) before clearing. Once cleared (**b**) the sample is washed and labelled with primary and secondary antibodies (**c**). The sample is them placed in a RIMS (**d**) to alter the refractive index before imaging. The images above were taken by myself from samples I processed within the Tobin group.

6.1.2 Large Sample Optimised Microscopy

Although they allow for high magnification and a high signal-to-noise ratio, confocal microscopes use powerful lasers to excite the fluorophores used to label the samples. This leads to the eventual bleaching of fluorescent tags on antibodies and proteins, reducing the signal over time and making the image darker. The high magnification and slow scanning of a confocal microscope means imaging of large sections through tissue could take a significant period of time. The fluorophores would likely bleach before the entire ROI had been imaged, limiting the usefulness of this technique.

Light sheet fluorescence microscopy (LSFM) uses lower powered light sources than confocal microscopes and a cylindrical lens to focus the light into a thin, wide plane through the sample (Fig 6.2). The original form of LSFM, published in 1993 by the Spelman lab (Voie et al., 1993), called orthogonal-plane fluorescence optical sectioning (OPFOS) was used to visualise the internal structure of chemically cleared guinea pig cochlea. This system could perform these kinds of larger sample analysis but only had a 10 µm to 26 µm resolution, making cellular and sub-cellular imaging impossible. Selective plane illumination microscopy (SPIM) is a more advanced form of LSFM, which can acquire higher resolution images than OPFOS. OPFOS uses an air objective lens which does not touch the RIMS in which the sample is suspended, but in SPIM systems immersion objectives are used (Huisken et al., 2004). Using immersion objectives, it is possible to achieve a higher numerical aperture than air objectives, increasing the magnification and resolution possible (Davidson, 2017; Royston-Pigott, 1870). Immersion media has this effect by reducing the refraction of light between objects of different RI. This refraction can distort the final image, reducing the potential resolution. Therefore, immersion media, tissue, and a sample holder with equal RIs, as well as an optimised objective, will reduce the distortion of light and increase the image quality.

SPIM systems use complementary metal-oxide-semiconductor (CMOS) or charge-coupled device (CCD) fluorescence microscope sensors rather than photomultipliers often used in laser scanning confocal microscopy (LSCM). LSCM uses a pinhole aperture between the sample and the sensor which blocks light from outside of the focal plane. Although this pinhole allows for a sharper image, the amount of light it blocks means a higher power laser light source is required to obtain an image with an acceptable signal-

noise ratio. Over a long period of time these light sources can bleach the fluorophores used in the labelling of samples, restricting the length of time the sample can be imaged for. In LSFM, the illumination of a specific plane through the tissue limits the exposure of regions outside of the focal plane to the light source. Without the pinhole, a lower powered laser light source can be used to illuminate the sample; and the use of a CMOS or CCD sensor allows for rapid image acquisition, further reducing potential bleaching of the sample.

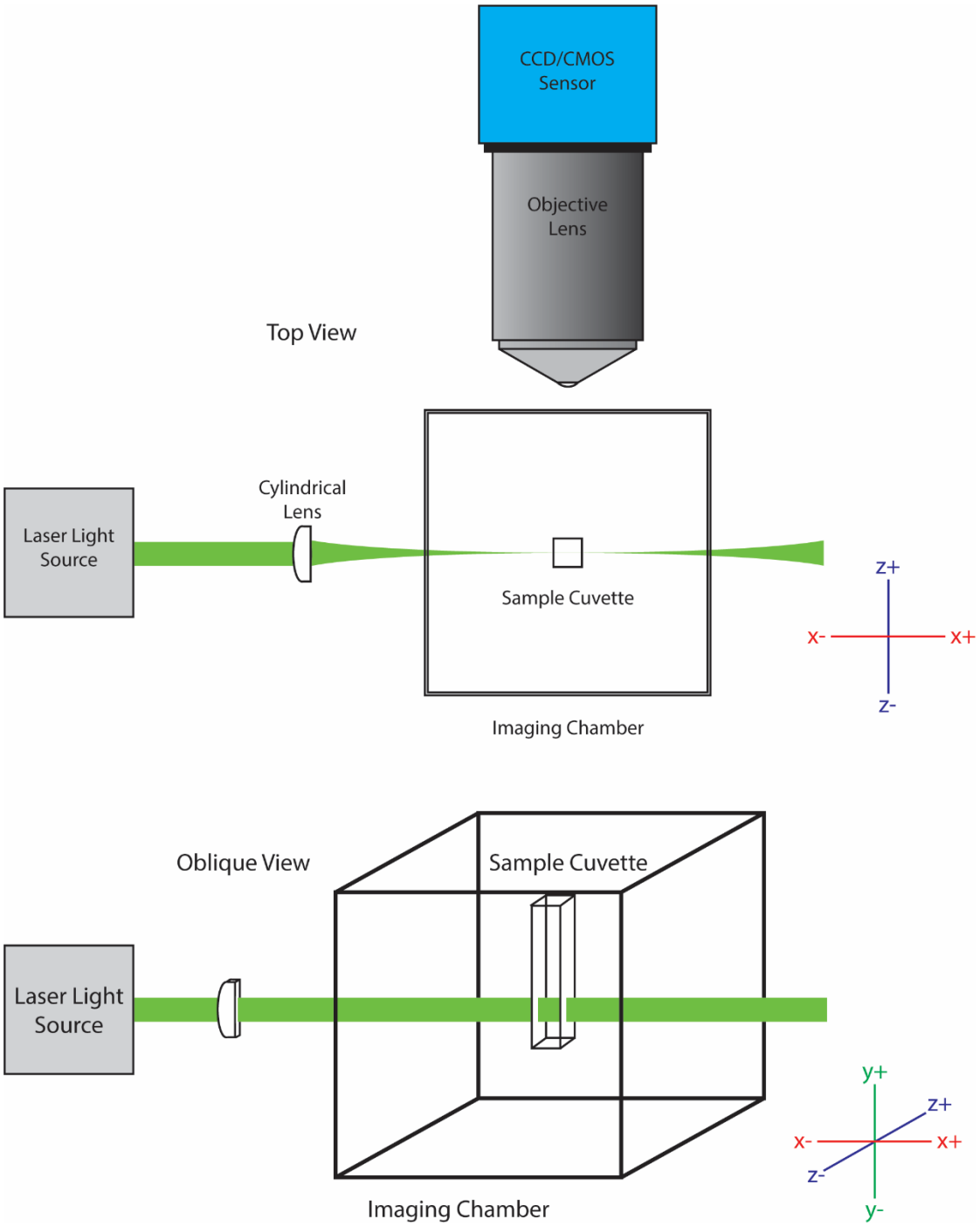

Figure 6.2: Schematic diagram of an OPFOS light-sheet microscope system.

Simplified schematic diagram showing the top and oblique view of an OPFOS LSFM system. The laser beam is passed through a cylindrical lens to change the shape of the laser beam into a sheet, with the thinnest portion of this sheet being within the sample. The objective lens is set perpendicular to the plane of the light sheet. The sample chamber and quartz glass cuvette contain 85% glycerol to maintain a continuous RI, reducing distortion of the image.

Working with Dr. Jonathon Taylor, at the University of Glasgow, we used CLARITY processed mouse tissue to optimise a custom LSM system for 3D IHC studies of hydrogel embedded samples. There are commercially available LSM systems developed by major manufacturers such as Zeiss and Leica. Although these systems will be optimised and are immediately ready to use, developing an in-house custom system allows for expansion of system capabilities, and does not incur the same cost as these commercial systems. The LSM we are currently using is an OPFOS system, using an air objective outside of the imaging chamber. The tissue, immersion media (85% glycerol), and quartz glass sample cuvette, all have a refractive index around 1.45 to reduce light path refraction as much as possible.

Ultimately, this technology will be used within the lab to visualise: structural changes, protein aggregation, neuronal loss, and gliosis in the prion model of neurodegenerative disease (Bradley et al., 2016a). Using samples from different time points it will be possible to track these changes, monitor the disease progression, and observe how potential therapeutic agents and tool compounds modify disease progression.

The aim of this chapter was to replicate the CLARITY tissue clearing technique (Chung et al., 2013; Yang et al., 2014), produce samples to identify cell-type markers and epitope tags within the sample, and use these samples to optimise a custom built LSM system. I will assess the quality of both CLARITY passively and electrophoretically cleared tissue; the image quality achievable with the current LSM system. Images from samples processed using the SWITCH technique, labelled with anti-GFAP, and imaged using the same LSM system, have also been presented here. Being a more rapid technique, if SWITCH processed tissue is of a comparably high quality it would be more convenient a technique to utilise going forward.

6.2 Results

6.2.1 Confocal Microscopy on sectioned CLARITY tissue.

The first samples processed using the CLARITY protocol were brains from mice treated with either a normal brain homogenate (NBH) control or with a prion protein containing brain homogenate (PBH). The mice treated with the prion protein will develop transmissible spongiform encephalopathy. Within the hippocampus, the presence of the misfolded prion protein promotes the invasion of microglia (microgliosis) and astrocytes (astrogliosis) (Bradley et al., 2016a), immune cells within the central nervous system. After polymerisation of the hydrogel, the brains were cut into 1 mm sections for passive clearing and antibody staining. Sections were stained with an antibody against GFAP. Sections were imaged using confocal microscopy and a z-stack was produced through the CA1 region (Fig. 6.3). The confocal microscopy results confirm that cellular resolution can be achieved in CLARITY processed tissue. It was reassuring proof that the process was not damaging the tissue to the point where high resolutions images could not be produced. In the confocal z-stacks, significant astrogliosis was present within the PBH treated brain compared to the NBH brain, with an increase in astrocytes within the polymorphic and molecular layers and invasion of astrocytes into the pyramidal cell layer.

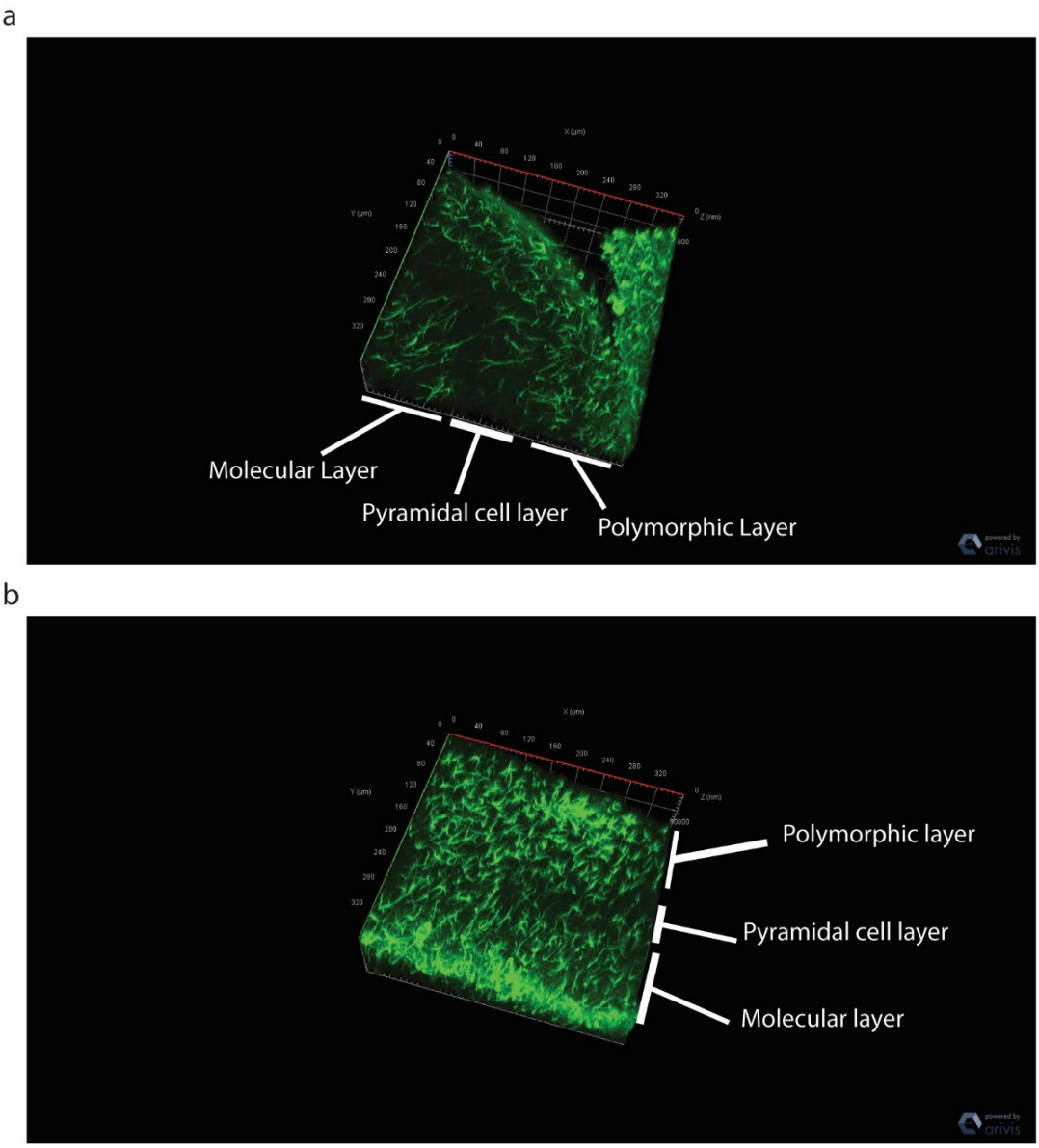

Figure 6.3: 3D representation of a confocal microscopy z-stack series through the CA1 region of the hippocampus stained with anti-GFAP antibody.

Mice treated with either NBH (**a**) or PBH (**b**) were perfusion fixed after 10 weeks with hydrogel and the brains were removed. Hydrogel was polymerised and the brains were cut into 1 mm thick sections, passively cleared, and stained with an anti-GFAP antibody (green). The PBH treated brain shows astrogliosis, with an increase in the astrocytes within the polymorphic and molecular layers as well as invasion into the pyramidal cell layer compared to the NBH brain. Images were taken using confocal microscopy and images were rendered using Carl Zeiss Zen Blue software.

6.2.2 Whole Tissue, Cleared with ETC and PTC, imaged using LSFM.

When clearing whole CLARITY tissue, both ETC and PTC were performed to compare clearing time and the condition of the tissue post-clearing. We also tried to use acrylamide and bis-acrylamide at half the original concentrations. This was in an effort to increase the permeability of the tissue for antibody staining and increase clearing rate. Lowering these concentrations could weaken the structural integrity of the cleared tissue and make it unsuitable for imaging. In total, passive clearing of a whole brain took around 3 months for the original hydrogel recipe and 2 months for the lowered acrylamide concentration to complete clearing. Tissue was stained for 2 weeks with each primary and secondary antibody. In between these steps was a wash step in PBS-T for 1 week.

Part of this study also included optimisation of the light-sheet microscope for imaging of the CLARITY processed tissue. Images of the first attempt of LSFM imaging (Fig 6.4) gave a certain amount of resolution at the surface, although there was diffuse fluorescence throughout the sample. There was also shadowing across the plane of the image, this shadowing is due to objects within the sample obstructing the light path. Deconvolution of the images in future acquisitions can help remove these artefacts and improve image resolution. When using ETC the process took just over 1 month but the tissue had lost its structural integrity and, after staining, very little specific staining could be seen within the samples. ETC has been shown to work previously (Chung et al., 2013), but it causes more swelling in the tissue than PTC. Knowing this it was decided that only the PTC method would be used, to avoid irreparable damage to the samples.

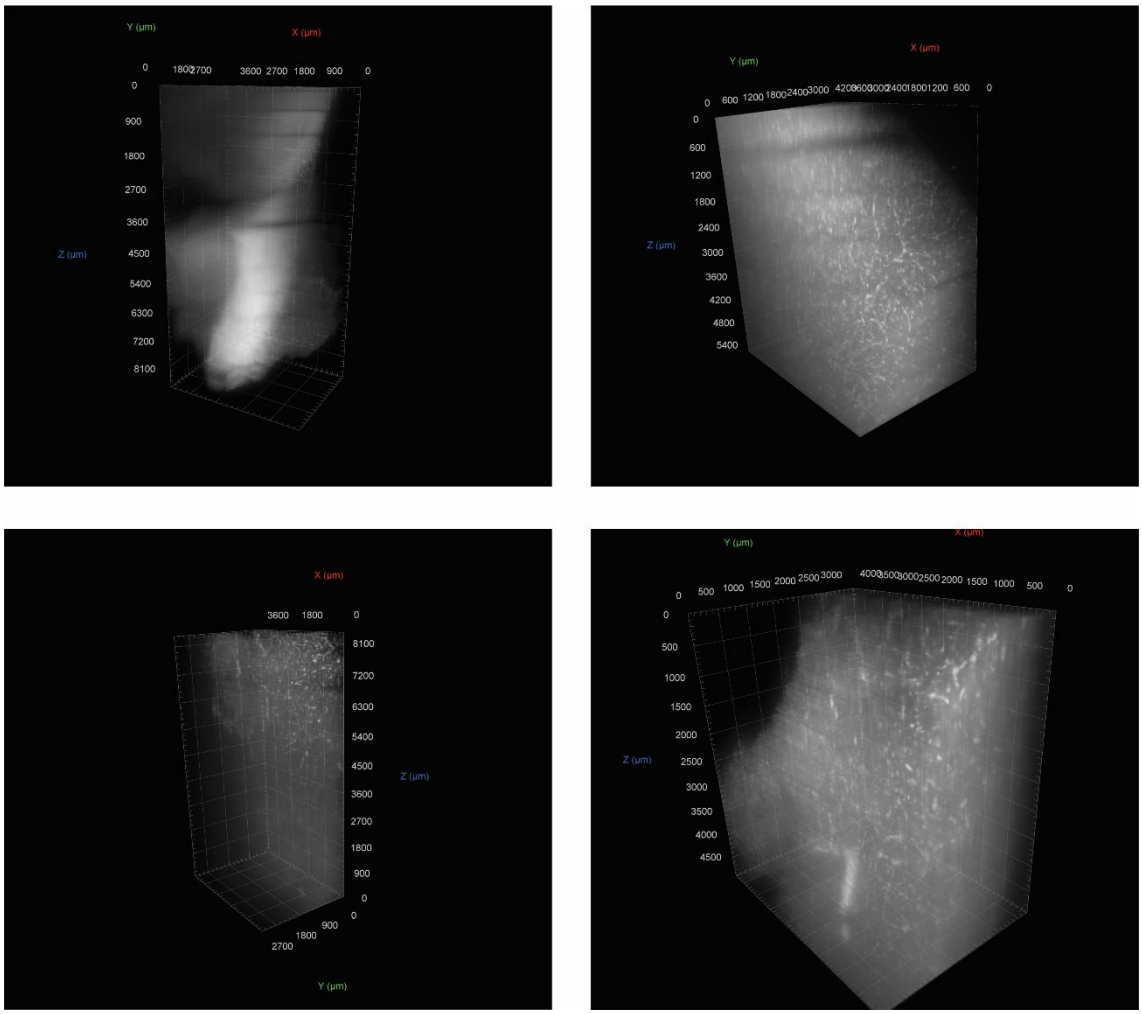

Figure 6.4: 3D representation of electrophoretically cleared CLARITY tissue using LSFM for the first time, showing brain tissue stained with GFAP.

Brains were taken from mice perfused with CLARITY hydrogel and, following degassing and polymerisation, the tissue was cleared using ETC. Once the samples were cleared they were labelled using anti-GFAP antibody and a secondary antibody conjugated to alexafluor488 (white). Images are from exploratory z-stacks through tissue; although staining can be seen there were no identifiable structures. Samples were then imaged using LSFM and 3D renders of the z-stacks were generated using Arivis Vision 4D. LSFM images were acquired with the assistance of Dr. Jonathon Taylor and Chiara Garbellotto.

Using tissue which had been processed using half the concentration of acrylamide and bis-acrylamide and stained with anti-GFAP antibody, we successfully acquired a z-stack through the hippocampus (Fig. 6.5-10). The CA1, CA2, CA3, and dentate gyrus are clearly visible within the stack (Fig. 6.11), as well as nuclei and small vessels in the region. The shadow artefacts across the image were less pronounced than seen in the ETC samples, but still present. The resolution of the image was not high enough to be able to discern between individual cells, as in the confocal images. This was due, in part, to the use of a lower magnification air objective lens in the current LSM system.

6.2.3 Whole Tissue Cleared using SWITCH and Imaged using LSFM

During the development of the CLARITY technique within the lab another technique called SWITCH was tested as an alternative. Tissue was processed by Dr. Sophie Bradley and Colin Molloy using the SWITCH protocol, labelled with anti-GFAP antibodies, and imaged using the same LSM. In these images acquired (Fig 6.12-15), the hippocampus was visible within the sample, and major structural features could be detected (Fig. 6.16), although not as pronounced as in the CLARITY images. This may mean that the brain required a longer incubation with the antibodies. In images from both CLARITY and SWITCH processed tissue cell bodies can be seen within the pyramidal cell layer. Unlike in the confocal microscopy images, the polymorphic and molecular layers only show diffuse staining, rather than being able to visualise individual astrocytes. This lower resolution is expected within the current LSM system.

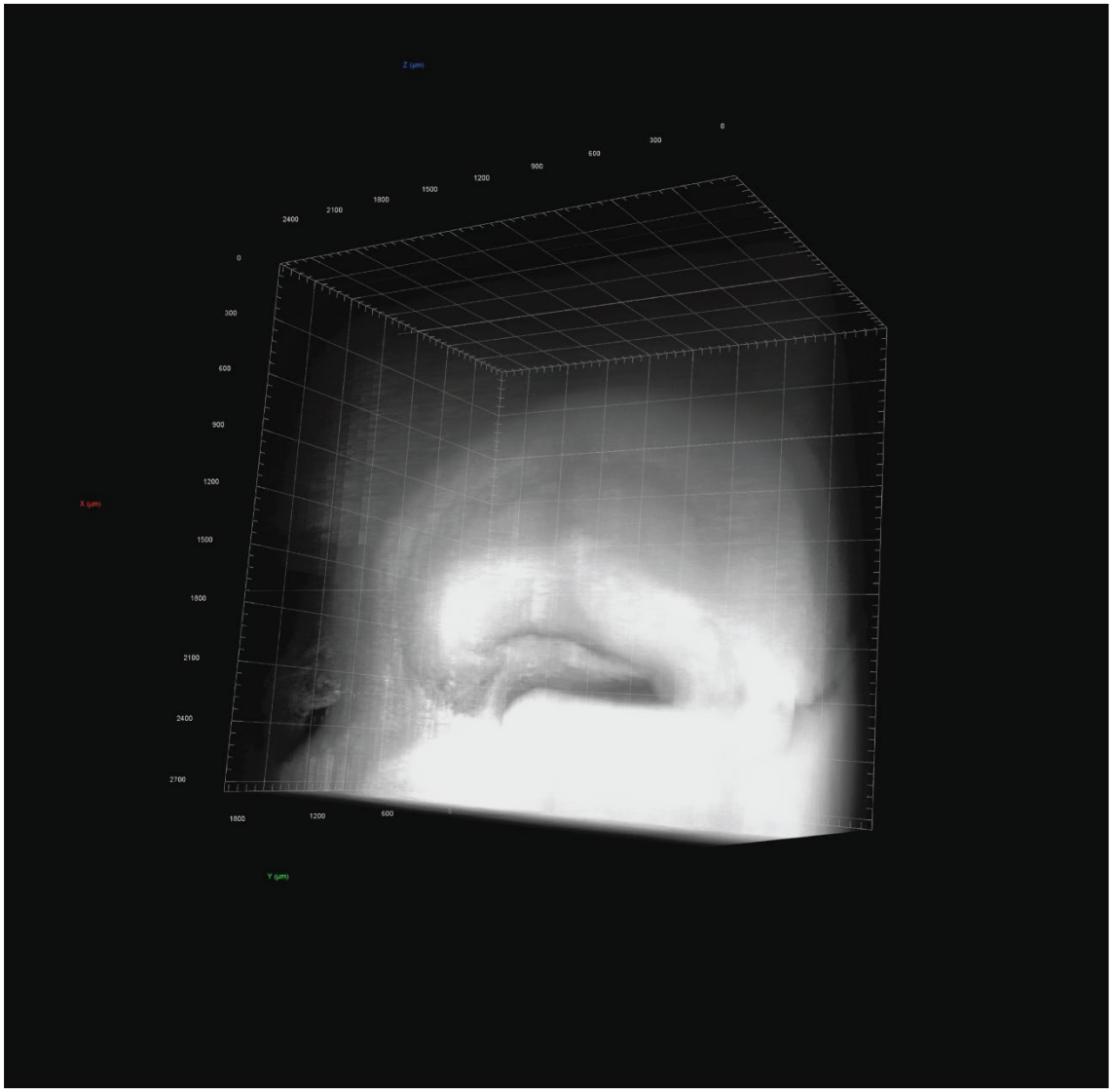

Figure 6.5: 3D representation of z-stack series using LSFM through CLARITY processed tissue, showing the hippocampus stained with anti-GFAP antibody.

A brain was taken from a mouse perfused with CLARITY hydrogel and, following degassing and polymerisation, the tissue was cleared using PTC. Once the samples were cleared they were labelled using anti-GFAP antibody and a secondary antibody conjugated to alexafluor488 (white) at 37°C. Samples were then imaged using LSFM and 3D renders of the z-stacks were generated using Arivis Vision 4D. The polymorphic and molecular layers of the hippocampus are clearly stained within the image, with the darker pyramidal cell layer visible between them. Samples were then imaged using LSFM and 3D renders of the z-stacks were generated using Arivis Vision 4D. LSFM images were acquired with the assistance of Dr. Jonathon Taylor and Chiara Garbellotto.

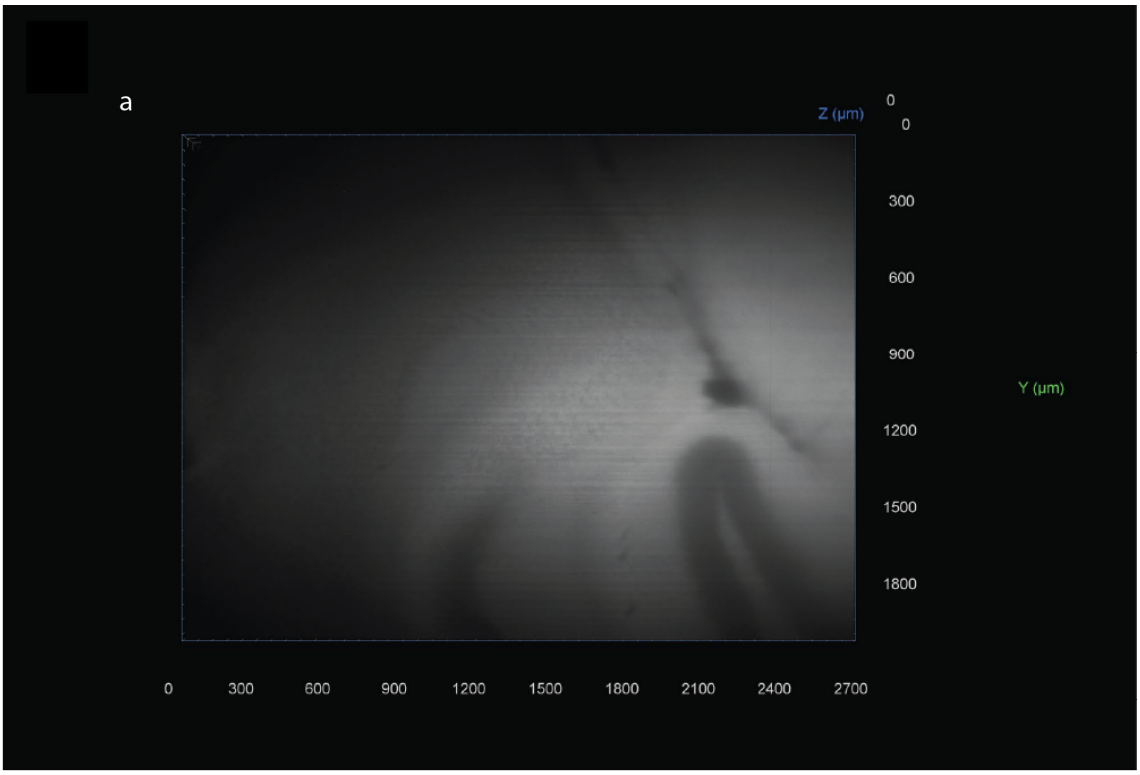

Figure 6.6: Representative images from the z-stack series through the hippocampus of a CLARITY processed mouse brain stained with GFAP

A brain was taken from a mouse perfused with CLARITY hydrogel and, following degassing and polymerisation, the tissue was cleared using PTC. Once the samples were cleared they were labelled using anti-GFAP antibody and a secondary antibody conjugated to alexafluor488 (white) at 37°C. Samples were then imaged using LSFM and 3D renders of the z-stacks were generated using Arivis Vision 4D (Fig. 6.5). Representative images through the brain labelled with anti-GFAP antibodies (**a**-**e**). A closer image (**e**) of the area highlighted in (**d**) shows individual nuclei visible within the pyramidal cell layer of the hippocampus. Samples were then imaged using LSFM and 3D renders of the z-stacks were generated using Arivis Vision 4D. LSFM images were acquired with the assistance of Dr. Jonathon Taylor and Chiara Garbellotto.

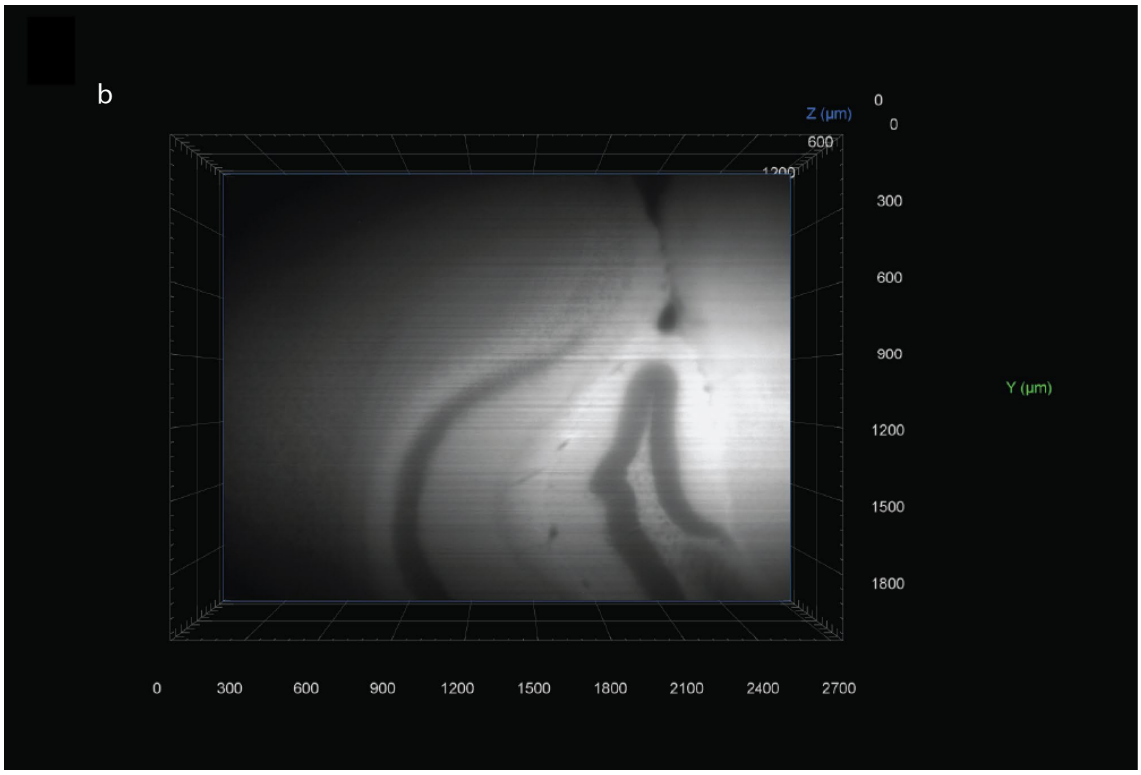

Figure 6.6: Representative images from the z-stack series through the hippocampus of a CLARITY processed mouse brain stained with GFAP

A brain was taken from a mouse perfused with CLARITY hydrogel and, following degassing and polymerisation, the tissue was cleared using PTC. Once the samples were cleared they were labelled using anti-GFAP antibody and a secondary antibody conjugated to alexafluor488 (white) at 37°C. Samples were then imaged using LSFM and 3D renders of the z-stacks were generated using Arivis Vision 4D (Fig. 6.5). Representative images through the brain labelled with anti-GFAP antibodies (**a-e**). A closer image (**e**) of the area highlighted in (**d**) shows individual nuclei visible within the pyramidal cell layer of the hippocampus. Samples were then imaged using LSFM and 3D renders of the z-stacks were generated using Arivis Vision 4D. LSFM images were acquired with the assistance of Dr. Jonathon Taylor and Chiara Garbellotto.

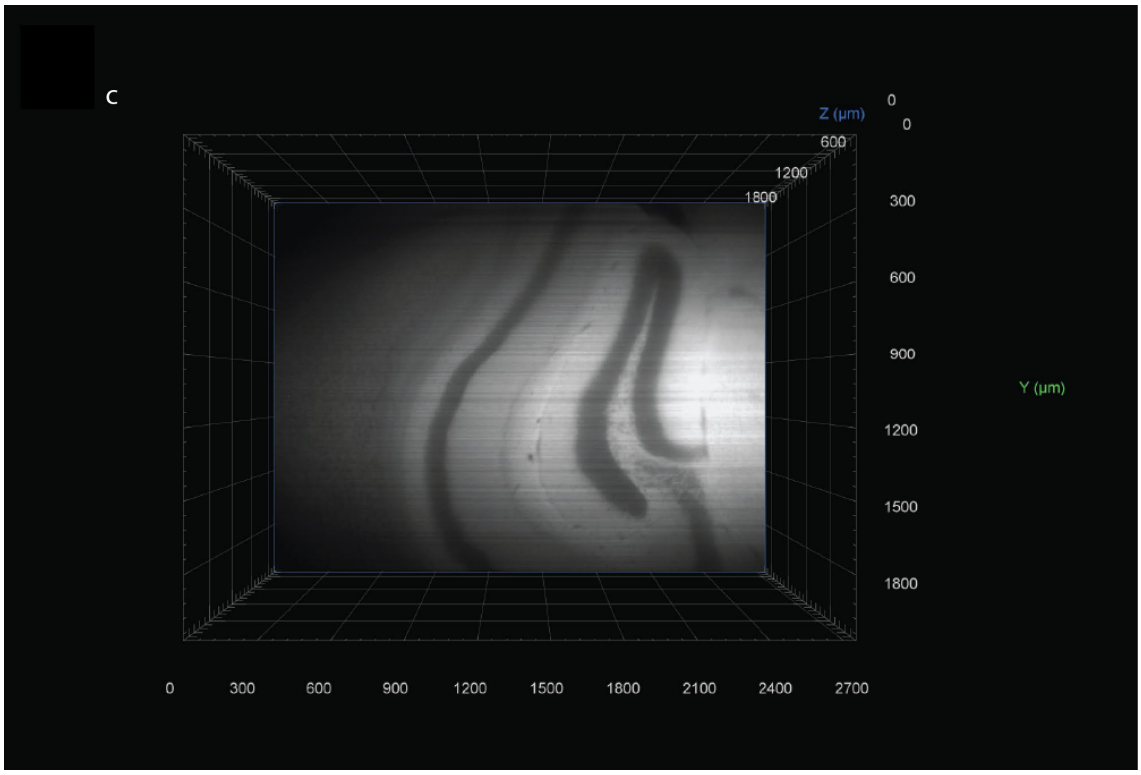

Figure 6.6: Representative images from the z-stack series through the hippocampus of a CLARITY processed mouse brain stained with GFAP

A brain was taken from a mouse perfused with CLARITY hydrogel and, following degassing and polymerisation, the tissue was cleared using PTC. Once the samples were cleared they were labelled using anti-GFAP antibody and a secondary antibody conjugated to alexafluor488 (white) at 37°C. Samples were then imaged using LSFM and 3D renders of the z-stacks were generated using Arivis Vision 4D (Fig. 6.5). Representative images through the brain labelled with anti-GFAP antibodies (**a-e**). A closer image (**e**) of the area highlighted in (**d**) shows individual nuclei visible within the pyramidal cell layer of the hippocampus. Samples were then imaged using LSFM and 3D renders of the z-stacks were generated using Arivis Vision 4D. LSFM images were acquired with the assistance of Dr. Jonathon Taylor and Chiara Garbellotto.

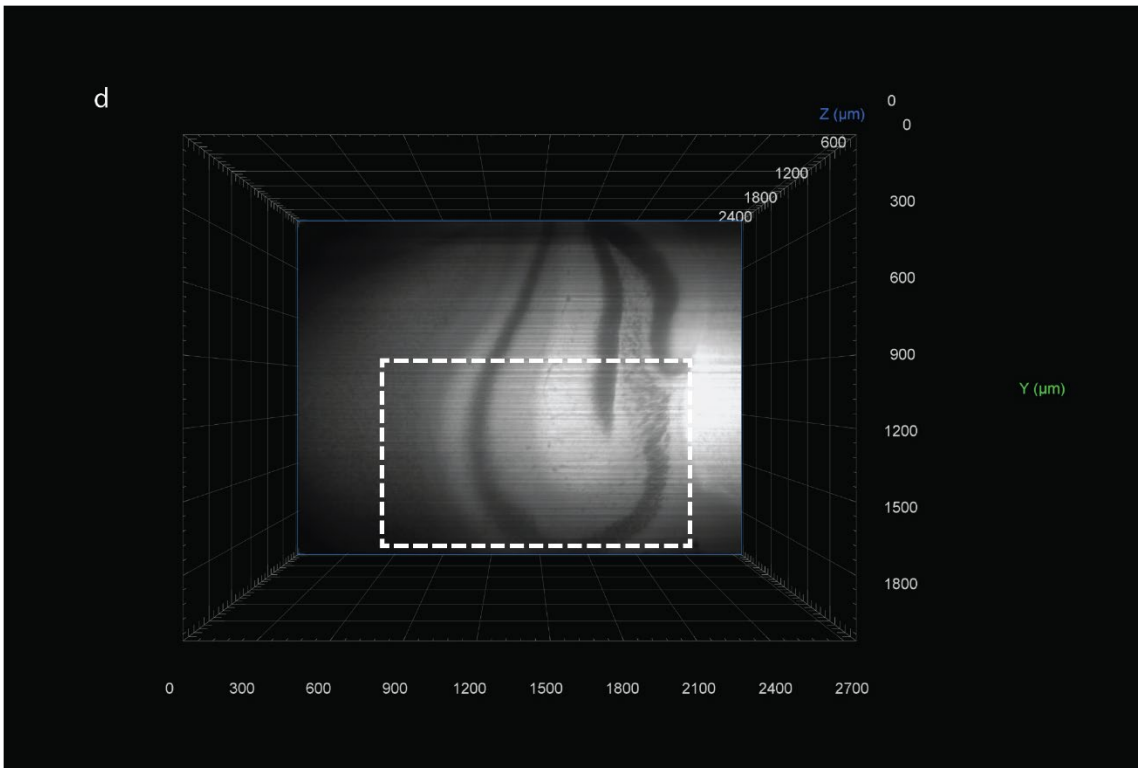

Figure 6.6: Representative images from the z-stack series through the hippocampus of a CLARITY processed mouse brain stained with GFAP

A brain was taken from a mouse perfused with CLARITY hydrogel and, following degassing and polymerisation, the tissue was cleared using PTC. Once the samples were cleared they were labelled using anti-GFAP antibody and a secondary antibody conjugated to alexafluor488 (white) at 37°C. Samples were then imaged using LSFM and 3D renders of the z-stacks were generated using Arivis Vision 4D (Fig. 6.5). Representative images through the brain labelled with anti-GFAP antibodies (**a-e**). A closer image (**e**) of the area highlighted in (**d**) shows individual nuclei visible within the pyramidal cell layer of the hippocampus. Samples were then imaged using LSFM and 3D renders of the z-stacks were generated using Arivis Vision 4D. LSFM images were acquired with the assistance of Dr. Jonathon Taylor and Chiara Garbellotto.

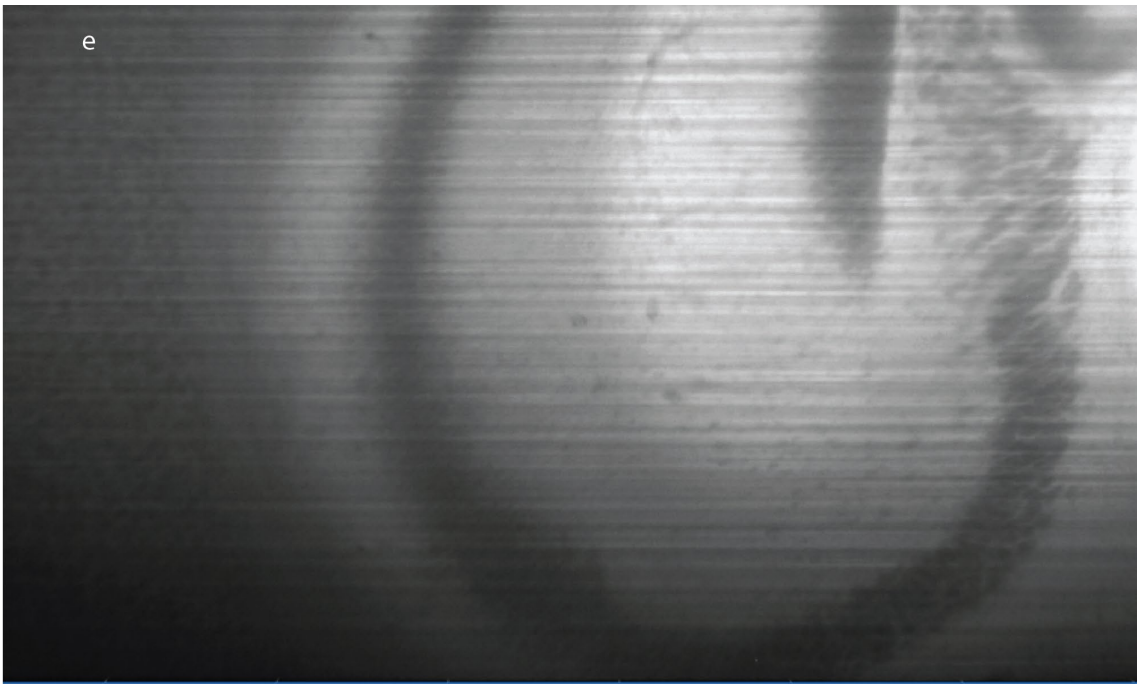

Figure 6.6: Representative images from the z-stack series through the hippocampus of a CLARITY processed mouse brain stained with GFAP

A brain was taken from a mouse perfused with CLARITY hydrogel and, following degassing and polymerisation, the tissue was cleared using PTC. Once the samples were cleared they were labelled using anti-GFAP antibody and a secondary antibody conjugated to alexafluor488 (white) at 37°C. Samples were then imaged using LSFM and 3D renders of the z-stacks were generated using Arivis Vision 4D (Fig. 6.5). Representative images through the brain labelled with anti-GFAP antibodies (**a**-**e**). A closer image (**e**) of the area highlighted in (**d**) shows individual nuclei visible within the pyramidal cell layer of the hippocampus. Samples were then imaged using LSFM and 3D renders of the z-stacks were generated using Arivis Vision 4D. LSFM images were acquired with the assistance of Dr. Jonathon Taylor and Chiara Garbellotto.

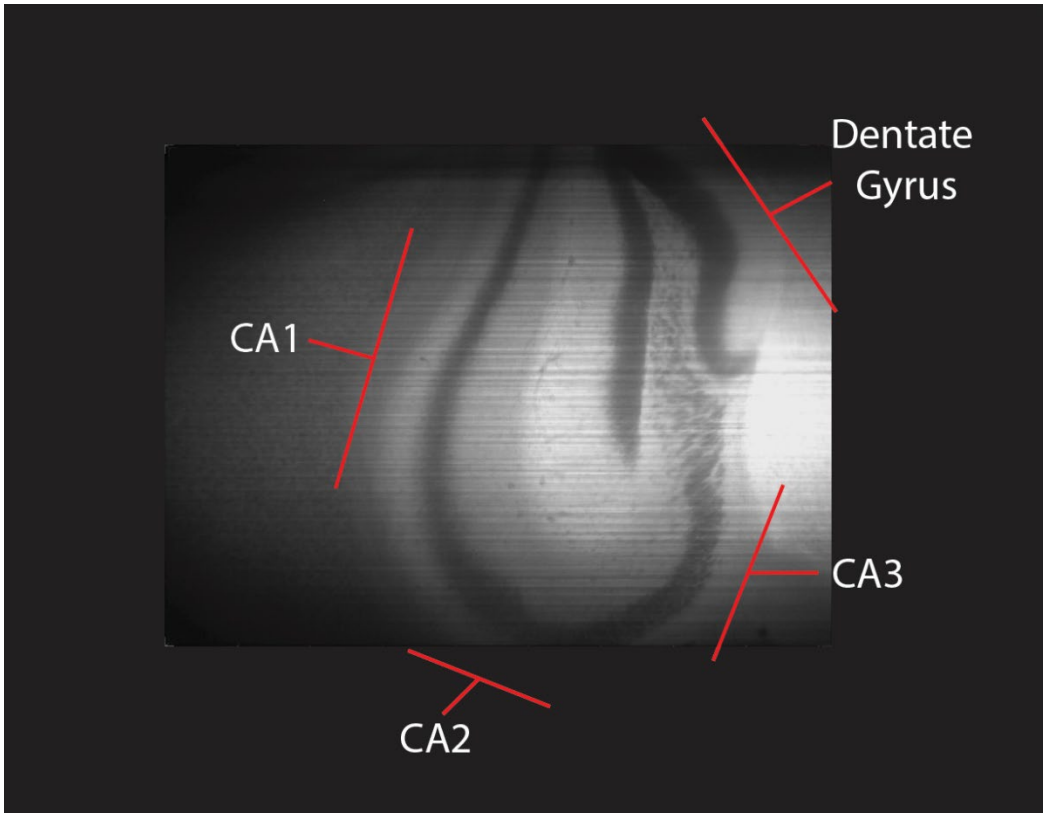

Figure 6.76.7: Section from a z-stack series through the hippocampus of a CLARITY processed mouse brain stained with GFAP

A brain was taken from a mouse perfused with CLARITY hydrogel and, following degassing and polymerisation, the tissue was cleared using PTC. Once the samples were cleared they were labelled using anti-GFAP antibody and a secondary antibody conjugated to alexafluor488 (white) at 37°C. Samples were then imaged using LSFM and 3D renders of the z-stacks were generated using Arivis Vision 4D. The CA1, CA2, CA3, and dentate gyrus regions of the hippocampus can be clearly seen within the z-stack. LSFM images were acquired with the assistance of Dr. Jonathon Taylor and Chiara Garbellotto.

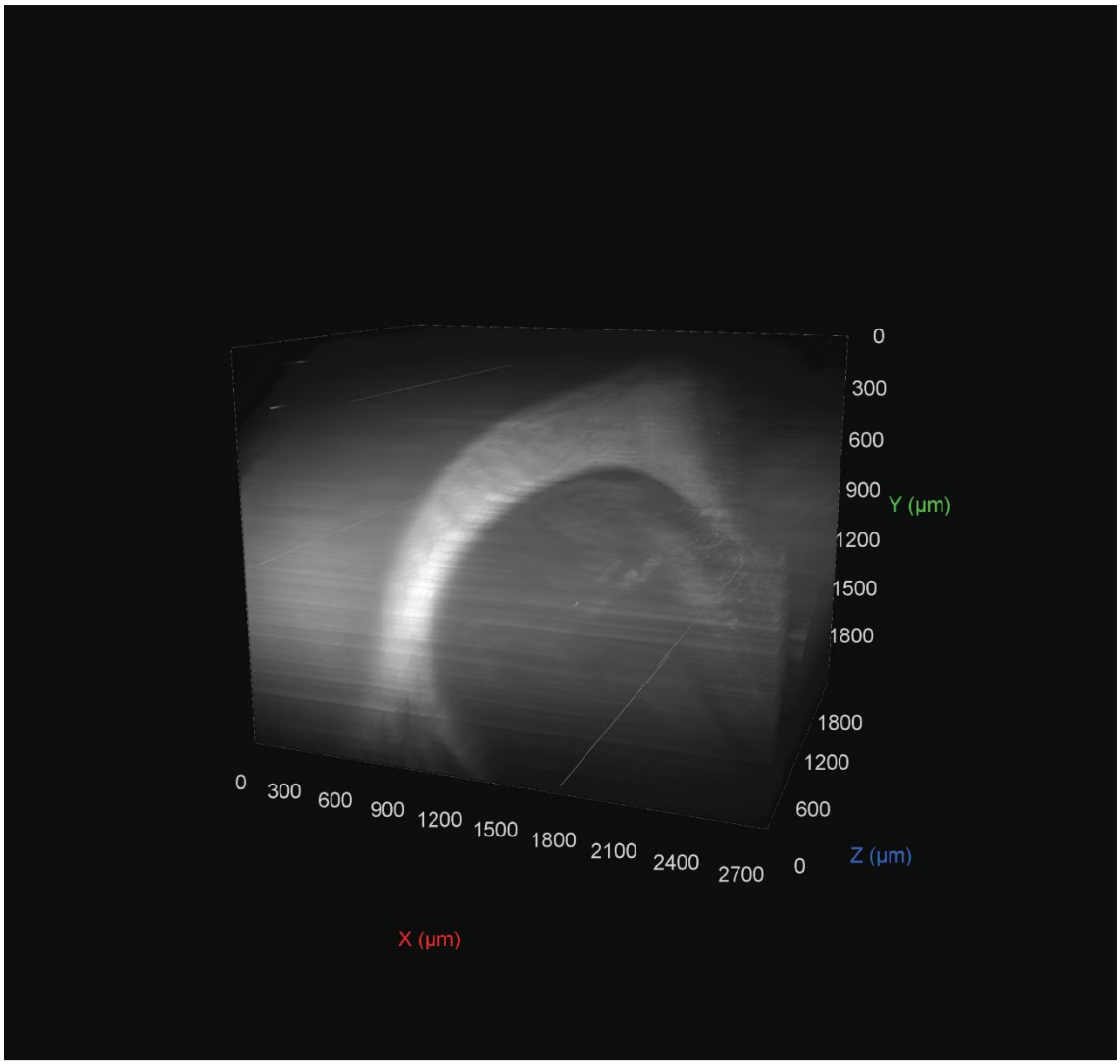

Figure 6.8: 3D representation of z-stack series using LSFM through SWITCH processed tissue, showing the hippocampus stained with anti-GFAP antibody.

A brain was taken from a mouse perfused with SWITCH-OFF and, following polymerisation with SWITCH-ON, the tissue was cleared at 70°C. Once the samples were cleared they were labelled using anti-GFAP antibody and a secondary antibody conjugated to alexafluor488 (white) at 37°C. Samples were then imaged using LSFM and 3D renders of the z-stacks were generated using Arivis Vision 4D. Staining is most pronounced in the region surrounding the hippocampus. Samples were then imaged using LSFM and 3D renders of the z-stacks were generated using Arivis Vision 4D. Samples were processed by Dr. Sophie Bradley and Colin Molloy. LSFM images were acquired with the assistance of Dr. Jonathon Taylor and Chiara Garbellotto.

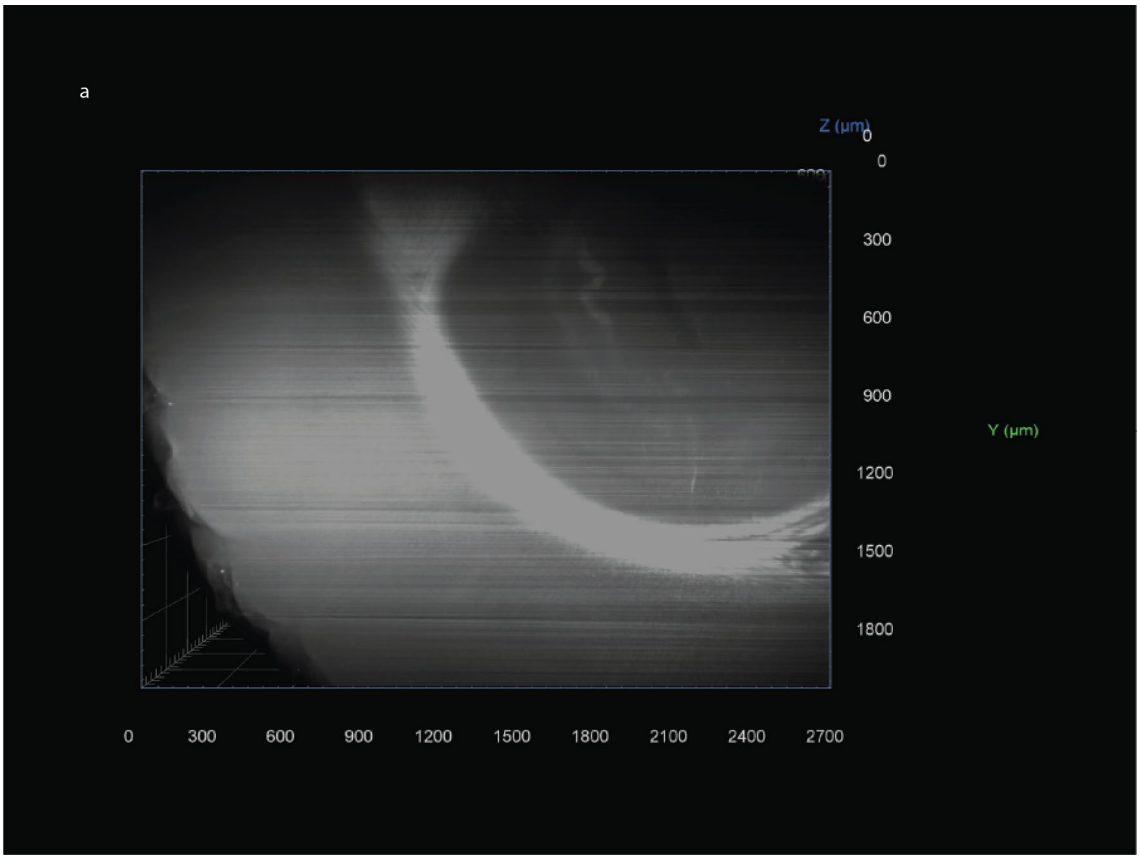

Figure 6.9: Representative images from the z-stack series through the hippocampus of a SWITCH processed mouse brain stained with GFAP.

A brain was taken from a mouse perfused with SWITCH-OFF and, following polymerisation with SWITCH-ON, the tissue was cleared at 70°C. Once the samples were cleared they were labelled using anti-GFAP antibody and a secondary antibody conjugated to alexafluor488 (white) at 37°C. Samples were then imaged using LSFM and 3D renders of the z-stacks were generated using Arivis Vision 4D (Fig. 6.8). Representative images through the brain labelled with anti-GFAP antibodies (**a-d**). Samples were then imaged using LSFM and 3D renders of the z-stacks were generated using Arivis Vision 4D. Samples were processed by Dr. Sophie Bradley and Colin Molloy. LSFM images were acquired with the assistance of Dr. Jonathon Taylor and Chiara Garbellotto.

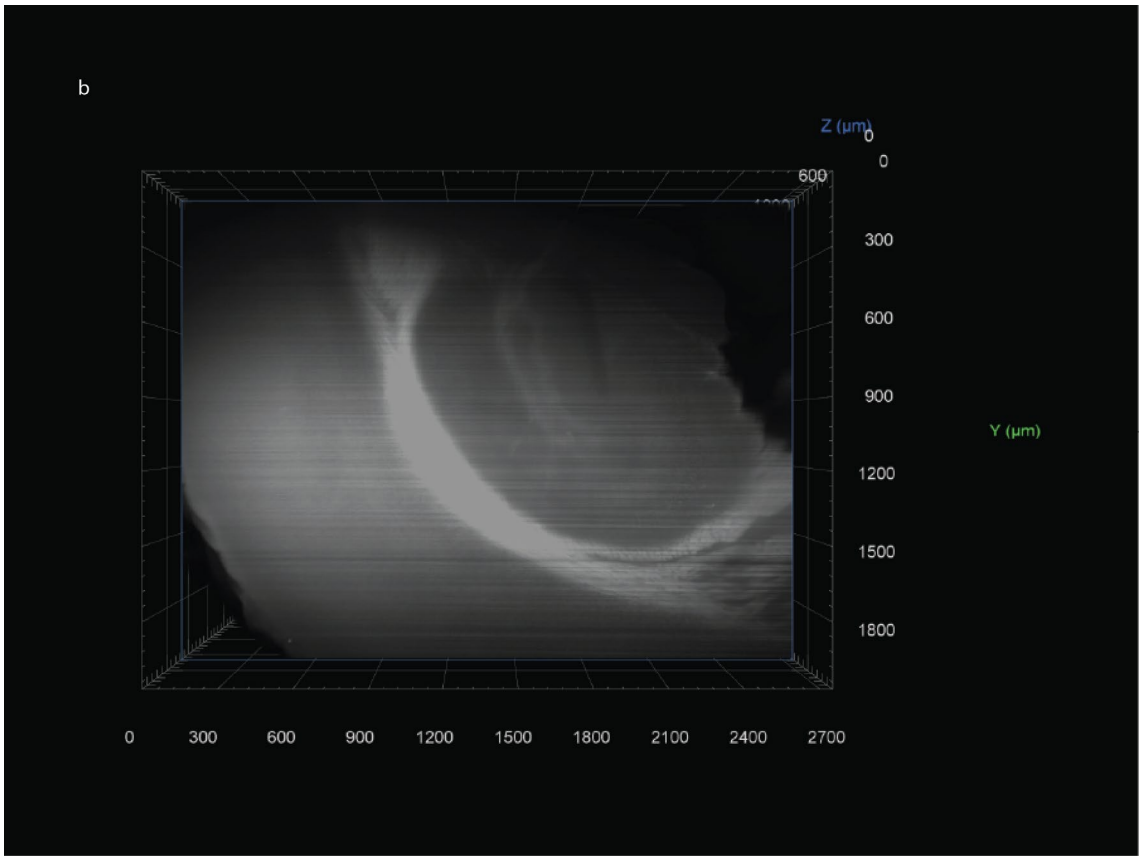

Figure 6.9: Representative images from the z-stack series through the hippocampus of a SWITCH processed mouse brain stained with GFAP cont.

A brain was taken from a mouse perfused with SWITCH-OFF and, following polymerisation with SWITCH-ON, the tissue was cleared at 70°C. Once the samples were cleared they were labelled using anti-GFAP antibody and a secondary antibody conjugated to alexafluor488 (white) at 37°C. Samples were then imaged using LSFM and 3D renders of the z-stacks were generated using Arivis Vision 4D (Fig. 6.8). Representative images through the brain labelled with anti-GFAP antibodies (**a-d**). Samples were then imaged using LSFM and 3D renders of the z-stacks were generated using Arivis Vision 4D. Samples were processed by Dr. Sophie Bradley and Colin Molloy. LSFM images were acquired with the assistance of Dr. Jonathon Taylor and Chiara Garbellotto.

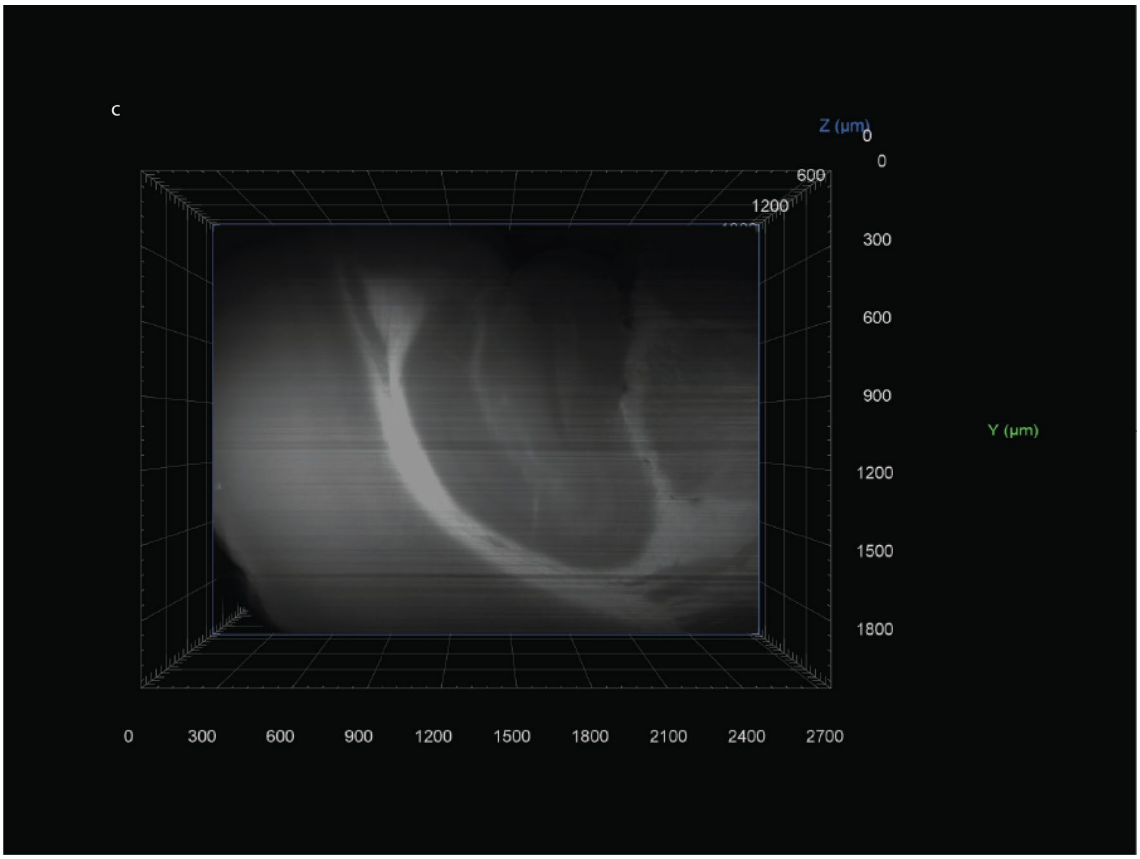

Figure 6.9: Representative images from the z-stack series through the hippocampus of a SWITCH processed mouse brain stained with GFAP cont.

A brain was taken from a mouse perfused with SWITCH-OFF and, following polymerisation with SWITCH-ON, the tissue was cleared at 70°C. Once the samples were cleared they were labelled using anti-GFAP antibody and a secondary antibody conjugated to alexafluor488 (white) at 37°C. Samples were then imaged using LSFM and 3D renders of the z-stacks were generated using Arivis Vision 4D (Fig. 6.8). Representative images through the brain labelled with anti-GFAP antibodies (**a-d**). Samples were then imaged using LSFM and 3D renders of the z-stacks were generated using Arivis Vision 4D. Samples were processed by Dr. Sophie Bradley and Colin Molloy. LSFM images were acquired with the assistance of Dr. Jonathon Taylor and Chiara Garbellotto.

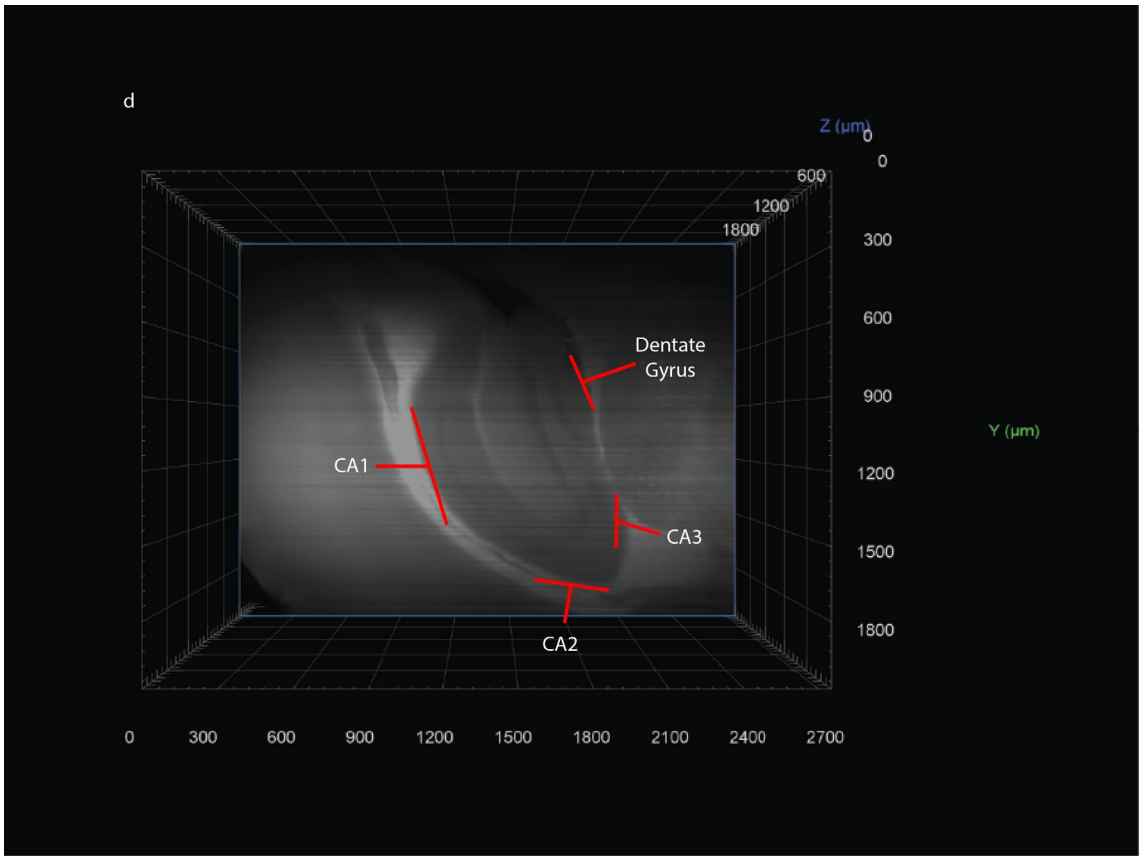

Figure 6.9: Representative images from the z-stack series through the hippocampus of a SWITCH processed mouse brain stained with GFAP cont.

A brain was taken from a mouse perfused with SWITCH-OFF and, following polymerisation with SWITCH-ON, the tissue was cleared at 70°C. Once the samples were cleared they were labelled using anti-GFAP antibody and a secondary antibody conjugated to alexafluor488 (white) at 37°C. Samples were then imaged using LSFM and 3D renders of the z-stacks were generated using Arivis Vision 4D (Fig. 6.9). Representative images through the brain labelled with anti-GFAP antibodies (**a-d**). Samples were then imaged using LSFM and 3D renders of the z-stacks were generated using Arivis Vision 4D. The labels within the above image are used to denote the location of the CA1, CA2, CA3, and dentate gyrus within the hippocampus. Samples were processed by Dr. Sophie Bradley and Colin Molloy. LSFM images were acquired with the assistance of Dr. Jonathon Taylor and Chiara Garbellotto.

6.3 Discussion

This chapter presents my current progress in the optimisation and implementation of advanced tissue processing and imaging techniques within the lab. This optimisation involved a collaboration with the laboratory of Dr. Jonathon Taylor at the University of Glasgow to build and optimise an LSM system to image optically cleared tissue.

Prior to the collaboration with Dr. Taylor, initial observations of CLARITY processed tissue were made using confocal microscopy (Fig. 6.3). Confocal microscopy of optically cleared tissue provided cellular resolution, proving that the process itself does not damage tissues to a point where detailed visualisation is not possible. This confirms what has been found in previous articles using the CLARITY technique (Chung et al., 2013; Yang et al., 2014). For use with the confocal microscope, tissue was cut into 1 mm sections prior to clearing and staining as larger sections could not be imaged. Using this sectioned tissue allowed for quicker clearing and improved labelling of the tissue, but was not practical for making observations through the hippocampus. The combination of thin sections and the confocal microscope also made imaging clearer than would be possible with other fluorescence microscopy systems. The low depth of the tissue, and the ROI being nearer the cover glass, reduced the amount of potential interference from objects and structures within the tissue. The confocal system itself allows for a higher resolution than standard fluorescence microscopy using high power lasers and a pinhole in front of the detector to prevent light from regions outside of the focal plane from reaching the detector. For imaging larger sections of tissue however, the use of a pinhole and high-power laser will eventually lead to bleaching of the fluorophore label on the antibodies used. With the advantage of CLARITY being the ability to image through large sections of tissue, confocal microscopy will be impractical and LSFM will need to be used.

Unlike in PTC, where tissue can be left for months in clearing solution and maintain its rigidity, tissue cleared electrophoretically would lose its structural integrity at a faster rate. This loss of integrity is from hydrogel embedded tissue swelling over time whilst in the clearing solution (Yang et al., 2014). Swelling was observed at a faster rate in ETC processed tissue and, if left for too long, would lead to the tissue structure degradation. Although it is possible to properly clear tissue using ETC there is a more limited window to preserve tissue structure. When attempts were made to clear brains using ETC (Fig.

6.4) samples lost their rigidity and, when visualised with LSFM little to no detail was visible within the sample. It was therefore decided that PTC would be used for future samples to avoid the irreparable damage which will waste animal tissue and a significant amount of time.

The quality of the images acquired from the PTC processed brain using LSFM (Fig. 6.5-11) was promising. Individual nuclei were visible within the pyramidal cell layer and the hippocampus was easily identifiable within the sample. Individual cells could not be visualised but this is expected as the objective lens used in the current system is an air objective. Air objectives have a lower magnification and numerical aperture than immersion lenses, reducing the maximum resolution which can be achieved. The shadows visible across the samples are caused by scattering of the light beam as it travels through the sample. Improvements in the LSM system can be made to reduce the shadowing across the sample (Girkin et al., 2018, Schwarz et al., 2015), such as implementing a scanning light sheet rather than a static cylindrical lens. By scanning a light sheet through multiple angles, the artefacts causing the shadows in one plane can be avoided in another plane. Removal of the shadowing will also allow for a better signal to noise ratio, with the gain and/or light source power no longer having to be increased to illuminate within the shadowed areas.

A brain processed using the SWITCH protocol (Fig 6.12-15) was also imaged using the same microscope as the CLARITY tissue. Although the staining penetration was lower than in the CLARITY tissue, making clear observations of the regions of the hippocampus difficult, the CA1, CA2, CA3, and dentate gyrus were all identifiable within the sample (Fig. 6.16). The rapid clearing time and successful staining of the hippocampus makes the SWITCH protocol an attractive option for future samples. Important considerations taking these protocols forward is the ability to perform multiple rounds of staining on the samples. Only being able to visualise a single protein within the samples would be incredibly wasteful, so it is important to test multiple rounds of staining and destaining.

The resolution obtained using the current LSM system was adequate to visualise structures within the brain; as well as pyramidal cell nuclei within the pyramidal cell layer of the hippocampus. It was not, however, possible to visualise individual astrocytes

within the polymorphic and molecular layers as with the confocal imaging. To improve the resolution, the lab has acquired a lens which is specifically designed for the imaging of cleared tissues with a RI of 1.45, such as CLARITY and SWITCH processed tissue. This new lens has a higher magnification and working distance than the current lens. As an immersion objective, rather than the current air objective, the new lens will also have a higher numerical aperture. In combination, these 3 factors can substantially increase the resolution of the images produced using our LSM system.

The samples process so far have all only been labelled with a single antibody, despite the laser light source being used having the ability to produce 5 different wavelengths of light. Working with Dr. Taylor's group, one future aim for this project is to modify the LSM system to allow for labelling of a sample with multiple antibodies, simultaneously. Although samples can be cleared of antibodies and relabelled, multicolour staining would allow for the co-localisation of proteins; such as prion proteins and receptors, cell types; such as astrocytes and microglia, structures; such as the hippocampus.

Through my work with the CLARITY technique I have found that, using passive tissue clearing, we can successfully label and observe individual cells within the hippocampus. Using light sheet fluorescence microscopy, structures within the brain such as the hippocampus can be well defined. With further development of the LSM system and software, we will be able to generate larger 3-D models of the hippocampus, labelling for important protein and cell types involved in the prion disease model. Making these observations within samples at multiple times points will provide more information about the progression of disease within a neurodegenerative model. As well as using the CLARITY technique, further optimisation should also be performed on the SWITCH protocol. Although internal structures were not seen as clearly within SWITCH tissue, further optimisation of both the CLARITY and SWITCH protocols is still required to consistently produce high quality samples and images. If these optimisations show the SWITCH protocol producing images of comparable quality it may be a preferable technique to use in the future due to the sped of the processing technique over CLARITY.

References

Abdul-Ridha, A., Lane, J.R., Sexton, P.M., Canals, M., Christopoulos, A., 2013. Allosteric modulation of a chemogenetically modified G protein-coupled receptor. Mol. Pharmacol. 83, 521–30. doi:10.1124/mol.112.083006

Adam, R., David, A.S., 2007. Patterns of anterior cingulate activation in schizophrenia: A selective review. Neuropsychiatr. Dis. Treat. 3, 87–101. doi:10.2147/nedt.2007.3.1.87

Aidoo, A.Y., Ward, K., 2006. Spatio-temporal concentration of acetylcholine in vertebrate synaptic cleft. Math. Comput. Model. 44, 952–962. doi:10.1016/j.mcm.2006.03.003

Ajima, A., Kato, T., 1987. Brain dialysis: Detection of acetylcholine in the striatum of unrestrained and unanesthetized rats. Neurosci. Lett. 81, 129–132. doi:10.1016/0304-3940(87)90352-1

Akam, E.C., Challiss, R. a, Nahorski, S.R., 2001. G(q/11) and G(i/o) activation profiles in CHO cells expressing human muscarinic acetylcholine receptors: dependence on agonist as well as receptor-subtype. Br. J. Pharmacol. 132, 950–958. doi:10.1038/sj.bjp.0703892

Akiba, I., Kubo, T., Maeda, A., Bujo, H., Nakai, J., Mishina, M., Numa, S., 1988. Primary structure of porcine muscarinic acetylcholine receptor III and antagonist binding studies. FEBS Lett. 235, 257–261. doi:10.1016/0014-5793(88)81274-2

Alagha, K., Palot, A., Sofalvi, T., Pahus, L., Gouitaa, M., Tummino, C., Martinez, S., Charpin, D., Bourdin, A., Chanez, P., 2014. Long-acting muscarinic receptor antagonists for the treatment of chronic airway diseases. Ther. Adv. Chronic Dis. 5, 85–98. doi:10.1177/2040622313518227

Alexander, G.M., Rogan, S.C., Abbas, A.I., Armbruster, B.N., Pei, Y., Allen, J.A., Nonneman, R.J., Hartmann, J., Moy, S.S., Nicolelis, M.A., McNamara, J.O., Roth, B.L., Alexander, G.M., Rogan, S.C., Rogan, S.C., Abbas, A.I., Abbas, A.I., Armbruster, B.N., Armbruster, B.N., Pei, Y., Pei, Y., Allen, J.A., Allen, J.A., Nonneman, R.J., Nonneman,

R.J., Hartmann, J., Hartmann, J., Moy, S.S., Moy, S.S., Nicolelis, M.A., Nicolelis, M.A., McNamara, J.O., McNamara, J.O., Roth, B.L., Roth, B.L., 2009. Remote control of neuronal activity in transgenic mice expressing evolved G protein-coupled receptors. Neuron 63, 27–39. doi:10.1016/j.neuron.2009.06.014

Alzheimer's Society, Society, A., 2014. Dementia UK: Update.

Armbruster, B.N., Li, X., Pausch, M.H., Herlitze, S., Roth, B.L., 2007. Evolving the lock to fit the key to create a family of G protein-coupled receptors potently activated by an inert ligand. Proc. Natl. Acad. Sci. U. S. A. 104, 5163–8. doi:10.1073/pnas.0700293104

Ashby, C.R., Wang, R.Y., 1996. Pharmacological actions of the atypical antipsychotic drug clozapine: A review. Synapse 24, 349–394. doi:10.1002/(SICI)1098-2396(199612)24:4<349::AID-SYN5>3.0.CO;2-D

Attramadal, H., Arriza, J.L., Aoki, C., Dawson, T.M., Codina, J., Kwatra, M.M., Snyder, S.H., Caron, M.G., Lefkowitz, R.J., 1992. Beta-arrestin2, a novel member of the arrestin/beta-arrestin gene family. J. Biol. Chem. 267, 17882–90.

Attwood, T.K., Findlay, J.B., 1994. Fingerprinting G-protein-coupled receptors. Protein Eng. 7, 195–203.

Avaliani, N., Andersson, M., Runegaard, A.H., Woldbye, D., Kokaia, M., 2016. DREADDs suppress seizure-like activity in a mouse model of pharmacoresistant epileptic brain tissue. Gene Ther. 1–7. doi:10.1038/gt.2016.56

Baltos, J.A., Gregory, K.J., White, P.J., Sexton, P.M., Christopoulos, A., May, L.T., 2016. Quantification of adenosine A1 receptor biased agonism: Implications for drug discovery. Biochem. Pharmacol. 99, 101–112. doi:10.1016/j.bcp.2015.11.013

Barlow, R.B., Berry, K.J., Glenton, P.A., Nilolaou, N.M., Soh, K.S., 1976. A comparison of affinity constants for muscarine-sensitive acetylcholine receptors in guinea-pig atrial pacemaker cells at 29 degrees C and in ileum at 29 degrees C and 37 degrees C. Br. J. Pharmacol. 58, 613–20. doi:10.1111/j.1476-5381.1976.tb08631.x

Basile, A.S., Fedorova, I., Zapata, A., Liu, X., Shippenberg, T., Duttaroy, A., Yamada, M.,

Wess, J., 2002. Deletion of the M5 muscarinic acetylcholine receptor attenuates morphine reinforcement and withdrawal but not morphine analgesia. Proc. Natl. Acad. Sci. U. S. A. 99, 11452–7. doi:10.1073/pnas.162371899

Bender, D., Holschbach, M., Stöcklin, G., 1994. Synthesis of n.c.a. carbon-11 labelled clozapine and its major metabolite clozapine-N-oxide and comparison of their biodistribution in mice. Nucl. Med. Biol. 21, 921–925. doi:10.1016/0969-8051(94)90080-9

Benovic, J.L., Pike, L.J., Cerione, R.A., Staniszewski, C., Yoshimasa, T., Codina, J., Caron, M.G., Lefkowitz, R.J., 1985. Phosphorylation of the mammalian Beta-adrenergic receptor by cyclic AMP-dependent protein kinase. Regulation of the rate of receptor phosphorylation and dephosphorylation by agonist occupancy and effects on coupling of the receptor to the stimulatory guan. J. Biol. Chem. 260, 7094–7101. doi:10.1038/333370a0

Benyamin, R., Trescot, A., Datta, S., Buenaventura, R., Adllaka, R., Sehgal, N., Glaser, S., Vallejo, R., 2008. Opioid complications and side effects. Pain Physician 11, S105–S120.

Birdsall, N.J.M., Hulme, E.C., 1983. Muscarinic receptor subclasses. Trends Pharmacol. Sci. 4, 459–463. doi:10.1016/0165-6147(83)90493-5

Birdsall, N.J.M., Nathanson, N.M., Schwarz, R.D., 2001. Muscarinic receptors: it's a knockout. Trends Pharmacol. Sci. 22, 215–219. doi:10.1016/S0165-6147(00)01660-6

Bjarnadóttir, T.K., Gloriam, D.E., Hellstrand, S.H., Kristiansson, H., Fredriksson, R., Schiöth, H.B., 2006. Comprehensive repertoire and phylogenetic analysis of the G protein-coupled receptors in human and mouse. Genomics 88, 263–73. doi:10.1016/j.ygeno.2006.04.001

Black, J.W., Crowther, A.F., Shanks, R.G., Smith, L.H., Dornhorst, A.C., 1964. A NEW ADRENERGIC: BETA-RECEPTOR ANTAGONIST. Lancet 283, 1080–1081. doi:10.1016/S0140-6736(64)91275-9

Bodick, N.C., Offen, W.W., Levey, A.I., Cutler, N.R., Gauthier, S.G., Satlin, A., Shannon, H.E., Tollefson, G.D., Rasmussen, K., Bymaster, F.P., Hurley, D.J., Potter, W.Z., Paul, S.M., 1997. Effects of xanomeline, a selective muscarinic receptor agonist, on cognitive function and behavioral symptoms in Alzheimer disease. Arch. Neurol. 54, 465–73. doi:10.1001/archneur.1997.00550160091022.

Bohn, L.M., Gainetdinov, R.R., Lin, F.-T., Lefkowitz, R.J., Caron, M.G., 2000. μ-Opioid receptor desensitization by β-arrestin-2 determines morphine tolerance but not dependence. Nature 408, 720–723. doi:10.1038/35047086

Bohn, L.M., Lefkowitz, R.J., Gainetdinov, R.R., Peppel, K., Caron, M.G., Lin, F.T., 1999. Enhanced morphine analgesia in mice lacking beta-arrestin 2. Science 286, 2495–8.

Bolden, C., Cusack, B., Richelson, E., 1992. Antagonism by Antimuscarinic and Neuroleptic the Five Cloned Human Muscarinic Cholinergic Expressed in Chinese Hamster Ovary Cells1 Compounds Receptors at. Pharmacol. Exp. Ther. 260, 576–580.

Bolognini, D., Moss, C.E., Nilsson, K., Petersson, A.U., Donnelly, I., Sergeev, E., König, G.M., Kostenis, E., Kurowska-Stolarska, M., Miller, A., Dekker, N., Tobin, A.B., Milligan, G., 2016. A Novel Allosteric Activator of Free Fatty Acid 2 Receptor Displays Unique G i -functional Bias. J. Biol. Chem. 291, 18915–18931. doi:10.1074/jbc.M116.736157

Bonner, T.I., Buckley, N.J., Young, A.C., Brann, M.R., 1987. Identification of a family of muscarinic acetylcholine receptor genes. Science 237, 527–532. doi:10.1126/science.3037705

Bonner, T.I., Modi, W.S., Seuanez, H.N., OBrien, S.J., 1991. Chromosomal mapping of the five human genes encoding muscarinic acetylcholine receptors., in: Cytogenetics and Cell Genetics. p. 1850.

Bonner, T.I., Young, A.C., Brann, M.R., Buckley, N.J., 1988. Cloning and expression of the human and rat m5 muscarinic acetylcholine receptor genes. Neuron 1, 403–10. doi:10.1016/0896-6273(88)90190-0

Bouvier, M., Leeb-Lundberg, L.M., Benovic, J.L., Caron, M.G., Lefkowitz, R.J., 1987. Regulation of adrenergic receptor function by phosphorylation. II. Effects of agonist occupancy on phosphorylation of alpha 1- and beta 2-adrenergic receptors by protein kinase C and the cyclic AMP-dependent protein kinase. J. Biol. Chem. 262, 3106–13. doi:10.1016/B978-0-12-152828-7.50007-X

Bradley, S.J., Bourgognon, J.-M., Sanger, H.E., Verity, N., Mogg, A.J., White, D.J., Butcher, A.J., Moreno, J.A., Molloy, C., Macedo-Hatch, T., Edwards, J.M., Wess, J., Pawlak, R., Read, D.J., Sexton, P.M., Broad, L.M., Steinert, J.R., Mallucci, G.R., Christopoulos, A., Felder, C.C., Tobin, A.B., 2016a. M1 muscarinic allosteric modulators slow prion neurodegeneration and restore memory loss. J. Clin. Invest. 127, 487–499. doi:10.1172/JCI87526

Bradley, S.J., Wiegman, C.H., Iglesias, M.M., Kong, K.C., Butcher, A.J., Plouffe, B., Goupil, E., Bourgognon, J.-M., Macedo-Hatch, T., LeGouill, C., Russell, K., Laporte, S.A., König, G.M., Kostenis, E., Bouvier, M., Chung, K.F., Amrani, Y., Tobin, A.B., 2016b. Mapping physiological G protein-coupled receptor signaling pathways reveals a role for receptor phosphorylation in airway contraction. Proc. Natl. Acad. Sci. 113, 201521706. doi:10.1073/pnas.1521706113

Braumann, U.-D., Scherf, N., Einenkel, J., Horn, L.-C., Wentzensen, N., Loeffler, M., Kuska, J.-P., 2007. Large Histological Serial Sections for Computational Tissue Volume Reconstruction. Methods Inf. Med. 46, 614–622. doi:10.1160/ME9065

Breitman, M.L., Tsuda, M., Usukura, J., Kikuchi, T., Zucconi, A., Khoo, W., Shinohara, T., 1991. Expression of S-antigen in retina, pineal gland, lens, and brain is directed by 5'-flanking sequences. J. Biol. Chem. 266, 15505–15510.

Brown, D.A., 2010. Muscarinic Acetylcholine Receptors (mAChRs) in the Nervous System: Some Functions and Mechanisms. J. Mol. Neurosci. 41, 340–346. doi:10.1007/s12031-010-9377-2

Bruno, J.P., Gash, C., Martin, B., Zmarowski, A., Pomerleau, F., Burmeister, J., Huettl, P., Gerhardt, G.A., 2006. Second-by-second measurement of acetylcholine release in prefrontal cortex. Eur. J. Neurosci. 24, 2749–2757. doi:10.1111/j.1460-

9568.2006.05176.x

Bruysters, M., Jongejan, A., Akdemir, A., Bakker, R.A., Leurs, R., 2005. A Gq/11-coupled mutant histamine H1 receptor F435A activated solely by synthetic ligands (RASSL). J. Biol. Chem. 280, 34741–34746. doi:10.1074/jbc.M504165200

Buck, S.H., Burcher, E., 1987. Differential sensitivity to phenoxybenzamine alkylation among types of neurokinin binding sites. Neuropeptides 9, 33–9.

Bullitt, E., 1990. Expression ofC-fos-like protein as a marker for neuronal activity following noxious stimulation in the rat. J. Comp. Neurol. 296, 517–530. doi:10.1002/cne.902960402

Burford, N.T., Tobin, A.B., Nahorski, S.R., 1995. Differential coupling of m1, m2 and m3 muscarinic receptor subtypes to inositol 1,4,5-trisphosphate and adenosine 3',5'-cyclic monophosphate accumulation in Chinese hamster ovary cells. J Pharmacol Exp Ther 274, 134–142.

Butcher, A.J., Bradley, S.J., Prihandoko, R., Brooke, S.M., Mogg, A., Bourgognon, J.-M., Macedo-Hatch, T., Edwards, J.M., Bottrill, A.R., Challiss, R.A.J., Broad, L.M., Felder, C.C., Tobin, A.B., 2016. An antibody biosensor establishes the activation of the M1 muscarinic acetylcholine receptor during learning and memory. J. Biol. Chem. 291, 8862–8875. doi:10.1074/jbc.M115.681726

Butcher, A.J., Prihandoko, R., Kong, K.C., McWilliams, P., Edwards, J.M., Bottrill, A., Mistry, S., Tobin, A.B., 2011. Differential G-protein-coupled receptor phosphorylation provides evidence for a signaling bar code. J. Biol. Chem. 286, 11506–11518. doi:10.1074/jbc.M110.154526

Calzetta, L., Rogliani, P., Ora, J., Puxeddu, E., Cazzola, M., Matera, M.G., 2017. LABA/LAMA combination in COPD: a meta-analysis on the duration of treatment. Eur. Respir. Rev. 26, 160043. doi:10.1183/16000617.0043-2016

Catapano, L.A., Manji, H.K., 2007. G protein-coupled receptors in major psychiatric disorders. Biochim. Biophys. Acta 1768, 976–93. doi:10.1016/j.bbamem.2006.09.025

Chang, W.H., Lin, S.K., Lane, H.Y., Wei, F.C., Hu, W.H., Lam, Y.W., Jann, M.W., 1998. Reversible metabolism of clozapine and clozapine N-oxide in schizophrenic patients. Prog. Neuropsychopharmacol. Biol. Psychiatry 22, 723–39. doi:10.1016/S0278-5846(98)00035-9

Chen, X., Choo, H., Huang, X.P., Yang, X., Stone, O., Roth, B.L., Jin, J., 2015. The first structure-activity relationship studies for designer receptors exclusively activated by designer drugs. ACS Chem. Neurosci. 6, 476–484. doi:10.1021/cn500325v

Cheryl, M., Craft, C.M., Whitmore, D.H., Wiechmann, A.F., Cheryl, M., Craft, C.M., Whitmore, D.H., Wiechmann, A.F., 1994. Cone arrestin identified by targeting expression of a functional family. J. Biol. Chem. 269, 4613–9.

Christopoulos, A., Birdsall, N.J.M., Brown, D.A., Buckley, N.J., Challiss, R.A.J., Eglen, R.M., Ehlert, F.J., Felder, C.C., Hammer, R., Kilbinger, H.J., Lambrecht, G., Langmead, C.J., Mitchelson, F., Mutschler, E., Nathanson, N.M., Tobin, A.B., Wess, J., Schwartz, R.D., 2017. Acetylcholine receptors (muscarinic) [WWW Document]. IUPHAR/BPS Guid. to Pharmacol. URL http://www.guidetopharmacology.org/GRAC/FamilyDisplayForward?familyId=2 (accessed 9.10.17).

Chung, K., Wallace, J., Kim, S.-Y., Kalyanasundaram, S., Andalman, A.S., Davidson, T.J., Mirzabekov, J.J., Zalocusky, K.A., Mattis, J., Denisin, A.K., Pak, S., Bernstein, H., Ramakrishnan, C., Grosenick, L., Gradinaru, V., Deisseroth, K., 2013. Structural and molecular interrogation of intact biological systems. Nature 497, 332–7. doi:10.1038/nature12107

Claeysen, S., Joubert, L., Sebben, M., Bockaert, J., Dumuis, A., 2003. A single mutation in the 5-HT4 receptor (5-HT4-R D100(3.32)A) generates a Gs-coupled receptor activated exclusively by synthetic ligands (RASSL). J. Biol. Chem. 278, 699–702. doi:10.1074/jbc.C200588200

Conklin, B.R., Bourne, H.R., 1993. Structural elements of Gα subunits that interact with Gβγ, receptors, and effectors. Cell 73, 631–641. doi:10.1016/0092-8674(93)90245-L

Conn, P.J., Christopoulos, A., Lindsley, C.W., 2009. Allosteric modulators of GPCRs: a novel approach for the treatment of CNS disorders. Nat. Rev. Drug Discov. 8, 41–54. doi:10.1038/nrd2760

Conrad, C.D., Grote, K.A., Hobbs, R.J., Ferayorni, A., 2003. Sex differences in spatial and non-spatial Y-maze performance after chronic stress. Neurobiol. Learn. Mem. 79, 32–40. doi:10.1016/S1074-7427(02)00018-7

Coward, D.M., 1992. General pharmacology of clozapine. Br. J. Psychiatry 160, 5–11. doi:10.1007/978-3-642-60551-2

Coward, P., Wada, H.G., Falk, M.S., Chan, S.D., Meng, F., Akil, H., Conklin, B.R., 1998. Controlling signaling with a specifically designed Gi-coupled receptor. Proc. Natl. Acad. Sci. U. S. A. 95, 352–7. doi:10.1073/pnas.95.1.352

Crilly, J., 2007. The history of clozapine and its emergence in the US market: a review and analysis. Hist. Psychiatry 18, 39–60. doi:10.1177/0957154X07070335

Daaka, Y., Luttrell, L.M., Lefkowitz, R.J., 1997. Switching of the coupling of the beta2-adrenergic receptor to different G proteins by protein kinase A. Nature 390, 88–91. doi:10.1038/36362

Dale, H.H.H., 1914. The Action of Certain Esters and Ethers of Choline, and Their Relation to Muscarine. J. Pharmacol. Exp. Ther. 6, 147–190.

Danysz, W., Parsons, C.G., 2003. The NMDA receptor antagonist memantine as a symptomatological and neuroprotective treatment for Alzheimer's disease: Preclinical evidence. Int. J. Geriatr. Psychiatry 18. doi:10.1002/gps.938

Davidson, M.W., 2017. Numerical Apeture [WWW Document]. URL https://www.microscopyu.com/microscopy-basics/numerical-aperture (accessed 9.7.17).

DD, F., Ferrari-DiLeo, G., DC, M., AI, L., 1995. Differential regulation of molecular subtypes of muscarinic receptors in Alzheimer's disease. J Neurochem 64, 1888–1891. doi:10.1046/j.1471-4159.1995.64041888.x/abstract

de Boer, P., Westerink, B.H.C., Horn, A.S., 1990. The effect of acetylcholinesterase inhibition on the release of acetylcholine from the striatum in vivo: Interaction with autoreceptor responses. Neurosci. Lett. 116, 357–360. doi:10.1016/0304-3940(90)90101-E

Dean, B., McLeod, M., Keriakous, D., McKenzie, J., Scarr, E., 2002. Decreased muscarinic1 receptors in the dorsolateral prefrontal cortex of subjects with schizophrenia. Mol. Psychiatry 7, 1083–91. doi:10.1038/sj.mp.4001199

DeWire, S.M., Yamashita, D.S., Rominger, D.H., Liu, G., Cowan, C.L., Graczyk, T.M., Chen, X., Pitis, P.M., Gotchev, D., Yuan, C., Koblish, M., Lark, M.W., Violin, J.D., 2013. A G protein-biased ligand at the μ-opioid receptor is potently analgesic with reduced gastrointestinal and respiratory dysfunction compared with morphine. J. Pharmacol. Exp. Ther. 344, 708–17. doi:10.1124/jpet.112.201616

Dhein, S., van Koppen, C.J., Brodde, O.E., 2001. Muscarinic receptors in the mammalian heart. Pharmacol. Res. 44, 161–82. doi:10.1006/phrs.2001.0835

Digby, G.J., Noetzel, M.J., Bubser, M., Utley, T.J., Walker, A.G., Byun, N.E., Lebois, E.P., Xiang, Z., Sheffler, D.J., Cho, H.P., Davis, A.A., Nemirovsky, N.E., Mennenga, S.E., Camp, B.W., Bimonte-Nelson, H.A., Bode, J., Italiano, K., Morrison, R., Daniels, J.S., Niswender, C.M., Olive, M.F., Lindsley, C.W., Jones, C.K., Conn, P.J., 2012. Novel allosteric agonists of M1 muscarinic acetylcholine receptors induce brain region-specific responses that correspond with behavioral effects in animal models. J. Neurosci. 32, 8532–44. doi:10.1523/JNEUROSCI.0337-12.2012

Disse, B., Speck, G. a, Rominger, K.L., Witek, T.J., Hammer, R., 1999. Tiotropium (Spiriva): mechanistical considerations and clinical profile in obstructive lung disease. Life Sci. 64, 457–464. doi:10.1016/S0024-3205(98)00588-8

Dodt, H., Leischner, U., Schierloh, A., Jährling, N., Mauch, C.P., Deininger, K., Deussing, J.M., Eder, M., Zieglgänsberger, W., Becker, K., Dodt, H., Leischner, U., Schierloh, A., Ja, N., Becker, K., Deininger, K., Deussing, J.M., Eder, M., Zieglga, W., 2007. Ultramicroscopy: three-dimensional visualization of neuronal networks in the whole mouse brain. Nat. Methods 4, 331–6. doi:10.1038/nmeth1036

Dortch-Carnes, J., Potter, D.E., 2005. Bremazocine: a kappa-opioid agonist with potent analgesic and other pharmacologic properties. CNS Drug Rev. 11, 195–212.

Dower, K., Zhao, S., Schlerman, F.J., Savary, L., Campanholle, G., Johnson, B.G., Xi, L., Nguyen, V., Zhan, Y., Lech, M.P., Wang, J., Nie, Q., Karsdal, M.A., Genovese, F., Boucher, G., Brown, T.P., Zhang, B., Homer, B.L., Martinez, R. V., 2017. High resolution molecular and histological analysis of renal disease progression in ZSF1 fa/faCP rats, a model of type 2 diabetic nephropathy. PLoS One 12, e0181861. doi:10.1371/journal.pone.0181861

Duttaroy, A., Zimliki, C.L., Gautam, D., Cui, Y., Mears, D., 2004. Muscarinic Stimulation of Pancreatic Insulin and Glucagon Release Is Abolished in M 3 Muscarinic Acetylcholine Receptor ⁒… Deficient Mice. Diabetes 53, 1714–1720.

Eglen, R.M., Harris, G.C., 1993. Selective inactivation of muscarinic M2 and M3 receptors in guinea-pig ileum and atria in vitro. Br. J. Pharmacol. 109, 946–52. doi:10.1111/j.1476-5381.1993.tb13712.x

Eglen, R.M., Nahorski, S.R., 2000. The muscarinic M 5 receptor: a silent or emerging subtype? Br. J. Pharmacol. 130, 13–21. doi:10.1038/sj.bjp.0703276

Eglen, R.M., Reddy, H., Watson, N., 1994. Selective inactivation of muscarinic receptor subtypes. Int. J. Biochem. 26, 1357–1368. doi:10.1016/0020-711X(94)90178-3

Eiermann, B., Engel, G., Johansson, I., Zanger, U.M., Bertilsson, L., 2003. The involvement of CYP1A2 and CYP3A4 in the metabolism of clozapine. Br. J. Clin. Pharmacol. 44, 439–446. doi:10.1046/j.1365-2125.1997.t01-1-00605.x

Ertürk, A., Becker, K., Jährling, N., Mauch, C.P., Hojer, C.D., Egen, J.G., Hellal, F., Bradke, F., Sheng, M., Dodt, H.-U., 2012. Three-dimensional imaging of solvent-cleared organs using 3DISCO. Nat. Protoc. 7, 1983–95. doi:10.1038/nprot.2012.119

Evans, B.A., Broxton, N., Merlin, J., Sato, M., Hutchinson, D.S., Christopoulos, A., Summers, R.J., 2011. Quantification of functional selectivity at the human α(1A)-adrenoceptor. Mol. Pharmacol. 79, 298–307. doi:10.1124/mol.110.067454

Ewins, A.J., 1914. Acetylcholine, a New Active Principle of Ergot. Biochem. J. 8, 44–9.

Fang, Y., Vilella-Bach, M., Bachmann, R., Flanigan, A., Chen, J., 2001. Phosphatidic acid-mediated mitogenic activation of mTOR signaling. Science 294, 1942–5. doi:10.1126/science.1066015

Ferguson, S.S.G., 2001. Evolving concepts in G protein-coupled receptor endocytosis: the role in receptor desensitization and signaling. Pharmacol. Rev. 53, 1–24.

Fernandez, N., Monczor, F., Baldi, A., Davio, C., Shayo, C., 2008. Histamine H2 receptor trafficking: role of arrestin, dynamin, and clathrin in histamine H2 receptor internalization. Mol. Pharmacol. 74, 1109–18. doi:10.1124/mol.108.045336

Fetscher, C., Fleichman, M., Schmidt, M., Krege, S., Michel, M.C., 2002. M(3) muscarinic receptors mediate contraction of human urinary bladder. Br. J. Pharmacol. 136, 641–3. doi:10.1038/sj.bjp.0704781

Fortress, A.M., Hamlett, E.D., Vazey, E.M., Aston-Jones, G., Cass, W.A., Boger, H.A., Granholm, A.-C.E.A.-C.E., 2015. Designer Receptors Enhance Memory in a Mouse Model of Down Syndrome. J. Neurosci. 35, 1343–1353. doi:10.1523/JNEUROSCI.2658-14.2015

Foster, D.A., 2009. Phosphatidic acid signaling to mTOR: signals for the survival of human cancer cells. Biochim. Biophys. Acta 1791, 949–55. doi:10.1016/j.bbalip.2009.02.009

Fraser, P.J., 1957. Pharmacological Actions of Pure Muscarine Chloride. Br. J. Pharmacol. Chemother. 12, 47–52. doi:10.1111/j.1476-5381.1957.tb01361.x

Fryer, A.D., Jacoby, D.B., 1998. Muscarinic receptors and control of airway smooth muscle. Am. J. Respir. Crit. Care Med. 158, S154-60. doi:10.1164/ajrccm.158.supplement_2.13tac120

Gautam, D., Duttaroy, A., Cui, Y., Han, S., Deng, C., Seeger, T., Alzheimer, C., Wess, J., 2006a. M1-M3 muscarinic acetylcholine receptor-deficient mice: novel phenotypes. J. Mol. Neurosci. 30, 157–60. doi:10.1385/JMN:30:1:157

Gautam, D., Gavrilova, O., Jeon, J., Pack, S., Jou, W., Cui, Y., Li, J.H., Wess, J., 2006b. Beneficial metabolic effects of M3 muscarinic acetylcholine receptor deficiency.

Cell Metab. 4, 363–75. doi:10.1016/j.cmet.2006.09.008

Gautam, D., Han, S.-J., Hamdan, F.F., Jeon, J., Li, B., Li, J.H., Cui, Y., Mears, D., Lu, H., Deng, C., Heard, T., Wess, J., 2006c. A critical role for β cell M3 muscarinic acetylcholine receptors in regulating insulin release and blood glucose homeostasis in vivo. Cell Metab. 3, 449–461. doi:10.1016/j.cmet.2006.04.009

Gautam, D., Heard, T.S., Cui, Y., Miller, G., Bloodworth, L., Wess, J., 2004. Cholinergic stimulation of salivary secretion studied with M1 and M3 muscarinic receptor single- and double-knockout mice. Mol. Pharmacol. 66, 260–7. doi:10.1124/mol.66.2.260

Gaven, F., Pellissier, L.P., Queffeulou, E., Cochet, M., Bockaert, J., Dumuis, A., Claeysen, S., 2013. Pharmacological profile of engineered 5-HT_4 receptors and identification of 5-HT_4 receptor-biased ligands. Brain Res. 1511, 65–72. doi:10.1016/j.brainres.2012.11.005

Gazi, L., Bobirnac, I., Danzeisen, M., Schüpbach, E., Langenegger, D., Sommer, B., Hoyer, D., Tricklebank, M., Schoeffter, P., 1999. Receptor density as a factor governing the efficacy of the dopamine D4 receptor ligands, L-745,870 and U-101958 at human recombinant D4.4 receptors expressed in CHO cells. Br. J. Pharmacol. 128, 613–620. doi:10.1038/sj.bjp.0702849

Gibbons, A.S., Scarr, E., Boer, S., Money, T., Jeon, W., Felder, C.C., Dean, B., 2013. Widespread decreases in cortical muscarinic receptors in a subset of people with schizophrenia. Int. J. Neuropsychopharmacol. 16, 37–46. doi:10.1017/S1461145712000028

GILLAM, P.M.S., PRICHARD, B.N.C., 1965. Use of Propranolol in Angina Pectoris. Br. Med. J. 2, 337–9. doi:10.1136/bmj.2.5457.337

Gilman, A., 1987. G Proteins: Transducers Of Receptor-Generated Signals. Annu. Rev. Biochem. 56, 615–649. doi:10.1146/annurev.biochem.56.1.615

Gomeza, J., Shannon, H., Kostenis, E., Felder, C.C., Zhang, L., Brodkin, J., Grinberg, A., Sheng, H., Wess, J., 1999a. Pronounced pharmacologic deficits in M2 muscarinic

acetylcholine receptor knockout mice. Proc. Natl. Acad. Sci. U. S. A. 96, 1692–7. doi:10.1073/pnas.96.4.1692

Gomeza, J., Zhang, L., Kostenis, E., Felder, C.C., Bymaster, F., Brodkin, J., Shannon, H., Xia, B., Deng, C., Wess, J., 1999b. Enhancement of D1 dopamine receptor-mediated locomotor stimulation in M(4) muscarinic acetylcholine receptor knockout mice. Proc. Natl. Acad. Sci. U. S. A. 96, 10483–8. doi:10.1073/pnas.96.18.10483

Goodman, O.B., Krupnick, J.G.. G.G., Santini, F., Gurevich, V. V., Penn, R.B., Gagnon, A.W., Keen, J.H., Benovic, J.L., 1996. Beta-arrestin acts as a clathrin adaptor in endocytosis of the beta2-adrenergic receptor. Nature 383, 447–50. doi:10.1038/383447a0

Graham, M.J., Lake, B.G., 2008. Induction of drug metabolism: Species differences and toxicological relevance. Toxicology 254, 184–191. doi:10.1016/j.tox.2008.09.002

Grant, M.K.O., El-Fakahany, E.E., 2005. Persistent binding and functional antagonism by xanomeline at the muscarinic M5 receptor. J. Pharmacol. Exp. Ther. 315, 313–9. doi:10.1124/jpet.105.090134

Griffin, M., Figueroa, K., Liller, S., Ehlert, F., 2007. Estimation of agonist activity at G protein-coupled receptors: analysis of M2 muscarinic receptor signaling through Gi/o, Gs, and G15. J. Pharmacol. Exp. Ther. 321, 1193–1207. doi:10.1124/jpet.107.120857.most

Guettier, J.-M.J.-M., Gautam, D., Scarselli, M., Ruiz de Azua, I., Li, J.H., Rosemond, E., Ma, X., Gonzalez, F.J., Armbruster, B.N., Lu, H., Roth, B.L., Wess, J., de Azua, I.R., Li, J.H., Rosemond, E., Ma, X., Gonzalez, F.J., Armbruster, B.N., Lu, H., Roth, B.L., Wess, J., Ruiz de Azua, I., Li, J.H., Rosemond, E., Ma, X., Gonzalez, F.J., Armbruster, B.N., Lu, H., Roth, B.L., Wess, J., 2009. A chemical-genetic approach to study G protein regulation of beta cell function in vivo. Proc. Natl. Acad. Sci. U. S. A. 106, 19197–202. doi:10.1073/pnas.0906593106

Gurevich, V. V., Chen, C.Y., Kim, C.M., Benovic, J.L., 1994. Visual arrestin binding to rhodopsin. Intramolecular interaction between the basic N terminus and acidic C terminus of arrestin may regulate binding selectivity. J. Biol. Chem. 269, 8721–

8727.

Gurwitz, D., Haring, R., Heldman, E., Fraser, C.M., Manor, D., Fisher, A., 1994. Discrete activation of transduction pathways associated with acetylcholine m1 receptor by several muscarinic ligands. Eur. J. Pharmacol. Mol. Pharmacol. 267, 21–31. doi:10.1016/0922-4106(94)90220-8

Hama, H., Kurokawa, H., Kawano, H., Ando, R., Shimogori, T., Noda, H., Fukami, K., Sakaue-Sawano, A., Miyawaki, A., 2011. Scale: a chemical approach for fluorescence imaging and reconstruction of transparent mouse brain. Nat. Neurosci. 14, 1481–8. doi:10.1038/nn.2928

Hammer, R., Berrie, C.P., Birdsall, N.J.M., Burgen, A.S., Hulme, E.C., 1980. Pirenzepine distinguishes between different subclasses of muscarinic receptors. Nature 283, 90–2. doi:10.1038/283090a0

Hammer, R., Giachetti, A., 1982. Muscarinic receptor subtypes: M1 and M2 biochemical and functional characterization. Life Sci. 31, 2991–2998. doi:10.1016/0024-3205(82)90066-2

Harrison, D.C., Griffin, J.R., Fiene, T.J., 1965. EFFECTS OF BETA-ADRENERGIC BLOCKADE WITH PROPRANOLOL IN PATIENTS WITH ATRIAL ARRHYTHMIAS. N. Engl. J. Med. 273, 410–5. doi:10.1056/NEJM196508192730802

Hartog, C. Den, Zamudio-Bulcock, P., Nimitvilai, S., Gilstrap, M., Fedarovich, H., Motts, A., Woodward, J.J., 2016. Inactivation of the lateral orbitofrontal cortex increases drinking in ethanol-dependent but not non-dependent mice. Neuropharmacology. doi:10.1016/j.neuropharm.2016.03.031

Hauser, A.S., Attwood, M.M., Rask-Andersen, M., Schiöth, H.B., Gloriam, D.E., 2017. Trends in GPCR drug discovery: New agents, targets and indications. Nat. Rev. Drug Discov. 16, 829–842. doi:10.1038/nrd.2017.178

Hauser, A.S., Chavali, S., Masuho, I., Jahn, L.J., Martemyanov, K.A., Gloriam, D.E., Babu, M.M., 2018. Pharmacogenomics of GPCR Drug Targets. Cell 172, 41–54.e19. doi:10.1016/j.cell.2017.11.033

Heinrich, J.N., Butera, J.A., Carrick, T., Kramer, A., Kowal, D., Lock, T., Marquis, K.L., Pausch, M.H., Popiolek, M., Sun, S.-C., Tseng, E., Uveges, A.J., Mayer, S.C., 2009. Pharmacological comparison of muscarinic ligands: historical versus more recent muscarinic M1-preferring receptor agonists. Eur. J. Pharmacol. 605, 53–6. doi:10.1016/j.ejphar.2008.12.044

Henderson, G., Johnson, J.W., Ascher, P., 1990. Competitive antagonists and partial agonists at the glycine modulatory site of the mouse N-methyl-D-aspartate receptor. J. Physiol. 430, 189–212.

Hermans, E., 2003. Biochemical and pharmacological control of the multiplicity of coupling at G-protein-coupled receptors. Pharmacol. Ther. 99, 25–44. doi:10.1016/S0163-7258(03)00051-2

Heusler, P., Bruins Slot, L., Tourette, A., Tardif, S., Cussac, D., 2011. The clozapine metabolite N-desmethylclozapine displays variable activity in diverse functional assays at human dopamine D 2 and serotonin 5-HT 1A receptors. Eur. J. Pharmacol. 669, 51–58. doi:10.1016/j.ejphar.2011.07.031

Higgins, S.T., Lamb, R.J., Henningfield, J.E., 1989. Dose-dependent effects of atropine on behavioral and physiologic responses in humans. Pharmacol. Biochem. Behav. 34, 303–311. doi:10.1016/0091-3057(89)90316-X

Hoyer, D., Boddeke, H.W.G.M., 1993. Partial agonists, full agonists, antagonists: dilemmas of definition. Trends Pharmacol. Sci. 14, 270–275. doi:10.1016/0165-6147(93)90129-8

Hu, J., Stern, M., Gimenez, L.E., Wanka, L., Zhu, L., Rossi, M., Meister, J., Inoue, A., Beck-Sickinger, A.G., Gurevich, V. V., Wess, J., 2016. A G Protein-biased Designer G Protein-coupled Receptor Useful for Studying the Physiological Relevance of G q/11 -dependent Signaling Pathways. J. Biol. Chem. 291, 7809–7820. doi:10.1074/jbc.M115.702282

Hucker, H.B., 1970. Species differences in drug metabolism. Annu Rev Pharmacol 10, 99–118. doi:10.1146/annurev.pa.10.040170.000531

Huisken, J., Swoger, J., Del Bene, F., Wittbrodt, J., Stelzer, E.H.K., 2004. Optical sectioning deep inside live embryos by selective plane illumination microscopy. Science 305, 1007–9. doi:10.1126/science.1100035

Hulme, E.C., Birdsall, N.J.M., Buckley, N.J., 1990. Muscarinic receptor subtypes. Annu. Rev. Pharmacol. Toxicol. 30, 633–673.

Hurowitz, E.H., Melnyk, J.M., Chen, Y.J., Kouros-Mehr, H., Simon, M.I., Shizuya, H., 2000. Genomic characterization of the human heterotrimeric G protein alpha, beta, and gamma subunit genes. DNA Res. 7, 111–120. doi:10.1093/dnares/7.2.111

Ikeda, T., Anisuzzaman, A.S.M., Yoshiki, H., Sasaki, M., Koshiji, T., Uwada, J., Nishimune, A., Itoh, H., Muramatsu, I., 2012. Regional quantification of muscarinic acetylcholine receptors and β-adrenoceptors in human airways. Br. J. Pharmacol. 166, 1804–14. doi:10.1111/j.1476-5381.2012.01881.x

Isberg, V., de Graaf, C., Bortolato, A., Cherezov, V., Katritch, V., Marshall, F.H., Mordalski, S., Pin, J.-P., Stevens, R.C., Vriend, G., Gloriam, D.E., 2015. Generic GPCR residue numbers - aligning topology maps while minding the gaps. Trends Pharmacol. Sci. 36, 22–31. doi:10.1016/j.tips.2014.11.001

Jaeger, W.C., Seeber, R.M., Eidne, K.A., Pfleger, K.D.G., 2014. Molecular determinants of orexin receptor-arrestin-ubiquitin complex formation. Br. J. Pharmacol. 171, 364–74. doi:10.1111/bph.12481

Jann, M.W., Lam, Y.W., Chang, W.H., 1994. Rapid formation of clozapine in guinea-pigs and man following clozapine-N-oxide administration. Arch. Int. Pharmacodyn. Ther. 328, 243–50.

Jat, K.R., Khairwa, A., 2013. Levalbuterol versus albuterol for acute asthma: A systematic review and meta-analysis. Pulm. Pharmacol. Ther. 26, 239–248. doi:10.1016/j.pupt.2012.11.003

Jeon, J., Dencker, D., Wörtwein, G., Woldbye, D.P.D., Cui, Y., Davis, A.A., Levey, A.I., Schütz, G., Sager, T.N., Mørk, A., Li, C., Deng, C.-X., Fink-Jensen, A., Wess, J., 2010. A subpopulation of neuronal M4 muscarinic acetylcholine receptors plays a critical

role in modulating dopamine-dependent behaviors. J. Neurosci. 30, 2396–405. doi:10.1523/JNEUROSCI.3843-09.2010

Johnson, M., 2001. Beta2-adrenoceptors: mechanisms of action of beta2-agonists. Paediatr. Respir. Rev. 2, 57–62. doi:10.1053/prrv.2000.0102

Jones, P., 2016. The therapeutic value of atropine for critical care intubation. Arch Dis Child 101, 77–80. doi:10.1136/archdischild-2014-308137

Kane, J., Honigfeld, G., Singer, J., Meltzer, H., 1988. Clozapine for the treatment-resistant schizophrenic. A double-blind comparison with chlorpromazine. Arch. Gen. Psychiatry 45, 789–96. doi:10.1001/archpsyc.1988.01800330013001

Kane, M., Terry, G., 2015. Dementia 2015 : Aiming higher to transform lives. Alzheimer's Soc. Lead. Fight against Dement. 1–84.

Ke, M.-T., Fujimoto, S., Imai, T., 2013. SeeDB : a simple and morphology-preserving optical clearing agent for neuronal circuit reconstruction. Nat. Publ. Gr. 16, 1154–1161. doi:10.1038/nn.3447

Kenakin, T.P., 2012. The potential for selective pharmacological therapies through biased receptor signaling. BMC Pharmacol. Toxicol. 13, 3. doi:10.1186/2050-6511-13-3

Kenakin, T.P., 1995. Agonist-receptor efficacy II: agonist trafficking of receptor signals. Trends Pharmacol. Sci. 16, 232–238. doi:10.1016/S0165-6147(00)89032-X

Kenakin, T.P., Watson, C., Muniz-Medina, V., Christopoulos, A., Novick, S., 2012. A simple method for quantifying functional selectivity and agonist bias. ACS Chem. Neurosci. 3, 193–203. doi:10.1021/cn200111m

Keov, P., Valant, C., Devine, S.M., Lane, J.R., Scammells, P.J., Sexton, P.M., Christopoulos, A., 2013. Reverse engineering of the selective agonist TBPB unveils both orthosteric and allosteric modes of action at the M_1 muscarinic acetylcholine receptor. Mol. Pharmacol. 84, 425–37. doi:10.1124/mol.113.087320

Kim, K.-S., Abraham, D., Williams, B., Violin, J.D., Mao, L., Rockman, H.A., 2012. β-

Arrestin-biased AT1R stimulation promotes cell survival during acute cardiac injury. Am. J. Physiol. Heart Circ. Physiol. 303, H1001-10. doi:10.1152/ajpheart.00475.2012

Knox, A.J., Tattersfield, A.E., 1995. Airway smooth muscle relaxation. Thorax 50, 894–901.

Kong, K.C., Butcher, A.J., McWilliams, P., Jones, D., Wess, J., Hamdan, F.F., Werry, T., Rosethorne, E.M., Charlton, S.J., Munson, S.E., Cragg, H.A., Smart, A.D., Tobin, A.B., 2010. M3-muscarinic receptor promotes insulin release via receptor phosphorylation/arrestin-dependent activation of protein kinase D1. Proc. Natl. Acad. Sci. 107, 21181–21186. doi:10.1073/pnas.1011651107

Kostenis, E., Waelbroeck, M., Milligan, G., 2005. Techniques: promiscuous Galpha proteins in basic research and drug discovery. Trends Pharmacol. Sci. 26, 595–602. doi:10.1016/j.tips.2005.09.007

Krasel, C., Dammeier, S., Winstel, R., Brockmann, J., Mischak, H., Lohse, M.J., 2001. Phosphorylation of GRK2 by protein kinase C abolishes its inhibition by calmodulin. J. Biol. Chem. 276, 1911–1915. doi:10.1074/jbc.M008773200

Kubo, T., Fukuda, K., Mikami, A., Maeda, A., Takahashi, H., Mishina, M., Haga, T., Haga, K., Ichiyama, A., Kangawa, K., Kojima, M., Matsuo, H., Hirose, T., Numa, S., 1986. Cloning, sequencing and expression of complementary DNA encoding the muscarinic acetylcholine receptor. Nature 323, 411–416. doi:10.1038/323411a0

Kühn, H., Hall, S.W., Wilden, U., 1984. Light-induced binding of 48-kDa protein to photoreceptor membranes is highly enhanced by phosphorylation of rhodopsin. FEBS Lett. 176, 473–8.

Kuwajima, T., Sitko, A.A., Bhansali, P., Jurgens, C., Guido, W., Mason, C., 2013. ClearT: a detergent- and solvent-free clearing method for neuronal and non-neuronal tissue. Development 140, 1364–1368. doi:10.1242/dev.091844

Lameh, J., Philip, M., Sharma, Y.K., Moro, O., Ramachandran, J., Sadée, W., 1992. Hm1 muscarinic cholinergic receptor internalization requires a domain in the third

cytoplasmic loop. J. Biol. Chem. 267, 13406–13412.

Langmead, C.J., Christopoulos, A., 2014. Functional and structural perspectives on allosteric modulation of GPCRs. Curr. Opin. Cell Biol. 27, 94–101. doi:10.1016/j.ceb.2013.11.007

Langmead, C.J., Watson, J., Reavill, C., 2008. Muscarinic acetylcholine receptors as CNS drug targets. Pharmacol. Ther. 117, 232–43. doi:10.1016/j.pharmthera.2007.09.009

Laporte, S.A., Oakley, R.H., Holt, J.A., Barak, L.S., Caron, M.G., 2000. The interaction of beta-arrestin with the AP-2 adaptor is required for the clustering of beta 2-adrenergic receptor into clathrin-coated pits. J. Biol. Chem. 275, 23120–23126. doi:10.1074/jbc.M002581200

Laporte, S.A., Oakley, R.H., Zhang, J., Holt, J.A., Ferguson, S.S., Caron, M.G., Barak, L.S., 1999. The beta2-adrenergic receptor/betaarrestin complex recruits the clathrin adaptor AP-2 during endocytosis. Proc. Natl. Acad. Sci. U. S. A. 96, 3712–3717. doi:10.1073/pnas.96.7.3712

Leaderbrand, K., Chen, H.J., Corcoran, K.A., Guedea, A.L., Jovasevic, V., Wess, J., Radulovic, J., 2016. Muscarinic acetylcholine receptors act in synergy to facilitate learning and memory. Learn. Mem. 23, 631–638. doi:10.1101/lm.043133.116

Lefkowitz, R.J., 1998. G protein-coupled receptors. III. New roles for receptor kinases and beta-arrestins in receptor signaling and desensitization. J. Biol. Chem. 273, 18677–80. doi:9668034

Lerea, C.L., Somers, D.E., Hurley, J.B., Klock, I.B., Bunt-Milam, A.H., 1986. Identification of specific transducin alpha subunits in retinal rod and cone photoreceptors. Science 234, 77–80.

Leucht, S., Corves, C., Arbter, D., Engel, R.R., Li, C., Davis, J.M., 2009. Second-generation versus first-generation antipsychotic drugs for schizophrenia: a meta-analysis. Lancet (London, England) 373, 31–41. doi:10.1016/S0140-6736(08)61764-X

Levey, A.I., Edmunds, S.M., Koliatsos, V., Wiley, R.G., Heilman, C.J., 1995. Expression of

m1-m4 muscarinic acetylcholine receptor proteins in rat hippocampus and regulation by cholinergic innervation. J. Neurosci. 15, 4077–4092.

Levey, A.I., Kitt, C. a, Simonds, W.F., Price, D.L., Brann, M.R., 1991. Identification and localization of muscarinic acetylcholine receptor proteins in brain with subtype-specific antibodies. J. Neurosci. 11, 3218–3226.

Lin, G., McKay, G., Midha, K.K., 1996. Characterization of metabolites of clozapine N-oxide in the rat by micro-column high performance liquid chromatography/mass spectrometry with electrospray interface. J. Pharm. Biomed. Anal. 14, 1561–1577. doi:10.1016/0731-7085(96)01738-4

Linnet, K., Olesen, O. V., 1997. Metabolism of clozapine by cDNA-expressed human cytochrome P450 enzymes. Drug Metab. Dispos. 25, 1379–1382.

Liu, A.K.L., Hurry, M.E.D., Ng, O.T.T.W., Defelice, J., Lai, H.M., Pearce, R.K.B., Wong, G.T.-C.C., Chang, R.C.-C.C., Gentleman, S.M., 2016. Bringing CLARITY to the human brain: visualization of Lewy pathology in three dimensions. Neuropathol. Appl. Neurobiol. 42, 573–587. doi:10.1111/nan.12293

Liu, B., Croy, C.H., Hitchcock, S.A., Allen, J.R., Rao, Z., Evans, D., Bures, M.G., McKinzie, D.L., Watt, M.L., Stuart Gregory, G., Hansen, M.M., Hoogestraat, P.J., Jamison, J.A., Okha-Mokube, F.M., Stratford, R.E., Turner, W., Bymaster, F., Felder, C.C., 2015. Design and synthesis of N-[6-(Substituted Aminoethylideneamino)-2-Hydroxyindan-1-yl]arylamides as selective and potent muscarinic M1 agonists. Bioorg. Med. Chem. Lett. doi:10.1016/j.bmcl.2015.08.011

Liu, J.K., Kato, T., 1994. Effect of physostigmine on relative acetylcholine output induced by systemic treatment with scopolamine in in vivo microdialysis of rat frontal cortex. Neurochem. Int. 24, 589–96.

Locht, C., Coutte, L., Mielcarek, N., 2011. The ins and outs of pertussis toxin. FEBS J. 278, 4668–4682. doi:10.1111/j.1742-4658.2011.08237.x

Lodowski, D.T., Pitcher, J.A., Capel, W.D., Lefkowitz, R.J., Tesmer, J.J.G., 2003. Keeping G proteins at bay: a complex between G protein-coupled receptor kinase 2 and

Gbetagamma. Science 300, 1256–62. doi:10.1126/science.1082348

Loewi, O., Navratil, E., 1926. Über humorale Übertragbarkeit der Herznervenwirkung. Pflüger's Arch. für die Gesamte Physiol. des Menschen und der Tiere 214–214, 678–688. doi:10.1007/BF01741946

Lohse, M., Andexinger, S., Pitcher, J., Trukawinski, S., Codina, J., Faure, J.-P., Caron, M.G., Lefkowitz, R.J., 1992. Receptor-specific Desensitization with Purified Proteins. J. Biol. Chem. 267, 8558–64.

Lohse, M.J., Benovic, J.L., Codina, J., Caron, M.G., Lefkowitz, R.J., 1990. beta-Arrestin: a protein that regulates beta-adrenergic receptor function. Science 248, 1547–50. doi:10.1126/science.2163110

Ma, P., Zemmel, R., 2002. Value of novelty? Nat. Rev. Drug Discov. 1, 571–2. doi:10.1038/nrd884

Machová, E., Jakubík, J., El-Fakahany, E.E., Dolezal, V., 2007. Wash-resistantly bound xanomeline inhibits acetylcholine release by persistent activation of presynaptic M(2) and M(4) muscarinic receptors in rat brain. J. Pharmacol. Exp. Ther. 322, 316–323. doi:10.1124/jpet.107.122093

MacLaren, D.A.A., Browne, R.W., Shaw, J.K., Krishnan Radhakrishnan, S., Khare, P., Espana, R.A., Clark, S.D., 2016. Clozapine-n-oxide administration produces behavioral effects in Long-Evans rats - implications for designing DREADD experiments. eNeuro 10, 219–16. doi:10.1523/ENEURO.0219-16.2016

Maehara, S., Hikichi, H., Ohta, H., 2011. Behavioral effects of N-desmethylclozapine on locomotor activity and sensorimotor gating function in mice-Possible involvement of muscarinic receptors. Brain Res. 1418, 111–119. doi:10.1016/j.brainres.2011.08.056

Malinow, R., 2012. New developments on the role of NMDA receptors in Alzheimer's disease. Curr. Opin. Neurobiol. 22, 559–563. doi:10.1016/j.conb.2011.09.001

Mangmool, S., Kurose, H., 2011. Gi/o protein-dependent and -independent actions of pertussis toxin (ptx). Toxins (Basel). 3, 884–899. doi:10.3390/toxins3070884

Marchese, A., Chen, C., Kim, Y.-M., Benovic, J.L., 2003. The ins and outs of G protein-coupled receptor trafficking. Trends Biochem. Sci. 28, 369–376. doi:10.1016/S0968-0004(03)00134-8

Mason, J.S., Bortolato, A., Congreve, M., Marshall, F.H., 2012. New insights from structural biology into the druggability of G protein- coupled receptors. Trends Pharmacol. Sci. 33, 249–260. doi:10.1016/j.tips.2012.02.005

Matsui, M., Motomura, D., Karasawa, H., Fujikawa, T., Jiang, J., Komiya, Y., Takahashi, S., Taketo, M.M., 2000. Multiple functional defects in peripheral autonomic organs in mice lacking muscarinic acetylcholine receptor gene for the M3 subtype. Proc. Natl. Acad. Sci. U. S. A. 97, 9579–84.

Matthes, H.W.D., Maldonado, R., Simonin, F., Valverde, O., Slowe, S., Kitchen, I., Befort, K., Dierich, A., Le Meur, M., Dollé, P., Tzavara, E., Hanoune, J., Roques, B.P., Kieffer, B.L., 1996. Loss of morphine-induced analgesia, reward effect and withdrawal symptoms in mice lacking the μ-opioid-receptor gene. Nature. doi:10.1038/383819a0

May, L.T., Leach, K., Sexton, P.M., Christopoulos, A., 2007. Allosteric Modulation of G Protein–Coupled Receptors. Annu. Rev. Pharmacol. Toxicol. 47, 1–51. doi:10.1146/annurev.pharmtox.47.120505.105159

McPherson, J., Rivero, G., Baptist, M., Llorente, J., Al-Sabah, S., Krasel, C., Dewey, W.L., Bailey, C.P., Rosethorne, E.M., Charlton, S.J., Henderson, G., Kelly, E., 2010. M-Opioid Receptors: Correlation of Agonist Efficacy for Signalling With Ability To Activate Internalization. Mol. Pharmacol. 78, 756–766. doi:10.1124/mol.110.066613

Miao, Y., Goldfeld, D.A., Moo, E. Von, Sexton, P.M., Christopoulos, A., McCammon, J.A., Valant, C., 2016. Accelerated structure-based design of chemically diverse allosteric modulators of a muscarinic G protein-coupled receptor. Proc. Natl. Acad. Sci. 201612353. doi:10.1073/pnas.1612353113

Michal, P., El-Fakahany, E.E., Dolezal, V., 2007. Muscarinic M2 receptors directly activate Gq/11 and Gs G-proteins. J. Pharmacol. Exp. Ther. 320, 607–614.

doi:10.1124/jpet.106.114314.There

Milligan, G., 1997. Is promiscuity of G protein interaction an issue in the classification of receptors? Ann. N. Y. Acad. Sci. 812, 126–132. doi:10.1111/j.1749-6632.1997.tb48152.x

Mimica, N., Presecki, P., 2009. Side effects of approved antidementives. Psychiatr. Danub. 21, 108–13.

Mirza, N.R., Peters, D., Sparks, R.G., 2003. Xanomeline and the antipsychotic potential of muscarinic receptor subtype selective agonists. CNS Drug Rev. 9, 159–86. doi:10.1111/j.1527-3458.2003.tb00247.x

Mota, S.I., Ferreira, I.L., Rego, A.C., 2014. Dysfunctional synapse in Alzheimer's disease - A focus on NMDA receptors. Neuropharmacology 76, 16–26. doi:10.1016/j.neuropharm.2013.08.013

Mrzljak, L., Levey, A.I., Belcher, S., Goldman-Rakic, P.S., 1998. Localization of the m2 muscarinic acetylcholine receptor protein and mRNA in cortical neurons of the normal and cholinergically deafferented rhesus monkey. J. Comp. Neurol. 390, 112–132. doi:10.1002/(SICI)1096-9861(19980105)390:1<112::AID-CNE10>3.0.CO;2-Z

Mrzljak, L., Levey, A.I., Goldman-Rakic, P.S., 1993. Association of m1 and m2 muscarinic receptor proteins with asymmetric synapses in the primate cerebral cortex: morphological evidence for cholinergic modulation of excitatory neurotransmission. Proc. Natl. Acad. Sci. U. S. A. 90, 5194–5198. doi:10.1073/pnas.90.11.5194

Mrzljak, L., Levey, A.I., Rakic, P., 1996. Selective expression of m2 muscarinic receptor in the parvocellular channel of the primate visual cortex. Proc. Natl. Acad. Sci. U. S. A. 93, 7337–7340.

Mundell, S.J., Matharu, A.-L., Nisar, S., Palmer, T.M., Benovic, J.L., Kelly, E., 2010. Deletion of the distal COOH-terminus of the A2B adenosine receptor switches internalization to an arrestin- and clathrin-independent pathway and inhibits

recycling. Br. J. Pharmacol. 159, 518–33. doi:10.1111/j.1476-5381.2009.00598.x

Murakami, A., Yajima, T., Sakuma, H., McLaren, M.J., Inana, G., 1993. X-arrestin: a new retinal arrestin mapping to the X chromosome. FEBS Lett. 334, 203–9.

Murray, E., Cho, J.H., Goodwin, D., Wedeen, V.J., Seung, H.S., Chung, K., 2015. Simple , Scalable Proteomic Imaging for High- Dimensional Profiling of Intact Systems Resource Simple , Scalable Proteomic Imaging for High-Dimensional Profiling of Intact Systems. Cell 163, 1500–1514. doi:10.1016/j.cell.2015.11.025

Nakajima, K., Wess, J., 2012. Design and functional characterization of a novel, arrestin-biased designer G protein-coupled receptor. Mol. Pharmacol. 82, 575–582. doi:10.1124/mol.112.080358

Nelson, C.D., Perry, S.J., Regier, D.S., Prescott, S.M., Topham, M.K., Lefkowitz, R.J., 2007. Targeting of diacylglycerol degradation to M1 muscarinic receptors by beta-arrestins. Science 315, 663–6. doi:10.1126/science.1134562

Nirogi, R., Mudigonda, K., Kandikere, V., Ponnamaneni, R., 2010. Quantification of acetylcholine, an essential neurotransmitter, in brain microdialysis samples by liquid chromatography mass spectrometry. Biomed. Chromatogr. 24, 39–48. doi:10.1002/bmc.1347

Nizri, E., Greenman-Maaravi, N., Bar-David, S., Ben-Yehuda, A., Weiner, G., Lahat, G., Klausner, J., 2016. Analysis of histological and immunological parameters of metastatic lymph nodes from colon cancer patients reveals that T-helper 1 type immune response is associated with improved overall survival. Medicine (Baltimore). 95, e5340. doi:10.1097/MD.0000000000005340

Nobles, K.N., Xiao, K., Ahn, S., Shukla, A.K., Lam, C.M., Rajagopal, S., Strachan, R.T., Huang, T., Bressler, E.A., Hara, M.R., Shenoy, S.K., Gygi, S.P., Lefkowitz, R.J., 2011. Distinct phosphorylation sites on the β(2)-adrenergic receptor establish a barcode that encodes differential functions of β-arrestin. Sci. Signal. 4, ra51. doi:10.1126/scisignal.2001707

Noetzel, M.J., Grant, M.K.O., El-Fakahany, E.E., 2009a. Immediate and delayed

consequences of xanomeline wash-resistant binding at the M3 muscarinic receptor. Neurochem. Res. 34, 1138–49. doi:10.1007/s11064-008-9886-3

Noetzel, M.J., Grant, M.K.O., El-Fakahany, E.E., 2009b. Mechanisms of M3 muscarinic receptor regulation by wash-resistant xanomeline binding. Pharmacology 83, 301–17. doi:10.1159/000214843

Noronha-Blob, L., Lowe, V., Patton, A., Canning, B., Costello, D., Kinnier, W.J., 1989. Muscarinic receptors: relationships among phosphoinositide breakdown, adenylate cyclase inhibition, in vitro detrusor muscle contractions and in vivo cystometrogram studies in guinea pig bladder. J. Pharmacol. Exp. Ther. 249, 843–851.

Oakley, R.H., Laporte, S.A., Holt, J.A., Caron, M.G., Barak, L.S., 2000. Differential affinities of visual arrestin, βarrestin1, and βarrestin2 for G protein-coupled receptors delineate two major classes of receptors. J. Biol. Chem. 275, 17201–17210. doi:10.1074/jbc.M910348199

Ohno-Shosaku, T., Sugawara, Y., Muranishi, C., Nagasawa, K., Kubono, K., Aoki, N., Taguchi, M., Echigo, R., Sugimoto, N., Kikuchi, Y., Watanabe, R., Yoneda, M., 2011. Effects of clozapine and N-desmethylclozapine on synaptic transmission at hippocampal inhibitory and excitatory synapses. Brain Res. 1421, 66–77. doi:10.1016/j.brainres.2011.08.073

Oldham, W.M., Hamm, H.E., 2008. Heterotrimeric G protein activation by G-protein-coupled receptors. Nat. Rev. Mol. Cell Biol. 9, 60–71. doi:10.1038/nrm2299

Olianas, M.C., Dedoni, S., Ambu, R., Onali, P., 2009. Agonist activity of N-desmethylclozapine at delta-opioid receptors of human frontal cortex. Eur. J. Pharmacol. 607, 96–101. doi:10.1016/j.ejphar.2009.02.025

Olianas, M.C., Maullu, C., Onali, P., 1999. Mixed agonist-antagonist properties of clozapine at different human cloned muscarinic receptor subtypes expressed in Chinese hamster ovary cells. Neuropsychopharmacology 20, 263–270. doi:10.1016/S0893-133X(98)00048-7

Onali, P., Olianas, M.C., 2002. Muscarinic M4 receptor inhibition of dopamine D1-like receptor signalling in rat nucleus accumbens. Eur. J. Pharmacol. 448, 105–11.

Ourselin, S., Roche, A., Subsol, G., Pennec, X., Ayache, N., 2001. Reconstructing a 3D structure from serial histological sections. Image Vis. Comput. 19, 25–31. doi:10.1016/S0262-8856(00)00052-4

Overk, C.R., Felder, C.C., Tu, Y., Schober, D.A., Bales, K.R., Wuu, J., Mufson, E.J., 2010. Cortical M1 receptor concentration increases without a concomitant change in function in Alzheimer's disease. J. Chem. Neuroanat. 40, 63–70. doi:10.1016/j.jchemneu.2010.03.005

Pal, K., Mathur, M., Kumar, P., DeFea, K., 2013. Divergent β-arrestin-dependent signaling events are dependent upon sequences within G-protein-coupled receptor C termini. J. Biol. Chem. 288, 3265–74. doi:10.1074/jbc.M112.400234

Papastylianou, A., Mentzelopoulos, S., 2012. Current Pharmacological Advances in the Treatment of Cardiac Arrest. Emerg. Med. Int. 2012, 1–9. doi:10.1155/2012/815857

Parnaudeau, S., Taylor, K., Bolkan, S.S., Ward, R.D., Balsam, P.D., Kellendonk, C., 2015. Mediodorsal thalamus hypofunction impairs flexible goal-directed behavior. Biol. Psychiatry 77, 445–53. doi:10.1016/j.biopsych.2014.03.020

Paronis, C.A., Nikas, S.P., Shukla, V.G., Makriyannis, A., 2012. Δ9-Tetrahydrocannabinol acts as a partial agonist/antagonist in mice. Behav. Pharmacol. 23, 802–805. doi:10.1097/FBP.0b013e32835a7c4d

Pauwels, P.J., Colpaert, F.C., 2000. Disparate ligand-mediated Ca(2+) responses by wild-type, mutant Ser(200)Ala and Ser(204)Ala alpha(2A)-adrenoceptor: G(alpha15) fusion proteins: evidence for multiple ligand-activation binding sites. Br J Pharmacol 130, 1505–1512.

Peppel, K., Boekhoff, I., McDonald, P., Breer, H., Caron, M.G., Lefkowitz, R.J., 1997. G protein-coupled receptor kinase 3 (GRK3) gene disruption leads to loss of odorant receptor desensitization. J Biol Chem 272, 25425–25428.

Peralta, E.G., Ashkenazi, A., Winslowl, J.W., Smith, D.H., Ramachandran, J., Capon, D.J., 1987. Distinct primary structures, ligand-binding properties and tissue- specific expression of four human muscarinic acetylcholine receptors Ernest. EMBO J. 6, 3923–3929.

Phillips, H.S., Kharbanda, S., Chen, R., Forrest, W.F., Soriano, R.H., Wu, T.D., Misra, A., Nigro, J.M., Colman, H., Soroceanu, L., Williams, P.M., Modrusan, Z., Feuerstein, B.G., Aldape, K., 2006. Molecular subclasses of high-grade glioma predict prognosis, delineate a pattern of disease progression, and resemble stages in neurogenesis. Cancer Cell 9, 157–173. doi:10.1016/j.ccr.2006.02.019

Phillips, R.G., LeDoux, J.E., 1992. Differential Contribution of Amygdala and Hippocampus to Cued and Contextual Fear Conditioning. Behav. Neurosci. 106, 274–285. doi:10.1037/0735-7044.106.2.274

Pirmohamed, M., Williams, D., Madden, S., Templeton, E., Park, B.K., 1995. Metabolism and bioactivation of clozapine by human liver in vitro. J. Pharmacol. Exp. Ther. 272, 984–90.

Pitcher, J., Lohse, M.J., Codina, J., Caron, M.G., Lefkowitz, R.J., 1992. Desensitization of the isolated beta 2-adrenergic receptor by beta-adrenergic receptor kinase, cAMP-dependent protein kinase, and protein kinase C occurs via distinct molecular mechanisms. Biochemistry 31, 3193–7. doi:10.1021/bi00127a021

Porter, A.C., Bymaster, F.P., DeLapp, N.W., Yamada, M., Wess, J., Hamilton, S.E., Nathanson, N.M., Felder, C.C., 2002. M1 muscarinic receptor signaling in mouse hippocampus and cortex. Brain Res. 944, 82–9.

Poulin, B., Butcher, A.J., McWilliams, P., Bourgognon, J.-M., Pawlak, R., Kong, K.C., Bottrill, A., Mistry, S., Wess, J., Rosethorne, E.M., Charlton, S.J., Tobin, A.B., 2010. The M3-muscarinic receptor regulates learning and memory in a receptor phosphorylation/arrestin-dependent manner. Proc. Natl. Acad. Sci. 107, 9440–9445. doi:10.1073/pnas.0914801107

Premont, R.T., Gainetdinov, R.R., 2007. Physiological Roles of G Protein–Coupled Receptor Kinases and Arrestins. Annu. Rev. Physiol. 69, 511–534.

doi:10.1146/annurev.physiol.69.022405.154731

Premont, R.T., Inglese, J., Lefkowitz, R.J., 1995. Protein kinases that phosphorylate activated G protein-coupled receptors. FASEB J. 9, 175–182. doi:10.1096/fasebj.9.2.7781920

Prihandoko, R., Alvarez-Curto, E., Hudson, B.D., Butcher, A.J., Ulven, T., Miller, A.M., Tobin, A.B., Milligan, G., 2016. Distinct Phosphorylation Clusters Determine the Signaling Outcome of Free Fatty Acid Receptor 4/G Protein-Coupled Receptor 120. Mol. Pharmacol. 89, 505–520. doi:10.1124/mol.115.101949

Prince, M., Bryce, R., Albanese, E., Wimo, A., Ribeiro, W., Ferri, C.P., 2013. The global prevalence of dementia: a systematic review and metaanalysis. Alzheimer's Dement. 9, 63–75. doi:10.1016/j.jalz.2012.11.007

Prince, M., Wimo, A., Guerchet, M., Gemma-Claire, A., Wu, Y.-T., Prina, M., 2015. World Alzheimer Report 2015: The Global Impact of Dementia - An analysis of prevalence, incidence, cost and trends. Alzheimer's Dis. Int. 84. doi:10.1111/j.0963-7214.2004.00293.x

Pronin, A.N., Benovic, J.L., 1997. Regulation of the G protein-coupled receptor kinase GRK5 by protein kinase C. J. Biol. Chem. 272, 3806–3812. doi:10.1074/jbc.272.6.3806

Pronin, A.N., Carman, C. V, Benovic, J.L., 1998. Structure-function analysis of G protein-coupled receptor kinase-5. Role of the carboxyl terminus in kinase regulation. J. Biol. Chem. 273, 31510–8.

Pronin, A.N., Satpaev, D.K., Slepak, V.Z., Benovic, J.L., 1997. Regulation of G protein-coupled receptor kinases by calmodulin and localization of the calmodulin binding domain. J Biol Chem 272, 18273–18280.

Pula, G., Mundell, S.J., Roberts, P.J., Kelly, E., 2004. Agonist-independent internalization of metabotropic glutamate receptor 1a is arrestin- and clathrin-dependent and is suppressed by receptor inverse agonists. J. Neurochem. 89, 1009–20. doi:10.1111/j.1471-4159.2004.02387.x

Qian, J., Wu, C., Chen, X., Li, X., Ying, G., Jin, L., Ma, Q., Li, G., Shi, Y., Zhang, G., Zhou, N., 2014. Differential requirements of arrestin-3 and clathrin for ligand-dependent and -independent internalization of human G protein-coupled receptor 40. Cell. Signal. 26, 2412–23. doi:10.1016/j.cellsig.2014.07.019

Rakha, E.A., Reis-Filho, J.S., Baehner, F., Dabbs, D.J., Decker, T., Eusebi, V., Fox, S.B., Ichihara, S., Jacquemier, J., Lakhani, S.R., Palacios, J., Richardson, A.L., Schnitt, S.J., Schmitt, F.C., Tan, P.-H., Tse, G.M., Badve, S., Ellis, I.O., 2010. Breast cancer prognostic classification in the molecular era: the role of histological grade. Breast Cancer Res. 12, 207. doi:10.1186/bcr2607

Rankin, M.L., Marinec, P.S., Cabrera, D.M., Wang, Z., Jose, P. a, Sibley, D.R., 2006. The D1 dopamine receptor is constitutively phosphorylated by G protein-coupled receptor kinase 4. Mol. Pharmacol. 69, 759–69. doi:10.1124/mol.105.019901

Rasmussen, S.G.F., DeVree, B.T., Zou, Y., Kruse, A.C., Chung, K.Y., Kobilka, T.S., Thian, F.S., Chae, P.S., Pardon, E., Calinski, D., Mathiesen, J.M., Shah, S.T.A., Lyons, J.A., Caffrey, M., Gellman, S.H., Steyaert, J., Skiniotis, G., Weis, W.I., Sunahara, R.K., Kobilka, B.K., 2011. Crystal structure of the β2 adrenergic receptor-Gs protein complex. Nature 477, 549–55. doi:10.1038/nature10361

Ray, R.S., Corcoran, A.E., Brust, R.D., Kim, J.C., Richerson, G.B., Nattie, E., Dymecki, S.M., 2011. Impaired respiratory and body temperature control upon acute serotonergic neuron inhibition. Science 333, 637–42. doi:10.1126/science.1205295

Reiner, S., Ziegler, N., Leon, C., Lorenz, K., von Hayn, K., Gachet, C., Lohse, M.J., Hoffmann, C., 2009. beta-Arrestin-2 interaction and internalization of the human P2Y1 receptor are dependent on C-terminal phosphorylation sites. Mol. Pharmacol. 76, 1162–71. doi:10.1124/mol.109.060467

Renier, N., Wu, Z., Simon, D.J., Yang, J., Ariel, P., Tessier-Lavigne, M., 2014. iDISCO: A Simple, Rapid Method to Immunolabel Large Tissue Samples for Volume Imaging. Cell 159, 896–910. doi:10.1016/j.cell.2014.10.010

Riker, W.F., Wescoe, W.C., 1951. The pharmacology of Flaxedil, with observations on certain analogs. Ann. N. Y. Acad. Sci. 54, 373–94. doi:10.1111/j.1749-6632.1951

Rollema, H., Coe, J.W., Chambers, L.K., Hurst, R.S., Stahl, S.M., Williams, K.E., 2007. Rationale, pharmacology and clinical efficacy of partial agonists of α4β2nACh receptors for smoking cessation. Trends Pharmacol. Sci. 28, 316–325. doi:10.1016/j.tips.2007.05.003

Roszkowski, A.P., 1961. An unusual type of sympathetic ganglionic stimulant. J. Pharmacol. Exp. Ther. 132, 156–70.

Roth, B.L., 2016. DREADDs for Neuroscientists. Neuron 89, 683–694. doi:10.1016/j.neuron.2016.01.040

Roth, B.L., Craigo, S.C., Choudhary, M.S., Uluer, a, Monsma, F.J., Shen, Y., Meltzer, H.Y., Sibley, D.R., 1994. Binding of typical and atypical antipsychotic agents to 5-hydroxytryptamine-6 and 5-hydroxytryptamine-7 receptors. J. Pharmacol. Exp. Ther. 268, 1403–1410.

Roth, B.L., Sheffler, D.J., Kroeze, W.K., 2004. Magic shotguns versus magic bullets: selectively non-selective drugs for mood disorders and schizophrenia. Nat. Rev. Drug Discov. 3, 353–359. doi:10.1038/nrd1346

Roth, B.L., Tandra, S., Burgess, L.H., Sibley, D.R., H.Y., M., 1995. D4 Dopamine receptor binding affinity does not distinguish between typical and atypical antipsychotic drugs. Psychopharmacology (Berl). 120, 365–368.

Royston-Pigott, 1870. On the Optical Advantages of Immersion Lenses and the Use of Deviation Tables for Optical Research. Mon. Microsc. J. 4, 20–26. doi:10.1111/j.1365-2818.1870.tb04974.x

Sarnago, S., Roca, R., de Blasi, A., Valencia, A., Mayor, F.J., Murga, C., 2003. Involvement of intramolecular interactions in the regulation of G protein-coupled receptor kinase 2. Mol. Pharmacol. 64, 629–639. doi:10.1124/mol.64.3.629

Scarr, E., Sundram, S., Keriakous, D., Dean, B., 2007. Altered hippocampal muscarinic M4, but not M1, receptor expression from subjects with schizophrenia. Biol. Psychiatry 61, 1161–70. doi:10.1016/j.biopsych.2006.08.050

Schlederer, M., Mueller, K.M., Haybaeck, J., Heider, S., Huttary, N., Rosner, M.,

Hengstschläger, M., Moriggl, R., Dolznig, H., Kenner, L., 2014. Reliable quantification of protein expression and cellular localization in histological sections. PLoS One 9, e100822. doi:10.1371/journal.pone.0100822

Schleicher, S., Boekhoff, I., Arriza, J., Lefkowitz, R.J., Breer, H., 1993. A beta-adrenergic receptor kinase-like enzyme is involved in olfactory signal termination. Proc. Natl. Acad. Sci. U. S. A. 90, 1420–4. doi:10.1073/pnas.90.4.1420

Schmiedeberg, O., Koppe, R., 1869. Das Muscarin, das giftige Alkaloid des Fliegenpilzes (Agaricus muscarius L.), seine Darstellung, chemischen Eigenschaften, physiologischen Wirkungen, toxicologische Bedeutung und sein Verhältniss zur Pilzvergiftung im allgemeine. Vergal von F. C. W. Vogel, Leipzig.

Schrage, R., Schmitz, A.-L., Gaffal, E., Annala, S., Kehraus, S., Wenzel, D., Büllesbach, K.M., Bald, T., Inoue, A., Shinjo, Y., Galandrin, S., Shridhar, N., Hesse, M., Grundmann, M., Merten, N., Charpentier, T.H., Martz, M., Butcher, A.J., Slodczyk, T., Armando, S., Effern, M., Namkung, Y., Jenkins, L., Horn, V., Stößel, A., Dargatz, H., Tietze, D., Imhof, D., Galés, C., Drewke, C., Müller, C.E., Hölzel, M., Milligan, G., Tobin, A.B., Gomeza, J., Dohlman, H.G., Sondek, J., Harden, T.K., Bouvier, M., Laporte, S.A., Aoki, J., Fleischmann, B.K., Mohr, K., König, G.M., Tüting, T., Kostenis, E., 2015. The experimental power of FR900359 to study Gq-regulated biological processes. Nat. Commun. 6, 10156. doi:10.1038/ncomms10156

Scimemi, A., Beato, M., 2009. Determining the neurotransmitter concentration profile at active synapses. Mol. Neurobiol. 40, 289–306. doi:10.1007/s12035-009-8087-7

Sco, M.D., Boger, H.A., Smith, R.J., Li, H., Haydon, P.G., Kalivas, P.W., Scofield Michael, D., Boger, H.A., Smith, R.J., Li, H., Haydon, P.G., Kalivas, P.W., Smith Rachel, J., Hao, L., 2015. Gq-DREADD Selectively Initiates Glial Glutamate Release and Inhibits Cue-induced Cocaine Seeking. Biol. Psychiatry 1–11. doi:10.1016/j.biopsych.2015.02.016

Scott, M.G.H., Pierotti, V., Storez, H., Lindberg, E., Thuret, A., Muntaner, O., Labbé-Jullié, C., Pitcher, J.A., Marullo, S., 2006. Cooperative regulation of extracellular signal-regulated kinase activation and cell shape change by filamin A and beta-arrestins.

Mol. Cell. Biol. 26, 3432–45. doi:10.1128/MCB.26.9.3432-3445.2006

Seeger, T., Fedorova, I., Zheng, F., Miyakawa, T., Koustova, E., Gomeza, J., Basile, A.S., Alzheimer, C., Wess, J., 2004. M2 muscarinic acetylcholine receptor knock-out mice show deficits in behavioral flexibility, working memory, and hippocampal plasticity. J. Neurosci. 24, 10117–27. doi:10.1523/JNEUROSCI.3581-04.2004

Seeman, P., Corbettand, R., Van Tol, H.H.M., 1997. Atypical neuroleptics have low affinity for dopamine D2 receptors or are selective for D4 receptors. Neuropsychopharmacology. doi:10.1016/S0893-133X(96)00187-X

Shannon, H.E., Bymaster, F.P., Calligaro, D.O., Greenwood, B., Mitch, C.H., Sawyer, B.D., Ward, J.S., Wong, D.T., Olesen, P.H., Sheardown, M.J., 1994. Xanomeline: a novel muscarinic receptor agonist with functional selectivity for M1 receptors. J. Pharmacol. Exp. Ther. 269, 271–81.

Shao, J.S., Cai, J., Towler, D.A., 2006. Molecular mechanisms of vascular calcification: Lessons learned from the aorta. Arterioscler. Thromb. Vasc. Biol. 26, 1423–1430. doi:10.1161/01.ATV.0000220441.42041.20

Shekhar, A., Potter, W.Z., Lightfoot, J., Lienemann, J., Dubé, S., Mallinckrodt, C., Bymaster, F.P., McKinzie, D.L., Felder, C.C., 2008. Selective muscarinic receptor agonist xanomeline as a novel treatment approach for schizophrenia. Am. J. Psychiatry 165, 1033–9. doi:10.1176/appi.ajp.2008.06091591

Shenoy, S.K., Modi, A.S., Shukla, A.K., Xiao, K., Berthouze, M., Ahn, S., Wilkinson, K.D., Miller, W.E., Lefkowitz, R.J., 2009. Beta-arrestin-dependent signaling and trafficking of 7-transmembrane receptors is reciprocally regulated by the deubiquitinase USP33 and the E3 ligase Mdm2. Proc. Natl. Acad. Sci. U. S. A. 106, 6650–5. doi:10.1073/pnas.0901083106

Shiina, T., Arai, K., Tanabe, S., Yoshida, N., Haga, T., Nagao, T., Kurose, H., 2001. Clathrin box in G protein-coupled receptor kinase 2. J. Biol. Chem. 276, 33019–33026. doi:10.1074/jbc.M100140200

Shiozaki, K., Iseki, E., Hino, H., Kosaka, K., 2001. Distribution of m1 muscarinic

acetylcholine receptors in the hippocampus of patients with Alzheimer's disease and dementia with Lewy bodies-an immunohistochemical study. J. Neurol. Sci. 193, 23–8.

Singh, S.N., Bakshi, K., Mercier, R.W., Makriyannis, A., Pavlopoulos, S., 2011. Binding between a distal C-terminus fragment of cannabinoid receptor 1 and arrestin-2. Biochemistry 50, 2223–34. doi:10.1021/bi1018144

Singla, N., Minkowitz, H.S., Soergel, D.G., Burt, D.A., Subach, R.A., Salamea, M.Y., Fossler, M.J., Skobieranda, F., 2017. A randomized, Phase IIb study investigating oliceridine (TRV130), a novel micro-receptor G-protein pathway selective (mu-GPS) modulator, for the management of moderate to severe acute pain following abdominoplasty. J. Pain Res. 10, 2413–2424. doi:10.2147/JPR.S137952

Smith, W.C., Milam, A.H., Dugger, D., Arendt, A., Hargrave, P.A., Palczewski, K., 1994. A splice variant of arrestin. Molecular cloning and localization in bovine retina. J. Biol. Chem. 269, 15407–15410.

Söderquist, F., Hellström, P.M., Cunningham, J.L., 2015. Human gastroenteropancreatic expression of melatonin and its receptors MT1 and MT2. PLoS One 10, e0120195. doi:10.1371/journal.pone.0120195

Soergel, D.G., Subach, R.A., Burnham, N., Lark, M.W., James, I.E., Sadler, B.M., Skobieranda, F., Violin, J.D., Webster, L.R., 2014. Biased agonism of the l-opioid receptor by TRV130 increases analgesia and reduces on-target adverse effects versus morphine: A randomized, double-blind, placebo-controlled, crossover study in healthy volunteers. Pain 155, 1829–1835. doi:10.1016/j.pain.2014.06.011

Sora, I., Takahashi, N., Funada, M., Ujike, H., Revay, R.S., Donovan, D.M., Miner, L.L., Uhl, G.R., 1997. Opiate receptor knockout mice define receptor roles in endogenous nociceptive responses and morphine-induced analgesia. Neurobiology 94, 1544–1549. doi:10.1073/pnas.94.4.1544

Spalteholz, W., 1911. Über das Durchsichtigmachen von menschlichen und tierischen Präparaten. Hirzel, Leipzig.

Stallaert, W., Christopoulos, A., Bouvier, M., 2011. Ligand functional selectivity and quantitative pharmacology at G protein-coupled receptors. Expert Opin. Drug Discov. 6, 811–825. doi:10.1517/17460441.2011.586691

Sterne-Marr, R., Gurevich, V. V., Goldsmith, P., Bodine, R.C., Sanders, C., Donoso, L.A., Benovic, J.L., 1993. Polypeptide variants of beta-arrestin and arrestin3. J. Biol. Chem. 268, 15640–8.

Stille, G., Sayers, A., Lauener, H., Eichenberger, E., 1973. 6-(4-methyl-1-piperazinyl)morphanthridine (perlapine), a new tricyclic compound with sedative and sleep-promoting properties - A pharmacological study. Psychopharmacologia 28, 325–337. doi:10.1007/BF00422753

Strader, C.D., Gaffney, T., Sugg, E.E., Candelore, M.R., Keys, R., Patchett, A.A., Dixon, R.A., 1991. Allele-specific activation of genetically engineered receptors. J. Biol. Chem. 266, 5–8.

Strathmann, M.P., Gautam, N., 1991. Diversity of G Proteins. Science (80-.). 252, 802–808. doi:10.1126/science.1902986

Sumara, G., Formentini, I., Collins, S., Sumara, I., Windak, R., Bodenmiller, B., Ramracheya, R., Caille, D., Jiang, H., Platt, K.A., Meda, P., Aebersold, R., Rorsman, P., Ricci, R., 2009. Regulation of PKD by the MAPK p38δ in Insulin Secretion and Glucose Homeostasis. Cell 136, 235–248. doi:10.1016/j.cell.2008.11.018

Susaki, E.A.A., Tainaka, K., Perrin, D., Kishino, F., Tawara, T., Watanabe, T.M., Yokoyama, C., Onoe, H., Eguchi, M., Yamaguchi, S., Abe, T., Kiyonari, H., Shimizu, Y., Miyawaki, A., Yokota, H., Ueda, H.R., 2014. Whole-brain imaging with single-cell resolution using chemical cocktails and computational analysis. Cell 157, 726–39. doi:10.1016/j.cell.2014.03.042

Sykes, D.A., Moore, H., Stott, L., Holliday, N., Javitch, J.A., Robert Lane, J., Charlton, S.J., 2017. Extrapyramidal side effects of antipsychotics are linked to their association kinetics at dopamine D2receptors. Nat. Commun. 8, 1–11. doi:10.1038/s41467-017-00716-z

Tanahashi, Y., Waki, N., Unno, T., Matsuyama, H., Iino, S., Kitazawa, T., Yamada, M., Komori, S., 2013. Roles of M2 and M3 muscarinic receptors in the generation of rhythmic motor activity in mouse small intestine. Neurogastroenterol. Motil. 25, 687–697. doi:10.1111/nmo.12194

Tangsucharit, P., Takatori, S., Zamami, Y., Goda, M., Pakdeechote, P., Kawasaki, H., Takayama, F., 2016. Muscarinic acetylcholine receptor M1 and M3 subtypes mediate acetylcholine-induced endothelium-independent vasodilatation in rat mesenteric arteries. J. Pharmacol. Sci. 1–9. doi:10.1016/j.jphs.2015.12.005

Tayebati, S.K., Di Tullio, M.A., Tomassoni, D., Amenta, F., Tullio, M.A.D.I., Tomassoni, D., Amenta, F., Di Tullio, M.A., Tomassoni, D., Amenta, F., 2003. Localization of the m5 muscarinic cholinergic receptor in rat circle of Willis and pial arteries. Neuroscience 122, 205–11. doi:10.1016/S0306-4522(03)00513-X

Thal, D.M., Sun, B., Feng, D., Nawaratne, V., Leach, K., Felder, C.C., Bures, M.G., Evans, D.A., Weis, W.I., Bachhawat, P., Kobilka, T.S., Sexton, P.M., Kobilka, B.K., Christopoulos, A., 2016. Crystal structures of the M1 and M4 muscarinic acetylcholine receptors. Nature 1–18. doi:10.1038/nature17188

Thompson, K.J., Khajehali, E., Bradley, S.J., Navarrete, J.S., Huang, X.-P., Slocum, S., Jin, J., Liu, J., Xiong, Y., Olsen, R., DiBerto, J., Boyt, K.M., Pina, M.M., Pati, D., Molloy, C., Bundgaard, C., Sexton, P.M., Kash, T.L., Krashes, M.J., Christopoulos, A., Roth, B.L., Tobin, A.B., 2018. Dreadd Agonist 21 (C21) Is an Effective Agonist for Muscarnic-Based Dreadds in Vitro and in Vivo. ACS Pharmacol. Transl. Sci. acsptsci.8b00012. doi:10.1021/acsptsci.8b00012

Tobin, A.B., Butcher, A.J., Kong, K.C., 2008. Location, location, location...site-specific GPCR phosphorylation offers a mechanism for cell-type-specific signalling. Trends Pharmacol. Sci. 29, 413–420. doi:10.1016/j.tips.2008.05.006

Tobin, G., Giglio, D., Lundgren, O., 2009. Muscarinic receptor subtypes in the alimentary tract. J. Physiol. Pharmacol. 60, 3–21.

Tsai, T.H., 2000. Separation methods used in the determination of choline and acetylcholine. J. Chromatogr. B Biomed. Sci. Appl. 747, 111–122.

doi:10.1016/S0378-4347(00)00268-1

Tsang, S.W.Y., Lai, M.K.P., Kirvell, S., Francis, P.T., Esiri, M.M., Hope, T., Chen, C.P.L.-H., Wong, P.T.-H., 2006. Impaired coupling of muscarinic M1 receptors to G-proteins in the neocortex is associated with severity of dementia in Alzheimer's disease. Neurobiol. Aging 27, 1216–23. doi:10.1016/j.neurobiolaging.2005.07.010

Tu-sekine, B., Goldschmidt, H., Raben, D.M., 2014. Diacylglycerol, phosphatidic acid, and their metabolic enzymes in synaptic vesicle recycling. Adv. Biol. Regul. 1–6. doi:10.1016/j.jbior.2014.09.010

Tuček, S., Michal, P., Vlachová, V., 2002. Modelling the consequences of receptor-G-protein promiscuity. Trends Pharmacol. Sci. 23, 171–176. doi:10.1016/S0165-6147(00)01996-9

Tyrer, P., Kendall, T., 2009. The spurious advance of antipsychotic drug therapy. Lancet 373, 4–5. doi:10.1016/S0140-6736(08)61765-1

Tzavara, E.T., Bymaster, F.P., Felder, C.C., Wade, M., Gomeza, J., Wess, J., McKinzie, D.L., Nomikos, G.G., 2003. Dysregulated hippocampal acetylcholine neurotransmission and impaired cognition in M2, M4 and M2/M4 muscarinic receptor knockout mice. Mol. Psychiatry 8, 673–9. doi:10.1038/sj.mp.4001270

Urban, J.D., Clarke, W.P., von Zastrow, M., Nichols, D.E., Kobilka, B.K., Weinstein, H., Javitch, J.A., Roth, B.L., Christopoulos, A., Sexton, P.M., Miller, K.J., Spedding, M., Mailman, R.B., 2007. Functional selectivity and classical concepts of quantitative pharmacology. J. Pharmacol. Exp. Ther. 320, 1–13. doi:10.1124/jpet.106.104463

Valant, C., Felder, C.C., Sexton, P.M., Christopoulos, A., 2012. Probe dependence in the allosteric modulation of a G protein-coupled receptor: implications for detection and validation of allosteric ligand effects. Mol. Pharmacol. 81, 41–52. doi:10.1124/mol.111.074872

Valant, C., May, L.T., Aurelio, L., Chuo, C.H., White, P.J., Baltos, J.-A., Sexton, P.M., Scammells, P.J., Christopoulos, A., 2014. Separation of on-target efficacy from adverse effects through rational design of a bitopic adenosine receptor agonist.

Proc. Natl. Acad. Sci. U. S. A. 111, 4614–9. doi:10.1073/pnas.1320962111

Varela, C., Weiss, S., Meyer, R., Halassa, M., Biedenkapp, J., Wilson, M.A., Goosens, K.A., Bendor, D., 2016. Tracking the Time-Dependent Role of the Hippocampus in Memory Recall Using DREADDs. PLoS One 11, e0154374. doi:10.1371/journal.pone.0154374

Veeraragavan, S., Bui, N., Perkins, J.R., Yuva-Paylor, L.A., Carpenter, R.L., Paylor, R., 2011. Modulation of behavioral phenotypes by a muscarinic M1 antagonist in a mouse model of fragile X syndrome. Psychopharmacology (Berl). 217, 143–51. doi:10.1007/s00213-011-2276-6

Veroff, A.E., Bodick, N.C., Offen, W.W., Sramek, J.J., Cutler, N.R., 1998. Efficacy of xanomeline in Alzheimer disease: cognitive improvement measured using the Computerized Neuropsychological Test Battery (CNTB). Alzheimer Dis. Assoc. Disord. 12, 304–12.

Vilaró, M.T., Palacios, J.M., Mengod, G., 1990. Localization of m5 muscarinic receptor mRNA in rat brain examined by in situ hybridization histochemistry. Neurosci. Lett. 114, 154–9.

Vincken, W., van Noord, J.A., Greefhorst, A.P.M., Bantje, T.A., Kesten, S., Korducki, L., Cornelissen, P.J.G., van de Bosch, J.M.M., Bunnik, M.C.M., Creemers, J.P.H.M., Dalinghaus, W.H., Eland, M.E., Evers, W.B.M., Gans, S.J.M., Gooszen, H.C., van Harreveld, A.J., van Kasteren, J.H.L.M., Kuipers, A.F., van Noord, J.A., Nossent, G.D., Pasma, H.R., Peters, A., Pieters, W.R., Postmus, P.E., Schreurs, A.J.M., Sinninghe Damsté, H.E.J., Sips, A.P., van Spiegel, P.I., Westbroek, J., Aumann, J.L., Janssens, E., Pauwels, R., Radermecker, M., Slabbynck, H., Stappaerts, I., Verhaert, J., Vermeire, P., Vincken, W., 2002. Improved health outcomes in patients with COPD during 1 yr's treatment with tiotropium. Eur. Respir. J. 19, 209–216. doi:10.1183/09031936.02.00238702

Violin, J.D., Dewire, S.M., Yamashita, D., Rominger, D.H., Nguyen, L., Schiller, K., Whalen, E.J., Gowen, M., Lark, M.W., 2010. Selectively engaging β-arrestins at the angiotensin II type 1 receptor reduces blood pressure and increases cardiac

performance. J. Pharmacol. Exp. Ther. 335, 572–9. doi:10.1124/jpet.110.173005

Violin, J.D., Lefkowitz, R.J., 2007. Beta-arrestin-biased ligands at seven-transmembrane receptors. Trends Pharmacol. Sci. 28, 416–22. doi:10.1016/j.tips.2007.06.006

Voie, A.H., Burns, D.H., Spelman, F.A., 1993. Orthogonal-plane fluorescence optical sectioning: three-dimensional imaging of macroscopic biological specimens. J. Microsc. 170, 229–236. doi:10.1111/j.1365-2818.1993.tb03346.x

Volpicelli, L.A., Levey, A.I., 2004. Muscarinic acetylcholine receptor subtypes in cerebral cortex and hippocampus. Prog. Brain Res. 145, 59–66. doi:10.1016/S0079-6123(03)45003-6

Volpicelli, S.A., Centorrino, F., Puopolo, P.R., Kando, J., Frankenburg, F.R., Baldessarini, R.J., Flood, J.G., 1993. Determination of clozapine, norclozapine, and clozapine-N-oxide in serum by liquid chromatography. Clin. Chem. 39, 1656–1659.

Von Voigtlander, P.F., Lewis, R.A., 1988. Analgesic and mechanistic evaluation of spiradoline, a potent kappa opioid. J.Pharmacol.Exp.Ther. 246, 259–262.

Wan, M., Zhang, W., Tian, Y., Xu, C., Xu, T., Liu, J., 2015. Unraveling a molecular determinant for clathrin- independent internalization of the M2 muscarinic acetylcholine receptor. Nat. Publ. Gr. 1–16. doi:10.1038/srep11408

Wang, C.-W., Budiman Gosno, E., Li, Y.-S., 2015. Fully automatic and robust 3D registration of serial-section microscopic images. Sci. Rep. 5, 15051. doi:10.1038/srep15051

Wang, P., Luthin, G.R., Ruggieri, M.R., 1995. Muscarinic acetylcholine receptor subtypes mediating urinary bladder contractility and coupling to GTP binding proteins. J. Pharmacol. Exp. Ther. 273, 959–66.

WANG, X., DEVAIAH, S.P., Zhang, W., WELTI, R., 2006. Signaling functions of phosphatidic acid. Prog. Lipid Res. 45, 250–78. doi:10.1016/j.plipres.2006.01.005

Warthen, D.M., Lambeth, P.S., Ottolini, M., Shi, Y., Barker, B.S., Gaykema, R.P., Newmyer, B.A., Joy-Gaba, J., Ohmura, Y., Perez-Reyes, E., Güler, A.D., Patel, M.K.,

Scott, M.M., 2016. Activation of Pyramidal Neurons in Mouse Medial Prefrontal Cortex Enhances Food-Seeking Behavior While Reducing Impulsivity in the Absence of an Effect on Food Intake. Front. Behav. Neurosci. 10, 1–17. doi:10.3389/fnbeh.2016.00063

Wasserman, D.I., Tan, J.M.J., Kim, J.C., Yeomans, J.S., 2016. Muscarinic Control of Rostromedial Tegmental Nucleus GABA Neurons and Morphine-induced Locomotion. Eur. J. Neurosci. n/a-n/a. doi:10.1111/ejn.13237

Watz, H., Mailänder, C., May, C., Baier, M., Kirsten, A., 2016. Fast onset of action of glycopyrronium compared with tiotropium in patients with moderate to severe COPD - A randomised, multicentre, crossover trial. Pulm. Pharmacol. Ther. 42, 13–20. doi:10.1016/j.pupt.2016.12.001

Weigmann, H., Hiemke, C., 1992. Determination of clozapine and its major metabolites in human serum using automated solid-phase extraction and subsequent isocratic high-performance liquid chromatography with ultraviolet detection. J. Chromatogr. 583, 209–16.

Wenk, G.L., Parsons, C.G., Danysz, W., 2006. Potential role of N-methyl-D-aspartate receptors as executors of neurodegeneration resulting from diverse insults: focus on memantine. Behav. Pharmacol. 17, 411–424. doi:10.1097/00008877-200609000-00007

Wenthur, C.J., Lindsley, C.W., 2013. Classics in chemical neuroscience: clozapine. ACS Chem. Neurosci. 4, 1018–25. doi:10.1021/cn400121z

Wess, J., Eglen, R.M., Gautam, D., 2007. Muscarinic acetylcholine receptors: mutant mice provide new insights for drug development. Nat. Rev. Drug Discov. 6, 721–33. doi:10.1038/nrd2379

Wilkie, T.M., Gilbert, D.J., Olsen, A.S., Chen, X., Amatruda, T.T., Korenberg, J.R., Trask, B.J., de Jong, P., Reed, R.R., Simon, M.I., Jenkins, N.A., Copeland, N.G., 1992. Evolution of the mammalian G protein α subunit multigene family. Nat. Genet. 1, 85–91. doi:10.1038/ng0592-85

Wipke, B.T., Allen, P.M., 2001. Essential Role of Neutrophils in the Initiation and Progression of a Murine Model of Rheumatoid Arthritis. J. Immunol. 167, 1601–1608. doi:10.4049/jimmunol.167.3.1601

Wortmann, M., 2015. World alzheimer report 2014: Dementia and risk reduction. Alzheimer's Dement. 11, P837.

Xu, M., Nakamura, Y., Yamamoto, T., Natori, K., Irie, T., Utsumi, H., Kato, T., 1991. Determination of basal acetylcholine release in vivo by rat brain dialysis with a U-shaped cannula: effect of SM-10888, a putative therapeutic drug for Alzheimer's disease. Neurosci. Lett. 123, 179–82.

Yamada, M., Basile, A.S., Fedorova, I., Zhang, W., Duttaroy, A., Cui, Y., Lamping, K.G., Faraci, F.M., Deng, C.X., Wess, J., 2003. Novel insights into M5 muscarinic acetylcholine receptor function by the use of gene targeting technology. Life Sci. 74, 345–53. doi:10.1016/j.lfs.2003.09.022

Yamada, M., Lamping, K.G., Duttaroy, A., Zhang, W., Cui, Y., Bymaster, F.P., McKinzie, D.L., Felder, C.C., Deng, C.X., Faraci, F.M., Wess, J., 2001a. Cholinergic dilation of cerebral blood vessels is abolished in M(5) muscarinic acetylcholine receptor knockout mice. Proc. Natl. Acad. Sci. U. S. A. 98, 14096–101. doi:10.1073/pnas.251542998

Yamada, M., Miyakawa, T., Duttaroy, A., Yamanaka, A., Moriguchi, T., Makita, R., Ogawa, M., Chou, C.J., Xia, B., Crawley, J.N., Felder, C.C., Deng, C.X., Wess, J., 2001b. Mice lacking the M3 muscarinic acetylcholine receptor are hypophagic and lean. Nature 410, 207–12. doi:10.1038/35065604

Yang, B., Treweek, J.B.B.B., Kulkarni, R.P.P.P., Deverman, B.E.E.E., Chen, C., Lubeck, E., Shah, S., Cai, L., Gradinaru, V., 2014. Single-Cell Phenotyping within Transparent Intact Tissue through Whole-Body Clearing. Cell 158, 945–958. doi:10.1016/j.cell.2014.07.017

Yang, W., Xia, S.-H., 2006. Mechanisms of regulation and function of G-protein-coupled receptor kinases. World J. Gastroenterol. WJG 12, 7753–7757.

Yang, Z., Yang, F., Zhang, D., Liu, Z., Lin, A., Liu, C., Xiao, P., Yu, X., Sun, J.-P., 2017. Phosphorylation of G Protein-Coupled Receptors: From the Barcode Hypothesis to the Flute Model. Mol. Pharmacol. 92, 201–210. doi:10.1124/mol.116.107839

Yau, J.O., Mcnally, G.P., 2015. Pharmacogenetic Excitation of Dorsomedial Prefrontal Cortex Restores Fear Prediction Error. J. Neurosci. 35, 74–83. doi:10.1523/JNEUROSCI.3777-14.2015

Yoshii, T., Hosokawa, H., Matsuo, N., 2016. Pharmacogenetic reactivation of the original engram evokes an extinguished fear memory. Neuropharmacology 113, 1–9. doi:10.1016/j.neuropharm.2016.09.012

Zavitsanou, K., Katerina, Z., Katsifis, A., Andrew, K., Mattner, F., Filomena, M., Huang, X.-F., Xu-Feng, H., 2004. Investigation of m1/m4 muscarinic receptors in the anterior cingulate cortex in schizophrenia, bipolar disorder, and major depression disorder. Neuropsychopharmacology 29, 619–25. doi:10.1038/sj.npp.1300367

Zhang, J., Ferguson, S.S., Barak, L.S., Ménard, L., Caron, M.G., 1996. Dynamin and beta-arrestin reveal distinct mechanisms for G protein-coupled receptor internalization. J. Biol. Chem. 271, 18302–18305. doi:10.1074/jbc.271.31.18302

Zhang, M.Y., Beyer, C.E., 2006. Measurement of neurotransmitters from extracellular fluid in brain by in vivo microdialysis and chromatography-mass spectrometry. J. Pharm. Biomed. Anal. 40, 492–499. doi:10.1016/j.jpba.2005.07.025

Zhu, X., Ottenheimer, D., DiLeone, R.J., 2016. Activity of D1/2 Receptor Expressing Neurons in the Nucleus Accumbens Regulates Running, Locomotion, and Food Intake. Front. Behav. Neurosci. 10, 1–10. doi:10.3389/fnbeh.2016.00066